UNIVERSITAT POLITÈCNICA DE CATALUNYA BARCELONATECH

A novel optimization methodology of modular wiring harnesses in modern vehicles : weight reduction and safe operation

Armand Rius i Rueda

A novel optimization methodology of modular wiring harnesses in modern vehicles

Weight reduction and safe operation

Thesis presented to obtain the qualification of Doctor from the Universitat Politècnica de Catalunya (ETSEIAT, Terrassa – March, 2017)

Author: Armand Rius i Rueda
Supervisor: Dr. Antoni Garcia Espinosa
SEAT Mentor: Manuel A. Díaz Millán

RÜCKER LYPSA EDAG GROUP

SEAT

UPC UNIVERSITAT POLITÈCNICA DE CATALUNYA BARCELONATECH
Escola Tècnica Superior d'Enginyeries Industrial i Aeronàutica de Terrassa

Abstract

The weight of electric and electronic components of cars has been uninterruptedly increasing through the last decades, and thus the weight of their wiring harnesses. This fact has awakened the interest of car manufacturers on the weight and cost optimization of automotive wiring harnesses. For this reason, this dissertation discusses and develops approaches to reduce the amount of copper for the purpose of current conduction, i.e. the cross-sections of all of the wires of the car, without endangering safety.

On the one hand, harnesses must withstand continuous operation currents. On account of this, it is necessary to know the characteristic flow of current of the in-vehicle electrical network. Nevertheless, the huge quantity of available combinations of equipment of the car produces a proportional variety of customer-specific wiring harnesses, and makes it unfeasible to simulate all of them. This thesis points attention on specific segments of the wiring harnesses. Some of them can have many possible compositions, which are related to the customer's car settings. Since computation time is a limiting factor here, it is proposed to predict the bundle heating behaviors by means of response surfaces, obtained from a set of finite element simulation results and the least squares method.

On the other hand, the correct wire sizes must ensure that they are protected by their associated melting fuses, so that their maximum acceptable temperature is not exceeded after short circuits. Since many wires in cars are connected to other wires with splices, or may suffer short-circuits in their electric loads, these short-circuits can flow across different wires. In modular wiring harnesses, each of the wires can have different lengths and different installation ratios, their cross-section affects the cost of the wire harness with different importance, as well as the short circuit and the final temperature of the wire. The finite volume method is used to simulate the short circuit of series-connected wires. Finally, non-linear optimization is used to find the minimum cross-sections of wires respecting the constraints of maximum temperature and minimum short-circuit current.

Finally, these two different criteria for optimal wire dimensioning are combined in the analysis of the on-board network of the vehicle in order to make a complete weight and cost minimization of the cable harnesses in a particular vehicle, considering also its modularity of loads.

Resum

El pes dels components elèctrics i electrònics dels automòbils ha crescut ininterrompudament al llarg de les darreres dècades, i conseqüentment ho han fet també els seus feixos de cables. Aquest fet ha despertat entre els fabricants de turismes un elevat interès en la minimització del pes i dels costos del cablejat del vehicle. Per aquest motiu, aquesta tesi desenvolupa mètodes per reduir la quantitat de coure destinat a la conducció de corrent, és a dir, les seccions de tots els fils elèctrics dins el cotxe, sense posar en risc la seguretat.

Per una banda, els feixos han de resistir els corrents d'operació continuada. Per a aquest propòsit, cal conèixer el flux de corrents característic de la xarxa de bord del vehicle. No obstant, la immensa quantitat de combinacions de diferents equipaments del vehicle produeix proporcionalment una enorme varietat de feixos personalitzats per als clients, fet que fa inviable simular totes aquestes combinacions. El primer dels mètodes d'optimització que es proposen en aquesta tesi estudia segments dels feixos de cables per separat un a un. Alguns d'ells poden tenir diferents composicions de fils en funció de la configuració aplicada pel client. Com que el temps de càlcul és un factor limitant, es proposa predir el comportament tèrmic dels segments per mitjà de superfícies resposta, que s'obtenen a través del mètode dels mínims quadrats i un conjunt de resultats de simulació de feixos pel mètode dels elements finits.

Per altra banda, les correctes seccions dels fils han de ser tals que els curtcircuits i les sobrecàrregues no puguin malmetre'ls, gràcies a la correcta coordinació amb els fusibles destinats a protegir-los. Atès que molts fils estan connectats amb altres fils per mitjà d'unions soldades i que molts curtcircuits són provocats directament en bornes de les càrregues elèctriques, els curtcircuits poden fluir a través de fils diferenciats connectats en sèrie. Als feixos modulars, cadascun dels fils té diferents longituds i ratis d'instal·lació. És per aquest darrer motiu que llur secció afecta de diferent manera al cost total del conjunt dels feixos de cables dels cotxes venuts. De la mateixa manera, les seves longituds diferents fan que les variacions en les seccions alterin els curtcircuits resultants amb diferent sensibilitat. És per això que es fa servir optimització no lineal per trobar les seccions separades de cadascun dels fils connectats en sèrie a través dels quals poden passar curtcircuits. Per a aquesta fi es fan simulacions en volums finits i models energètics dels fusibles integrades dins de l'optimització no lineal.

Finalment, aquestes dues vies de dimensionament es combinen dins una anàlisi íntegra de la xarxa de bord per dimensionar de forma òptima cadascun dels fils del vehicle, tenint en compte les interconnexions entre feixos i totes les combinacions d'equipament.

.

Acknowledgements

There are so many people I would like to thank for their active participation in this research and for their support during these nearly four years of my life. I feel so grateful that it would take several pages to describe how much I will remember what they did for me, and I am sorry I cannot go into detail here.

I need to reserve some lines to say thanks to my incomparable friend Oriol Bergadà, who left us on July 2014, at the age of 24. Oriol was a promising engineer whose creativeness inspired me and many others every day, and whom I have missed ever since he left. Thank you for the years you gave us Uri, I wish you were still here.

In a rigorous chronological order, I must thank my old friend, Dr. Sergi Rotger, because he was the person who insistently encouraged me to start this research, in spite of my hesitations. I also want to acknowledge my friend Dr. Dr. F. Xavier López for his constant presence despite we are thousands of kilometers away from each other.

The second two participants of this story are Manel Díaz and Dr. Antoni Garcia, whom I must acknowledge for choosing me for this research and for their guidance along these years. But most of all, I want to thank them for their affection and particularly for their extensively proven patience with me.

And once the research started, of course, I wish to say thanks to all the people who actively and invaluably helped me with their work, who are Ana Cristina Hernández, Albert Garrell, Juan Andrés Pérez and Octavian Rotariu. I also want to thank Rosa Nogales, Eva M. Baña, Anna Fontarnau, Miguel Ferrer, Alexia Soria, Enric Canadell, Eduard Rodellas and Pedro Manonelles for sharing their wisdom, for every answer they had to my numerous questions, and also for their unconditional affection and support. And I must say thanks to all members of the MCIA group in Terrassa, especially to Carles Colls, Carlos López and Enric Sala.

And of course, I cannot forget this wonderful team of doctoral students in Seat –some of whom have already become doctors–, which I need to acknowledge for their friendship, all of the knowledge, and all of the ideas I have received from them. Daniel Dorribo, Jorge López, Miguel Galarza, Javier Gómez, Carlos Viñolo, Lluc Canals and Adrián Schiffer: thank you guys.

And finally, I wouldn't like to finish this thesis without acknowledging the rest of my friends, my family and specially my parents. Because they are the source of everything I am. Because they have always prioritized their sons in front of anything else. Because they have always forgiven my faults and my scarcities and respected my decisions. Because they are whom I must thank every step I have made in my life, and all the good I have taken from them. Thank you, mum and dad.

Table of contents

List of figures 11
List of tables 15
1. Introduction 19
1.1. The need for a weight reduction of the vehicle wiring 20
1.2. Weight reduction strategies 21
1.3. The complexity of customer-specific wiring harnesses 28
1.4. The problem of the temperature prediction and the need for reliability 39
1.5. Single-wire wire parameters and definitions 41
1.6. Automotive fuse parameters and definitions 44
1.7. The standard dimensioning method 47
2. Statement of the problem 53
3. The state-of-the-art automotive wire modelling and optimization 57
3.1. Analytical solution of the heat transfer equation for single wires 59
3.2. Numerical solution of temperature transients for single wires 63
3.3. Interpolation of numerical results 70
3.4. Coordinate transformation of the multi-wire bundle geometry 72
3.5. The finite volume method for wire bundles (2D) 74
3.6. The finite element method for multi-wire bundles 78
3.7. The fixed-point approach in multi-wire bundles 81
3.8. Efficiency-oriented optimization of wiring systems in vehicle applications 87
3.9. Optimization of current-carrying multi-wire cables 94
3.10. Optimization of multi-voltage automotive power supply systems 100
4. Hypotheses 107
5. Objectives of the thesis 113
6. Methodology 117
6.1. The dimensioning concept 119
6.2. Reliability and relevant concepts for optimization 123
6.3. FEM wire bundle simulator for multiple cases 130
6.4. Comparison of the FEM simulator with COMSOL® Multiphysics 136
6.5. Optimization process proposal 143
6.6. Optimization approaches for wire bundles 146
6.7. Simulation and optimization of series connected wires subject to short circuit 161
6.8. Entire network optimization 190
7. Conclusions 205

Bibliography 209
Conference presentations 211
Publications 211

List of figures

Fig. 1: Overall view of the wiring system 29
Fig. 2: Classification of different wiring approaches 30
Fig. 3: Example of modules of the airbag family 35
Fig. 4: Example of routing definition of the driver's door 36
Fig. 5: Rated current, continuous current and time-current characteristic of a fuse 44
Fig. 6: Fuse typical temperature rerating curves for medium blade fuses 45
Fig. 7: Fuse cold resistance versus operating time 46
Fig. 8: Fuse time-current spread characteristic given by Littelfuse 46
Fig. 9: Wire and fuse dimensioning process diagram 47
Fig. 10: Example of fuse and wire current-time characteristic curves under correct coordination 48
Fig. 11: VW75212 dimensioning process diagram (skipping optimization) 49
Fig. 12: Section of a wire for the analytical solution of the heat transfer equation [1] 61
Fig. 13: Scheme of the cable model in the thermal equivalent circuit approach 63
Fig. 14: Comparison of the pde solution with the thermal equivalent circuit 64
Fig. 15: Comparison of simulated and measured steady temperatures 64
Fig. 16: Comparison of simulated and measured temperature transients 64
Fig. 17: Comparison of measured and modeled current of a single wire in a wiring system 65
Fig. 18: The finite volume grid of round wires [1] 67
Fig. 19: The model of heat conduction in round electrical wires [1] 68
Fig. 20: Measured temperature of a round wire conductor (cross-section = 35mm²) as function of the electric load [1] 69
Fig. 21: Thermo-electrical characteristic $\Delta T(I)$ of round insulated wire (FLRY-B, 2.5mm²) obtained from numerical calculation and approximated by polynomial function [1] 70
Fig. 22: Heating-up time characteristic of round insulated wire (FLRY-B, 2.5mm²) obtained from numerical calculation and approximated by a logarithmical function [1] 70
Fig. 23: Insulated single (a) and multi-wire conductor (b) [1] 72
Fig. 24: Transformation of insulated round conductors (a) into squares of the same area (b) [1] 72
Fig. 25: Determination of the mixed area conductivity: (a) assembly, (b) circuitry [1] 72
Fig. 26: Experimental versus theoretical results of the wire bundle (environment temperature = 23ºC) [1] 73
Fig. 27: Discretisation: a) discrete grid showing how neighbours out of the domain are removed, b) basic grid and the obtained discretisation of the computational domain [4] 74
Fig. 28: Experimental and computer simulation results for electro-wires with different numbers of wires, filling factors and heat conductivities of materials between the wires 76
Fig. 29: Schematic cross-section of a multi-wire cable and a single cable 78
Fig. 30: Single cable with solid interior conductor 81
Fig. 31: Geometrical model for the determination of the average heat conductivity 82
Fig. 32: Power balance of a combustion-engine car, as in equation (72) 90
Fig. 33: Power balance of an electric-driven car (ignoring regenerative braking) 91
Fig. 34: Comparison of temperature distributions for equally composed multi-wire bundles with different layouts 94
Fig. 35: Optimization strategy 95
Fig. 36: Initial template for the circle-packing algorithm used in [12] 96
Fig. 37: Diagram of the genetic algorithm 97
Fig. 38: Programmatic flowchart of the entire process of multi-wire cable optimization 98

Fig. 39: Temperature distributions in 33-wire bundles for: (a) inner layout; (b) outer layout; (c) opposed layout 99
Fig. 40: Improved cable configurations obtained by application of the genetic algorithm for 33 single cables. (a) best; (b) second best; (c) third best 99
Fig. 41: Equivalent thermal circuit for a short cable segment, with length *dz*, axial heat power $P(z,t)$ ... 100
Fig. 42: Simple behavioral model for a DC/DC converter and its efficiency with respect to its rated power, *Pnom* 100
Fig. 43: Different architectures 101
Fig. 44: Example of a system with 6 possible spaces for DC/DC converters 101
Fig. 45: Cost function over cross-section of wires from 1mm² to 100mm² 102
Fig. 46: Weight for DC/DC converters depending on the rated power 102
Fig. 47: Cost function of DC/DC converters with respect to their rated power 103
Fig. 48: Optimization process for cable cross-sections (A) regarding temperature (T) and voltage (U) .. 103
Fig. 49: Flow chart of the optimization process 104
Fig. 50: Different architectures of the first example of power supply system 104
Fig. 51: Different architectures of the second example of power supply system 105
Fig. 52: Installation spaces (K_{xx}) for the second example of power supply system 105
Fig. 53: Cable heating characteristic cloud of infinite cases, given min and max time constants and steady temperatures 109
Fig. 54: Thermal response of seven cases of cable segment 111
Fig. 55: Fuse-wire matching diagram - hypothetical wire optimization 119
Fig. 56: Potentially unprotected currents and times 121
Fig. 57: Example of parallel connection of loads to a shared fuse 122
Fig. 58: Experimental and simulated heating curves for bundle and free convection branch segments of one wire 123
Fig. 59: Experimental and simulated heating curves for bundle and free convection branch segments of two wires 124
Fig. 60: Different types of branch segments of a wiring harness with different thermal behaviors 125
Fig. 61: Cross-section view of the listed types of segments 126
Fig. 62: High resolution versus the finally chosen resolution for the FEM mesh 131
Fig. 63: Effects of variations of the time step in the transient, near $t = 0$ 131
Fig. 64: Effects of variations of the time step 132
Fig. 65: Measured results and simulations of multiple cases of wire bundles 132
Fig. 66: Experimental and simulated heating curves for bundle and free convection branch segments of one wire 133
Fig. 67: Experimental and simulated heating curves for bundle and free convection branch segments of two wires (12A) 134
Fig. 68: Experimental and simulated heating curves for bundle and free convection branch segments of two wires (24A) 135
Fig. 69. Overview of the COMSOL project for comparing FEM results 136
Fig. 70. List of global definitions showing parameters, variables, analytic formulas and look-up tables 137
Fig. 71. Definition of the global parameters 137
Fig. 72. Definition of the global variables 138
Fig. 73. Definition of variables for copper + air 138
Fig. 74. Structure of the geometry description 138
Fig. 75. Caption of the geometry description in Fig. 74 139
Fig. 76. Definition of the polyvinylchloride material 139
Fig. 77. Definition of the mixed air and copper material, depending on the β parameter 140
Fig. 78. Structure of the heat transfer definition of the 0.35mm² wire 140

Fig. 79. Caption of the mesh definition of the wire 140
Fig. 80. Position of the temperature probe 141
Fig. 81. Results of the transient simulation showing maximum temperature of the polyvinylchloride insulator of the wire 141
Fig. 82. Results of simulation of a 0.35mm² wire made with the FEM simulator described in section 6.3 142
Fig. 83: Diagram of the proposed optimization method 143
Fig. 84. Ideal cylindrical conductor exposed to air, with uniform current density J 147
Fig. 85. Center temperature of a conductive cylinder with uniform current density and cross-section A 147
Fig. 86. Maximum area of a cylindrical conductor set to current density J 148
Fig. 87. Minimum cross-sectional area of a cylindrical conductor subjected to a current I and uniform current density. Smaller areas would produce temperatures above T_{max} 148
Fig. 88. Maximum current for a cylindrical conductor with cross-sectional area A. Greater currents would produce temperatures above the maximum acceptable value 148
Fig. 89. a. Bundle geometry decomposition b. Mesh detail 149
Fig. 90. Experimental results vs. FEM simulation of a single wire 149
Fig. 91. Experimental results vs. FEM simulation of a wire bundle 150
Fig. 92. Diagram of the factorial experiment, where a is the cross section of the conductors, n is the number of wires and T_{amb} is the ambient temperature. 150
Fig. 93. Response surface: minimum area of the bundle versus its sum of currents and different ambient temperatures 151
Fig. 94. Response surface: maximum current of the bundle versus its sum of cross-sections and different ambient temperatures 151
Fig. 95. Comparison of the computation times of 200 optimization cases using the three different methods 157
Fig. 96. Relative difference in total area of copper in the bundle compared to the linear method, calculated for 200 cases 157
Fig. 97. Probability density function fit of the maximum temperature and their mean values 157
Fig. 98. Temperature evolution measured in three different points of a bundle dimensioned via the custom method with area criterion 157
Fig. 99. Detail of an ultrasonic splice between two wires 163
Fig. 100. Short circuit under study composed by series-connected wires 163
Fig. 101. Electric equivalent circuit for thermal fuse model 165
Fig. 102. Results of curve fitting to determine R for a commercial fuse 166
Fig. 103. Scheme of the finite volumes used for the wire heating model 167
Fig. 104. Equivalent thermal circuit of the finite volume scheme 168
Fig. 105. Radial temperature distribution of wires 169
Fig. 106. Experimental validation of a short circuit (one wire) a. Experimental versus simulated short-circuit current b. Experimental (thick solid line) versus simulated (thin and dashed lines) temperatures of the wire 174
Fig. 107. Experimental validation of a short circuit (three wires) a. Experimental versus simulated short-circuit current b. Experimental (thick solid line) versus simulated (thin and dashed lines) temperatures of the wires 175
Fig. 108. Short circuit current for different cross-sections of two series-connected wires of equal lengths 176
Fig. 109. Maximum reached temperature along two wires of equal lengths after the short circuit, for different cross-sections a_1 and a_2 177
Fig. 110. Cost function seen as plane of two variables, representing different cross-sections of two series-connected wires with equal lengths and mixes 178

Fig. 111. Feasible (green) and unfeasible (red) combinations of cross-sections a1 and a2 according to the minimum short circuit current constraint 179
Fig. 112. Constraint boundary of the minimum short circuit current for three variable cross-sections. Values of [a_1, a_2, a_3] below the surface are unfeasible solutions and vice versa 180
Fig. 113. Evaluation of four different standard values of cross sections around the found floating optimum (blue point): only one combination of standard cross section is feasible (check) and the other three are unfeasible (cross) 181
Fig. 114. Evaluation of four different standard values of cross sections around the found floating optimum (blue point), for dissimilar mixes: the standard optimum is encircled 182
Fig. 115. Results of optimization for one wire. The active constraint is the short circuit current 183
Fig. 116. Results of optimization for one wire. The active constraint is the wire temperature. 184
Fig. 117. Results of optimization for two wires. The active constraint is the short circuit current 184
Fig. 118. Results of optimization for two wires. Better angle to see the gradient vector and its perpendicularity to the boundary 185
Fig. 119. Results of optimization for three wires, showing the short circuit boundary, the optimum and the gradient vector 185
Fig. 120. Results of optimization for three wires. The tangency of the plane defined by the gradient vector (red) with respect to the short circuit current boundary indicates that the optimum is correct 186
Fig. 121. Test points of the tangent plane of a 2-wire problem. These two points propagate outwards checking for compatible solutions in the optimality test algorithm 188
Fig. 122. Test points of the tangent plane of a 3-wire problem. These eight points propagate outwards checking for compatible solutions in the optimality test algorithm 188
Fig. 123. Entire network optimization flux diagram 190
Fig. 124. Concept of optimization tool for wiring harnesses 192
Fig. 125. Scope of the KBL data container within the harness design process 194
Fig. 126. Prototype process of optimization using the *QT* file 196

List of tables

Table 1: Characteristics of the different wiring approaches 32
Table 2: Example of modules of the airbag family 34
Table 3: Presence matrix of airbag functions 34
Table 4: Computational results for different values of *N* 76
Table 5: Comparison of measured and computed temperature differences in Kelvin (EXP = Measurement, FE = Finite elements approach, FP = Fixed-point approach 85
Table 6: Relative error of simulations compared to measurements 85
Table 7. Optimization results (FEM) – Coldest 158
Table 8. Optimization results (FEM) – Warmest 158
Table 9. Experimental bundle setup 159
Table 10. Example of the list of harnesses in the *QT* file 197
Table 11. Example of the battery information in the *QT* file 197
Table 12. Example of the location master table in the *QT* file 198
Table 13. Example of the wires-segment table in the *QT* file 199
Table 14. Example of the segments-junctions table in the *QT* file 199
Table 15. Example of the *junctions* table in the *QT* file 199
Table 16. Example of the *modules* table in the *QT* file 200
Table 17. Example of the *device pin-out* table in the *QT* file 200
Table 18. Example of the pin master table in the *QT* file 201
Table 19. Example of the couplings table in the *QT* file 201
Table 20. Example of the fuse box pin-out table in the *QT* file 201
Table 21. Example of a fuse box modularity table in the *QT* file 202

A Oriol Bergadà

1. Introduction

1.1. The need for a weight reduction of the vehicle wiring

For the first time in 2009, the EU introduced mandatory passenger cars CO_2 standards. Currently, a target value of 95g/km of CO_2 is set for the new car fleet in 2020. In order to accomplish this regulation, the goal of the automotive industry is to reduce the weight of the wiring systems along with every component of their vehicles in order to lower their fuel consumption and CO_2 emissions. In addition, if the weight reduction of the wiring system is performed by means of a smaller amount of conductor metal, it will also involve a reduction of manufacturing costs.

The weight reduction of the on-board power supply network is a challenging objective, since electric components in road vehicles have slowly gained importance throughout decades [1]. Nowadays, they have become a large percentage of the manufacturing costs, just as the wiring system has become more and more heavy, complex and expensive [2]. E.g., medium range cars can already have more than 3km of wires with a total mass above 50kg.

A potential of weight reduction is suspected to exist, to the extent to which the regulations regarding the dimensioning process for automotive wiring are similar to those written for stationary applications [3], such as power distribution lines. However, stationary and automotive applications differ in some aspects. Their first difference lies in the lengths of wires, which are considerably smaller for the latter [1]. This allows wires in road vehicle applications to have greater current densities [4]. Secondly, the fact that cables are generally shorter places their temperature as the most constraining parameter, more than the voltage drop. The voltage drop must be always validated, but the temperature is generally the limiting factor to dimension an automotive cable.

The weight reduction may be performed by means of empirical techniques, but the complexity of the on-board networks is so high, that it cannot be carried out within an affordable time. Likewise, simulations may not be useful if an engineer must initialize each simulation, wire-by-wire, case-by-case. Even though simulations and models may be a good alternative to experimentation, the attempts to institute the simulation-based optimization [5] of the entire wiring system have been difficult, for reasons that will be discussed along this document.

1.2. Weight reduction strategies

As previously explained, lightening the wiring system of the car is one of the goals of weight reduction of medium passenger cars in order to achieve the required reduction of CO_2 emissions in the next years. For this purpose, various strategies can be carried out, yet all of them must be economically measured in such a way that the cost of the weight reduction strategy does not exceed its profit. This is needed to achieve success in a research project, as well as a balance between excellence and affordability, which is precisely the motivation of research in industry.

In this section, different approaches of weight reduction of the wiring system of a vehicle are going to be summarized. Some of them are not profitable regarding costs, but some other can bring both the reduction of CO_2 emissions and manufacturing costs, which makes them appealing for the car industry.

It is remarkable that the following strategies are compatible amongst them; they are based on improving independent parameters of the wiring system. None of the described strategies disables using any of the rest. On the contrary, all of them might be applied at the same time in an inclusive way, yet they would be redundant in some cases.

Despite a description of different optimization strategies is given below, this research is only related to one of them: the cable thermal simulation. Regardless of which technique is used to reduce the weight of the wiring system, the dimensions of the cable always affect the temperature and the voltage drop of the cable. Therefore, it is necessary to assure a correct temperature of the wire in any case. Since the voltage drop is much easier to calculate, especially in DC applications such as automotive, the prediction of temperature stays as the most important and complex aspect of the wire dimensioning process.

Moreover, the cable thermal simulation might be one of the most appealing approaches, capable of reducing weight and manufacturing costs at the same time. After the introduction of the other strategies, this document will only address topics or aspects related directly or indirectly to the cable thermal modeling and simulation.

1.2.1. Cable thermal simulation

Many methods can be applied to reduce the weight of the wiring system. However, all of the methods need a temperature validation. The capability of predicting the heating characteristics of wires composing the on-board supply network is crucial for weight optimization, as well as for assuring reliability. That is why the method of assisting the dimensioning process with simulations or models is chosen in this dissertation. In the following, an introduction to the strategy is given, yet the state-of-the-art chapter of this dissertation addresses the topic completely.

The complexity of the automotive wiring systems makes it unaffordable to use experimentation to validate manually all of the single wires in the car. In order to assure reliability, wires tend to be

oversized. If materials and topologies are kept while thinner cables are used, immediate profitability and CO_2 emissions reduction will be obtained.

The temperature of a wire is a constraint. It is actually derived from the most restrictive constraint regarding temperature, which is the integrity of the insulation. Cable standards demand cables in automotive systems to withstand a minimum amount of hours before losing its capability to isolate their inner conductor from the environment. In other terms, temperature produces the so-called ageing of the insulation.

Generally, cables are protected from ageing by assuring they do not exceed certain values of temperature, but it is not the only constraint when dimensioning a cable. The rest of restrictions must be observed with no exception. Nonetheless, it is usually the most restrictive constraint in automotive applications, since most of the wires are sufficiently short to consider the voltage drop a secondary constraint.

It is important to notice that the relation between the temperature and premature ageing of a cable is visible in the fact that the maximum acceptable temperature of a wire depends merely on its insulator material. Therefore, the constraint (maximum acceptable temperature) is a constant for all of the wires of the same type, and the variable of cross-section modifies their weight and heating characteristics. The loss of margin of this variable, which gets closer to its constraint (temperature towards its maximum acceptable value), forces to adopt measures in order ensure the variable does not exceed its restriction. In this case, the solution is either measuring the temperature empirically or using mathematical models and simulators.

Traditionally, tables of ampacity for cables have been useful, yet they are unable to consider several parameters affecting the thermal behavior of a cable, such as bundles wherein many cables conduct current at the same time. In stationary applications, rerating factors are used to adapt certain current-carrying capacities of cables to especial conditions. They are reliable ways of dimensioning cables, but they have been made in order to assure reliability in any case, which explains why the final dimensions of the cable are believed to be excessive in most of cases. The only way to address this matter is performing more accurate temperature predictions by considering as many parameters as possible with models and simulators.

As previously discussed, the accurate prediction of the heating behavior of a cable corresponds to reducing the margin between a variable and its restriction, in mathematical terms (temperature versus maximum acceptable temperature). Nevertheless, some approaches allowing a weight reduction consist of modifying the constraint itself or the thermal behavior of the cable; they are explained below.

1.2.2. New alloys for improved tensile strength of signal wires

Usually, the amount of current being carried by signal wires is so small that their theoretical and minimal cross-section would be very thin. This cross-section would be limited by a maximum acceptable resistance of the wire. However, when it comes to thin wires, mechanical requirements are often more important than the electrical. As a result, signal wires in automotive applications usually need to be thicker than how they would be according electrical restrictions.

Cable standards like ISO 8820 impose mechanical demands establishing what wires must withstand during the manufacturing process, workers' handling and assembly. In addition, they must resist the entire life of a car maintaining their integrity. For these reasons, wires must behave correctly when subjected to a list of mechanical tests that emulate the entire mechanical efforts along one real life cycle. It is then necessary to keep a minimum diameter of the conductor or to apply strengthening measures if it is desired to downsize the wire.

Some copper alloys such as CuAg, CuMg or CuSn can be used as the conductor material in order to obtain an improved tensile strength compared to simple copper. In addition, copper-clad steel allows a reduction of the wire cross-section as well as improving enormously –much more than those previously mentioned alloys– its maximum number of bending cycles before breaking. These alternative conductor materials let the manufacturers downsize the diameter of their wires from 0.35mm² to 0.13mm², which leads to a weight reduction around 55%, depending on the specific choice (according to Leoni).

Amongst others, USB, LVDS, Ethernet, IEEE 1394 (Firewire), APIX®, CAN (Controller Area Network) and MHL™ (Mobile High-Definition Link) are types of signals that can be found in a car network. Signal and data wires can easily stand for more than 20% of the total weight of the wiring set of a car.

1.2.3. Replacing copper by aluminum for lighter wires

Changing the material of the conductor is also the answer when the approach is to lower the weight of wires directly by reducing their material density. This could be the case of thick copper wires carrying large currents. In this case, the aim is to reduce the weight of the wiring system without reducing its current conduction capacity, unlike the previously mentioned need for reducing cross-sections of signal wires to the limit. It means that the temperature of the wire must be the same for the same currents. However, this can be only done if there is no restriction regarding the wire diameter.

The conductivity to weight ratio k / ρ (electrical conductivity divided by the density) determines the potential current capacity of a conductor material for a specific weight per unit length of wire. In a list of pure metals sorted by descending k / ρ, Lithium would be at the top, followed by Calcium and Magnesium. Nevertheless, in spite of their weight reduction potential, these metals are unsuitable for this purpose, due their chemical instability, their poor mechanical properties and their cost. Nonetheless, the

fourth place is for aluminum. One kilogram of aluminum can approximately replace two kilograms of copper, providing equal unit-length resistance.

The use of aluminum for power wires is not a novelty. In fact, during the mid-sixties into the mid-seventies copper reached a high price level, which made it cost-prohibitive for use in residential wiring. In fact, the price of aluminum and copper nowadays tend to diverge, making it more and more favorable to the latter. Nowadays it is also used in aircraft power wiring due to its weight advantages.

As early as in 1945, aluminum was approved for interior wiring purposes, providing it be properly installed. Almost all reported problems involved circuit connections wherein installers did not follow its installation guidelines.

The first and most evident reason for aluminum to be a challenging material is its lower conductivity as compared to Copper, which forces to use thicker wires in order to equal the unit length resistance of Copper wires. In second place, there is the fact that the surface of an aluminum conductor is immediately covered in a non-conducting oxide layer upon exposure to oxygen. This characteristic leads to an increase in the resistance between the aluminum conductors and metallic terminals of connectors, which can lead to overheating and, in the worst case, to fire. Normally, the exposed surface of the conductor must be scraped under special conditions and protected with alkali free grease immediately before the final connection.

Unlike with copper wires, galvanic corrosion does occur when aluminum is in contact with other metals and a drop of electrolyte (such as seawater) is in contact with their surface. A car wiring must withstand a long time of exposure to electrolytes, humid or wet areas, so that the combination of copper and aluminum would need an adequate insulation to prevent the junction from galvanic corrosion. Whereas metals such as Nickel or Copper have low and similar anodic indices, aluminum is reactive enough to produce a notable chemical reaction when combined with copper, brass or stainless steel in presence of electrolyte.

Stress relaxation and creep are also matters to be considered when using aluminum wires. The flow tendency in aluminum makes it necessary to tighten the terminal clamps in interior installations before start up and at a certain time after the first hours of use. For the automotive use, it is necessary to design robust and maintenance-free aluminum terminal systems. Moreover, the thermal expansion coefficient of aluminum is significantly higher than that of common metals used in devices, outlets, switches and screws. This implies that connections get progressively loose over time due to thermal loads, thus causing overheating.

Despite the disadvantages of aluminum, it is a feasible solution, and the increasing price of copper is leading automotive wire manufacturers to perform investments in this area.

1.2.4. Insulating material

The current-carrying capacity of a wire will be higher if the insulating material withstands higher temperatures. Loads could have thinner wires with higher temperatures by upgrading their insulation material to a higher temperature class. As a result, it is possible to use thinner wires with the same rated current.

Nevertheless, it is important to say that in many occasions, this strategy can be limited by the temperature resistance of the materials around the cable (e.g. the connectors).

1.2.5. Increasing battery voltage and multi-level voltage

Car manufacturers have decided to introduce an additional level of voltage (48V) in order to be able to supply powerful loads more efficiently. This change is an opportunity to apply an interesting electrical principle that allows a reduction of the mass of electric conductors: Keeping the powers constant, a variation of voltage involves an inversely proportional variation of current. Thus, changing the 12V supply voltage of some loads into 48V involves a theoretical and proportional reduction of the mass of copper, if the current density of all of the wires is kept unvaried.

The main reason of this change is the unprofitability of supplying all of the loads with one voltage level. It is cheaper to classify loads into different levels of voltages [6]. Of course, using larger voltages allows a reduction of all of the currents and thus a reduction of the overall weight of the wiring system, but not all of the loads can operate with the same voltage. It is necessary to use power converters to adapt the battery voltage to their needs, which increases the overall price.

1.2.6. Fuse distribution optimization

The simplest way to design a reliable wiring system is to have one fuse per one load. Because of the characteristics of fuses, their circuit-breaking capacity is dependent on their rated current: the higher rated current, the slower the fuse is. As a result, when loads share a fuse, their cables must be sometimes oversized in order to assure they will be protected in case of short-circuit.

Therefore, separating fuses for every load produces savings of copper. However, in many cases the cost of an additional fuse in contrast with the price of copper makes it more profitable to group electric loads under one fuse. This is especially visible when the power of the loads is low: the use of a higher number of fuses would entail a general wire size reduction, yet not implying a sufficient savings of copper to make these additional fuses profitable. Additionally, the use of many fuses entails a problem of space.

The VW75212 standard recommends using wire cross-sections large enough so that their fuses protect them under any circumstances. This way, the shared fuse prevents all the wires from short-circuit overheating with no kind of doubt. However, the fuse rating of a set of loads must be higher than the sum of their currents. This fact makes these parallel wires have a current capacity above their maximum

expected current. Wire ramifications after splices are probably going to be underexploited along the entire life cycle of the car, if one follows this recommendation.

1.2.7.Electronic fusing

The use of electronic fuses instead of conventional passive ones introduces many advantages for the electric distribution system, amongst which there is also the possibility of downsizing many wires. The cost of this technology makes it unprofitable for currently applications and targets, but it is a good solution, for example, for arcing when using higher battery voltages instead of 12V.

An electronic fuse might be used to avoid arcing with higher voltages, and then it will be controlled by certain software capable of detecting electric arcs. Therefore, the same software can be extended in order to control the fuse so that it can control the power of the load.

For some loads, the operation currents can be hard to predict, due to some variability factors ranging from the temperature of the battery and its voltage, to how the user handles the features of the car. The more uncertain is the maximum current, the larger the load factor applied to the fuse rating must be. All of the relevant values of current are taken from datasheets, but one must be careful because sometimes the conditions that component manufacturers use to assure values given in datasheets can be unaccomplished. If an engineer trusts certain values of maximum currents provided by a datasheet without any kind of margin, they run the risk of either finding actual currents exceeding the theoretical values, or never being reached.

In addition, passive fuses can experience nuisance trips if designers have not chosen the rated current of the fuse correctly. It is necessary to prevent the systems from nuisance trips, as well as from premature ageing. For this purpose of robustness, one must select fuses with a margin between the maximum expected operation current and their rated current. It is thus necessary to know the maximum operation current (I_0) and the overload current of a load and then apply a safety coefficient before choosing the fuse rated current, which depends on the load and is usually called the *load factor* (*LF*).

$$LF \cdot I_R \geq I_0 \tag{1}$$

After applying a load factor, a standard fuse must be selected, and its rated current (I_R) must be equal or larger than the maximum operation current of the load. This is going to add even an extra margin between the maximum operation current of the load and the rated current of the fuse. Probably, the wire is also going to have this margin because the short-circuit protection of the fuse can be the most limiting factor.

By contrast, electronic fusing with an embedded power control can soften inrush currents as well as, for example, stall currents for motors. These would entail a completely new way of dimensioning the wiring system of cars, in such a way that wires could have in general, smaller cross-sections.

Furthermore, electronic fuses do not need to be placed in a particular place of the car. They can rather be placed wherever the design of the wiring system demands. This is because the matter is about semiconductor devices that can be easily controlled, and nobody will need to replace them after they have blown. In addition, the temperature does not affect their characteristic, which allows for placing them in places that could have been originally unsuitable for passive fuse boxes.

All of the new possibilities would allow a complete fuse system optimization, as described in section 1.2.6 (for example, each load has one electronic fuse).

1.3. The complexity of customer-specific wiring harnesses

1.3.1. Introduction to the development of automotive electric distribution systems

The development of the electric distribution system is one of the most complex processes within the conception of a car, due to the large number of involved components and its enormous variety.

The starting point is the technical report of the product, which contains all of the conclusions obtained during the stage of pre-development of the vehicle. In the case of the wiring system, the most important conclusions are those regarding which specific equipment will be finally installed in the car. Once these functions are known, the architecture of the components is defined independently, system by system.

By means of this information, one can elaborate the electric schematics, which are merely indicating how components are interconnected. Nevertheless, and due to the large variety of equipment offered by European car manufacturers, it is necessary to define a robust relation between the selectable equipment of the car and its involved sets of components.

Once the electric schematics are complete, the next step is to extend the information of the electric schematics with data regarding palpable and non-electric parameters of the wiring system: wire types, connectors, fuses, etc. At this point, it is necessary to know the positions of all of the components in order to define the routing of the wiring system by means of CAD tools.

Lastly, engineers elaborate the assembly drawing, which describes the wiring system taking into account all of the different combinations of equipment. This drawing, with some adaptations, is the one that is finally used for the production of the wiring harnesses.

The entire process of design of the wiring harnesses will be explained in the following sections.

1.3.2. Functional systems and electric schematics

As it has been previously explained, the independent establishment of the architecture of each of the functional systems is the first step of the design of the wiring system.

A functional system can be defined as a set of components performing a specific function of the vehicle. For example, the lighting system is a functional system composed by the brake lights, the number plate lights, the fog lights, the headlights, the rear lamps, indicators, etc. The front passenger airbag is also an example, composed by the front airbag, the head airbag, the side airbag, the airbag disconnection switch, the indicator light, airbag control unit, etc.

It is remarkable that some components belong to more than one functional system. This occurs when an electric component carries out more than one function, which is the case of the wheel rotational speed sensor: this component provides information to both the ABS and the navigation systems. Since they are

separated functional systems, the rotational speed sensor of the wheels is a component belonging to two systems.

The information of the connections between all of the components belonging one functional family is contained in the electric schematics. Additionally, the schematics must include some important data of the wires and the connectors, such as the identification of twisted pairs or the conductor metal of the terminals of the connectors (gold, silver, tin…).

1.3.3. Different wiring system approaches

The use of wiring harnesses is a way of gathering a set of elements (wires, connectors, protections, fasteners, etc.) into a single part of the car. A harness thus becomes a part that will be assembled at a certain point of the assembly line, just like any other part of the vehicle.

Therefore, the definition of the assembly line affects the definition of the wiring harness. For example, doors in cars are mounted when they are completely assembled, which forces their internal wires to be already installed when the door is finally mounted on the car. It is thus necessary to design a separated wiring harness for the doors. In other terms, the wiring system of the car must have cut-off points with which the main harness is connected to the auxiliary wiring harnesses of the doors, instead of being a one-piece wiring harness. Besides, there are some other factors forcing the division of the wiring system into smaller wiring harnesses, such as the impossibility of handling some wiring harnesses on account of their size.

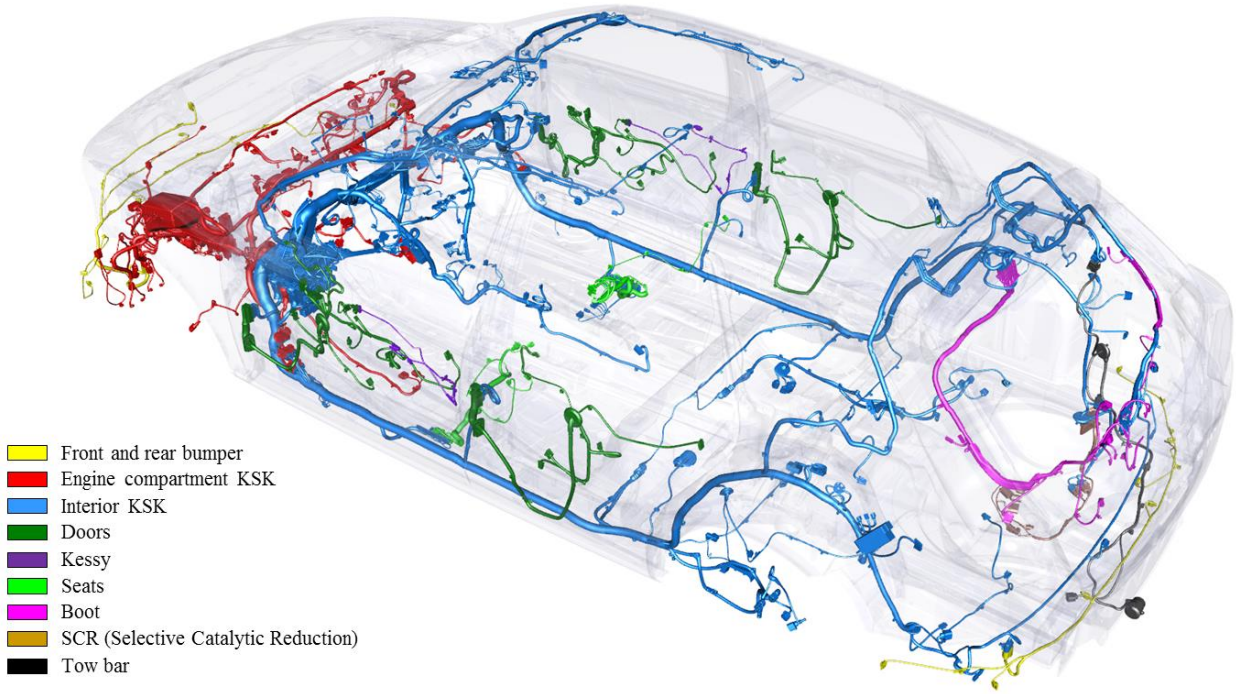

Fig. 1: Overall view of the wiring system

Fig. 1 shows the different wiring harnesses composing the wiring system of a car. One can distinguish between the main wiring harness (interior and engine KSK's) and the auxiliary ones. These two wiring harnesses are called KSK, which stands for ***k****undens****p****ezifischer* ***K****abelstrang* (German for customer-specific wiring harness). This concept will be explained later in this section.

The main wiring harness includes most of the functions of the vehicle, whereas the auxiliary harnesses gather a smaller number of functions due to their size. Both types must be manufactured in such a way that they be able to meet all of the desired varieties of equipment.

First, one must distinguish two different approaches as regards the desired variety for the market. For the Asiatic and American market, a lower number of variants are offered, whereas the European market offers much more variants for each car model.

Amongst car manufacturers offering a high level of variability, there are two contrary trends:

a) Grouping as many functions as possible in the main wiring harness

b) Dividing the wiring system into smaller wiring harnesses

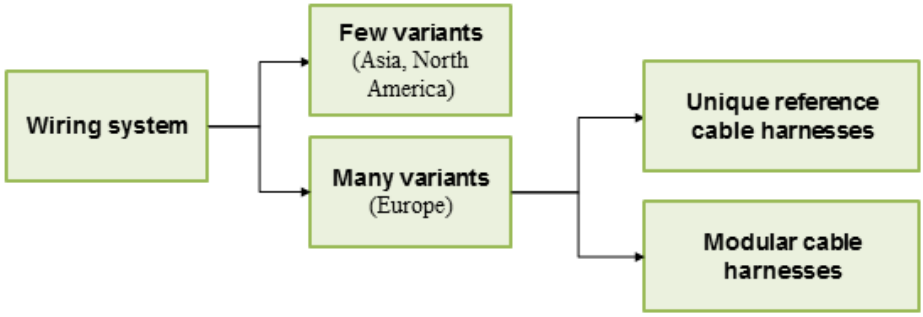

Fig. 2: Classification of different wiring approaches

The wiring systems with a low number of variants is designed independently for each grade of equipment, i.e., for each available configuration of the car. This is only possible when the car is only sold with a few different sets of equipment, for example "basic", "standard" and "premium".

The advantage of this approach is a minimized complexity of industrialization and logistical processing, due to the small variety. This reduced complexity involves also a reduction of costs in other areas. One more advantage is that its assembly results simpler for the workers in the assembly line.

Besides the limited availability of combinations of features, this system sometimes brings some disadvantages. The need for subdividing the electric distribution system into some smaller wiring harnesses might not be avoided by the reduction of variety. Then, some of these designed wiring harnesses might be shared in some different configurations of the car, which would force to dimension the wiring system so that the different wiring harnesses are compatible between them. As a result, in least

equipped cars, some wires or other components would be installed but not needed, which is a waste of material.

The wiring systems with a large number of variants are industrialized in two ways according Fig. 2. Functions can be combined either by subdividing the wiring system into many harnesses or by assembling customer-specific wiring harnesses. They are respectively called *unique reference* and *modular* wiring systems.

1.3.3.1. *Unique reference wiring systems*

The unique-reference wiring system approach consists of dividing the wiring system into several smaller harnesses, so that each of them comprehends a relatively small number of variants. This approach enables a specific reference number to be associated to every variety of wiring harness, thus facilitating the spare parts logistics when the wiring harness needs to be replaced.

Its main drawback is the higher complexity of assembly. Workers in the assembly lines must manage different wiring harnesses as well as plugging their connectors between them. Furthermore, this approach implies a high number of connections among harnesses. Since a connection implies two connectors and two wires, this approach brings a multiplied number of quality problems in comparison with other approaches.

1.3.3.2. *Modular wiring systems*

The modular wiring systems approach consists of grouping all of the variants in rather big-sized wiring harnesses. The number of harnesses defining the entire electric distribution system is smaller than compared to the other wiring approaches. This is the strategy followed by the Volkswagen Group.

Each installed selectable component of the car is related to its so-called *module*, and the wiring harness is defined by a combination of these *modules*. The modules of a family are oriented to the customers as packs of functions they can select, so that just one module can be selected for one functional family.

Still, when many functional families are supplied by a shared wiring harness, it entails that there are as many configurations of this harness, as combinations of modules of all of the functional families.

This approach brings the advantage of allowing a large variety of features, because the wiring system supports all of the possible combinations of modules. This has a positive effect on the manufacturing costs of the wiring harness, because each harness is going to have only the necessary parts and dimensions for its modules, unlike the prior approaches.

Nevertheless, this approach brings a great complexity for development, industrialization and logistics, and complicates the spare parts management system, because each wiring harness is customized for the

customer according their selection of equipment. Table 1 sets a comparison between the different discussed approaches of vehicle wiring.

Aspect	Few variants	Unique reference wiring	Modular wiring
Number of combinations	~10^2	~10^5	~10^{10}
Complexity of industrialization and logistics	Low	High	Very high
Costs of industrialization and logistics	Low	High	Very high
Unit cost of parts	High	High	Low
Complexity of development	Low	High	Very high
Complexity of assembly	Low	High	Low
Pre-allocated elements	~5%	Up to ~3%	0
Complexity of the spare parts management	Low	High	Low

Table 1: Characteristics of the different wiring approaches

The modular wiring includes always a *basic* module, which lacks any alternative. All of the wiring harnesses of the same type (e.g. doors of the same car model) share their basic module regardless of the equipment of the car. For example, in many car models, the basic module of the doors consists of the speaker set. On the contrary, the *variable modules* can be chosen from a list, so the final installed module depends on the selection of the customer. Using the same example, some of the wiring harnesses will include wires for the electric side mirrors, and some others will not. The same occurs with heated side mirrors.

At the same time, there are *optional* and *obligatory* functional families. The basic module is fixed, but variable modules can be either active or inactive. Both of them belong to the variable group, but they differ because in the obligatory families exactly one module from each must be mandatorily chosen, while in optional functional families one can dispense with selecting any module. Summarizing:

Basic module:

- No available selections
- It is present in all of the manufactured instances of the car model

Variable modules:

a) Obligatory functional families
   - Exactly one module **must** be selected

b) Optional functional families

- One module **can** be selected
- The absence of selected modules is also allowed

Therefore, a wiring harness will be necessarily defined by the basic module and one module of each of the obligatory functional families. Moreover, it will also include modules of some of the optional functional families. This modular structure can be exemplified with an office desktop, where one can have different types of tables, computers and the options of one additional screen and a telephone on the desktop:

"Office desktop"
Basic module:
- Table board

Variable modules:

a) Obligatory functional families:
   - Table legs
     - 4 plastic legs
     - 6 plastic legs
     - 4 metal legs
     - 6 metal legs
   - Computer
     - Laptop
     - PC

b) Optional functional families:
   - Additional screen
     - 1600x900 screen
     - 1920x1200 screen
   - Telephone
     - Telephone (land line)

Now returning to cars, let us consider the functional family called "fog lights". Considering a car with two different designs of front bumper (*standard* and *sport*), the wires of the fog lights are going to have different routes depending on the selection, because the position of the fog lights depends on the physical shape of the front bumper. Therefore, there should be at least two modules for the fog lights.

In the latter example, two variants of the same function were forming two modules, and they were not shared, which defines a particular case of functional family. However, functional families can have modules sharing functions. Let the airbag family be considered as an example of this. Consider a basic airbag system composed by the driver's airbag. One can add a side airbag, and this selection can be optionally extended by including a head airbag as well. Additionally, one can choose whether the passenger airbag can be deactivated with a switch. In summary, there are six possible modules for the *airbag family* as in Table 2, which is enough to understand modules in the same functional family cannot be combined, because it would entail duplicating functions.

Airbag family	Description
Module 1	Basic airbag
Module 2	Basic airbag + Side
Module 3	Basic airbag + Passenger disconnection
Module 4	Basic airbag + Side + Passenger disconnection
Module 5	Basic airbag + Side + Head
Module 6	Basic airbag + Side + Head + Passenger disconnection

Table 2: Example of modules of the airbag family

Whereas only one module can be selected for a functional family, functions such as "side airbag" can be shared among modules. In this way, it is possible to build a *presence matrix* (Table 3), so that all of the functions are listed separately. The belonging of each function to each module is expressed in this table as an answer to the question: *is the function* f *included in module* m*?*

The actual definition of the modules as in Table 2 cannot be visualized in any of the electric schematics used in the wiring development process. Instead, all of the components have their information of presence in the different modules, as in Table 3.

Airbag family	Module 1	Module 2	Module 3	Module 4	Module 5	Module 6
Basic airbag	✓	✓	✓	✓	✓	✓
Side airbag	✗	✓	✗	✓	✓	✓
Passenger disconnection	✗	✗	✓	✓	✗	✓
Head airbag	✗	✗	✗	✗	✓	✓

Table 3: Presence matrix of airbag functions

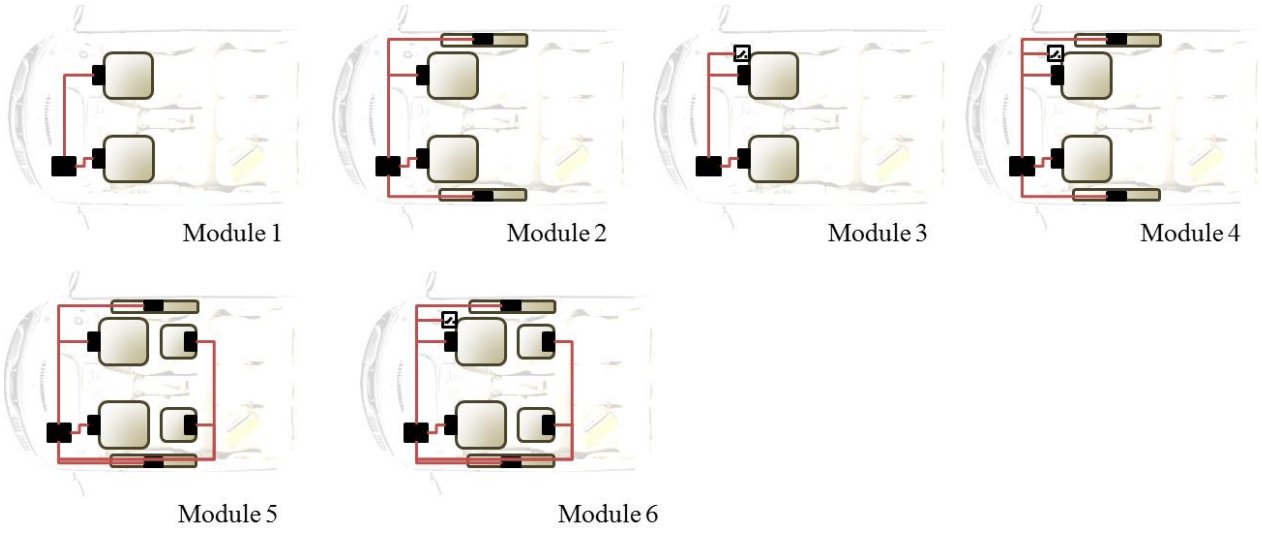

Fig. 3: Example of modules of the airbag family

The distinction between obligatory and optional functional families is useful to translate the demands of variety of the car into industrialized wiring harnesses. The wiring harnesses are assembled on special platforms, starting from wires and components belonging to the basic module. The variable modules are assembled in separated platforms, and they are later coupled to the basic wiring harness, until the customer-specific wiring harness is complete.

1.3.4. Wiring schematics

The electric schematics lack information about the size, the color, and any other non-electric parameters of the wiring. This information is provided by the wiring schematics.

The scope of this schematic is often between an electric schematic and an assembly drawing. For its definition, one starts with the electric schematics of all of the functional systems. The components, already included in the electric schematics, are directly imported. Afterwards, all of the wire cross-sections and colors of the wires are assigned. The components to which one or more connectors are associated are given a connector depending on the involved wires, and on the size, color, and other parameters of the connector. The equipotential *splices* are also established, which are the soldering points between wires.

Besides the mentioned information, the wiring schematics also include all of the relevant data such as the characteristics of the wires and the contacts. For instance, a wire can be related to a twisted pair, or it might be a shielded wire. With respect to contacts, their material is also specified (tin-plated, gold-plated…).

During the definition of the wiring schematics, the electrical protections (fuses) of the electric distribution system are also defined. Fuses are designed to protect the wiring system in case of overcurrent, and they are all placed in fuse boxes.

A very important property of the wiring schematics is the fact that it contains all of the possible variants of connections that can be found due to the variety of equipment. It depicts all of the combinations in a unique schematic. This is achieved, as it has been previously discussed, by associating the presence of each component to modules, as in Table 3. Thus, for a specific combination of modules, a particular interpretation of the wiring schematic will be obtained.

1.3.5. Wire routing definition

The physical implementation of the wires inside the vehicle takes place within the routing definition. At this stage, all of the prior information is needed, as well as the location of the components, which is defined by the *package* of the car. This routing definition is carried out by means of 3D graphic representation software tools allowing the DMU (Digital Mock-up) of the car (Fig. 4).

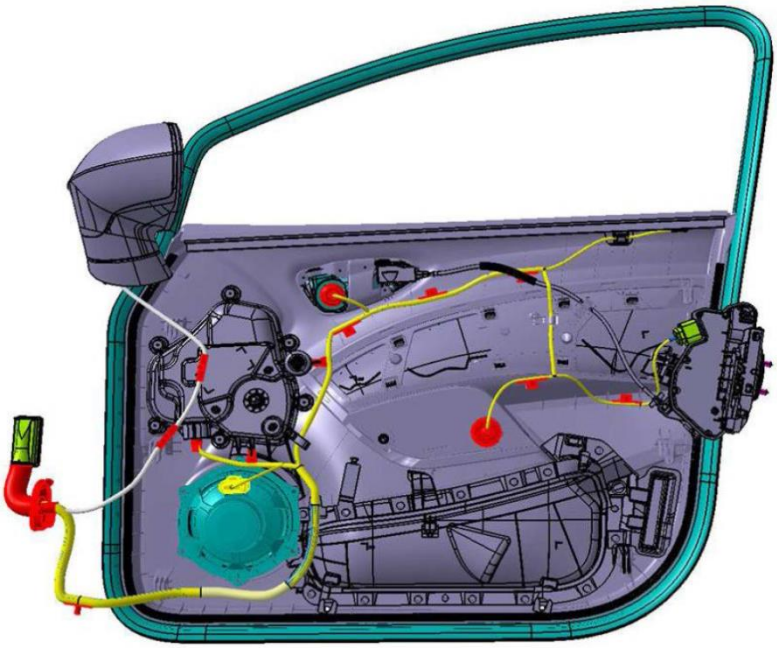

Fig. 4: Example of routing definition of the driver's door

The routing definition does not work with single wires, but with the bundle branches of the harnesses containing a certain number of wires [2]. These bundles are joined with tape, as well as other protection or driving elements. The thickness and the maximum curvature of every branch segment are defined by the wires it contains, although at this stage the CAD tool does not include this information. Their position, orientation and type of fasteners, as well as their amount are defined by the three-dimensional structure of the car. The ease for placing fasteners and the possibility of including holes for clamps are important aspects during the design of the bodywork of the car.

The routing definition uses the highest number of components and bundle branches. This case comprehends any of the other possibilities of wiring system with less equipment.

If different modules imply different locations of the components and thus different routes, all of the possible routes must be defined. During the routing process, some modifications of the bodywork are likely to be necessary.

The result of the routing definition contains also all of the protection elements of the harnesses. Depending on the surroundings of the wires, different types of protection are used. For example, near the sharp edge of a steel plate, where there is a risk of breaking, abrasion-resistant protections are used. On the contrary, when such risks do not exist, a spiral wrapping is applied, just to keep wires forming a bundle.

1.3.6. The assembly drawings

The assembly drawing is a 2D arrangement of the routing, which also includes all of the information of the wiring system. Again, this drawing contains all of the possible combinations of modules, as well as all of the necessary information for the manufacture of the wiring harness. Like any other part drawing, it is delivered in paper format to the wiring harness manufacturer.

At this stage, some rules are added so that the obtained circuit is consistent. Some of these rules are:

- Electric coupling from the limits of the wiring harness to the connectors
- Close the electric circuit formed by the harness
- Wires continuity at *nodes* (points where a bundle branch bifurcate into two branches)

This geometrical representation with electrical consistency joins the electrical data of the electric schematics, which involves the following topics:

- Identification of the connectors
- Properties of each module (name of the modules, identification number of the wires, weight of each module, etc.)
- Selection of one module and one reference for each component
- Definition of parts of the harness that come already mounted with the part

The assembly drawing provides the following essential information:

- Physical description of the wiring harness: lengths of the bundle branch segments, positions of all of the components and splices, type of wrappings for each branch, etc.
- Wire list: reference number of each wire and modules to which it belongs
- Component list: reference number of each component and modules to which it belongs

Besides, the assembly drawing includes further information such as standards, modifications, detailed views of some components, etc.

One single drawing is sufficient to interpret all of the possible combinations of modules for a given harness. The use of the modular reference enormously eases tasks of modification, since they affect only to one drawing.

1.4. The problem of the temperature prediction and the need for reliability

The prior explained complexity of the wiring system entails a great problem when it comes to perform predictions of temperature of one or more of its wires.

First, the tree shape of a harness and the fact that cables belong to different segments of the harness with different bundle compositions and packing systems, produces several different thermal environments for a wire, along its length. A complete thermal characterization of the cable must consider all of the thermal parameters along the entire cable.

In order to overcome this problem, the worst case is used. Generally, it is assumed that a cable surrounded by air is a fairly worst case of heat dissipation [7]. However, when many cables are near to each other and conducting current simultaneously, this is a worse situation. As one can easily understand, the ease to find a worse case than the single cable surrounded by air reveals a certain lack of reliability within the assumption. In other terms, one cannot rely on this model because it is easy to find hot spots whose temperature will not be predicted by the model.

Exactly for that reason, the automotive wiring regulations demand that the wiring system be validated by experimentation, in order to avoid unexpected and excessively high temperatures. The behavior of the single cable surrounded by air is already described by regulations with respect to the ambient temperature. Therefore, simulating the same case is not useful in many cases, because, at the end of the day, an experiment must be carried out to prevent hot spots. Performing one experiment for each of the current-carrying wires takes certainly too much time, due to the tremendous complexity of the modular wiring systems.

Moreover, reliability can only be assured if all of the modular combinations are checked: the immediate surroundings of a cable depend on the modular combination (i.e. which cables are near to a certain observed cable). This makes even more unaffordable to program simulations manually cable-by-cable, or even worse, to measure their temperature experimentally.

Assuring reliability implies especially preventing damages produced by electrical faults. The need for assuring safety in case of overloads or short-circuits is one more reason why nowadays most of the cables are oversized. The cable cross-section must match its corresponding fuse, which must be able to prevent the cable from overheating in case of short-circuit. This is directly related to the necessary time for the fuse to break the circuit. Among other considerations, fuses must be selected considering the sum of currents of all of the loads they protect. For this reason, squeezing cables can cause the loss of their protection, which is produced when there is a short circuit and the fuse melts too late. In this case, the cable has exceeded the maximum acceptable temperature due to the short-circuit current.

Based on this, standards like ISO 8820 or VW74212 detail how to select cross-sections for cables protected by automotive melting fuses, but this is not generally considered by simulators suggesting optimized cable sizes. Since it is desired to use thinner cables in the automotive wiring systems without compromising their reliability, simulators will not be useful unless they provide a solution based on both the weight reduction and the safety concept, in such a way that no subsequent experiments are needed.

1.5. Single-wire wire parameters and definitions

1.5.1. Maximum permissible conductor temperatures

Every single wire in the car must be given a specific cross-section, which must be chosen in consideration of the power of the load and some thermal parameters of its environment. In this section, the most basic parameters and definitions used for this purpose are going to be explained.

High temperatures can be produced by an external source such as the exhaust pipe, but normally the temperature rise is due to the Joule effect inside the cable. Thus, a certain current density produces a certain temperature, and a certain temperature produces a certain degradation rate of the polymer. In the end, engineers must consider the relation between current and temperature, because the degradation of the polymer is hard to predict.

A cable must withstand a certain life cycle. In automotive applications, it is desired that all of the cables live as long as the car wherein they have been installed. Different types of degradation have been observed and standards have been written, so that complying cables withstand all of them as long as demanded.

Polymers deteriorate through chemical reactions such as the anaerobic thermal decomposition (or thermolysis) and the thermo-oxidative ageing. The molecular structure of the material changes along time due to these reactions, and it can be measured. These differences produce changes in the material characteristics, being the most relevant the mechanical characteristics. In the case of cables, a maximum degradation level is defined, so that the properties of the material are at a critical point.

Temperature affects the reaction rates increasingly. Therefore, the higher the temperature, the faster the degradation. The rates of the different degradation reactions are not linear with respect to temperature, and they can be dependent on the stage of the reaction (i.e. the concentration of product molecules).

Predicting slow and sensible chemical reactions such as the mentioned thermal degradation is complex. In order to simplify this task, regulations demand the definition of three temperatures related to three degradation rates and periods defining mean degradation rates.

If the maximum temperatures are not exceeded, then the maximum rates will neither be. Facing a certain uncertainty, it is a good solution to demand that these temperatures are never exceeded, so that the maximum degradation rates are neither exceeded. The selection of the correct wire cross-section must assure this latter demand.

Accordingly, the endurance of the wire insulator is defined by its long-term, short-term and thermal overload temperatures (ISO 8820):

- T_{LT} Long-term temperature: Wires withstand this temperature or less for 3,000 hours.
- T_{ST} Short-term temperature: Wires withstand between T_{LT} and this temperature for 240 hours.
- T_{OL} Thermal overload temp.: Wires withstand between T_{ST} and this temperature for 6 hours.

If the wire is held above these temperatures and times, the integrity of the wire insulator cannot be assured. In order to have a better idea of these times, let us imagine a period of 10 years. Then, 3,000 hours stand for an average use of 50 minutes per day; 240 hours stand for 4 minutes per day; and 6 hours are only 6 seconds per day (or 3 minutes per month).

Albeit, just as discussed, these are mean degradation rates. The degradation level is the integral of the degradation rate along time. Then, since the instantaneous value of degradation rate is unknown, the degradation level cannot be estimated. For example, it is unclear how long the cable will last after being 1,500 hours under the long-term temperature and 5 hours between the short-term and the thermal overload temperature.

Therefore, the strategy is never to exceed the long-term temperature. The opposite is undesirable, because if the temperature exceeds the long-term temperature, the degradation level of the polymer will be unclear. Standards tolerate cases when cables exceed the long-term temperature, but just in rare cases related to faults, in such a way that the increase of the degradation rate does not affect substantially the degradation level of the cable.

1.5.2. Simplified equations used in standards

The following simplified equations are used to calculate the steady temperature rise of wires caused by a current conduction. ISO 8820 standard considers these approximations sufficient for automotive wire dimensioning. Nonetheless, it warns the reader about the possibility of differing results when the ambient temperature deviates heavily from the temperatures at which experiments have been carried out in order to write this standard.

$$\Delta T(I) = aI + bI^2 \tag{2}$$

Equation (2) describes the temperature rise, ΔT, in Celsius or Kelvin, expressed as the difference between the wire temperature and the ambient temperature in steady state. I is the current flowing to the conductor, in Amperes. a is the linear current dependence of the conductor heating in steady state ($\mathrm{K} \cdot \mathrm{A}^{-1}$). b is the quadratic current dependence coefficient ($\mathrm{K} \cdot \mathrm{A}^{-2}$).

$$\Delta T(t) = \Delta T_{max} \cdot \left(1 - e^{-\frac{t}{\tau}}\right) \tag{3}$$

$$\Delta T_{max} = \Delta T(I) \tag{4}$$

Equation (3) describes the first order response of the temperature rise, with a maximum value of ΔT_{max} and a time constant τ (seconds). ΔT_{max} is used instead of $\Delta T(I)$ from equation (2) in order to remark that equation (3) works only with a constant value of current, since it is the step response of the wire temperature, assuming perfect first order behavior.

The conductor resistance depends on its temperature. This is one of the factors breaking the ideal first order behavior of this system, because the Joule power of a constant current is not constant. Instead, the Joule power increases as the temperature rises. The relation between the temperature and the wire resistance can be used as equation (5).

$$\frac{dR}{dL}(T) = \frac{\rho(T)}{A} = \frac{\rho_{T_0}}{A} \cdot \left[1 + \alpha_\rho (T - T_0) + \beta_\rho (T - T_0)^2\right] \quad \left(\frac{\Omega}{m}\right) \tag{5}$$

Where $\frac{dR}{dL}(T)$ is the resistance per unit length ($\Omega \mathrm{m}^{-1}$) of the conductor material at a temperature T. $\rho(T)$ is the resistivity of the conductor material (Ωm), and ρ_{T_0} is the resistivity of the conductor material at a reference temperature T_0, in such a way that $\rho(T_0) = \rho_{T_0}$. A is the wire cross-section (m²). Note that this parameter is usually given in mm², but units must be consistent, and then m² must be used if the calculation is carried out through the resistivity given in standard units. Lastly, α_ρ and β_ρ are respectively the linear and quadratic temperature coefficients of the material resistivity (K^{-1} and K^{-2}).

With a specified ambient temperature, one can know how long it takes for the wire to reach a certain temperature, when subjected to a continuous current I, by evaluating equation (6). This equation is derived from equations (2) and (3), and assumed the current is kept constant from $t = 0$ to $t = t_h$. T_{amb} is the ambient temperature and T_x is the temperature for which heating times are desired to know.

$$t_h = \tau \ln \frac{\Delta T(I)}{\Delta T(I) - (T_x - T_{amb})} \tag{6}$$

When this equation (6) is plotted in a graph, it provides useful information for understanding the correct coordination of fuse protection and wire heating. For this purpose T_x takes values of T_{LT}, T_{ST} and/or T_{OL}, and a fuse characteristic curve is also added to the graph. This fuse curve shows its pre-arcing times for any value of current. An example of fuse-wire coordination can be seen in Fig. 10.

1.6. Automotive fuse parameters and definitions

1.6.1. Rated current and continuous current

Since wires must be protected in case of overcurrent, the dimensioning process must include an interdependent consideration of wires and fuses. In this section, the basic definitions and formulae for fuses will be explained.

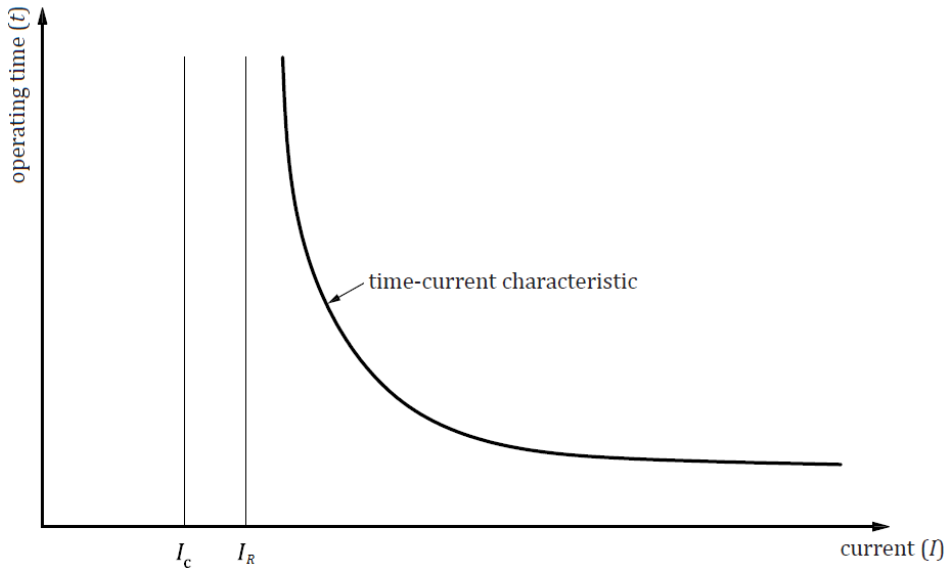

Fig. 5: Rated current, continuous current and time-current characteristic of a fuse

The value of rated current of a fuse (I_R) is merely one of the distinctive parameters used to identify this type of fusible link. By contrast, the continuous operation current (I_C) (Fig. 5) is the value of maximum current the fuse can be conducting during an indefinite time, which must be strictly and sufficiently lower than I_R. Otherwise, the fuse would age prematurely, causing an accidental trip (the so-called *nuisance* trips). Nuisance trips are undesirable because they interrupt unnecessarily the electrical operation of a system. Yet they are unwanted because they can jeopardize driver's safety, if they stop critical functions.

In order to prevent any kind of unexpected trip, it is crucial that maximum operation currents of the loads be a certain percentage lower than the rated current. This percentage must be chosen in consideration of the type of fuse and its characteristics. According to the ISO 8820-3 standard, 70% coefficient for medium blade-type fuses can be used, so that the continuous current of the loads never exceeds 0.7 times the rated current of the fuse. The same standard recommends using a coefficient equal to 50% for any other kind of fuse.

1.6.2. Temperature rerating

The maximum and minimum ambient temperature of the fuse must be considered in any given situation, in such a way that its behavior is delimited. Fuse manufacturers usually provide the value of rated current

for room temperature, so that the dimensioning process requires a temperature rerating for any other ambient temperature in order to predict its operation parameters. The fuse manufacturer must provide the rerating curves (Fig. 6).

Again, the maximum ambient temperature of a fuse must be considered when comparing its characteristic curve with the operation currents of the electrical device. By contrast, the minimum ambient temperature of the fuse should be used when considering short-circuits, because a lower ambient temperature delays the fuse melting, thus exposing the wires to higher temperatures.

1.6.3. Cold resistance and dispersion

The cold resistance of a fuse is defined as the resistance of a fuse without self-heating at a defined ambient temperature. It can be calculated by means of the voltage drop across the contacts of a fuse when conducting a certain test current.

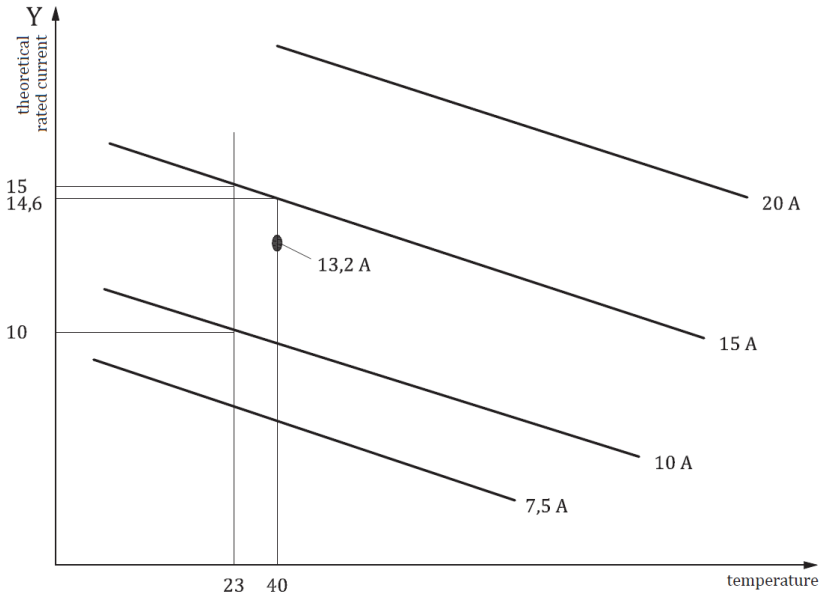

Fig. 6: Fuse typical temperature rerating curves for medium blade fuses

If the cold resistance of a sample of fuses is measured, a certain statistical dispersion will be found. This dispersion causes unavoidably dispersion in the dissipated Joule heat when the fuse conducts current, and therefore in the melting time (Fig. 7) and characteristic time-current curves (

Fig. 8). Then, operation currents and non-faulty phenomena must be compared with the lower curve, whereas short-circuit currents and other electrical failures must be compared with the upper curve.

In general, when a certain situation demands that the fuse have unquestionably blown, one must consider the upper curve, which is the case of a short circuit. On the other hand, if the situation demands that the fuse be still in correct operation, one must consider the lower curve, which is the case of a current peak or the stall current of an electric motor.

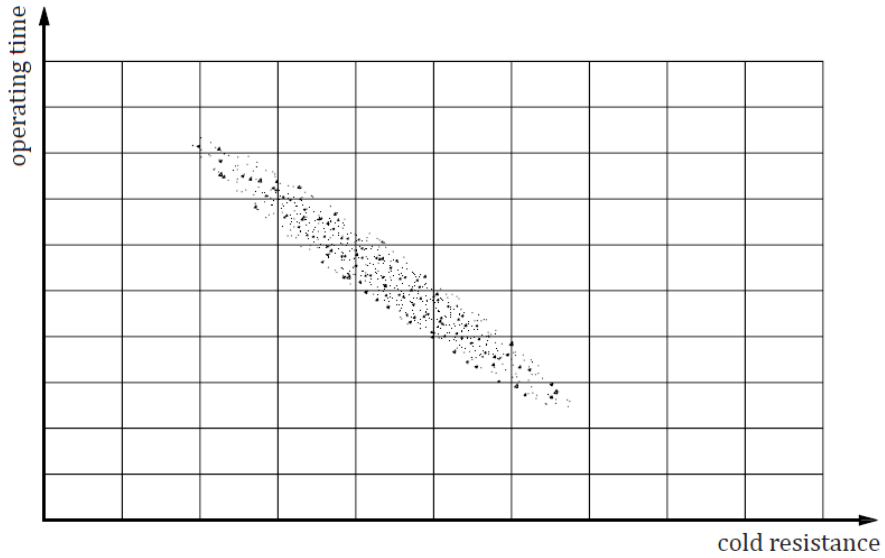

Fig. 7: Fuse cold resistance versus operating time

1.6.1. Inrush tolerance characteristics of fuses

The selection of a fuse does not depend merely on the continuous current and the rated current. Besides, one must consider also the inrush characteristics of electrical devices.

It is easy to establish a value of the maximum operation current of loads having continuous and constant power consumptions. For other types of loads, such as electric actuators that operate only occasionally, it is necessary to study their root-mean-square values of current at maximum acceptable frequency and power of operation. This applies for loads with current peaks, which must be studied in the same way.

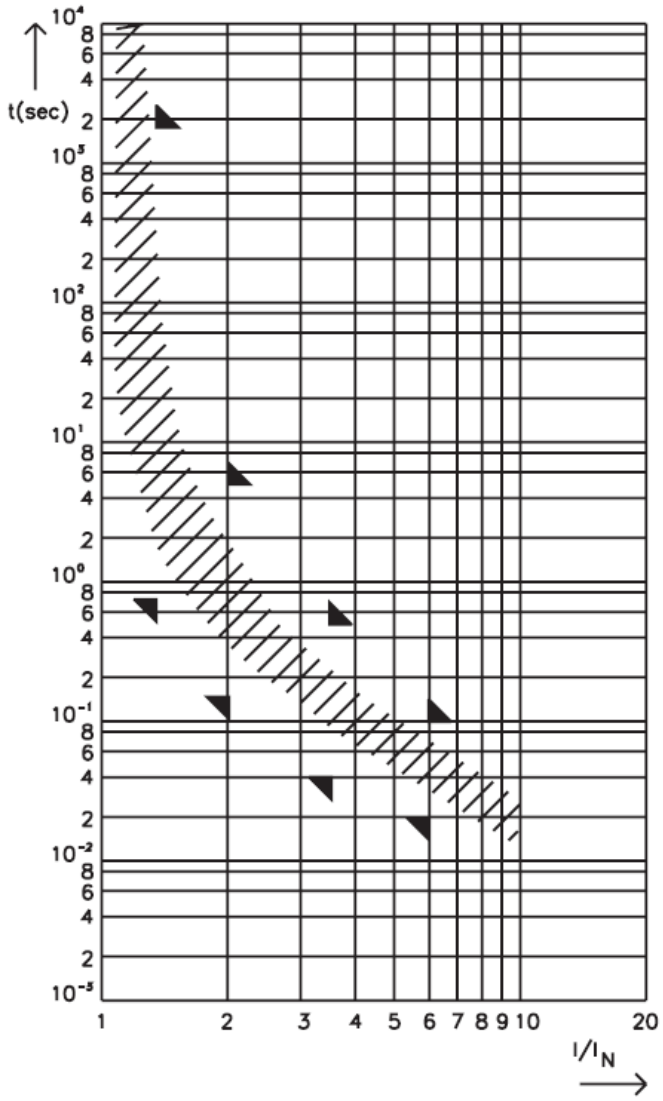

Fig. 8: Fuse time-current spread characteristic given by Littelfuse

1.7. The standard dimensioning method

The prior explained definitions and formulae have been used to elaborate automotive cable standards, with the aim of simplifying the dimensioning process and providing robustness to the system.

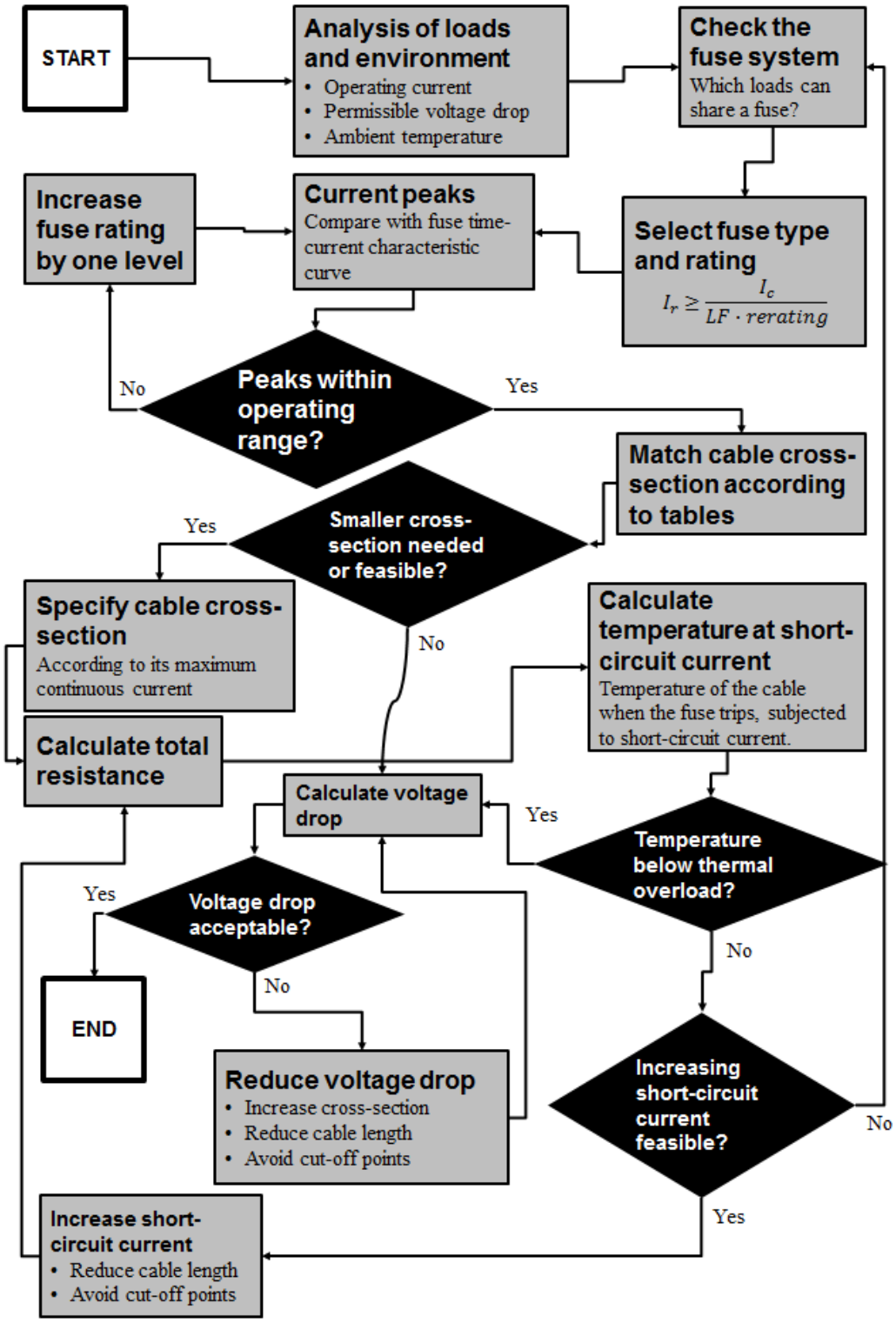

Fig. 9: Wire and fuse dimensioning process diagram

In Fig. 9, a diagram of the actual VW75212 standard dimensioning method can be seen. The gauge selection is bound indivisibly to the selection of a fuse. Both the wire and the fuse must withstand the maximum operation current of the loads. However, the fact that the fuse must protect the wire from the prior temperatures sets the fuse to be the first being dimensioned.

The fuse must withstand the maximum non-faulty currents of all of its loads at the same time, including their current peaks. As Fig. 9 shows, the first step is to apply a load factor coefficient to the continuous rated current of the loads, to get the rated current of the fuse. Afterwards, it must be ensured that current peaks do not make the fuse blow, if there are any. Then it is necessary to upsize the fuse until the peak point lays inside the operation zone of its time-current characteristic curve, whenever there are any loads with current peaks in this fuse.

A standard matching between a fuse and a wire can be seen in Fig. 10. The red curve defines the average characteristic of a 20A fuse. Above the line, the fuse has tripped; below the line, the fuse is still conducting; near the curve, it is unclear how long the fuse will last. In this figure, one can see also a maximum operation current value (12A) and the same current divided by a load factor (17.1A). Therefore, the standard fuse for this application must have a rated current of 20A. Assuming an ambient temperature of 55ºC, the standard recommends using one 1.5mm² cable.

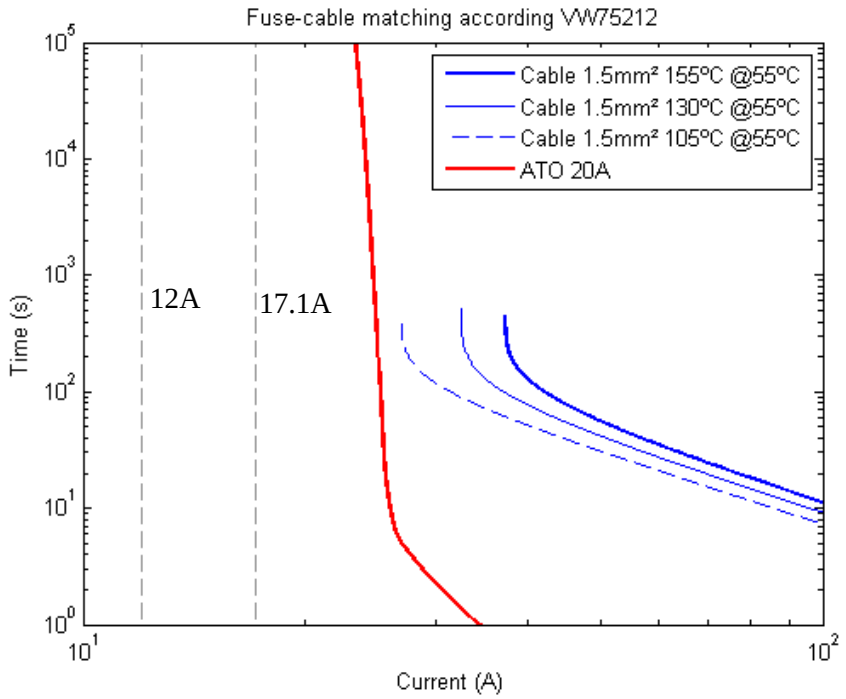

Fig. 10: Example of fuse and wire current-time characteristic curves under correct coordination

Setting a value for the maximum operation current and the current peaks requires experimentation. It is worth mentioning that the thermal behavior of fuses is affected by wires in contact with them, because

wires can conduct a significant amount of heat in such a way that they delay the fuse trip. On the contrary, a hot wire can dissipate sufficient heat across the fuse to advance its tripping time.

Once the fuse is decided, the wire size is specified by a few tables in this standard, depending on the selected fuse. Fig. 10 shows actually a fuse-wire matching recommended by W75212, included in these tables. These tables assure the correct temperature of wires assuming they are exclusively surrounded by still air, and under any current, and even in case of short-circuit.

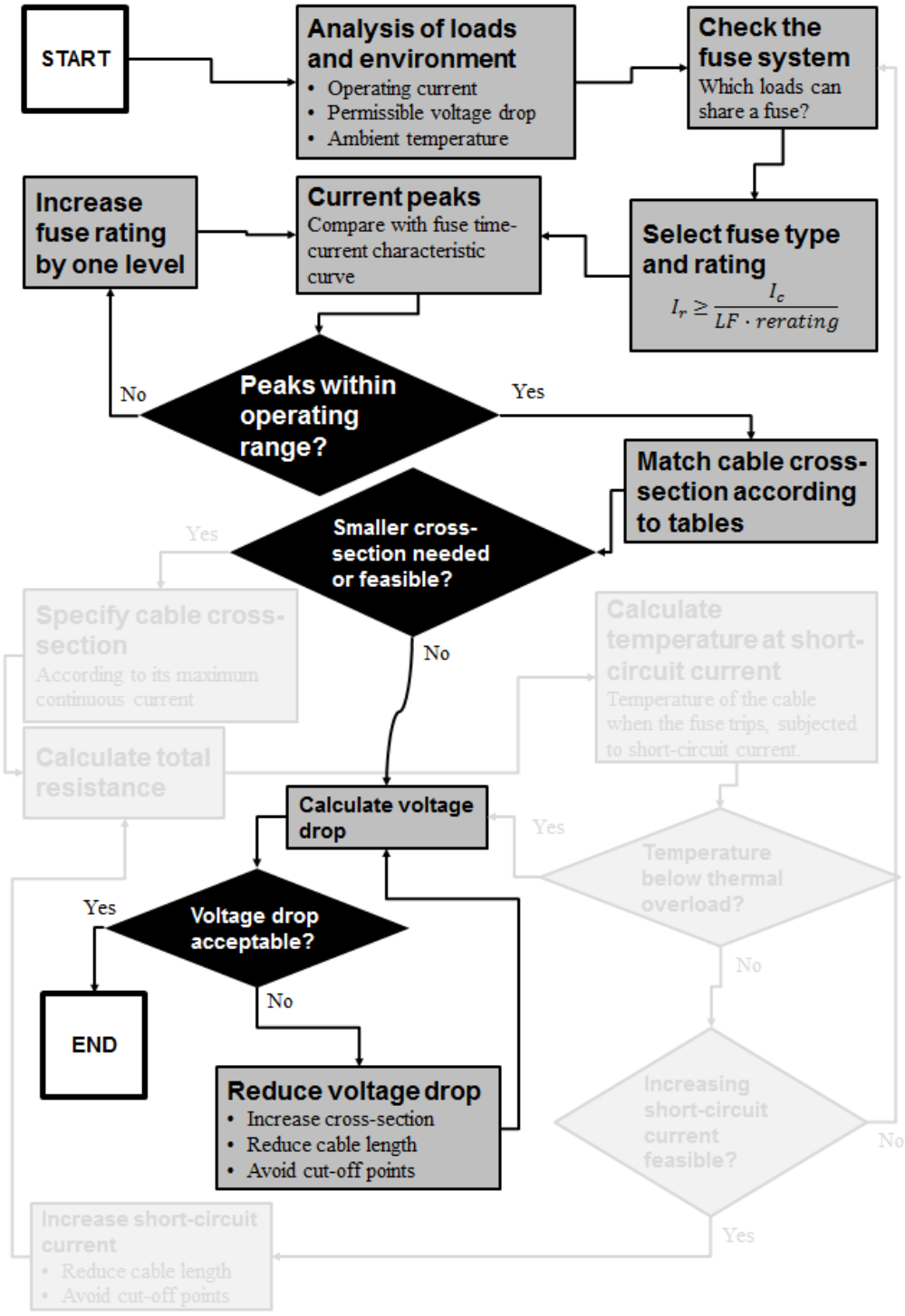

Fig. 11: VW75212 dimensioning process diagram (skipping optimization)

The temperature of the air around a wire is selected as the worst-case temperature of the different environments inside a car. For example, the greenhouse has an associated temperature of 70ºC due to the possibility of the sun heating all of the surfaces in the passenger compartment.

The dimensioning process in Fig. 9 considers the possibility of reducing the wire size by means of optimization. It means that wire sizes might be smaller than proposed by those tables. However, their correct operation must be proved either by simulation or by direct experimentation. Since this process takes time, it is normally carried out just for some wires and the recommended cross-sections from VW75212 are usually taken with no more considerations for the rest of wires (Fig. 11).

A wire must not exceed its maximum acceptable temperature:

a) Under fault-free operation
b) Subjected to short-circuit

Fig. 10 shows a conservative choice of wire cross-section because, as one can see, the maximum value of operation current is actually far from the long-term temperature asymptote of the wire (105ºC, dashed line). In the following, it will be explained how to choose a reliable and smaller cross-section, following the diagram path in Fig. 9.

1.7.1. Fault-free operation conditions

Unless there is an electric fault, the temperature of a wire must be less than or equal to T_{LT} (long term), whereas the temperature can reach a maximum value of T_{OL} (thermal overload) in case of short-circuit. This is due to the definition of long-term and thermal overload temperatures, the wire must withstand temperatures between -40ºC and 105ºC for 3,000 hours; from 105ºC to 130ºC for 240 hours; and from 130ºC to 155ºC for 6 hours. This can be seen in Fig. 10, where the dashed blue line has an asymptote on the right of the operation current of 25A. It assures that the wire never exceeds its long-term temperature during normal operation.

As for the continuous operation current, one must consider the maximum power of the load. For this power, the wire must never exceed the long-term temperature, T_{LT}. In the characteristic curves diagram, it implies the asymptote of the wire to be equal or greater than the value of maximum operation current.

On the other hand, when parallel wires are carrying current at the same time, hot spots can appear, so that the assumption that the wire is going to be surrounded only by air is no longer the worst case. This extra temperature can lower the current-carrying capacity of some wires. Connector designers consider this matter, so that current-carrying wires are placed as much separated as possible. However, sometimes this is not possible, and the dimensioning process needs experimentation to be validated.

Besides the continuous operation current, one must be careful not to neglect the overload currents. The dimensioning process is simple for static loads such as lights, but not as much for pulsating loads such as

electronic side mirrors, which could be blocked causing a stall current. Their maximum power depends on how the user manipulates them and these aspects must be especially taken into account.

1.7.2. Short-circuit conditions

A thick blue line was also plotted, depicting the necessary time for the wire to reach the temperature of thermal overload in Fig. 10, and it is in the tripping range for any values of current. This assures the wire never reaches this temperature, whatever the current is.

One can see how the fuse characteristic and the wire characteristic diverge as current increases. Hence, the larger the current applied to the system is, the wider the margin between the moment of tripping and the moment of the wire reaching its thermal overload temperature. On the contrary, the smallest margins occur when unexpected currents are relatively low, close to the fuse ratings. Therefore, one must pay special attention to the minimum short-circuit currents, because unexpectedly low faulty currents could make the fuse blow too late, and then the wire would be damaged.

2. Statement of the problem

It is desired to reduce the weight of the automotive wiring systems to its optimum, without a loss of reliability. The size reduction of a wire increases the temperature rise due to its current conduction, which is more difficult to predict that the voltage drop, because it depends on the thermal parameters of its immediate environment. Since a cable can extend across different nodes of the harness and thus have different bundle branch segments composed by different sets of cables, each of the bundle branch segments will have a different thermal behavior, with different time constant and different steady temperature.

Normally and for simplicity, the case of the wire being just surrounded by air has been used as the worst-case as a reference to dimension wires. Considering only one of the thermal behaviors leads to dismiss the fact that cables in bundles have slower time constants but they are likely to have higher steady temperatures in some cases (e.g. when hot cables surround the observed cable in the center of the bundle). Likewise, the single cable surrounded by air has the fastest time constant, but, in some cases, its steady temperature is lower than compared to cases where other hot cables are close.

Additionally, the modular complexity implies that one wire in a drawing with only one dimension can have different sets of thermal behaviors simultaneously in two different cars. Therefore, it is necessary to consider all of the modular combinations in order to find the absolute worst cases among all of the future manufactured instances of the wire in the harness, and to use this worst case to select the cross-section of the cable. Since the amount of cases is enormous, the use of iterative simulations appears to involve excessively long computation times.

Furthermore, the need for considering the capacity of fuses to protect the wires forces to consider worst cases of heating time, besides the more evident need for being aware of the steady temperature of the cable. That is why the thermal behaviors of all of the segments of the wire must be considered and compared in order to assure reliability even in the case of short circuit, not only using their steady temperature, but also their time constant. Additionally, it is necessary to foresee the minimum short-circuit current of all of the sets of series-connected wires in order to know the temperature of the wire after the fuse melts.

Summarizing:

- Cars have electric loads.
- Each of the loads needs a power supply cable.
- It is desired to reduce the weight of all of the cables.
- The thinner the cable is, the more it heats up and the greater its voltage drop is.
- The exact voltage drop and temperature rise depend on the conducted current.

- The voltage drop is relatively easy to predict and usually less restrictive than the temperature rise.
- The temperature rise is difficult to predict because it also depends on the thermal environment.
- Normally, researchers have used the assumption of the wire being just surrounded by air. However, wires are actually together in a cable harness.
- Some others have considered the thermal behavior of wires in bundles as well.
- The thermal behaviors of both the above cases are very different and must be considered at the same time, because they have crossed bad cases of time constant and steady temperature and because one cable is present in different segments of a harness, thus experiencing various thermal behaviors.
- The different segments are characterized also depending on the modular complexity. A segment defined by two specific nodes can be different in composition comparing two cars.
- The possible simultaneity of loads is also important (some loads cannot conduct current at the same time, which is a better case). This allows being more realistic with constraints.
- The above points reveal that a particular worst case for each of the cables can be found, instead of considering just one for all of the cases.
- The cable is protected by a fuse, and after giving a new optimized cross-section for the wire, it must be ensured that the fuse protects it in case of short-circuit.
- This depends not only on one wire, but also on all of the series-connected wires, because the worst short circuit is the one causing the smallest current.
- The short circuit maximum resistance must be lowered by increasing the size of the cables, and both their weight and their so-called *mix* must be considered in order to add the least possible weight to the system.
- Since the amount of thermal characterizations is enormous, using iterative simulations involves an inconvenient computation time for the optimization.

3. The state-of-the-art automotive wire modeling and optimization

3.1. Analytical solution of the heat transfer equation for single wires

The characteristic geometry of a wire and the variety of spaces where it can be installed makes its temperature prediction complex. Especially if one considers wire bundles, whose exact reproduction with a mathematical model is usually unlikely to be achieved because of the large number of degrees of freedom of the system.

A wire in an automotive harness can experience situations wherein its heating behavior can be worse than the heating behavior of the single wire exposed to still air. However, this assumption has been used to dimension wires, as well as motivating the development of methods, models and algorithms capable of predict the temperature of single wires surrounded by air.

All of the methods must start from the general heat transfer equation in its conservative form [1]:

$$\frac{\partial}{\partial x}\left(\lambda\frac{\partial T}{\partial x}\right)+\frac{\partial}{\partial y}\left(\lambda\frac{\partial T}{\partial y}\right)+\frac{\partial}{\partial z}\left(\lambda\frac{\partial T}{\partial z}\right)+q_v=\gamma\rho\frac{\partial T}{\partial t} \tag{7}$$

In some cases, the same equation is used in cylindrical coordinates:

$$\frac{\partial}{\partial x}\left(\lambda\frac{\partial T}{\partial x}\right)+\frac{1}{r}\frac{\partial}{\partial r}\left(\lambda r\frac{\partial T}{\partial y}\right)+\frac{1}{r^2}\frac{\partial}{\partial \phi}\left(\lambda\frac{\partial T}{\partial \phi}\right)+q_v=\gamma\rho\frac{\partial T}{\partial t} \tag{8}$$

In both equations (7) and (8), γ stands for the volumetric heat capacity, ρ for density and q_v for the volumetric heat generation.

Reference [1] describes a method for obtaining the steady temperature of a single wire surrounded by still air, either with analytical and numerical methods. Analytical solutions for heat transfer equations (7) and (8) have the advantage of a reduced computation time in comparison to numerical methods. As a drawback, they generally need simplifications of the differential equations in order to linearize them. This makes them not as accurate.

Despite this, mismatches between simulations and reality are acceptable most of times, especially when the number of calculations is large and fast computations are needed. Considering the extreme difficulty of reproducing the exact conditions of a wire in automotive applications as input data for a thermal simulator, it is a waste of efforts to pursuit high accuracy. Instead, the optimum balance resides in fast simulators whose result can be taken as a reliable reference for dimensioning wires. That is why the analytical solutions are so interesting.

The following assumptions are made in order to simplify the partial differential equations:

a) Steady-state conditions
b) One-dimensional conduction
c) Constant or linear material properties
d) Uniform volumetric heat generation
e) Constant heat transfer coefficients

The radial heat transfer must consider infinite length of the cylindrical wires, neglecting the heat transmission in their limits. According to [1], this assumption is acceptable if the radius of the cylinder (r) and its length (L) are such that $L / r > 10^3$. Thus, this approach assumes a wire to be an infinitely long horizontal cylinder, which general heat equation corresponds to equation (9):

$$\frac{1}{r}\frac{\partial}{\partial r}\left[r\frac{\partial T(r,t)}{\partial r}\right]+\frac{E\cdot I}{\lambda A}-\frac{\gamma}{\lambda}\frac{\partial T(r,t)}{\partial t}=0 \tag{9}$$

T is the temperature, t is the time, E is the electric field or the unit length voltage drop (Vm^{-1}), I is the current (A), λ is the thermal conductivity ($Wm^{-1}K^{-1}$), A is the cross-section of the wire, and γ is the volumetric heat capacity $Jm^{-3}K^{-1}$.

Equation (9) describes a radial heat transfer with temperature-independent coefficients. In order to consider the effects of the temperature rise in the properties of the materials, the author in [1] considers the variation of the resistivity of copper as in equation (10):

$$\rho(T)=\rho_0\{1+\alpha_\rho[T(r,t)-T_0]\} \tag{10}$$

In this equation, ρ is the resistivity of copper; ρ_0 is the resistivity of copper at the reference temperature, T_0; α_ρ is the linear temperature coefficient of resistance. This considered variation in the electric resistivity affects the voltage drop, expressed in this case as the unit-length voltage drop or electric field E, which affects at the same time the unit-length Joule power $E{\cdot}I$. This variable E is expressed in equation (11), which uses the same temperature dependence as equation (10).

$$E(T)=E_0\{1+\alpha_\rho[T(r,t)-T_0]\} \tag{11}$$

The result of introducing equation (11) into the linear general heat equation (9) leads to equation (12), which describes the non-linear heat equation of an infinitely long cylinder considering variations in resistivity as a function of the temperature.

$$\frac{1}{r}\frac{\partial}{\partial r}\left[r\frac{\partial T(r,t)}{\partial r}\right]+\frac{\alpha_\rho E_0\cdot I}{\lambda A}\Delta T(r,t)+\frac{E_0\cdot I}{\lambda A}-\frac{\gamma}{\lambda}\frac{\partial T(r,t)}{\partial t}=0 \tag{12}$$

These equations are solved assuming the temperature gradient of the inner metal conductor of the wire to be zero, which is a good approximation considering the low heat conductivity of plastic materials compared to copper's.

For the steady state, the last term of equation (12) equals to zero, leading to equation (13):

$$\frac{1}{r}\frac{\partial}{\partial r}\left[r\frac{\partial T(r,t)}{\partial r}\right]+\frac{\alpha_\rho E_0 \cdot I}{\lambda A}\Delta T(r,t)+\frac{E_0 \cdot I}{\lambda A}=0 \tag{13}$$

A scheme of the system can be seen in Fig. 12. The following boundary conditions must be considered to solve equation (13) for the set of metallic conductor and plastic insulator:

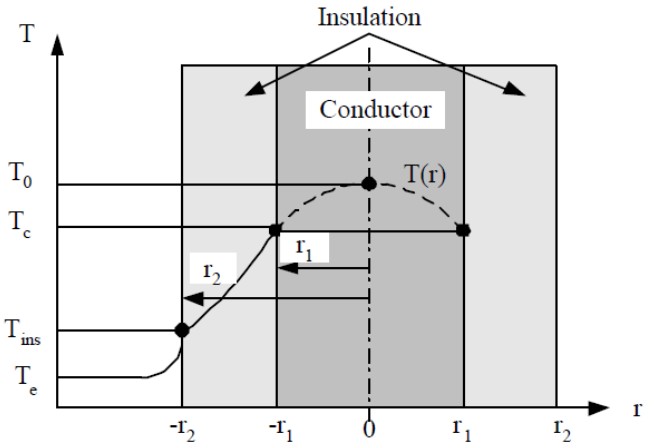

Fig. 12: Section of a wire for the analytical solution of the heat transfer equation [1]

a) The total heat crossing the surface of the inner cylinder at $r = r_1$ equals the Joule heat:

$$-2\pi r_1 \cdot \lambda_{ins} \cdot \left.\frac{\partial T}{\partial r}\right|_{r=r_1} = E \cdot I$$

b) Neglecting radiation, the total heat crossing the outer surface of the insulator at $r = r_2$, equals the heat dissipated by convection [8]:

$$2\pi r_2 \cdot \lambda_{ins} \cdot \left.\frac{\partial T}{\partial r}\right|_{r=r_2} = -2\pi r_2 \cdot \alpha(T - T_{env})$$

$$\Rightarrow \left.\frac{\partial T}{\partial r}\right|_{r=r_2} = -\frac{\alpha}{\lambda_{ins}}(T - T_{env})$$

Using the boundary condition of the zero-gradient for $r = 0$ and integrating, equation (14) is obtained:

$$T(r) = \frac{E \cdot I}{2\pi\lambda_{ins}} \ln\frac{r_2}{r} + \frac{E \cdot I}{2\pi r_2 \alpha} + T_{env} \tag{14}$$

This latter equation provides the steady temperature at any radius of the wire. The maximum acceptable temperature of a wire is given by the temperature endurance of the wire insulator. For that reason, the applicable temperature of the wire is the maximum temperature of the insulator, which occurs exactly at $r = r_1$. Using equation (14), this temperature is expressed for any current I and ambient temperature as in equation (15):

$$\boxed{T(r) = \frac{E \cdot I}{2\pi\lambda_{ins}} \ln\frac{r_2}{r_1} + \frac{E \cdot I}{2\pi r_2 \alpha} + T_{env}} \tag{15}$$

This latter equation is the result of considering an infinitely long wire surrounded by still air, whose materials experience no changes due to temperature (except from the resistivity of copper), and wherein the effects of radiation have not been considered.

3.2. Numerical solution of temperature transients for single wires

The mentioned non-linearity and non-homogeneity of the partial differential equations of a single wire exposed to air forces to use numerical solutions if a transient result is desired. Nonetheless, analytical steady state and experimental results are useful for verifying the accuracy and validity of numerical results.

3.2.1. Solution of the heat transfer equation in transient state

The heat transfer equation (12) cannot be solved analytically in transient state. Despite that, this partial differential equation can be discretized in one dimension in order to solve a set of ordinary differential equations. This is known as the initial-boundary value problem for parabolic partial differential equations in one dimension. This is carried out in [7] in order to compare different single-wire thermal simulation approaches.

3.2.2. Thermal equivalent circuit approach

Diebig includes in her comparison the thermal equivalent approach in [7]. It consist of converting the thermal equation into an electric circuit where current, capacitors and resistors are respectively the heat power (*P*), the heat capacity and the thermal resistance, which is the inverse of the thermal conductivity. This can be seen in Fig. 13.

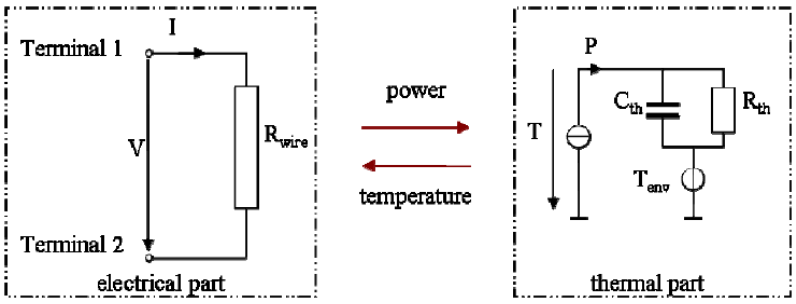

Fig. 13: Scheme of the cable model in the thermal equivalent circuit approach

The equivalent thermal resistor R_{th} and capacitor C_{th} need to be defined according the following equations (16) and (17). Again, r_1 and r_2 are the radii of the conductor and of the outer surface, respectively. L stands for the length of the cable. (18) is the differential equation for the temperature derived from this model.

$$R_{th} = \frac{\lambda_{ins} + r_2 \cdot \alpha(T) \cdot \ln\left(\frac{r_2}{r_1}\right)}{\lambda_{ins} \cdot 2\pi r_2 \cdot \alpha(T) \cdot L} \tag{16}$$

$$C_{th} = \pi L \cdot [\gamma_{wire} \cdot r_1^2 + \gamma_{ins} \cdot (r_2^2 - r_1^2)] \tag{17}$$

$$\frac{dT}{dt} = \frac{I^2 R_{wire}(T) - \frac{1}{R_{th}}(T - T_{env})}{C_{th}} \tag{18}$$

This approach is compared with the discretization of the heat transfer equation described in section 3.2.1 (carried out via Matlab®), and it can be seen in Fig. 14. It shows a simulated cable of a 0.5mm² and polyethylene insulation, subjected to 18 amperes for 200 seconds. A good agreement between the approaches can be observed.

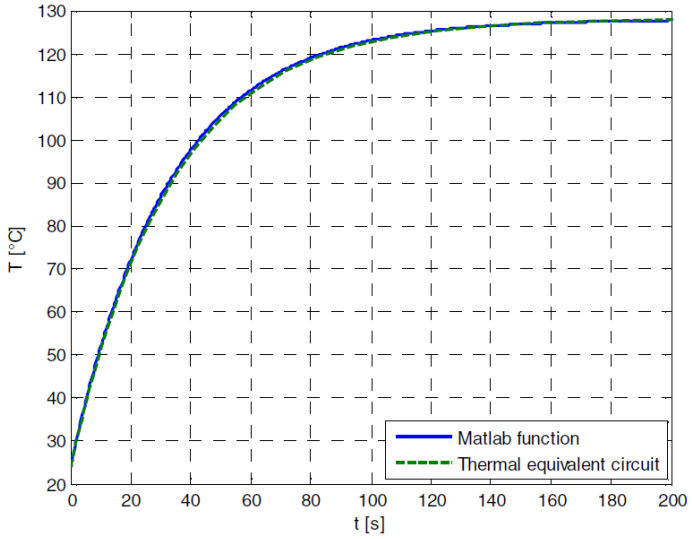

Fig. 14: Comparison of the PDE solution with the thermal equivalent circuit

Fig. 15 shows the comparison between the simulated and measured steady temperatures for different current loadings, as well as Fig. 16 shows the temperature transients.

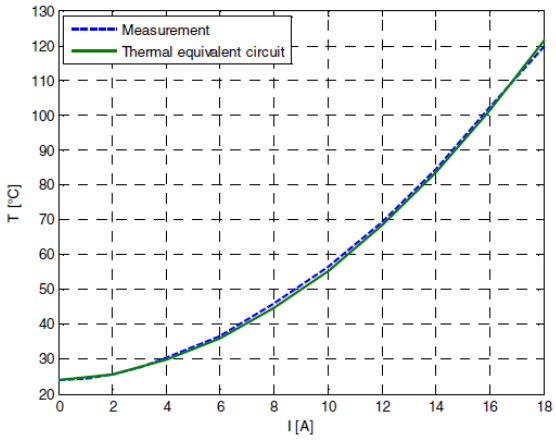

Fig. 15: Comparison of simulated and measured steady temperatures

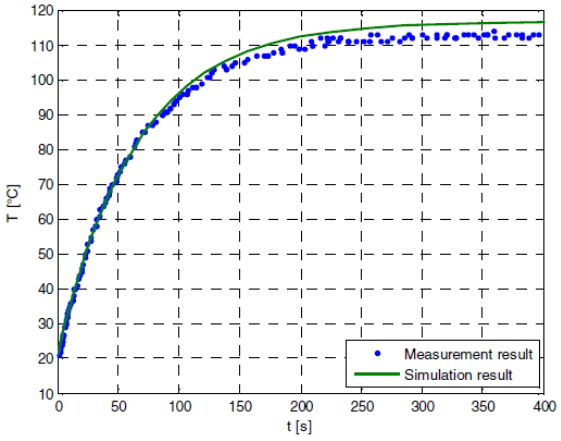

Fig. 16: Comparison of simulated and measured temperature transients

This simulation approach was implemented via the VHDL-AMS language in [7], which has become more and more famous in the automotive industry in the last years. Additionally, there are free libraries available allowing the reproduction of complex systems with the purpose of simulation.

The aim of the simulators is to be able to simulate complete wiring systems, and thus a full simulator was implemented using this described approach and the typical formats of the car industry containing all the information of the wiring systems. These files come in KBL format, which is standardized as STEP AP 212 according standard VHDL.

The pre-processor of the harness simulator was written in Matlab, and it builds a data model from de KBL files, which have been previously adjusted by means of the Harness Studio software (EMCoS). The comparison between measured results and simulated results of a real current profile in a cable harness can be seen in Fig. 17.

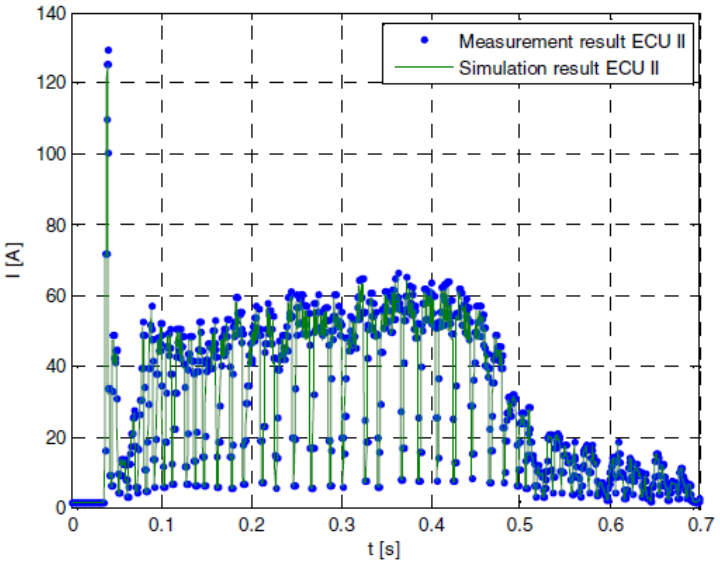

Fig. 17: Comparison of measured and modeled current of a single wire in a wiring system

3.2.3. Solution with power flow balance

This approach considers that the only relevant thermal effects explaining the temperature evolution of a single wire are the Joule heat P_e, the convection heat dissipation P_c, and radiation P_r. All of them depend on the temperature of the wire, and the latter two depend also on the surrounding air temperature. This is an assumption that disregards the axial heat conduction, which will be correct if the cable is long enough.

Conservation of energy implies that the difference between the generated heat and the dissipated heat equals the rate of stored heat:

$$\frac{dQ}{dt} = P_e - P_r - P_c \tag{19}$$

From equation (19), one can derive the isolated term of the temperature derivative as a function of the temperature, using the expressions of P_e, P_r and P_c, as well as the expression of the stored heat Q.

$$\frac{P_c}{L} = \alpha_c \cdot 2\pi r_2 \cdot (T - T_{env}) \tag{20}$$

$$\frac{P_r}{L} = \alpha_r \cdot 2\pi r_2 \cdot (T^4 - T_{env}^4) \tag{21}$$

$$\frac{Q}{L} = \frac{C_{th}}{L} \cdot (T - T_{env}) \tag{22}$$

$$\frac{dT}{dt} = \frac{I^2 \frac{R_{wire}(T)}{L} - \frac{\lambda_{ins} \cdot 2\pi r_2 \cdot \alpha(T) \cdot (T - T_{env})}{\lambda_{ins} + r_2 \cdot \alpha(T) \cdot \ln\left(\frac{r_2}{r_1}\right)}}{\frac{C_{th}}{L}} \tag{23}$$

Equation (23) is derived from (19) by means of equations (20) to (22). Note that some parameters appear divided by L, because it is easier to consider only unit-length values in this case where the length of the cable is not considered.

3.2.4. The finite volume method (1D)

The basis of the finite volume method [9] consists of discretizing the integral form of the behavioral equations under study, rather than their differential forms. This assures that these equations can be converted into partial differential equations even in case of discontinuities [1].

The discretization method is similar to that of the well-known finite elements method. Due to the enormous complexity of the automotive wiring, it is unaffordable to perform complete 3D temperature estimations, using the finite elements method. In general, researches using this method with the purpose of assisting their dimensioning process have used 2D finite elements, as well as with the *finite volume* method discussed in this section.

The advantage of the finite volume method is that, unlike the finite elements method, the finite volumes can have any shape, and various shapes combined in one domain. Moreover, the solution of the equations is not so strongly related to the geometric representation of the domain.

Equation (7) can be rewritten in its integral form over a small fixed volume V:

$$\oint_V \nabla(\lambda \nabla T) dV + \oint_V q_v dV = \oint_V \gamma \frac{\partial T}{\partial t} dV \tag{24}$$

Equation (24) can be rewritten as a surface integral by means of the divergence theorem:

$$\oint_V \lambda \frac{\partial T}{\partial n} dS + \oint_V q_v dV = \oint_V \gamma \frac{\partial T}{\partial t} dV \tag{25}$$

This latter equation represents the conservation of energy in a control volume *V*. The sum of the energy entering the region throughout its external surface S and the generated energy inside the region equals the rate of increase of the stored energy. Since the heat flux among finite regions, the conservation principle is also accomplished for a set of finite volumes.

Like in the described analytical method brought by [1], the axial heat conduction is neglected, assuming long wires, so that the heat conduction is only radial. Therefore, the finite element grid in this research consists of several concentric pipes of two materials. Actually, these pipes are rings because only the radial flux is considered. All of the parameters are unit-length and temperature variations are only calculated in a cross-section plane, which is the same along the *infinitely long* wire.

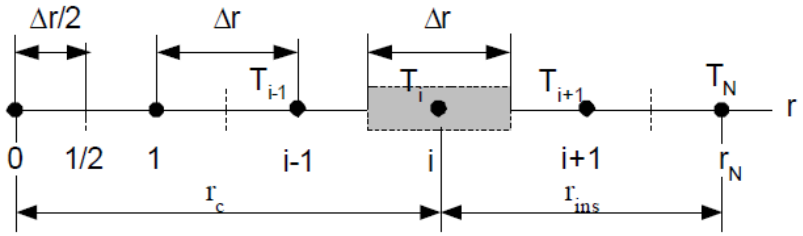

Fig. 18: The finite volume grid of round wires [1]

Fig. 18 shows the multiple temperatures of *N* finite-volume rings T_i, and the radii they represent. Finite volumes within r_c are made of copper and those within r_{ins} are made of PVC (copper and PVC could be other materials in some cases, such as aluminum or TFE). Each of the finite-volume rings has a thickness of Δr, except from the first volume, which is round and has a radius equal to $\Delta r/2$. This can be seen also in Fig. 19.

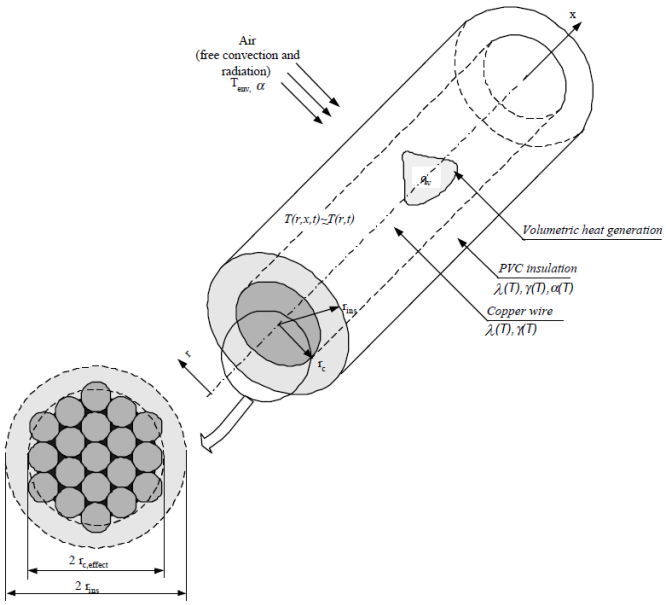

Fig. 19: The model of heat conduction in round electrical wires [1]

Equation (26) is obtained by applying the integral form of the governing equations to the finite volume $V=[i - ½; i + ½]$ and solving the integrals. In this equation, the partial derivatives have been replaced by central differences and time derivatives have been replaced by backward time differences.

$$\boxed{-\frac{r_{i+½}\cdot\lambda_{i+½}}{\Delta r_{i+½}}\left(T_{i+1}^{n}-T_{i}^{n}\right)+\frac{r_{i-½}\cdot\lambda_{i-½}}{\Delta r_{i-½}}\left(T_{i}^{n}-T_{i-1}^{n}\right)+\frac{r_i\cdot\gamma_i^n\cdot\Delta r_i}{\Delta t}\left(T_{i}^{n}-T_{i}^{n-1}\right)=r_i q_i \Delta r_i} \qquad (26)$$

In order to solve the problem, the boundary conditions must be imposed as following:

$$\begin{cases} T(r,0)=T_{env}(r), \qquad r\in[r_{½},r_N] \\ \lim\limits_{r\to 0} r\lambda_0(r)\dfrac{\partial T}{\partial r}=0, \quad t\geq 0 \\ -\lambda_N\left.\dfrac{\partial T}{\partial r}\right|_{r=r_N}=\alpha_c(d,T)(T_N-T_{env})+\epsilon\sigma[(T^*)^4-(T_{env}^*)^4], \quad t\geq 0 \end{cases} \qquad (27)$$

These conditions lead to special equations for the first and the last rings of the finite volume discretization:

$$\boxed{\begin{gathered} -\frac{r_{½}\cdot\lambda_{½}}{\Delta r_{½}}\left(T_1^n-T_0^n\right)+\frac{r_{½}\cdot\gamma_{½}^n\cdot\Delta r_0}{\Delta t}\left(T_0^n-T_0^{n-1}\right)=r_{½}q_0\Delta r_0 \\ \alpha(T_N^n-T_{env})+\varepsilon\sigma[(T_N^{*n})^4-(T_{env}^*)^4]+\frac{r_{N-½}\cdot\lambda_{N-½}}{\Delta r_{N-½}}\left(T_N^n-T_{N-1}^n\right)+\frac{r_N\cdot\gamma_N^n\cdot\Delta r_N}{2\Delta t}\left(\Delta T_N^n-T_N^{n-1}\right)= \\ =\frac{1}{2}r_N q_N^n\Delta r_N \end{gathered}} \qquad (28)$$

The resulting problem is a non-linear system of equations because the heat capacity is second order temperature dependent, as well as the radiation boundary condition, which is fourth order temperature

dependent. Ilgevičius states in [1] that the electrical resistance of copper and the dependence of the thermal conductivity with temperature can be considered linear if the temperature does not exceed 150ºC, with no relevant changes in the result.

Since the problem has been reduced to one dimension, the Gauss elimination method is used by means of the Thomas Algorithm, which is a very efficient method for solving large numbers of equations like these.

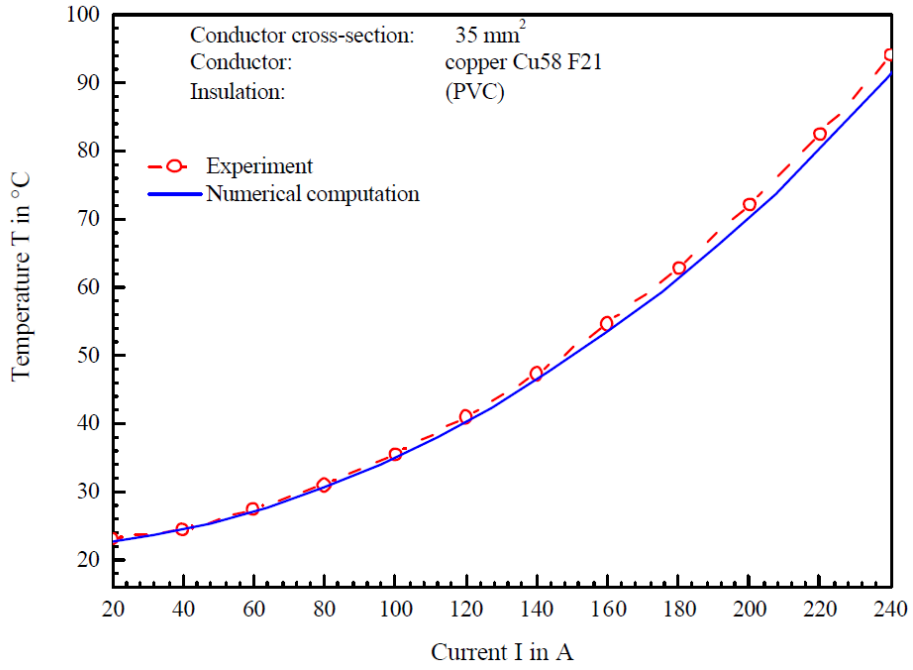

Fig. 20: Measured temperature of a round wire conductor (cross-section = 35mm²) as function of the electric load [1]

Since an experimental validation of the thermal conductivity coefficient λ of all of the insulating materials was not carried out in [1], its final value was determined after fitting the computation with the experimental results. For PVC, the results were satisfactory with no fitting, as can be seen in Fig. 20.

3.3. Interpolation of numerical results

The complexity of the design and manufacturing process of the automotive electric distribution networks (section 1.3) demands the fastest methods of calculations. Therefore, Ilgevičius proposes in [1] to fit curves to the numerical computations when possible, so that simple analytical formulae describe accurately with low computation times the behavior of a single round wire (Fig. 21 and Fig. 22).

These formulae are the fastest method among the proposed methods, and they can be as accurate as the numerical method can be. The fastest level of accuracy corresponds to fitting and obtaining these formulae from numerical computations with a high number of finite volumes, that matches perfectly the experimental results.

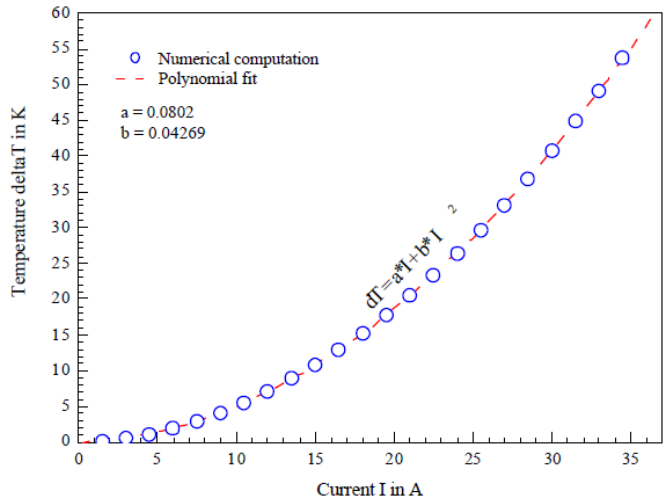

Fig. 21: Thermo-electrical characteristic $\Delta T(I)$ of round insulated wire (FLRY-B, 2.5mm²) obtained from numerical calculation and approximated by polynomial function [1]

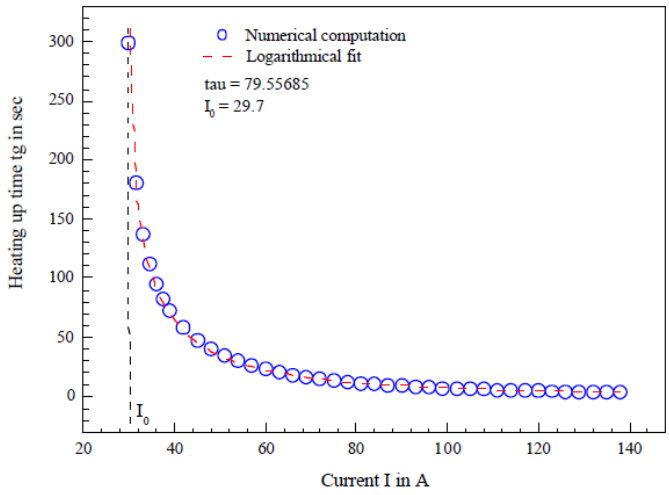

Fig. 22: Heating-up time characteristic of round insulated wire (FLRY-B, 2.5mm²) obtained from numerical calculation and approximated by a logarithmical function [1]

Fig. 22 shows the fitted heating time of a round wire, which is a useful formula for validating the wire dimensions, as explained in section 1.7.

3.4. Coordinate transformation of the multi-wire bundle geometry

In reference [1], Ilgevičius introduces a novel method for calculating the temperature of wire bundles. This approach is based in the calculation of averaged conductivities of the bundle system under study by means of the linear coordinate transformation and averaging method for layered media.

Fig. 23 and Fig. 24 show the wire bundle model and its transformation to square frames of the same area, respectively.

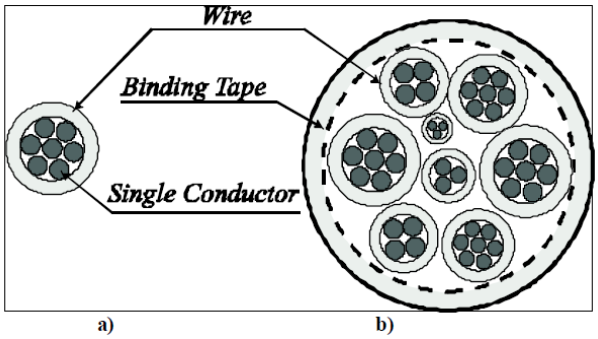

Fig. 23: Insulated single (a) and multi-wire conductor (b) [1]

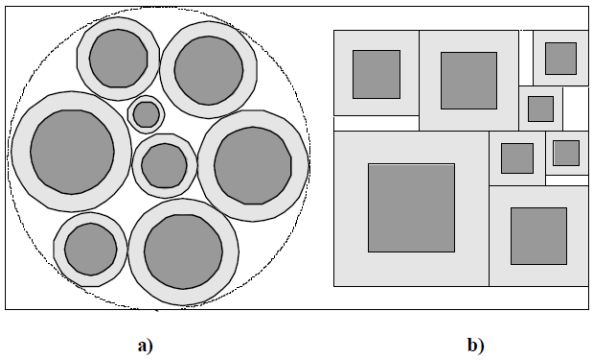

Fig. 24: Transformation of insulated round conductors (a) into squares of the same area (b) [1]

This transformation into a square structure allows the use of a serial-parallel lumped model, wherein air has been removed, thus having three layers, as shown in Fig. 25. Air gaps are removed from the geometrical representation, but included in the calculation by means of a *filling factor*, which is multiplied by the cross-section of the conductor core in order to obtain the effective cross-section of the conductor.

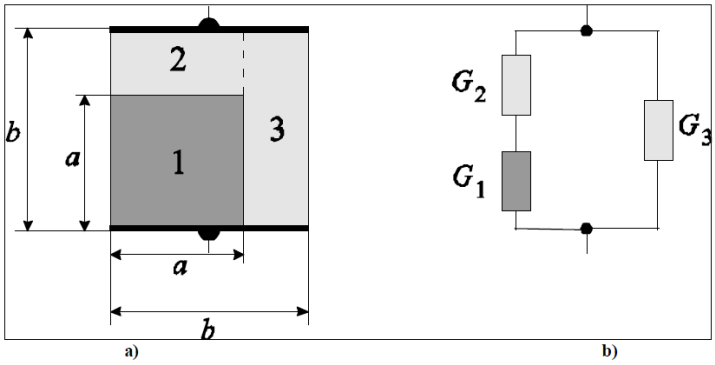

Fig. 25: Determination of the mixed area conductivity: (a) assembly, (b) circuitry [1]

The thermal conductivity coefficients are calculated by means of equation (25), which was developed as a solution for mixed materials.

$$\lambda = \lambda_2 \left(\frac{1}{\frac{\lambda_2}{\lambda_1} + \frac{b}{a} - 1} - \frac{a}{b} + 1 \right) \tag{29}$$

Experimental results are compared with the result of the latter method, which can be seen in Fig. 26. A difference between the curves can be noticed, for which Ilgevičius writes "there is some error between curves, which cannot be fully explained yet" [1]. The same author observes that this difference could be justified by:

a) The model does not completely describe reality from a geometrical point of view

b) Low accuracy of those parameters involved in radiative heat dissipation

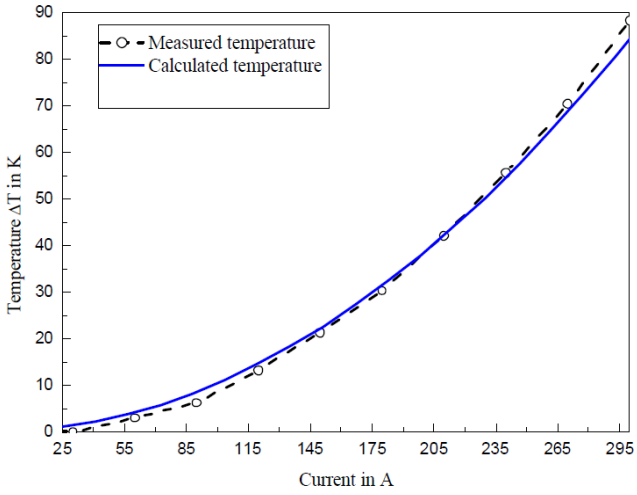

Fig. 26: Experimental versus theoretical results of the wire bundle (environment temperature = 23ºC) [1]

3.5. The finite volume method for wire bundles (2D)

After the development of the 1D finite volume method approach in [1], Čiegis made a specific finite volume methodology for wire bundles in [4], which approximates the differential problem of heat transfer on non-rectangular regions with smooth boundaries by means of a square mesh (Fig. 27).

This approach appears to be promising because it consists of a combination of the finite volume method and a finite-difference scheme, which approximates well with second order of accuracy both the solution and the normal flux through the interface. These schemes use a minimal discretization stencil while preserving a local discrete conservation.

This model neglects complicated models of heat transfer throughout air gaps inside the wire bundles, because in terms of air convection, the closest layer of air carries heat by conduction. The air movement that defines the heat convection takes place further from the surface. Therefore, small gaps of air can be considered *still*, just as a solid material with low heat conductivity. The air gaps are thus included in the problem definition by means of a filling factor that lowers the average heat conductivity of the bundle.

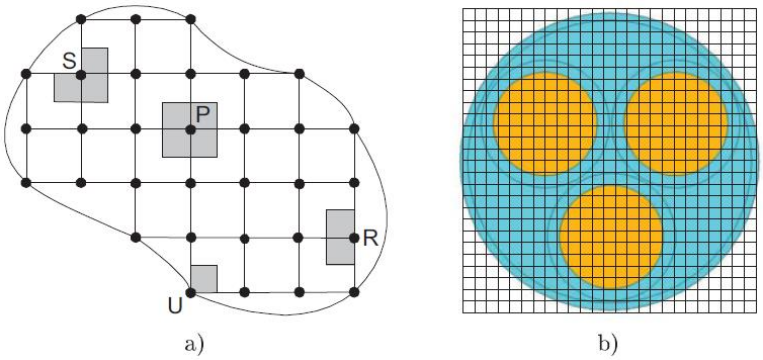

Fig. 27: Discretization: a) discrete grid showing how neighbors out of the domain are removed, b) basic grid and the obtained discretization of the computational domain [4]

The discretization works in such a way that a binary mask activates or deactivates the convection and radiation terms of the heat transfer equations, depending on whether the cells represent the external surface of the bundle or not. In this way, all of the cells have the same formula for the heat flux calculation, but a binary parameter sets the terms of convection and radiation to zero when they are not applicable. This mask must be identified before as one of the first stages of the method.

Thermal parameters are considered functions of the temperature when necessary, which is the case of the specific heat capacity. This parameter depends on the material as well as on its temperature.

$$c = \begin{cases} 381 + 0.17T, & 0 \leq 200ºC \quad \text{(Cu)} \\ 920 - 1.3T + 0.074T^2, & 0 \leq T \leq 100ºC, \quad \text{(PVC)} \end{cases}$$

One more temperature-dependent parameter is the heat generation *f*, because the electrical resistivity of copper increases linearly with temperature. On the contrary, both the density of copper and polyvinyl chloride are considered constant, as well as their thermal conductivities.

Each square cell defines a control volume using minimum and maximum coordinates, such as minimum and maximum *x* and *y*, where the main differential equation can be integrated. The diffusion coefficients between every pair of cells, *k*, are calculated using the harmonic mean of the heat conductivities between neighbor cells. Likewise, there is an area for each cell, *S*. Since the mesh is square-centered, the value of *S* depends on the number of quarters of the volume (Fig. 27.a).

Equation (30) shows how the heat flux q is calculated for a cell in a compact way. This expression here is to explain the calculation approximately. Please refer to [4] if a detailed explanation is desired. The heat flux q appears as the sum of the heat flux produced by a difference of between the temperatures of its neighbor cells and of its own ($q_{cond.}$), and the nonlinear generalized coefficient of convection and radiation (α_G). The k subscripts (k = 0, 1, 2, 3) denote parameters depending on the neighbor. Then, r_k is the division of height and width of adjacent cells, and it depends on whether the k neighbor lies on top or beside the current cell. Likewise, h_k is the width or the height of the neighbor, and δ_k activates or deactivates the nonlinear term depending on the position of the neighbor. Subscripts k_1, k_2 and k_3 take the values of neighbors for the calculation of equation (30), in such a way that $k_i \equiv k_i(k)$, i = 1, 2, 3.

$$\begin{aligned} q_k(\bar{T}, T) &= \sum \frac{r_{k1} \cdot q_{cond.}}{2} + \frac{h_{k2}}{2}(1 - \delta_{k3}) \cdot \alpha_G(\bar{T}) \cdot (T - T_{env}) \\ \alpha_G(\bar{T}) &= \alpha_k(\bar{T}) + \varepsilon\sigma(\bar{T}^3 + \bar{T}^2 T_{env} + \bar{T} T_{env}^2 + T_{env}^3) \end{aligned} \tag{30}$$

The use of the predictor-corrector method allows the approximation of the system of nonlinear equations. For each time step, the system of equations is solved twice, obtaining each time a solution vector for temperatures. The first one (predictor) is considered the initial guess vector $\tilde{T}_n$. In order to obtain this vector, all of the thermal parameters with nonlinear expressions are calculated with the last values of temperature, T_{n-1}, so that they become a constant for this step of the calculation. In this way, the system can be solved like a linear system. Now having the initial guess vector $\tilde{T}_n$, the final solution vector for this time step can be obtained. Again, the thermal parameters with nonlinear expressions are evaluated so that they become constants in this step of calculation, but this time they are evaluated with the initial guess temperatures $\tilde{T}_n$.

Predictor: $$S \cdot \rho \cdot c_{n-1} \cdot \frac{\tilde{T}_n - T_{n-1}}{\tau} = S \cdot f_{n-1} + \sum_{k=0}^{3} \delta_k \cdot q_k\left(\bar{T}_{n-1}, \tilde{T}_n\right) \tag{31}$$

Corrector: $$S \cdot \rho \cdot \tilde{c}_n \cdot \frac{T_n - T_{n-1}}{\tau} = S \cdot \tilde{f}_n + \sum_{k=0}^{3} \delta_k \cdot q_k\left(\tilde{\bar{T}}_n, T_n\right) \tag{32}$$

A wire bundle with 27 wires was simulated and experimented. Twelve wires were carrying current, and the real distribution, currents and temperatures were known. The simulation was carried out with an $N \times N$ grid, with N = 100, 200, 300, 400. Results are shown in table 4, from where one can conclude that the algorithm is robust and that the discrete model provides accurate results starting from low-resolution grids.

N	T_{min}	T_{max}	C. time (s)
100	83.43	88.98	11.6
200	83.53	89.09	125
300	82.94	88.47	456
400	82.60	88.15	1892

Table 4: Computational results for different values of N

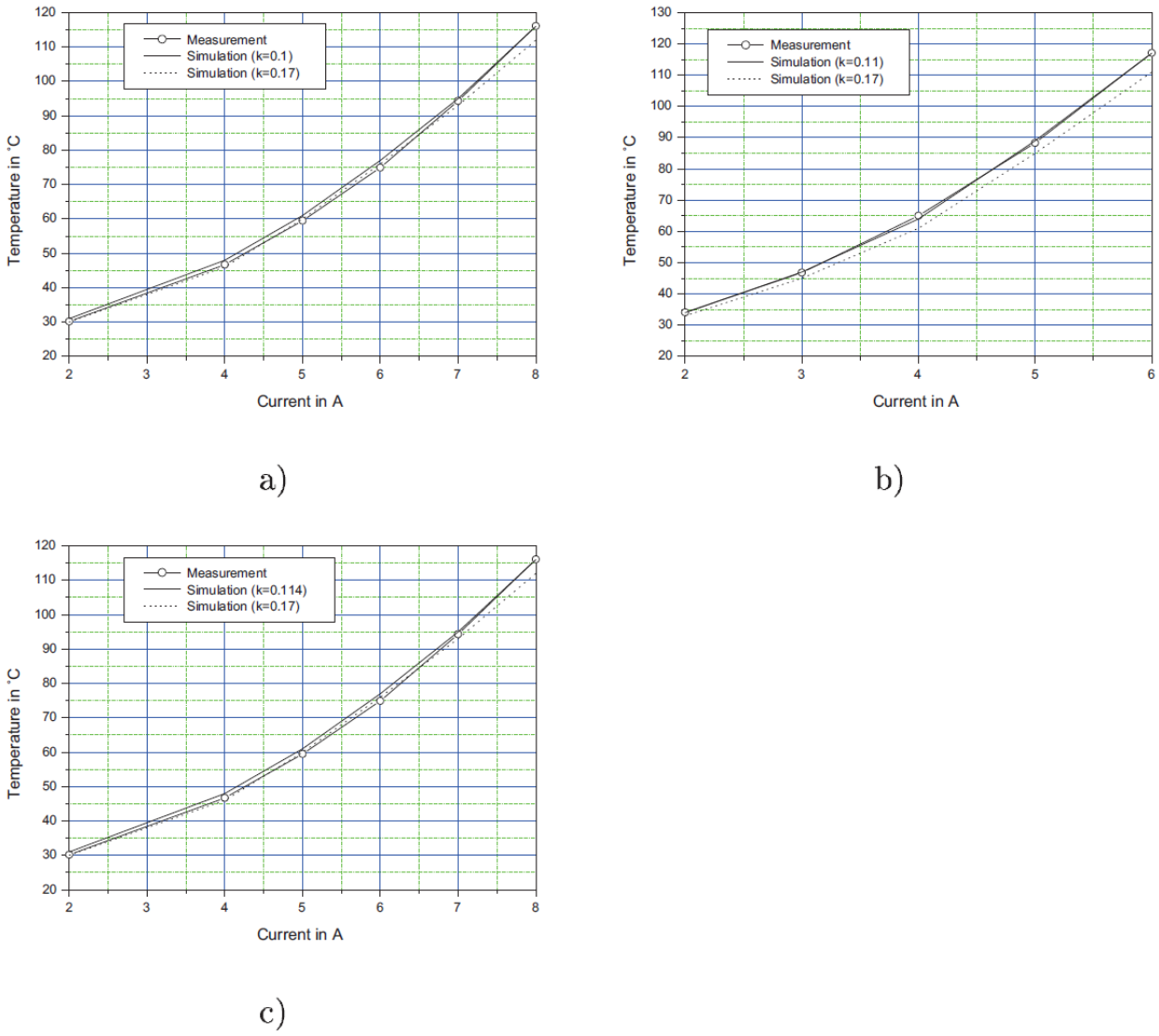

Fig. 28: Experimental and computer simulation results for electro-wires with different numbers of wires, filling factors and heat conductivities of materials between the wires

In Fig. 28.a and Fig. 28.b one can see how considering a filling factor and a lower heat conductivity for gaps makes the simulation curve get closer to experimental results. In Fig. 28.c, the number of wires was greater, which produced a smaller influence of the different heat conductivity coefficients in the result. In other terms, the filling factor is higher, which makes the air affect less to the other two cases.

With the purpose of finding better heat conductivity coefficients, Ilgevičius used the inverse problem solution method in [10]. Some experiments were carried out, and the temperature of each of the wires for known currents was obtained. Nevertheless, the exact distributions of the cables inside the bundles were unknown. Then, in order to reproduce the experiments by simulation, 10 random bundle distributions were generated for each of the wire bundles. The mean temperatures of the simulated cases were taken as results, with very good agreement with the experimental data after fitting the heat conductivity coefficients.

3.6. The finite element method for multi-wire bundles

3.6.1. Problem definition

The finite element method is widely used in many applications [11]. Due to the complexity and anisotropy of cable bundles, it is often used to estimate their temperature when subjected to current, especially when there is a simultaneous current conduction in various cables. Normally, and in this case too, the finite element method is only used to validate other simulation methods or for simulating simple problems.

Problems needing hundreds or thousands of iterative results of simulation would entail a huge computation time if the finite element method were used (e.g. genetic optimization algorithms). However, if the application requires just a few simulations, the finite element method is the one providing the most reliable results, compared to the rest of methods included in this document.

In [12], the finite element method is used to simulate multi-wire cables, which are thick and composed of various thinner cables, each of them with its own insulation. Results are compared to those of the so-called *fixed-point approach* (section 3.6.2).

Loos introduces a circle-packing algorithm in order to characterize the geometry of a cable bundle before generating a mesh for the 2D FEM (cross-section temperature distribution ignoring axial heat flux), obtaining a good accordance between experimental and simulation results.

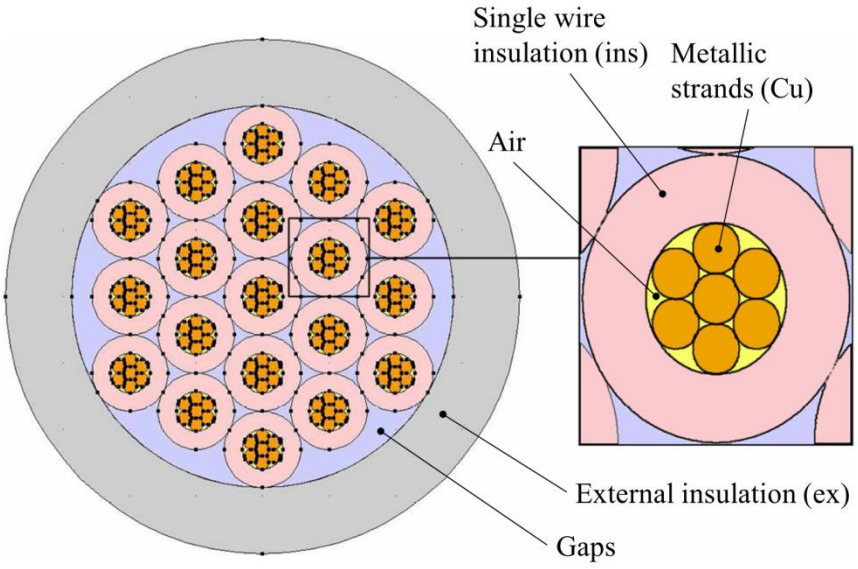

Fig. 29: Schematic cross-section of a multi-wire cable and a single cable

The FEM model uses the assumption of all of the thermal conductivities k to be invariable with respect to temperature, since they are actually considered weakly temperature-dependent. The starting point of the model is the general expression of the heat equation:

$$-\nabla(k\nabla T) = f \tag{33}$$

Both the heat conductivity *k* and the heat power density *f* are discontinuous, i.e. they have different values for each subdomain. Subdomains are noted as Ω_i, e.g. the insulation of one cable is one subdomain, and its conductor core is a different subdomain. The temperature dependence of the electric resistivity of the conductor material is considered linear as following:

$$\rho = \rho_0 \cdot \left[1 + \alpha_\rho (T - T_0)\right] \tag{34}$$

The linear consideration is sufficient when the temperature does not exceed 200ºC. Now having the expression for the linear dependence of the electrical resistivity with temperature, an expression for *f* can be obtained. First, the Ohm's law is used to establish a relation between *f* (W/m³) and the current, *I*. Equation (35) shows how integrating *f* in all the volume V^{core} (which is the volume of the inner cylinder of the cable, including air gaps) equals the total Joule heat of the cable. Then, since *f* is assumed constant, the result of the integral is the product of *f* and V^{core}, which enables to express *f* as in the second line of (35). Note that the division of the volume by the length of the cable *L* produces the cross-section area of the core $A^{core} = \pi r_{in}^2$. This area differs from A^{Cu}, which is the effective electrical cable cross-section, i.e. the sum of areas of all of the conductor strands in the core of the cable, excluding the air gaps. Note that the *Cu* superscript is used to refer the conductor material for clarity, but it could be also *Al* for aluminum or others.

$$\begin{aligned} \int_{V^{core}} f dx &= U \cdot I = RI^2 = \frac{\rho L}{A^{Cu}} I^2 \\ f &= \frac{\rho L}{V^{core} A^{Cu}} I^2 = \frac{\rho}{A^{core} A^{Cu}} I^2 \end{aligned} \tag{35}$$

Since the area of the domain wherein $f > 0$ is made of metal and small gaps of air, it is necessary to use a mixed conductivity k^{core}:

$$\begin{aligned} k^{core} &= \beta k^{Cu} - (1 - \beta) k^{air} \\ \beta &= \frac{A^{Cu}}{A^{core}} \end{aligned} \tag{36}$$

Now regarding the complete bundle, in practice multi-wire cables are pressed, so that air gaps inside them are also small. It is thus convenient to apply the same mixed conductivity for the gaps between cables:

$$k^{gaps} = \frac{k^{air} \cdot A^{gaps} + \sum_{n=1}^{N} k_n^{ins} \cdot A_n^{ins}}{A^{gaps} + \sum_{n=1}^{N} A_n^{ins}} \tag{37}$$

The boundary conditions of the multi-wire bundle are first defined by the air convection and radiation, applied to the external contour of the multi-wire bundle:

$$\begin{aligned} \alpha(T) &= \underbrace{\left(\frac{\alpha_d}{\sqrt{d^{ex}}} + \alpha_T \sqrt[6]{T - T_{env}}\right)^2}_{convection} + \underbrace{\varepsilon\sigma(T^4 + T_{env}^4)(T + T_{env})}_{radiation} \\ -k^{ex}\frac{\partial T}{\partial n} &= \alpha(T)(T - T_{env}) \end{aligned} \tag{38}$$

It is important to keep in mind that the radiation term of $\alpha(T)$ must use temperatures in Kelvin.

Unlike other methods, the FEM needs a description of the multi-wire bundle geometry, which can be achieved by applying a circle-packing algorithm to the set of circles representing the different diameters of wires inside the multi-wire bundle. Once the circle packing is completed, it is easy to solve the problem with usual software tools for FEM.

The geometry description needs the position, the core and the insulator diameter of each of the wires, as well as the inner and the outer diameter of the external insulation. Since the distribution of the wires in the bundle after the packing algorithm is unknown and irregular, the outer insulation must be fit by a simple optimizing algorithm capable of finding the smallest circle enclosing all of the wires of the bundle. All of this is detailed in [12].

This set of information is used to carry a discretization of the domain out, before the resolution of the elliptic problem. In this reference, the used solver is COMSOL Multiphysics 3.5a in combination with Matlab, with an automatic mesh generator into triangular elements with quadratic basis functions.

3.6.2. Comparison of calculation and measurement results

The comparison between the finite-element approach and experimental results of [12] is included in section 3.7.5, along with the results of the fixed-point approach, which is explained in the next section.

3.7. The fixed-point approach in multi-wire bundles

3.7.1. Single wire

Loos applies conservation of energy in order to derive formulae enabling estimations of temperature distributions inside single wires. Obtained results are used thereafter to predict multi-wire bundle temperatures by means of average value expressions. Lastly, the fixed-point equation is derived in order to determine unknown temperatures.

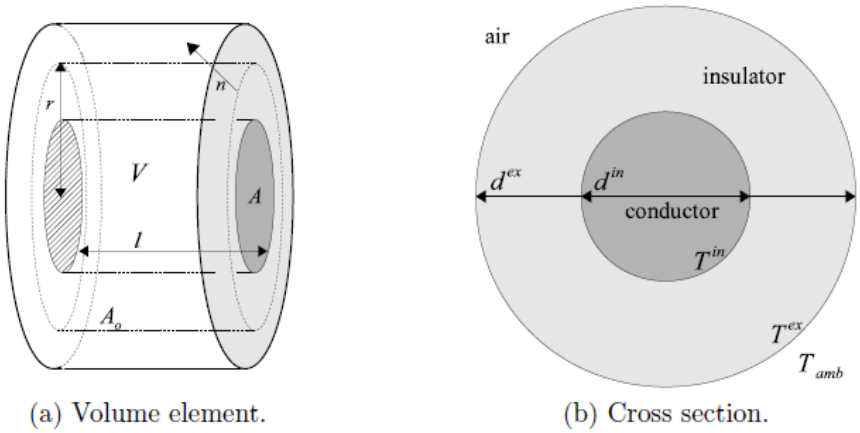

(a) Volume element. (b) Cross section.

Fig. 30: Single cable with solid interior conductor

In a similar manner to (15), an analytical expression for the temperature is derived, based on the conservation of energy. It establishes a relation between the external and the internal temperature of a single wire, assuming rotational symmetry:

$$T^{in} - T^{ex} = \frac{\rho I^2}{2\pi k^{ex} A^{in}} \ln \frac{d^{ex}}{d^{in}} \tag{39}$$

At the same time, the relation between the external temperature and the ambient temperature comes as the following:

$$T^{ex} - T_{amb} = \frac{\rho I^2}{\pi d^{ex} \alpha(T^{ex}) A^{in}} \tag{40}$$

3.7.2. Multi-wire cables

Similar expressions can be obtained for the multi-wire bundle, by means of isotropization, as described in section 3.4. De external and the internal diameters are defined as:

$$D^{ex} = \sqrt{\sum_{n=1}^{N} (d_n^{ex})^2} \quad \text{and} \quad D^{in} = \sqrt{\sum_{n=1}^{N} \left(d_n^{in}\right)^2} \tag{41}$$

Likewise, the cross-sectional areas are also defined as following:

$$\begin{aligned} A^{cond} &= \sum_{n=1}^{N} A_n^{core} \\ A^{iso} &= \frac{\pi}{4}\left((D^{ex})^2 - \left(D^{in}\right)^2\right) \\ A^{air} &= \frac{\pi}{4}\left(\left(d^{in}\right)^2 - (D^{ex})^2\right) \end{aligned} \tag{42}$$

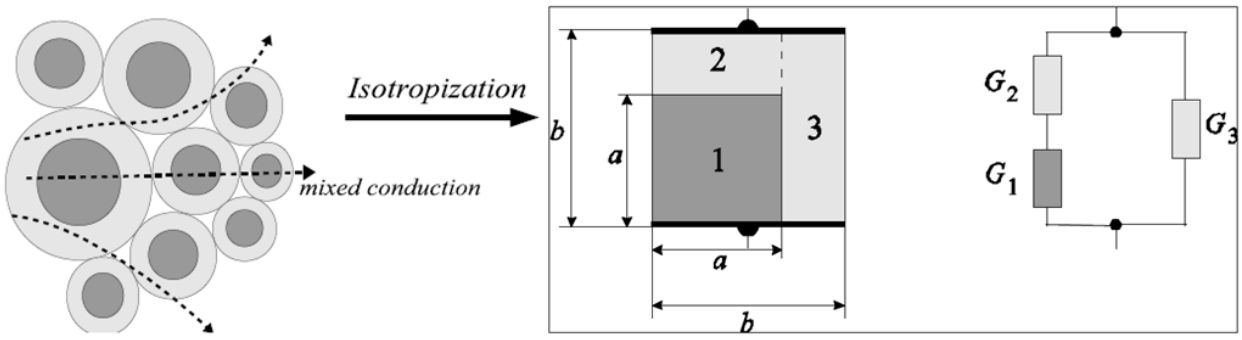

Fig. 31: Geometrical model for the determination of the average heat conductivity

The conductivities of the cores and the insulations k^{cond} and k^{iso} are calculated as the weighted arithmetic mean of their respective conductivities:

$$\begin{aligned} k^{cond} &= \frac{\sum_{n=1}^{N} A_n^{core} k_n^{Cu}}{A^{cond}} \\ k^{iso} &= \frac{\pi}{4} \frac{\sum_{n=1}^{N} \left((d_n^{ex})^2 - \left(d_n^{in}\right)^2\right) k_n^{iso}}{A^{iso}} \end{aligned} \tag{43}$$

The heat conduction is considered rotationally symmetrical in this approach. Hence, a part of the heat flows throughout both the cable cores and their insulations, and the rest is conducted only across the insulations, as one can see in Fig. 31. In this figure, one can see the parameters *a* and *b*, which must be determined preserving the cross-sectional areas:

$$\begin{aligned} A^{cond} &= a^2 \\ A^{iso} &= b^2 - a^2 \end{aligned} \tag{44}$$

Adding the parallel resistances one obtains the equivalent conductivity in vertical position:

$$k^{c/i} = \frac{1}{\frac{1}{k^{cond}} + \frac{b-a}{a} \cdot \frac{1}{k^{iso}}} + \frac{b-a}{a} \cdot k^{iso} \tag{45}$$

Now the mean heat conductivity can be obtained by weighting with respect to the corresponding areas:

$$k^{mean} = \frac{A^{iso} + A^{cond}}{A^{iso} + A^{cond} + A^{air}} k^{c/i} + \frac{A^{air}}{A^{iso} + A^{cond} + A^{air}} k^{air} \tag{46}$$

Lastly, the specific Joule heat is expressed in unit-length units (W/m):

$$p(T) = \frac{P}{L} = \sum_{n=1}^{N} \frac{\rho_n(T) I_n^2}{A_n^{Cu}} \tag{47}$$

Using the latter derivations, equations (39) and (40) can be rewritten:

$$\begin{aligned} T^{in} - T^{ex} &= \frac{p(T)}{2\pi k^{ex}} \ln \frac{d^{ex}}{d^{in}} \\ T^{ex} - T_{amb} &= \frac{p(T)}{\pi d^{ex} \alpha(T^{ex})} \end{aligned} \tag{48}$$

In order to calculate the value of the electric resistivity ρ, it is necessary to estimate the temperature distribution also over the cable core. For this purpose, one can express de unit-length specific heat inside a cylinder for radius $r \leq r^{in}$:

$$p(r) = \frac{4r^2}{(d^{in})^2} p(T) \tag{49}$$

Additionally, the definition of k^{mean} implies that $p(r)$ can be expressed as a function of r and the temperature distribution, as in (50). Integrating over $r \in [0, r^{in}]$ yields equation (51), which introduces T^{centre}, the temperature in the center of the wire.

$$p(r) = -2\pi r \cdot k^{mean} \cdot \frac{dT(r)}{dr} \tag{50}$$

$$T^{centre} - T^{in} = \frac{p(T)}{4\pi k^{mean}} \tag{51}$$

3.7.3. Temperature dependence of the resistivity and the heat transfer coefficient

In the context of the fixed-point approach, Loos sets the resistivity of the conductor material to be calculated using the mean temperature of the core:

$$T^{mean} = \frac{1}{2}\left(T^{centre} + T^{in}\right) \tag{52}$$

$$\rho(T^{mean}) = \rho_0\left[1 + \alpha_\rho(T^{mean} - T_0)\right] \tag{53}$$

3.7.4. Fixed point mapping

A fixed-point iterative approach is carried out in order to determine the three temperatures T^{ex}, T^{in} and T^{centre}. The following iterative sentence is defined:

$$T^{k+1} = h\left(T^k\right)$$
$$\text{where } T^k = \begin{pmatrix} T^{ex} \\ T^{in} \\ T^{centre} \end{pmatrix}^k \tag{54}$$

The $h(T)$ term in the sequence is a temperature mapping as defined in (55). It is proven in [12] that there exists a unique solution of $T \in \mathbb{R}^3$ such that $h(T) = T$.

$$h(T) = \begin{pmatrix} T_{env} + \dfrac{p(T^{mean})}{\pi d^{ex}\alpha(T^{ex})} \\ T^{ex} + \dfrac{p(T^{mean})}{2\pi k^{ex}} \ln\dfrac{d^{ex}}{d^{in}} \\ T^{in} + \dfrac{p(T^{mean})}{4\pi k^{mean}} \end{pmatrix}, \qquad h \in C^1 : \mathbb{R}^3 \longrightarrow \mathbb{R}^3 \tag{55}$$

3.7.5. Comparison of calculation and measurement results

A multi-wire cable composed by 33 single wires belonging to the main harness of a car, provided by an automotive cable supplier. With the aim of observing the importance of the cable layout, the experiment was carried out with three bundles with three different layouts and diameters:

1. Inner layout: Current-carrying wires centered in the bundle
2. Outer layout: Current-carrying wires at the outline of the bundle layout
3. Monte Carlo layout: Random distribution of currents inside the bundle

The layout definitions are qualitative, because the exact distribution of the bundle layout is not available in [12], and it is difficult to obtain in most situations.

Table 5 contains the results of the measurement (EXP), along with those of the finite elements approach (FE) and the fixed-point approach (FP). In this table, T_{avg} stands for the weighted average temperature of the metallic conductors.

Measurements reveal that inside a bundle, current-carrying cables that are in contact reach higher temperatures than the same cables when they are placed as in the outer layout, because they are capable of

transferring heat to the environment. However, whereas the *worst case* of a cable bundle layout corresponds to the inner layout described in this section, it is remarkable that the *best-case* layout is not trivial. This is discussed in [13] and studied in [14], that there are some layouts capable of lowering the temperature below the values achieved by the outer layout.

	Inner layout			Outer layout			Monte Carlo layout		
	EXP	FE	FP	EXP	FE	FP	EXP	FE	FP
$T_{avg} - T_{env}$	61.6	65.6	60.8	63.0	61.7	61.8	61.0	63.6	62.2
$T_{max} - T_{env}$	69.7	74.2	–	66.6	65.2	–	64.5	67.2	–
$T_{min} - T_{env}$	55.0	57.2	53.5	57.4	58.0	55.1	54.6	57.9	55.2

Table 5: Comparison of measured and computed temperature differences in Kelvin (EXP = Measurement, FE = Finite elements approach, FP = Fixed-point approach

Comparing the finite-element approach with measured results, one can see that the temperature rises differ 6.46% in the inner layout, 2.10% in the outer layout, and 4.19% in the Monte Carlo layout. Measuring inaccuracies, numerical errors and uncertainties in all of the parameters are included in these percentages of discrepancy. One of the factors explaining this rather large difference is the fact that the finite elements approach needs the exact distribution of the wire-bundle layout (precisely, the fixed-point approach cannot provide the maximum temperature of the bundle because the position of the single wires is ignored). The lack of a reproduction of the layout of the measured bundle entails a visible error in the result. The layout in the finite elements approach is prepared by means of a circle-packing algorithm, but the final layout has not been found to be similar in the measured bundle.

	Inner layout		Outer layout		Monte Carlo layout	
	Finite elements	Fixed point	Finite elements	Fixed point	Finite elements	Fixed point
T_{avg}	6.5%	1.3%	2.1%	1.9%	4.3%	2.0%
T_{max}	6.5%	–	2.1%	–	4.2%	–

Table 6: Relative error of simulations compared to measurements

The resulting average and minimum temperatures of the fixed-point approach are relatively similar for the three layouts. This is an expected result, since the fixed-point approach does not use the position of each cable for the calculation. That is precisely the reason why only the average and minimum temperatures (T^{mean} and T^{ex}) temperatures are given in Table 5. The slight differences are due to actual differences in the environment temperature and the diameter of the bundle.

The results of the fixed-point approach only comprehend the average and minimum temperatures, but they have better accordance with the measurements, compared to the case of the finite elements approach.

Discrepancy in terms of the average temperature is as low as 1.3%, 1.9% and 2.0% for the inner, outer and Monte Carlo layouts.

3.8. Efficiency-oriented optimization of wiring systems in vehicle applications

Just as it has been discussed in the introduction of this thesis and in many other occasions along the document, the weight reduction of the wiring systems pursuits a reduction of the CO_2 emissions. A second but not less important aspect of the weight reduction is the wish that the extra cost is zero or even a benefit.

Ließ describes in [15] considerations about the optimal dimensions of the wires in a car caring only about efficiency. The heavier the wiring system is, the more energy the car needs to gain speed. On the contrary, the thinner the wires are, the more power is lost as Joule heat. These opposed laws make it easy to understand that there is an optimum point for the dimensions of the wires, i.e. their current density.

3.8.1. Power requirements

The relevant parameters of a wire in this optimization are the Joule power P_J and its mass m_{wire}, which are expressed as in equations (56) and (57). L stands for the length of the wire, k for the electrical conductivity of the conductor material, A for the cross-section area of the wire and ρ for the density of the conductor material.

$$P_J = \frac{L}{k \cdot A} I^2 \tag{56}$$

$$m_{wire} = \rho \cdot L \cdot A \tag{57}$$

The idea is to provide in one expression the entire power consumption of a car. The latter P_{wire} must be summed to the required power for moving the car against the mechanical friction, P_f; to the necessary mechanical power to surmount slopes, P_s; the necessary mechanical power to accelerate, P_a; and to the required power for moving the car against the aerodynamic resistance, P_w. Their expressions are represented by equations (58) to (61), where:

- g is the gravitation constant (9.81m/s²)
- m is the mass of the vehicle, expressed as $m = m_{wire} + m_{veh} = \rho\ L\ A + m_{veh}$ (m_{veh} is the mass of the vehicle without the wiring system)
- v is the speed of the vehicle
- θ is the ascending angle in a slope
- α is the relative acceleration coefficient expressed as $\alpha = a / g$ (the acceleration measured as the g-force)
- c_w is the specific air resistance in s^2N/m^4
- A_w is the drag plane area in m^2.

$$P_f = \mu \cdot g \cdot m \cdot v \tag{58}$$

$$P_s = \sin\theta \cdot g \cdot m \cdot v \tag{59}$$

$$P_a = \alpha \cdot g \cdot m \cdot v \tag{60}$$

$$P_w = c_w \cdot A_w \cdot v^3 \tag{61}$$

$$P = P_J + P_f + P_s + P_a + P_w \tag{62}$$

A complete expression of equation (62) can be rewritten as in equation (63):

$$P = \frac{L}{kA} I^2 + (\mu + \sin\theta + \alpha)(\rho LA + m_{veh}) gv + c_w A_w v^3 \tag{63}$$

3.8.2. Optimization of the power requirements

Optimal current density, J

Equation (63) can be differentiated with respect to the cross-sectional area of the wire, *A*, and then equaled to zero in order to find the relative optimal points as following:

$$\begin{aligned} &\frac{dP}{dA} = -\frac{LI^2}{kA^2} + (\mu + \sin\theta + \alpha)\rho Lgv = 0 \\ &\frac{I^2}{A^2} = \left(\frac{I}{A}\right)^2 = J^2 \end{aligned} \tag{64}$$

As a result, the optimal current density *J* is obtained, as shown by equation (65):

$$J = \sqrt{(\mu + \sin\theta + \alpha) k\rho gv} \tag{65}$$

It is remarkable that those parameters on which the optimum *J* depends are variable throughout time, such as the speed, the slope and the acceleration. On the other hand, the aerodynamic resistance does not play any role in its expression, because this power is completely independent of the size of the cables.

Optimal unit-length voltage drop, E

According to the Ohm's law, $E = J / k$, where *E* is the electric field intensity or the unit-length voltage drop. Therefore:

$$E = \frac{J}{k} = \frac{\sqrt{(\mu + \sin\theta + \alpha) k\rho gv}}{k} = \sqrt{\frac{(\mu + \sin\theta + \alpha)\rho gv}{k}} \tag{66}$$

Minimum power requirements

Replacing *J* by its expression and introducing the mass of conductor material m_{wire} in equation (62) provides the expression of the minimum required total power P_{min} for a vehicle operating in optimized state:

$$P_{min} = (\mu + \sin\theta + \alpha)(2m_{wire} + m_{veh})gv + c_w A_w v^3 \tag{67}$$

In this latter equation, the mass of the conductor material appears twice, resulting from the sum of the mechanical and the electrical losses. Note that this expression corresponds to the optimum power demands only if *J* accomplishes the equation (65). In the same way, one can easily derive from the latter equations that *J* is optimum if the electric losses equal the required mechanical power for moving the mass of conductor m_{wire} (equation (68)).

$$\begin{gathered} P_J = \frac{L}{k \cdot A} I^2 = \frac{L}{k} \cdot A \cdot J^2 = L \cdot A \cdot \rho \cdot (\mu + \sin\theta + \alpha)gv = m_{wire}(\mu + \sin\theta + \alpha) \cdot gv \\ P_{wire,\ min} = 2m_{wire}(\mu + \sin\theta + \alpha) \cdot gv = 2P_e \end{gathered} \tag{68}$$

Optimal material properties for a conductor

Being η_{wire} the efficiency of the wire, expressed as the fraction of power that arrives to the load with respect to the total transferred power, equation (69) shows how the unit-length voltage drop is affecting negatively this parameter (*U* is the supply voltage).

$$\eta_{wire} = 1 - \frac{P_e}{P_{supp.}} = 1 - \frac{I \cdot L \cdot E}{I \cdot U} = 1 - \frac{L}{U} \cdot E \tag{69}$$

Equation (66) can be rewritten as in (70), from where it is seen that *E* is proportional to the square root of the density-to-conductivity ratio, i.e. ρ / *k*.

$$\begin{gathered} E = \frac{J}{k} = C_1 \cdot \sqrt{\frac{\rho}{k}} \\ C_1 = \sqrt{(\mu + \sin\theta + \alpha)gv} \end{gathered} \tag{70}$$

Now retaking equation (69), it proves that lowering $\sqrt{\rho/k}$ increases the efficiency of the wire. Therefore, the most suitable material for a conductor –in electrical terms– is the one with higher k/ρ. Then, it is proved that aluminum is more suitable for vehicle applications than copper (k_{Al}/ρ_{Al}= 14.07m²Ω^{-1}kg^{-1}, k_{Cu}/ρ_{Cu}= 6.83m²Ω^{-1}kg^{-1}).

3.8.3.Extension of the basic equation

Mechanical-electrical conversion

Normally, the electric power of cars is converted from a mechanical source, which is the combustion engine. Thus, the electrical and the mechanical powers can be related by a mechanical-electrical conversion efficiency, $\eta_e < 1$, so that $P_e = \eta_e \cdot P_m$ (Fig. 32). Then, the total consumed power can be expressed as the sum of all the different mechanical powers fed by the engine, now including this P_m, which is the input mechanical power of the generator. Equation (71) shows how the generated electric power P_e is related to the Joule power of the wire, P_J, and the power transferred to the electrical loads, P_{tr}.

$$P_m = \frac{P_e}{\eta_e} = P_J + P_{tr} = \frac{LI^2}{kA} + P_{tr} \tag{71}$$

Now, the total power consumption expressed by equation (62) can be rewritten including the input power of the generator, P_m:

$$P = P_f + P_s + P_a + P_w + P_m = P_f + P_s + P_a + P_w + \frac{P_e}{\eta_e} \tag{72}$$

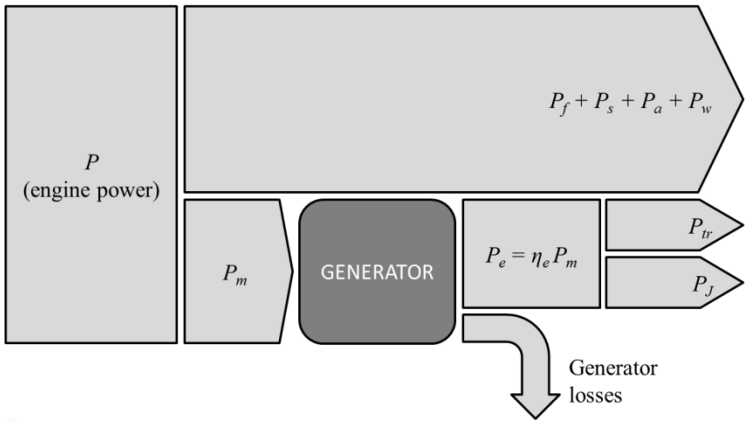

Fig. 32: Power balance of a combustion-engine car, as in equation (72)

Reproducing the derivation of equation (65) to find the optimum current density, J, it is now found including the mechanical-electrical conversion efficiency, η_e:

$$\frac{P_e}{\eta_e} = P_J + P_{tr} = \frac{LI^2}{kA} + P_{tr}$$

$$\frac{dP}{dA} = -\frac{LI^2}{\eta_e k A^2} + (\mu + \sin\theta + \alpha)\rho L g v = 0 \tag{73}$$

$$\boxed{J = \sqrt{\eta_e(\mu + \sin\theta + \alpha)k\rho g v}}$$

Since electric-driven vehicles have a different power balance (Fig. 33), the same extension for *J* may be done, which result is given by equation (74).

$$J = \sqrt{\frac{1}{\eta_{motor}}(\mu + \sin\theta + \alpha)k\rho g v} \tag{74}$$

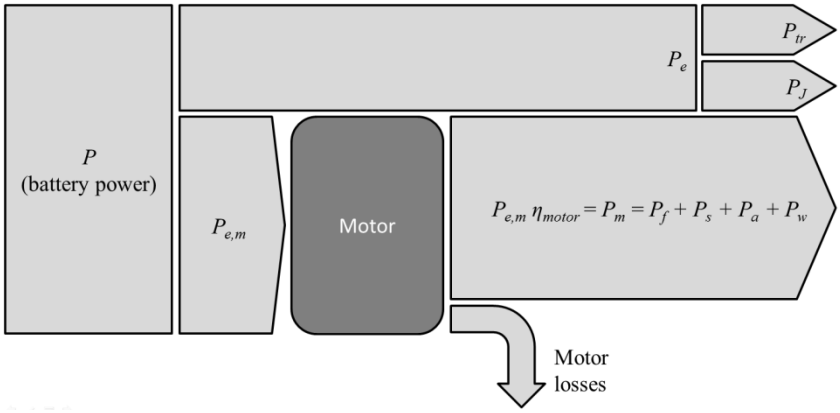

Fig. 33: Power balance of an electric-driven car (ignoring regenerative braking)

Ließ actually uses in [15] the same formula (73) for both electric and combustion cars, but reversing η_e in such a way that for electric cars this parameter is mandatorily greater than one. In other terms, $\eta_e = \eta_{motor}^{-1}$.

Mechanical recovering degree of efficiency

The regenerative braking must be also included in the optimization. It is characterized by a recovering efficiency, η_r:

$$\eta_r = \frac{(\sin\theta + \alpha)_{recovered}}{\sin\theta + \alpha} \tag{75}$$

Therefore, *J* can be rewritten as following:

$$J = \sqrt{\eta_e[\mu + (\sin\theta + \alpha)(1 - \eta_r)]k\rho g v} \tag{76}$$

Temperature influence in the electrical conductivity

The electrical conductivity *k* can be rewritten expressing its dependence on the temperature, as following:

$$k = \frac{k_0}{1 + \alpha_\rho(T - T_0)} \tag{77}$$

Where k_0 is the electrical conductivity of the conductor material at a reference temperature T_0; T is the temperature of the conductor; and α_ρ is the temperature coefficient of the electrical conductivity in K^{-1}. Therefore, J can be rewritten including these parameters:

$$J = \sqrt{\frac{\eta_e[\mu + (\sin\theta + \alpha)(1 - \eta_r)]k\rho g v}{1 + \alpha_\rho(T - T_0)}} \tag{78}$$

Insulation thickness

The minimum insulation thickness can be found by means of the maximum acceptable intensity of the electric field at the inner surface of the cable insulation. The electric field is related to the power supply voltage, U, as following:

$$U = rE_i \ln\frac{r + s}{r} \tag{79}$$

where r is the radius of the thinnest conductor among all cable sizes, s is the isolation thickness, and E_i is the intensity of the electric field at the inner insulation radius. s can be isolated in order to find an expression for its minimum value:

$$s = r\left(\exp\frac{U}{rE_i} - 1\right) \tag{80}$$

Mass of the insulation

Since the total mass of the insulation can be expressed as a function of the insulation thickness as in equation (81), an expression for the mass as a function of the power supply voltage can be also found using equations (80) and (81), as in equation (82), where ρ_i stands for the density of the insulation material.

$$m_i = \pi\rho_i L[(r + s)^2 - r^2] \tag{81}$$

$$m_i = \pi\rho_i L r^2\left(\exp\frac{2U}{rE_i} - 1\right) \tag{82}$$

3.8.4. Optimum current density

Considering all the prior aspects influencing the expression of the current density, its expression finally becomes as the following:

$$J = \sqrt{\frac{[\mu + (\sin\theta + \alpha)(1 - \eta_r)]k_0\eta_e g v}{1 + \alpha_\rho(T - T_0)}\left[\rho + \rho_i\left(\exp\frac{2U}{rE_i} - 1\right)\right]} \tag{83}$$

3.8.5. Quantitative values

Ließ evaluates his equations for the optimum current density and unit-length voltage drop, assigning possible values to all of the parameters:

Friction coefficient:	$\mu = 0.2$
Ascending slope coefficient:	$\sin\theta = 0.2$
Relative acceleration:	$\alpha = 0.2$
Electrical conductivity (copper):	$k_0 = 58.5 \cdot 10^6\ \Omega^{-1}\mathrm{m}^{-1}$
Temperature coefficient of electrical resistivity:	$\alpha_\rho = 4 \cdot 10^{-3}\ \mathrm{K}^{-1}$
Conductor material density:	$\rho = 8930 \frac{\mathrm{kg}}{\mathrm{m}^3}$
Insulation material density:	$\rho_i = 1100 \frac{\mathrm{kg}}{\mathrm{m}^3}$
Mechanical-electrical efficiency:	$\eta_e = 0.8$
Mechanical recovering efficiency:	$\eta_r = 0.0$
Gravitation constant:	$g = 9.81 \frac{\mathrm{m}}{s^2}$
Conductor radius:	$r = 3\ \mathrm{mm}$
Vehicle speed:	$v = 200\ \frac{\mathrm{km}}{\mathrm{h}}$
Electric field intensity in the insulation:	$E_i = 10^6\ \frac{V}{m}$
Power supply voltage:	$U = 1000\ \mathrm{V}$
Operating temperature:	$T = 120\ ^\circ\mathrm{C}$
Reference temperature:	$T_0 = 20\ ^\circ\mathrm{C}$

The result of this calculation is J = 10.4 A/mm² and E = 250mV/m.

3.9. Optimization of current-carrying multi-wire cables

3.9.1. Overview

In [14], Harbrecht formulates an optimization problem with the aim of finding the best bundle layout for a given set of wires. It consists of lowering the maximum steady temperature of the bundle down to its optimized value.

The packing density of the wire bundle must be considered in order to select the most convenient optimization strategy: the gradient-based strategy can be used for loose bundles, whereas densely packed bundles are optimized by means of layout heuristics, by means of a genetic algorithm. Mixed strategies are used as well. They are based on simulation, using the approaches described in sections 3.6 and 3.7.

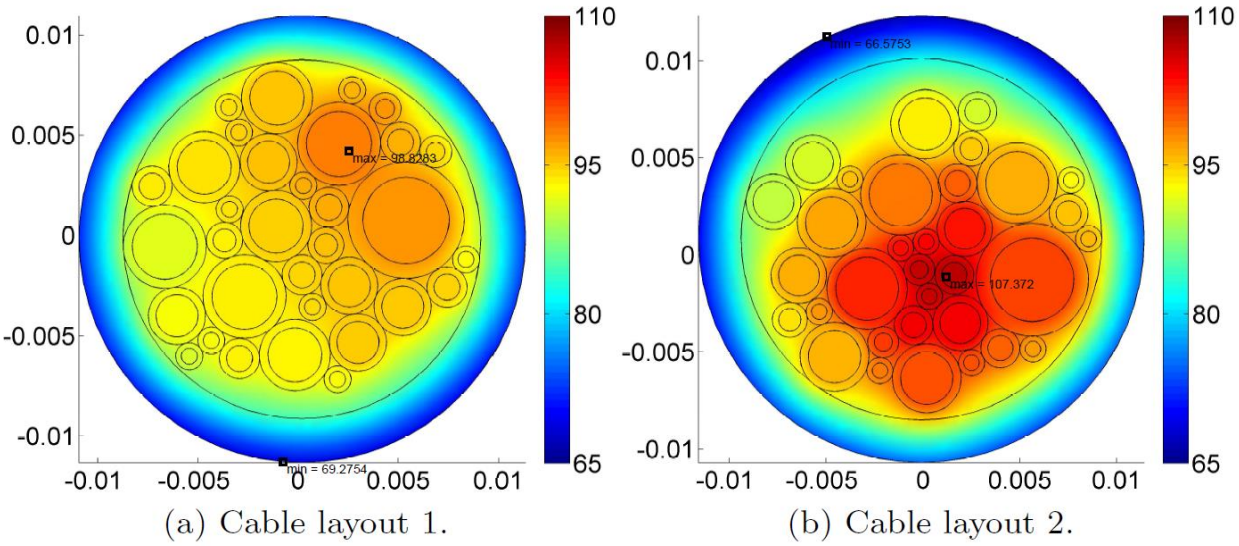

Fig. 34: Comparison of temperature distributions for equally composed multi-wire bundles with different layouts

An example of the importance of the bundle layout can be seen in Fig. 34, where two different layouts of 33 single wires are shown with different maximum temperatures (98.8ºC and 107.4ºC).

3.9.2. Optimization problem

The problem considers the dimensions of all of the wires in the bundle given and invariable. The currents are also given, as well as their electrical and thermal parameters. Therefore, the heat capacity, conductivity and specific heat generation are known from the beginning.

The optimization algorithm varies the bundle layout and thus the inner shape of the interior domain by positioning each single wire. In order to produce feasible results, it is necessary to keep constraints regarding the geometry of the bundle. First, none of the cables can overlap either between them or with the external insulation. In fact, the must be separated a certain distance to allow the creation of correct meshes for the finite-element simulation. It is important to fix de position of some cables to avoid axial

symmetry. For that reason, the first cable is centered, and the second is obligatorily placed on the right half of the interior domain.

Different algorithms are combined in order to solve the problem of the optimum bundle layout (Fig. 35). First, a global minimum is approximated by using *M* different initial layouts, obtained by heuristics and the application of the circle-packing algorithm described in [12], here referred as *squeezing algorithm*.

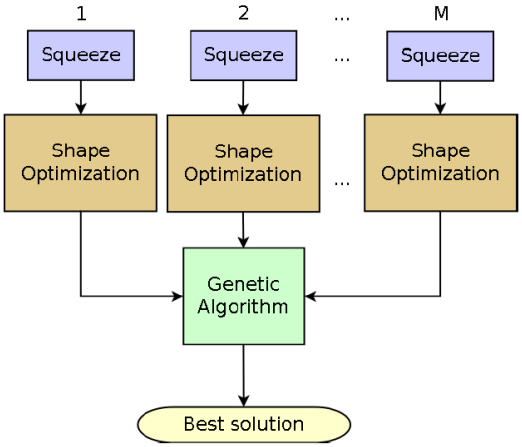

Fig. 35: Optimization strategy

The shape optimization is a gradient-based strategy, which is not always satisfactory. That is why *M* local minima candidates are passed to the genetic algorithm, which tries to find better solutions for each of them. The final solutions can be the exact or similar local minima. It is convenient to couple these algorithms because using exclusively a genetic algorithm would have an excessively long and unpractical resolution time.

3.9.3. Initialization

The circle-packing algorithm starts from an initial template wherein all of the cables are sufficiently separated, and then they are pressed towards the center iteratively. Since in this optimization problem the diameter of the external insulation is given and invariable, they are pressed together until they fit the outer circumference. If this is unachievable, the template is not accepted.

When the conductor materials of the wires are the same, higher current densities *J* imply higher specific heat generations (f). Then the wires can be sorted with different strategies considering this fact.

The template creation consists of assigning a position from one to *N* to each of the wires, being no. 1 the center of the template. The following positions form circumference layers around the center, with spiral assignment (Fig. 36).

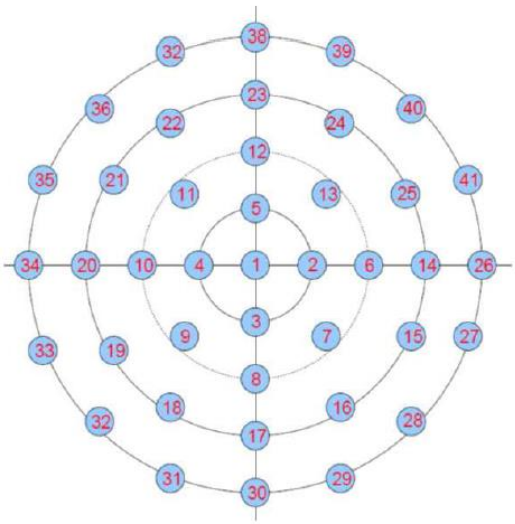

Fig. 36: Initial template for the circle-packing algorithm used in [12]

The different template types are:

1. Inner layout: descending order of J_n (wires with highest J gathered near the center)
2. Outer layout: ascending order of J_n (wires with highest J near the outer contour of the template)
3. Alternative outer layout: ascending order of J_n, but not assigned consecutively, but with steps of 2, 3, 4 or 5 positions (outer layout 2, outer layout 3, outer layout 4 and outer layout 5).
4. Opposed layout: in every template layer, consecutive wires (according to ascending order of J_n) are placed in such a way that they are as far as possible from each other.
5. Monte Carlo layout: Randomly assigned positions

3.9.4. Genetic algorithm

A genetic algorithm is a stochastic optimization method that uses the concept of the natural evolution. It starts with an initial population of individuals, and they evolve throughout several generations by means of the operations *crossover* and *mutation* (Fig. 37). In each generation, the fittest individuals survive and reproduce.

In this case, the initial population is composed by the first M bundle layouts described in section **¡Error! No se encuentra el origen de la referencia.**. In order to determine which layouts are better than others, their temperatures are simulated. From one generation to the next, the coordinates of the wires will change.

- The k best individuals are directly transmitted to the next generation as *elite*. Parents are randomly selected from the rest of the population.
- The coordinates of the parents are *crossed* and *mutated* to produce *children*.
- The new population of coordinates replaces the old one.

In Harbrecht's solution, the genetic algorithm proposes a bundle layout. This is expected to approximate a local minimum. First, it must be converted to a physically feasible wire bundle. Therefore, the circle-packing algorithm is applied to the genetic algorithm's solution in order to avoid overlapping. In addition, the shape optimization algorithm is applied to convert the approximated minimum into a strict local minimum.

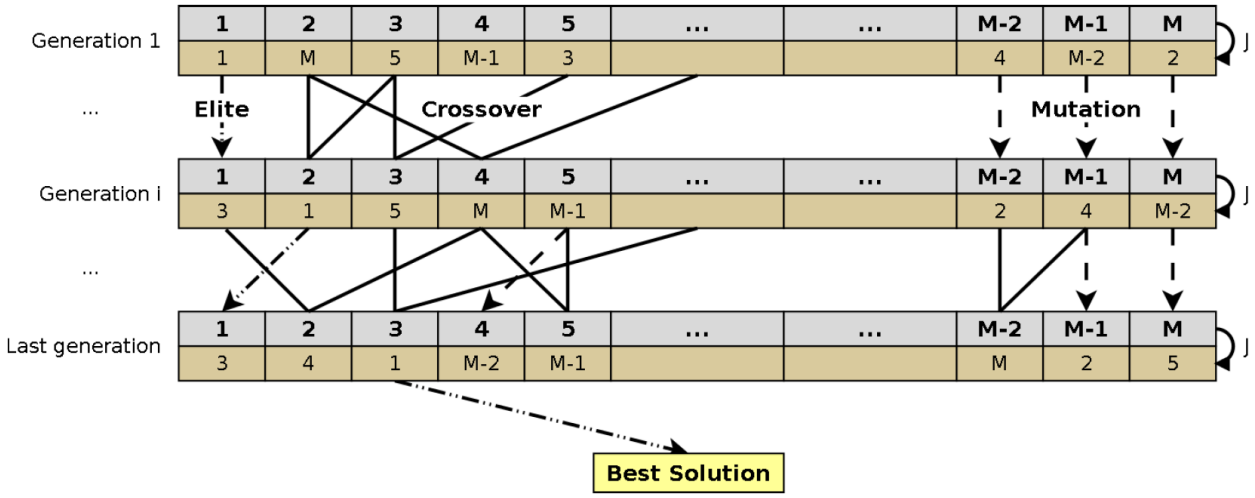

Fig. 37: Diagram of the genetic algorithm

Crossover

Each individual is expressed as a vector. The reproduction of two of them (a pair of parents) gives a new vector (child), for which each component is a randomly selected value from one individual of the pair.

$$\text{parents}\begin{cases} a = [a_1, a_2, a_3, a_4, a_5, \dots, a_m] \\ b = [b_1, b_2, b_3, b_4, b_5, \dots, b_m] \end{cases}$$
$$\text{child} \longrightarrow c = [b_1, b_2, a_3, b_4, a_5, \dots, a_m]$$

Mutation

Mutation consists of modifying some of the components of a parent vector. For example (given in [14]), selecting a random number of components and averaging them with a random number, *r*.

$$\text{parent}\,\{a = [a_1, a_2, a_3, a_4, a_5, \dots, a_m]$$
$$\text{child} \longrightarrow c = \left[a_1, \frac{1}{2}(a_2 + r_2), a_3, a_4, \frac{1}{2}(a_5 + r_5), \dots, a_m\right]$$

The child individuals must be feasible, i.e. constraints are accomplished. Otherwise, the packing algorithm is applied. If constraints cannot be accomplished, then a new one is created.

Stopping criterion

The genetic algorithm has no implicit manners to detect when to stop. In order to stop the execution of the optimization, it is defined in [14] to stop after a certain number of generations if the fitness of the best individual does not improve during a certain number of steps.

3.9.5. Complete algorithm

A flowchart of the entire process of optimization can be seen in Fig. 38. First, all the input data, such as physical parameters, is read from input files. If it is necessary, one can specially provide at this stage specific convergence criteria. Additionally, the filling factor of the bundle is determined, so that the optimization algorithm can start.

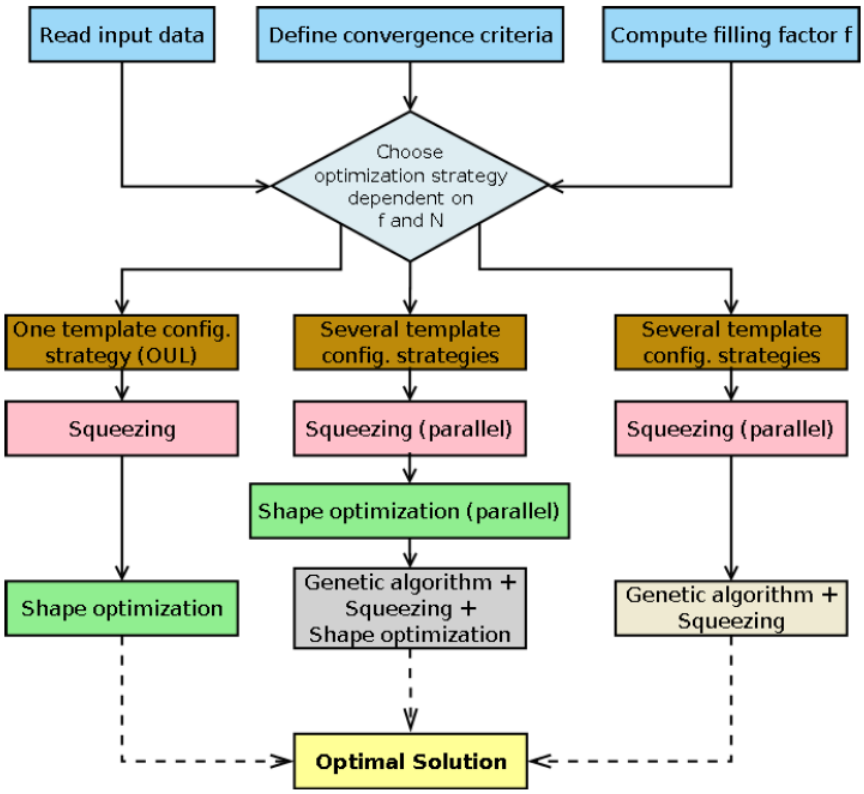

Fig. 38: Programmatic flowchart of the entire process of multi-wire cable optimization

Depending on the filling factor and the number of wires, the optimization engine will carry out different strategies. In cases of few wires and low filling factors, only one initial template is used ($M = 1$). In [14], Harbrecht recommends using the outer layout template considering his own experience. After the *squeezing* algorithm has packed the wires, one shape optimization attempt is performed, which approximates the best solution.

In contrast, for densely packed cables the shape optimization is not used. Instead, the prior detailed template configurations are initialized and then taken by the genetic algorithm, where all of the new configurations will be made feasible by means of the squeezing algorithm. According to Harbrecht, this

process takes a long time and is often unable to provide a better solution than the best among the *M* initial layouts.

The most complex branch of the program corresponds to moderately packed bundles, with which all of the mentioned algorithms are used in combination.

3.9.6. Results

In the following example, the environment temperature was 33.2ºC and the filling factor around 63%, with an inner diameter of the external insulation equal to 19.2mm and outer equal to 23.6mm. Fig. 39 depicts the temperature distributions of three of the initial layouts (inner, outer and opposed), with a maximum temperature of 108.5ºC for the inner layout.

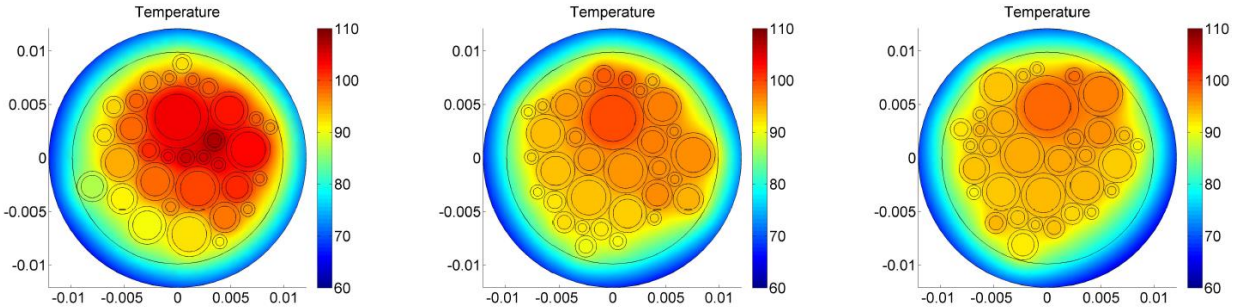

Fig. 39: Temperature distributions in 33-wire bundles for: (a) inner layout; (b) outer layout; (c) opposed layout

The result of the genetic algorithm provides a maximum temperature of 92.4ºC, which brings a 16.1ºC temperature difference between the worst and the best layouts. Considering strictly the temperature rise, the reduction is about 21%. The entire optimization process took about 42 hours.

Temperature distributions of the best three individuals of the genetic algorithm can be seen in Fig. 40.

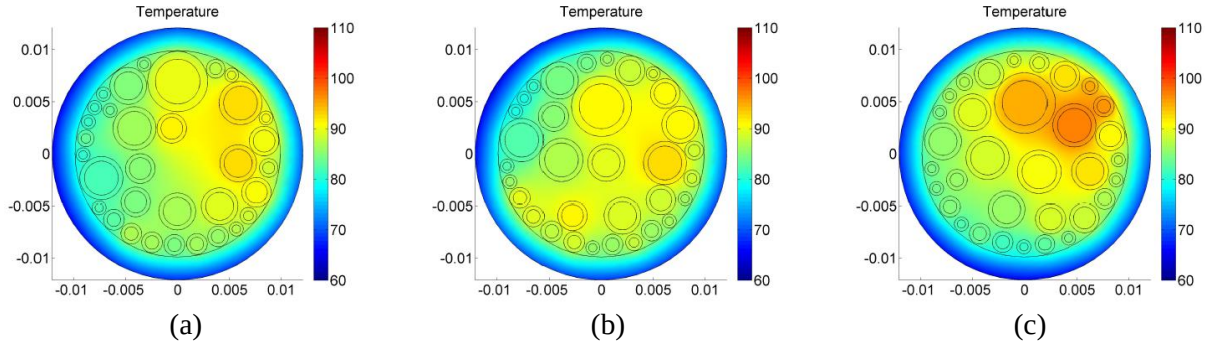

Fig. 40: Improved cable configurations obtained by application of the genetic algorithm for 33 single cables. (a) best; (b) second best; (c) third best

3.10. Optimization of multi-voltage automotive power supply systems

3.10.1. Definitions

The introduction of micro-hybrid, hybrid and electric vehicles is one of the reasons why the topic of on-board multi-voltage power supply systems has gained importance in recent years. With the aim of minimizing the cost, weight and volume of such wiring systems, an optimization method is introduced in [6]. This method is based on the simulation system from [7], extended for axial heat conduction using an equivalent-circuit method based on the transmission lines theory (Fig. 41).

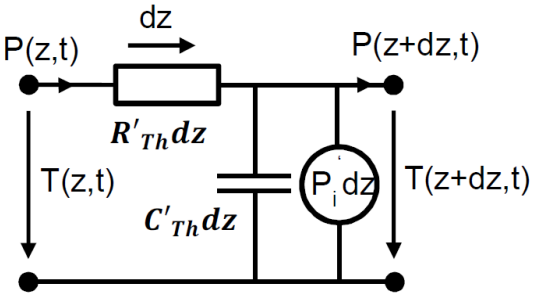

Fig. 41: Equivalent thermal circuit for a short cable segment, with length *dz*, axial heat power *P*(*z*,*t*)

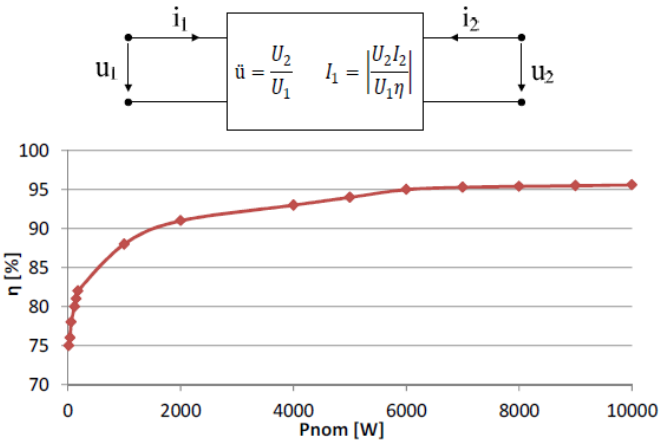

Fig. 42: Simple behavioral model for a DC/DC converter and its efficiency with respect to its rated power, *Pnom*

The approach here uses models for the main electric components of the car, such as batteries, contacts, or fuses. Electric loads are represented as controlled current-sources with rated currents and maximum acceptable voltage drops. The DC/DC converters are modeled considering their efficiency (Fig. 42).

3.10.2. Structure of the on-board power supply system

Multi-voltage systems can be outlined through different architectures. Diebig considers two possibilities:

1. Every DC/DC converter is connected to the main power supply (Fig. 43.a).
2. One DC/DC converter is connected to the main power supply, being the rest connected in series with it (Fig. 43.b).

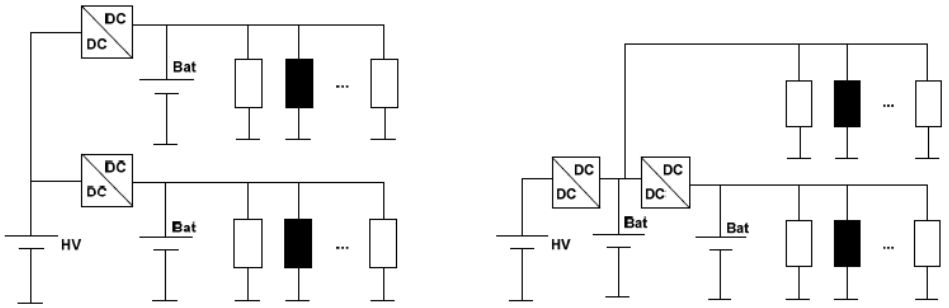

Fig. 43: Different architectures

In Fig. 43, HV stands for *high voltage*, and it represents the battery of an electric vehicle. However, these architectures are characterized in the same way if the converters are connected to the alternator of a combustion engine car.

An important aspect of the feasibility of the power supply system is the available space. This is also considered in the optimization process: available positions for the DC/DC converters are given, in such a way that the distances between components are known (Fig. 44).

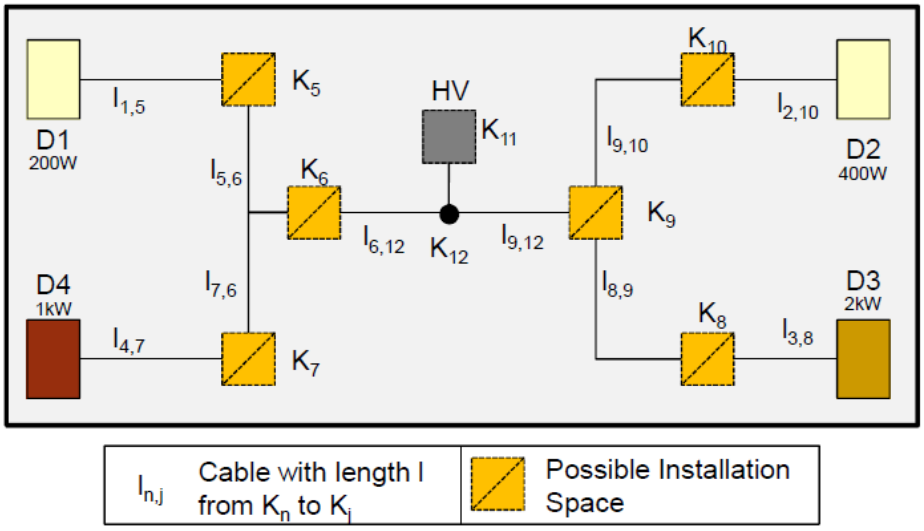

Fig. 44: Example of a system with 6 possible spaces for DC/DC converters

2.10.3. Rating functions

Cables

It is considered in [6] that the weight of the cable insulation can be neglected, due to its low density in comparison to copper's. The weight of the cable conductor can be easily estimated using the density of the conductor material (e.g. copper), its cross-section and the cable length. In order to include the unconsidered weight of the connectors and the neglected weight of the insulation, a 50% is added to the weight of the metallic core of the wires.

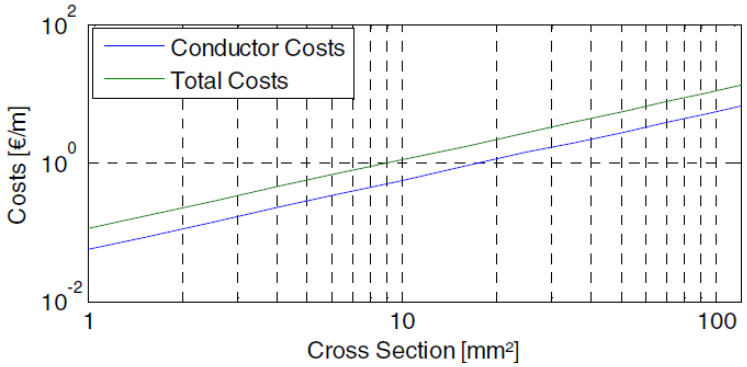

Fig. 45: Cost function over cross-section of wires from 1mm² to 100mm²

The costs of the wire (Fig. 45) are calculated by means of its weight. The price for copper in February, 2013 was 5.85€/kg according to [6]. A correction factor equal to 2 is used in order to comprehend the insulation and manufacturing costs.

DC/DC converters

In order to create a function capable of predict the weight of a converter with respect to its rated power, the weights of various existing power DC/DC have been gathered. The weight function is obtained by fitting a 2nd-order polynomial to the power-weight points (Fig. 46).

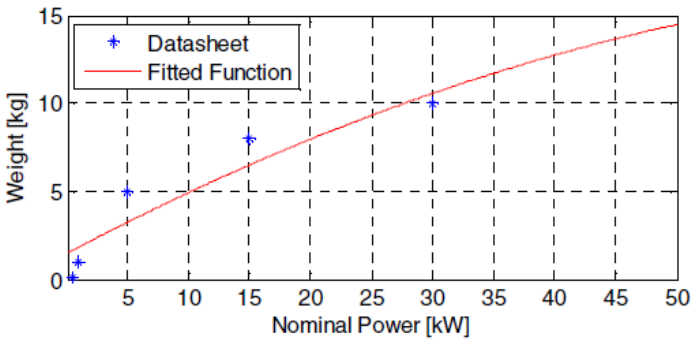

$$m(P) = aP^2 + bP + c$$

$$a = -2 \cdot 10^{-6}\,\frac{\mathrm{kg}}{\mathrm{W}^2}$$

$$b = 0.37\,\frac{\mathrm{kg}}{\mathrm{W}}$$

$$c = 1459\ \mathrm{kg}$$

Fig. 46: Weight for DC/DC converters depending on the rated power

The cost of the converters is estimated using as a reference the cost of the single components composing them, such as diodes, transistors, and heat sinks.

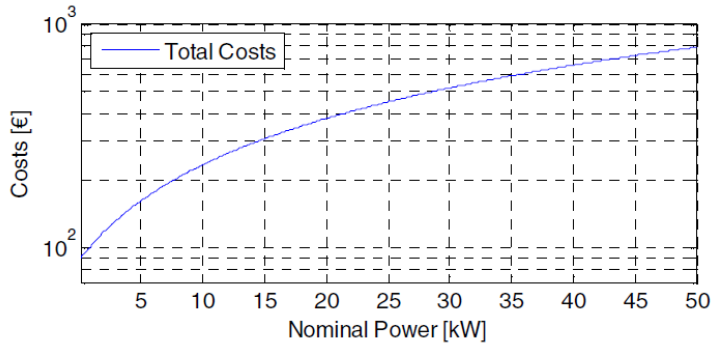

Fig. 47: Cost function of DC/DC converters with respect to their rated power

2.10.4. Cable optimization

With every modification of the architecture, the cables have to be optimized in order to evaluate the overall cost and weight of the system.

The prior mentioned simulation system is able to compute the temperature of the wires, as well as their voltage drop. By comparing them with the maximum allowed values, one sets the constraints of the optimization (Fig. 48).

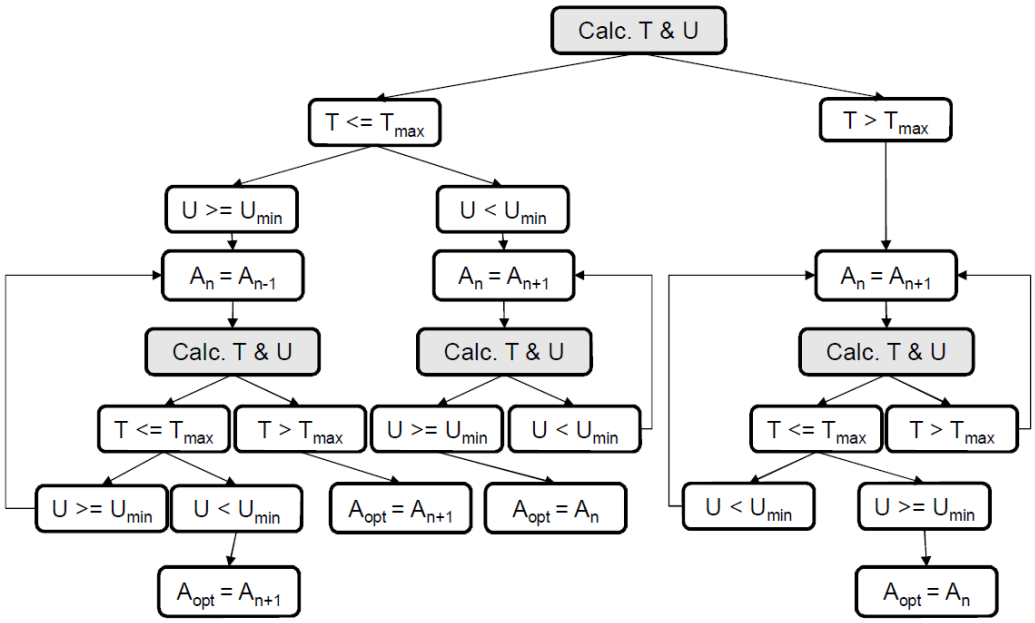

Fig. 48: Optimization process for cable cross-sections (*A*) regarding temperature (*T*) and voltage (*U*)

Once the components of the car are identified, all of the possible distributions of the DC/DC converters are simulated and optimized. The weight and cost of all of them are calculated and compared.

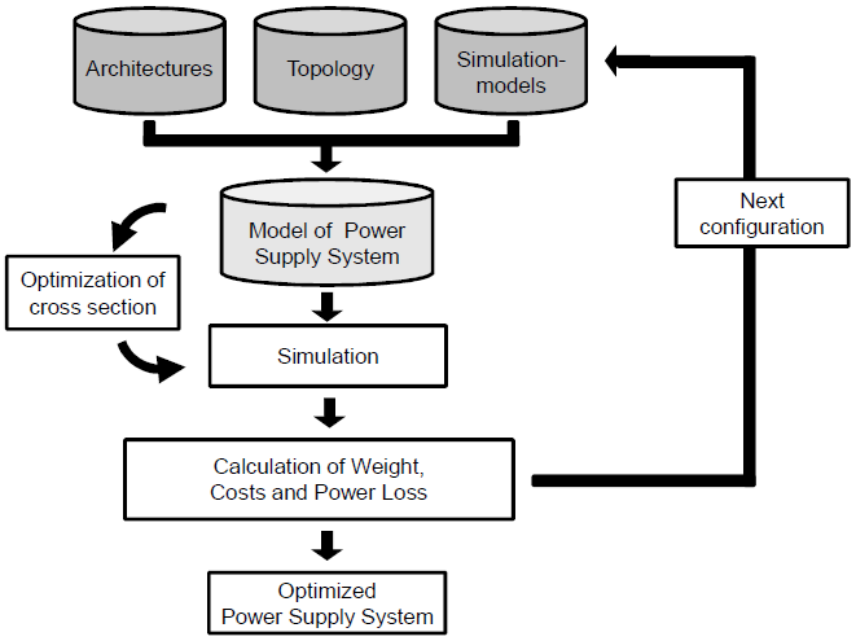

Fig. 49: Flow chart of the optimization process

2.10.5. Results

Example 1

An initial power supply system is optimized, with four components and three converters. Two electronic components are connected to the 5V power supply; another electronic component is connected to the 12V power supply, and the last one to the 48V power supply. The different configurations (architectures) of this system are compared, as in Fig. 50.

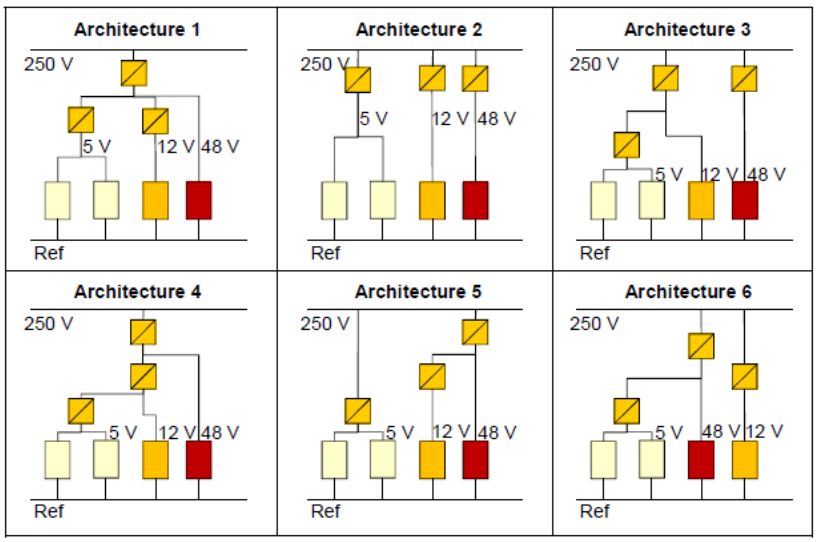

Fig. 50: Different architectures of the first example of power supply system

For every architecture, different topologies are compared, considering routing options and installation spaces of the converters. The optimal cross-section of the cables is also determined. The total number of

topologies for each of the architectures is 120. Evaluating the cost of each of the topologies, it is found that the optimum architecture is number 2, with all of the converters connected to the main power supply, and in particular positions.

Example 2

In this case, there are eight components and two converters. The components have two voltage levels, 5V and 12V, and have thus two contacts, one for each. The length of the wires between the installation spaces is assumed 1.5m.

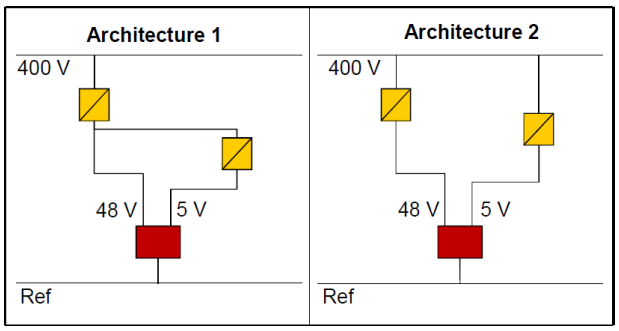

Fig. 51: Different architectures of the second example of power supply system

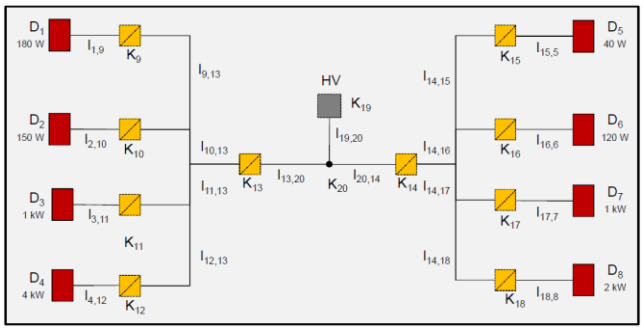

Fig. 52: Installation spaces (K_{xx}) for the second example of power supply system

For this example, the optimum is defined by architecture number 2, placing the 48V-converter in space K_{13} (Fig. 52) and the 5V-converter in space K_{14} (these are the closest spaces to the 400V power supply).

4. Hypotheses

In this thesis, it is hypothesized that a complete optimization of a wiring system can be performed, from which both a weight reduction and an improved reliability will emerge. It is based in a better geometrical characterization of the wiring harnesses, which allows a closer study of the thermal behavior of wires entirely along their extents. Moreover, this optimization must use the correct coordination of all of the cables with their fuses and thermal switches as a constraint, in order to assure reliability even in the case of short circuits.

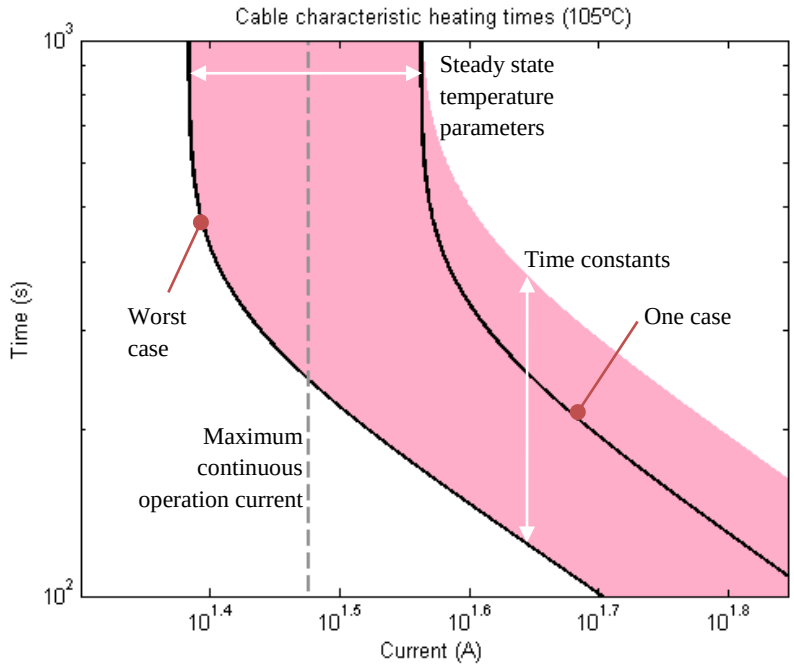

Fig. 53: Cable heating characteristic cloud of infinite cases, given min and max time constants and steady temperatures

The same wire with one specific cross-section can be included in infinite cable harnesses and have infinite thermal behaviors, i.e. infinite steady temperatures along with infinite time constants. This is shown in Fig. 53, where the characteristic heating of a cable with a specific cross section is plotted. In this figure, minimum and maximum steady behaviors and time constants have been defined, with a unique ambient temperature. The colored area depicts their continuous spectrum like a cloud, made of all of the thermal behaviors between the minimum and maximum steady behaviors and time constants. It must be interpreted as a set of infinite heating curves of infinite cases. As indicated with white arrows, the variability of steady state characteristics produces a spread on the position of the vertical asymptotes. Likewise, the variability of time constants produces a spread in the heating time, so that the colored area is enlarged crosswise. This figure also shows two black curves representing just one thermal case. The lower one defines the limit of the colored area, which defines the absolute worst case. The one on the right is just one case, and it might be the well-defined case of the single cable exposed to still air at the given ambient temperature.

As one can see in Fig. 53, considering just one thermal response (the black curve on the right) dismisses many different thermal responses. The existing colored area under this upper black line denoted as “one case” reveals that, if one takes this curve as a reference for selecting the size of the wire, in some cases the decision would be wrong: many possible thermal responses are worse than the considered.

In order to make this more comprehensible, the maximum operation current of the load is plotted with a dashed line. There is one question: is this cable cross-section suitable for this operation current? If one considers the worst case of the cable (the lower black curve), the answer will be negative, because the curve intersects the line of the maximum operation current. On the contrary, if the other case is used, the answer is positive. As a conclusion, in some cases a cable cross-section can be considered suitable or not depending on the accuracy of the reference thermal response.

In the case of Fig. 53, if one selects the size of the cable considering the absolute worst case, the cable cross-section will be larger. If, on the contrary, the assumption of the wire exposed to air is used, the cable cross-section will be thinner. This reveals how dismissing worse cases leads to reduce the cable size. Nevertheless, safety is jeopardized if the dismissed cases can actually happen. It must be guaranteed that these dismissed worse cases will never exist considering the particular conditions of this wire. For example, the cable is only in contact with data and signal cables in a bundle. Then, the worst case is the segment where this cable is alone and exposed to air. In this case, the absolute worst case cannot happen and it can be dismissed. But if, on the contrary, this cable is included in a bundle where other hot cables are included, this worst case cannot be dismissed.

The latter paragraph reveals a great potential of reliability improvement and optimization. It is hypothesized that considering all of the possible curves for a wire cross-section and then discard worse cases that cannot happen is the way to increase the reliability and optimizing at the same time. The improved reliability will reduce the need for experimentation and it will be assured that the wire cross-sections are minimal.

Achieving the cloud of thermal responses shown in Fig. 53 is impossible due to the enormous computational time it would demand, especially if all of the wires in all of the modular combinations of a car are desired. However, cable cross-sections are discrete and the considered cases can be discrete too. This means that the thermal response cloud can be discretized, divided into some cases and sub-clouds. From these sub-clouds, only the worst case is needed.

This idea is represented in Fig. 54, where the same cable is considered and just seven curves are shown in blue, including the absolute worst case. Four of the cases would conclude the cable size is not suitable for this continuous current, and the other three on the right would conclude the opposite. Note that the consideration of “worst case” depends on whether the curves are compared to a maximum operation current or coordinated with a fuse. As explained in section 1.7, the minimum short-circuit current is

needed for this. The worst case of steady heating might be different from the worst-case curve in case of short circuit, because they intersect with each other: some curves have lower steady temperatures than other and a faster behavior at the same time, so that they are more unfavorable for high currents, and more favorable for low currents.

There is a large amount of available geometrical parameters of the wires, because the harnesses are designed in 3D with CAD tools. This geometrical information can be used to classify each segment of the cable into one of the sub-clouds, and then consider the sub-worst case of the sub-cloud. The fact that cable cross-sections are discrete values leads to believe that there are a maximum number of sub-cases, for which an increase of studied sub-cases will hardly produce any difference in the weight of the wiring system. It is desired to find this optimum number of sub-cases, so that the optimum weight of the wiring system is achieved. The most convenient number of cases is expected to be able to be found by heuristics.

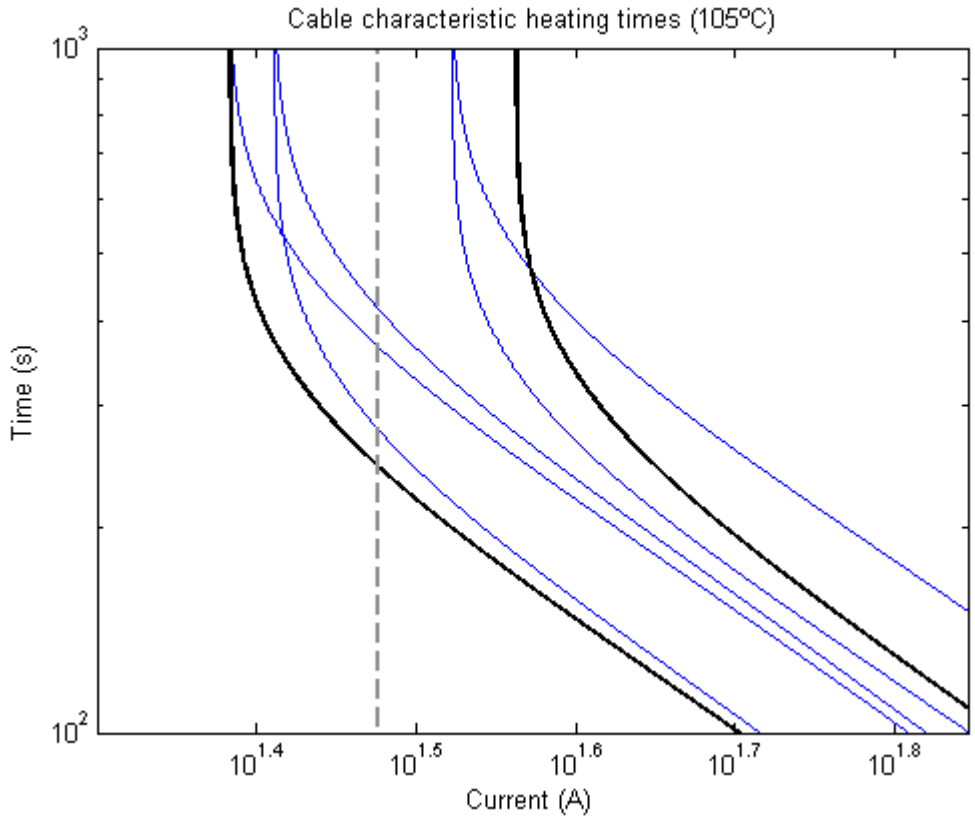

Fig. 54: Thermal response of seven cases of cable segment

The identification of sub-cases allows the use of memory instead of CPU, because each of the thermal cases can be defined by look-up tables or with an exponential behavior with just three parameters. This makes the proposal computationally affordable.

This research is based on the following hypotheses:

1. Each of the bundle branch segments has a different thermal behavior, with different time constant and different steady temperature.

2. The thermal parameters of each of the segments have influence on the other segments, but the obtained thermal response by considering zero axial heat transmission is one reasonable worst case.

3. It is necessary to consider all of the segments in all of the modular combinations to find the worst cases of steady behavior and short-circuit temperature. This will assure reliability.

4. Using custom worst cases for every cable brings an optimization potential, whereas using the same worst-case for all of the cables produces oversizing for a large percentage of the wires.

5. It is necessary to predict the minimum short-circuit current among all of the possible modular combinations to validate the correct coordination between the cable and its fuse.

6. There is a certain optimization potential, to the extent to which there is no automatic tool capable of solving the prior points and whenever they must be overcome, it is performed with experimentation. If this is not possible, standard dimensions are applied.

5. Objectives of the thesis

The aim of this research is to provide a tool capable of performing a complete optimization of the wiring system of a car, with a reliable and notable result, that assures optimum weight of the cables as well as the reliability of the result. The goals of this thesis are summarized as following:

1. To create an algorism capable of performing a geometric analyzing the wiring system of a car, so that the different branch segments of the harness can be identified and modeled, in order to consider all of the different thermal environments of each of the wires

2. To provide an optimum cross-section to all of the wires of the analyzed car, based on the operation of the electric loads and the correct coordination of the protection devices (fuses and others)

3. To assure reliability of the result, so that it be immediately useful without the need for experimentation, by means of:

    a. The use of worst-case parameters and models for all of the necessary estimations

    b. A thermal analysis of the cable harnesses via characterization of the bundle branch segments

    c. Consideration of the simultaneity of current consumption of electric loads

    d. Ensuring the correct coordination between fuses and cables

    e. Considering thermal switches and other protections (when applicable)

The novelty of this research in comparison to others is the aim for providing an optimization method that replaces the empirical task of assuring the reliability of the dimensioning process, based on the knowledge of the industry. This is focused on two points, which are the inclusion of the fuse system as a constraint and the consideration of the harnesses' geometry. None of these two points has been considered in previous optimization methods that having accomplished objectives one and two of the list above.

6. Methodology

6.1. The dimensioning concept

Just as previously explained, the size of the wire will be correct if it withstands the maximum operation current of the load under continuous operation and does not reach the thermal overload temperature when subjected to short-circuit.

Fig. 55 shows a minimum cross-section (blue), and its characteristic isotherm can be compared to those of two larger cross-sections. The largest corresponds to the first proposed in Fig. 10 in section 1.7, which is a standard matching value. The medium one is immediately smaller standard cross-section (1mm²), and the blue one is the proposed optimized value, the smallest (0.5mm²). This dimensioning method is described in ISO8820, which recommends selecting, first, the cable cross-section in consideration of the maximum operation current, and then ensuring that the minimum short-circuit current does not produce overheating.

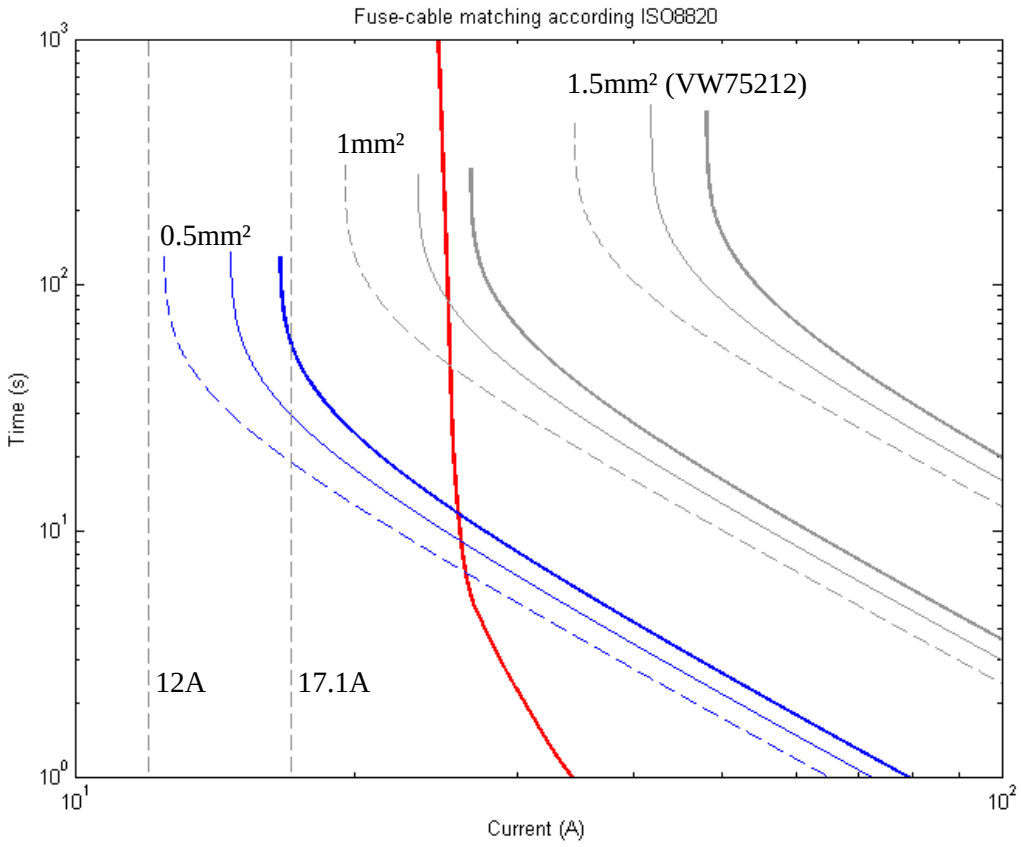

Fig. 55: Fuse-wire matching diagram - hypothetical wire optimization

As explained in section 1.7, the standard dimensioning method in VW75212 suggests wire cross-sections that will be protected by their corresponding fuses for any values of current. Since the current rating of the fuse must be always higher than the maximum operation current in order to prevent ageing, the heating characteristic of the wire is far from the maximum operation current. This is why the standard

matching (1.5mm²) shown in Fig. 55 may be considered conservative, because the current that makes the wire heat up to its long-term temperature is considerably higher than the maximum expected current. This is a good solution either when the electrical behavior of the load is unknown or when the wire ends in a connector where different loads can be connected [16].

Nevertheless, there is a minimum and a maximum value of short-circuit current, and they can be estimated, regardless of whether the load is known or not. The correct delimitation of the possible short-circuit currents allows the selection of smaller cross-sections.

The worst case of short-circuit current corresponds to a low value, because the fuse characteristic and the wire characteristic are divergent along a wide domain of currents. This divergence implies higher short-circuit currents to cause lower temperatures in the wire, providing the fuse blows on time. Therefore, it is enough to calculate the minimum short-circuit current in order to assure the protection of the wire under short-circuits.

The short-circuit current can be calculated by means of the Ohm's law and the impedance along the wire path, from the battery to the failure point. In this case, one must ensure the characteristic time-current curve of the wire to be above the one of the fuse at this magnitude of current, in such a way that the temperature of the wire does not exceed T_{OL}.

One can see how the asymptote for the 105ºC isotherm of the 0.5mm² wires lies near the maximum operation current (12A), which is a good example of wire optimization: the necessary time for the wire to reach the long-term temperature at maximum power is infinite. In other terms, the wire will be exploited at its maximum capacity, when it comes to a fault-free operation.

It is worth mentioning that if currents above this value of maximum operation currents occur, then the wire could theoretically reach temperatures above 105ºC (Fig. 56). That is why the given value for maximum operation current must be reliable.

The case of a blocked motor is an interesting one to explain this matter. Their stall current must be known, and it must be ensured that this current cannot make the wire reach any temperature above T_{ST}. In many cases, motors include a thermal relay that prevents them from overheating. Its time-current curve could be added to Fig. 56 (red thin curve), so that this curve lies for any current under the short-term temperature curve (under the orange region). Whenever such protection is lacking or its characteristic is unclear, then it must be ensured that the fuse blows before the wire reaches 130ºC for the minimum value of stall current.

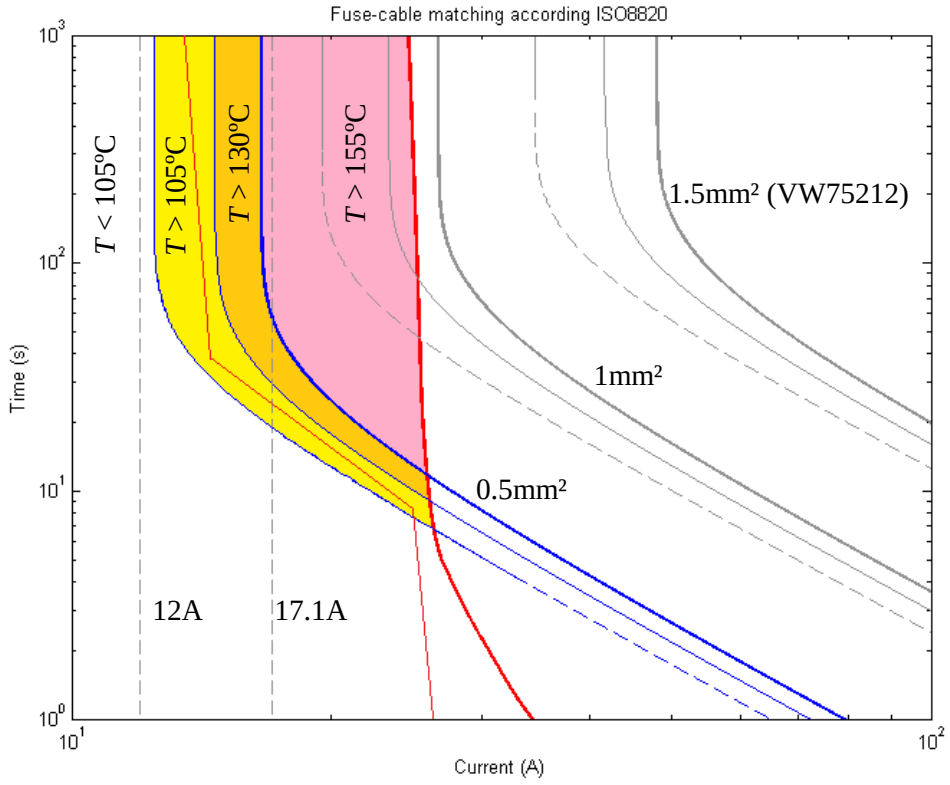

Fig. 56: Potentially unprotected currents and times

As regards the short-circuit current, its minimum value is defined by the intersection point of the 155ºC isotherm and the fuse characteristic. If a short circuit ever produced an overcurrent below this value, the wire would reach temperatures above 155ºC (it would take the cable into the pink area), which is unacceptable.

When the maximum short-circuit impedance is low enough, this optimization will be correct. If the minimum short-circuit current were too low, then it might be enough to choose larger wire cross-sizes, so that the same current cannot make them heat up as rapidly. For example, the 1mm² one. Again, it is worth mentioning that the result of the optimization is specific for a maximum power of a load. If this maximum power is exceeded, then the wire cross-section is not correct anymore.

Optimization processes similar to this one are likely to be applicable to all loads having a considerably smaller maximum operation current than their fuse rating. Since the fuse rating is selected after dividing the maximum operation current by a load factor, this example of optimization is likely to be applicable for almost every single wire of the car. Especially for all the wires supplying parallel loads sharing one fuse (Fig. 57), because their operation currents are particularly different of the fuse rated current, which has been calculated as the sum of the maximum operation currents of its loads.

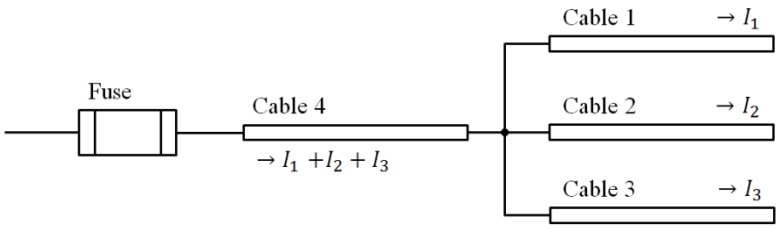

Fig. 57: Example of parallel connection of loads to a shared fuse

VW75212 standard recommends using exactly the same wire cross-section for all the wires protected by the same fuse, in order to assure that wires are protected against short circuits without calculating the short-circuit current. Nevertheless, the standard itself reminds the readers that they can perform a size reduction if needed.

6.2. Reliability and relevant concepts for optimization

6.2.1. The worst-case thermal behavior of a wire

A wire heats up roughly following first-order behavior, so that the coordination analysis with fuses and other protectors are performed using continuous current. In regards of the immediate environment of the wire, it is remarkable that solid media surrounding a cable are beneficial for its heating behavior: they absorb heat, increasing considerably its heating time. Additionally, transmitting heat to a solid body incorporates an extra heat-dissipation surface, which also lowers considerably the steady temperature. That is why a single cable in contact with still air has a worse heating behavior in comparison to a cable inside a bundle of cables (providing these latter do not conduct current).

Fig. 58 shows simulated (blue) and experimental (red) heating curves for a wire. These curves symbolize the evolution of the temperature of the wire along the time. The experiment here consists of one wire in a harness. A part of the cable is inside bundle segments, and the other part is out of the harness. The curve with a higher temperature belongs to the segment where the wire is exposed to air, whereas the other curve depicts the temperature of the wire inside a bundle.

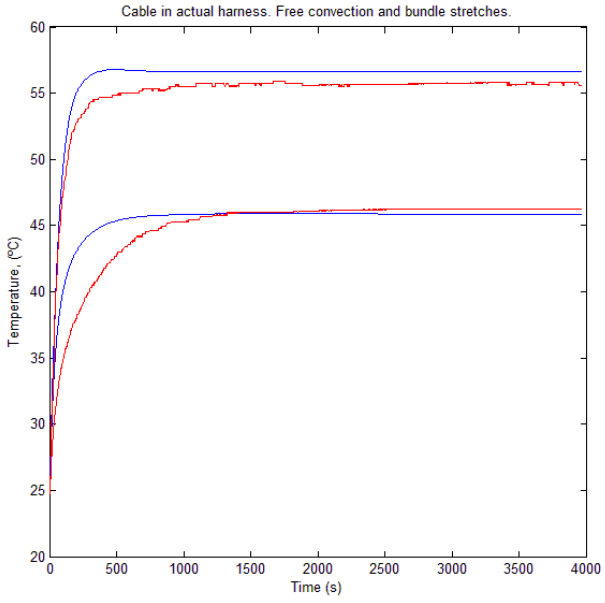

Fig. 58: Experimental and simulated heating curves for bundle and free convection branch segments of one wire

In the VW75212 standard, all dimensions of wires are chosen according to the assumption that the wire is surrounded by air and nothing else. A calculation of the steady temperature will use the ambient temperature and the characteristic of the specific cross-section. However, when some other wires are carrying current near a studied wire, their heat makes the effective ambient temperature increase, so that the temperature of the studied wire rises above the obtained value.

Hence, it is true that the still air around a wire causes the lowest time constants, but it is crucial to know what else surrounds the wire. Otherwise, the considered *ambient* temperature would be wrong. In this case, since the surrounding medium of the wire would not be the ambient, this temperature might be called *surrounding temperature* instead. The presence of hot wires around the observed wire causes a high surrounding temperature, which must be studied.

This can be seen in Fig. 59, where the same experiment has been carried out. In this case, two of the cables were conducting current at the same time. The blue and golden lines represent the single cable exposed to air (simulated and measured). The cyan and red lines represent the cable inside the bundle (simulated and measured). Since the two cables were in contact, the temperature of the cable inside the bundle (cyan, red) rises slowly, but reaches a steady temperature above the expected temperature for the single cable surrounded by air (blue). The measured temperature of the cable out of the bundle does not match the single cable model (blue), because there is another cable next to the observed one, which rises the *surrounding temperature*, as the air heats up.

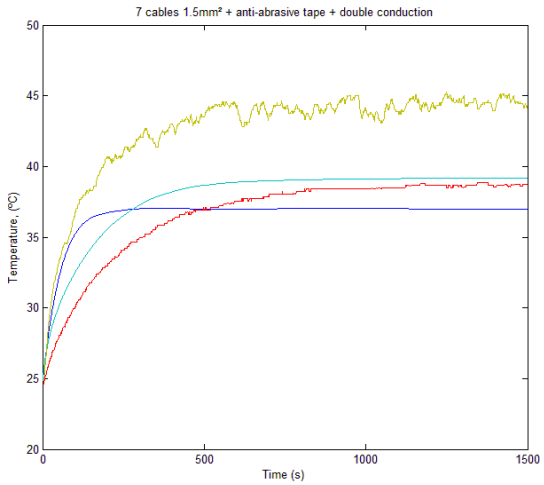

Fig. 59: Experimental and simulated heating curves for bundle and free convection branch segments of two wires

The heating curve of a wire will be considerably different depending on which materials are in contact with the wire. The variability of this aspect is enormous, as it has been explained in section 1.3, so that every single wire can experience many different geometrical configurations with additional manufacturing dispersion. A complete analysis of the worst-case of a specific wire would need to simulate loose wire bundles surrounded by air, in consideration of the particular neighbor wires around with their specific dimensions and current consumptions. This approach would have an enormous computational cost, which would be useless for optimizing a set of wiring harnesses of a vehicle.

Nevertheless, this research proposes an approach consisting of identifying different cases of geometrical configuration defining different thermal behaviors. These cases are deduced from a simplified geometrical characterization of the environment, which consists of classifying what surrounds the wire:

- Inside a wire bundle or in contact with air
- Neighbor wires are carrying current or not
- Number of cables in the bundle

If the wire under study crosses different geometrical environments, the thermal conductivity of copper will let the heat flow along the wire, causing a diffusion of the temperature. However, if the wire is thin enough and the differing branch segments are sufficiently long, the heating curves of all of the branch segments are expected to behave independently. Then, it is a reliable worst case to consider the worst-case segment branch along the wire as it was infinitely long.

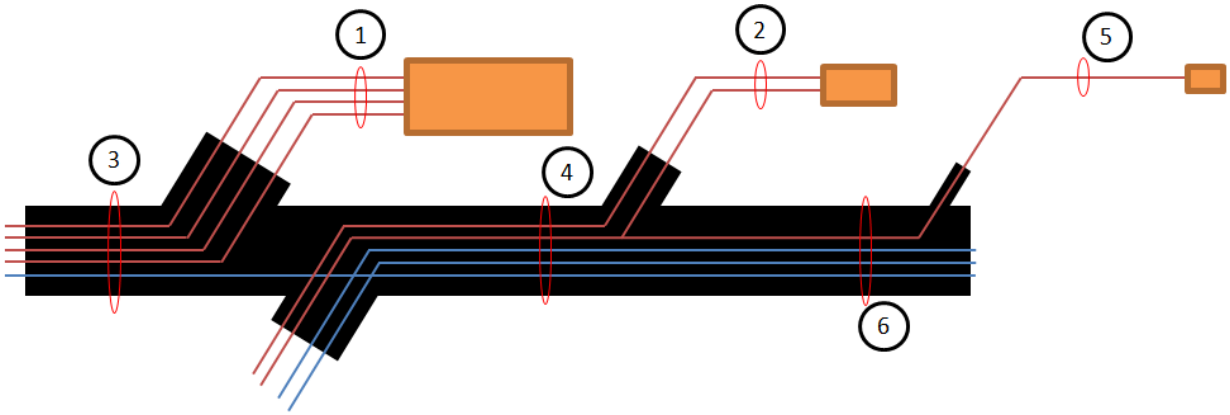

Fig. 60: Different types of branch segments of a wiring harness with different thermal behaviors

The following list is an observation of the different type of branch segments in consideration of the geometry of a the example wiring harness in Fig. 60 and the relevant thermal effects:

Out of the bundle, close to various hot wires:
- A. Four or more
- B. Three (Fig. 60, 1)
- C. Two
- D. One (Fig. 60, 2)

In a bundle, in contact with various hot wires:
- F. Four or more
- G. Three (Fig. 60, 3)
- H. Two
- I. One (Fig. 60, 4)

J. Out of the bundle, alone (Fig. 60, 5)
K. In a bundle, in contact with *cold* wires (Fig. 60, 6)

Some of these types of branch segments in a wiring harness are represented in Fig. 60, where current-carrying (hot) wires are red and zero-current or signal wires (cold) are blue. Actually, every wire will have a unique thermal behavior, but this classification is to allow an optimization of the entire wiring harnesses, so that it provides a useful and mostly fast way to get on the worst-case of every wire.

Fig. 61 shows the cross-section view of the listed types of segments. The current-carrying wires are represented with red color. Note that the layout of the cables in bundles is shown randomly, as in reality. There are many degrees of freedom, but the thermal behavior must be considered in the worst case, which is a specific layout not shown in this figure.

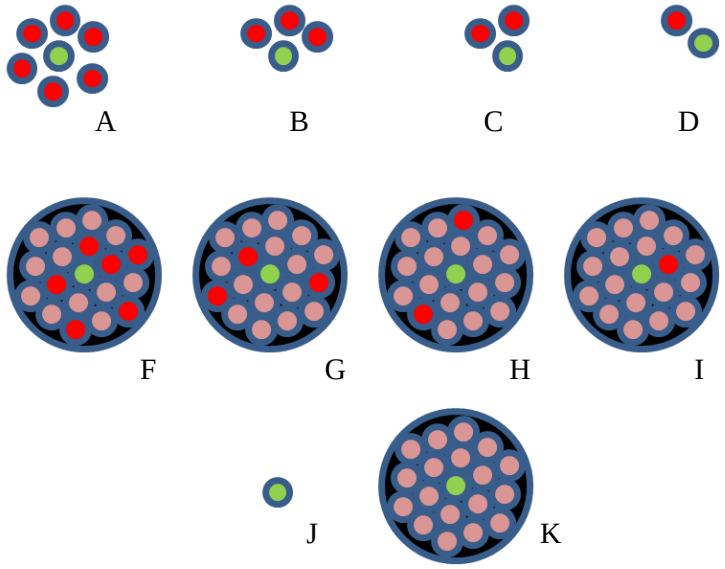

Fig. 61: Cross-section view of the listed types of segments

When it comes to a short circuit or any other failure that must make the fuse blow, one must assure the correct coordination and it is thus necessary to use the time-current characteristics. This time, the worst case refers to the *fastest* characteristic rather than the *hottest*. That is why the wire fuse coordination will use the single wire model instead of the bundle environment.

6.2.2.Fuses as circuit-breakers and overcurrent

The latter considerations about the worst case of steady temperature would be sufficient to dimension the wires if there were no protection device involved in the system. Yet, the presence of fuses and protections for some loads can make the system more reliable, providing their coordination is correct. If the correct coordination is not ensured, then the fuse system is useless.

Fuses behave like a circuit breaker. Just as it has been previously explained, the time it takes for them to blow depends on the amount of current. It must be ensured that, for any faulty current, the fuse blows before the wire is exposed to thermal damage. The greater the current is, the faster the fuse blows, and the lower the maximum temperature of the wire is.

Therefore, the worst-case of a faulty current is a low one, which could heat the wire for a long time before the fuse blows, damaging the wire. The most important point for this optimization method is being aware of which is the lowest faulty current. If the consideration is wrong and an unexpected lower current occurs in an actual situation, the wire could be overheated, demonstrating a wrong design of the wiring.

What is more, the temperature of the fuse determines the melting time in the event of a short circuit. The hotter the fuse is, the faster it blows. That is why manufacturers provide rerating methods with respect to their ambient temperature. In the same way, when the fuse has been conducting its maximum power for some time, it is at its highest temperature. In this case, the melting time is expected to be the shortest for any current.

However, in spite of the convenience of considering the actual temperature of the fuse during the steady operation of its loads, the worst case corresponds to the slowest melting time. The colder the fuse is in the moment of a failure, the longer it will take to blow. Therefore, the characteristic of the fuse will be evaluated at low temperature in order to be always in the worst case.

For example, if a short circuit is the result of a wrong modification of a circuit, it will happen right after switching the circuit on, when the fuse is initially cold, which is the worst-case. Nevertheless, differences are expected to be slight, unless the temperature of the fuse in the moment of a short circuit is extremely low.

Overload currents

Overload currents are the candidate for lowest unexpected currents above the maximum power value. A good separation of the overload and the maximum operation current is essential for a reliable and optimized wiring system. From the electrical point of view, they are caused by a non-faulty operation of a load, but under undesired conditions. From the point of view of the wire dimensioning, the overload current must be the maximum value of current a load can consume, regardless of whether it is an instantaneous or continuous value of current.

Some loads have overload currents that are much higher than their maximum operation currents. These electric consumers are susceptible of being damaged if they lack a self-protection, because fuses are to protect the wiring system, yet not the loads. Therefore, whenever a value of overload current is given, a value of time might be also given, which would indicate the maximum time this current can be consumed before the self-protection of the load opens the circuit.

Electric motors consume their maximum flowing current when stalled. They are prone to overheating and possible damage in these conditions, so they normally include their own thermal switch protecting them in case of stalling. Additionally, some of them can include an electronic power control unit, so that the stall currents do not exceed certain maximum values or times.

If the protection against overload current is lacking, the value of overload current must be considered the minimum faulty current: it must make the fuse blow before the wire reaches its short-term temperature.

The worst short-circuit current

The short-circuit current depends on various parameters. For a given fuse-wire pair, the worst short-circuit is the one achieving the highest temperature of the wire in the moment of the trip. As it has been prior discussed, the longest delays in tripping occur when the short-circuit current is low. In addition, the fuse is slowest when it is cold.

Then, all of the parameters defining the short-circuit current across the observed wire must be selected so that the short-circuit current is minimum. This involves finding the short-circuit path with highest impedance, as well as all the maximum expectable values of resistance of the entire short-circuit path, including connectors. Moreover, the voltage must correspond to the uncharged battery, which will lower the current according the Ohm's Law.

Note that the *path with highest impedance* must be found among all of the possibilities of series connections of the observed wire. These possibilities are defined by the modular compatibility. Moreover, the paths must be explored beyond all the couplings between harnesses, thus requiring the analysis of all of them as one group. Splices play an important role in this matter. Considering a wire that starts after a fuse and ends in a splice, all of the wires rising from that splice are associated to possible worst short-circuit paths. As a conclusion, many wires will have a tree structure of possible short circuits to be explored.

If the found minimum short-circuit current is too low the fuse will blow too late. Then the cable would reach excessive temperatures. In order to avoid this, the wire cross-section can be increased in order to obtain a more favorable thermal behavior that withstands better the overcurrent. The reached temperature would be lower in the event of a short circuit. Nevertheless, the short-circuit impedance can depend on series-connected wires with different cross-sections after the process of optimization, which involves the existence of different solutions. The final valid solution of dimensioning must be the lightest, i.e. the added mass must be evaluated before selecting which cable to thicken.

Fortunately, both the CO_2 emissions reduction regulations and the manufacturing costs' savings of the industry coincide in the fact that they are valued in an overall view. The CO_2 reduction affects the entire fleet of cars. At the same time, the reduction of costs must be designed in such a way that the overall profitability is increased. Therefore, choosing the *least mass* to be added in every step of correction of the wires' cross-sections involves something more than just the weight difference: the *mix*.

The *mix* is a percentage related to a part of the vehicle, which expresses how many of the cars include this part, over one hundred. Some features of the car are rather rare, so that their related parts, including wires, have low mixes. For example, if a certain wire has a related mix of 1%, it means that this wire appears only in one car per one hundred. Then, it is less worth downsizing this wire if it is optional to downsize

another cable with a higher mix. It would imply no significant extra cost or CO_2 emissions to oversize this particular cable with a mix of 1%, despite one particular instance of this car has a heavier cable.

6.3. FEM wire bundle simulator for multiple cases

6.3.1. Description

In this research, a simulator for cable bundles has been developed with Matlab®. It is based on its integrated tool for partial differential equations. The simulator has been developed following the guidelines of [12].

The objective is to obtain reliable results for any bundle configuration. Therefore, all of the parameters introduced to the simulator have been considered in the worst case, so that the obtained results are close to reality, but corresponding to the worst probability queue. In this manner, reality is desired to be normally more favorable than simulations, even though in some unfavorable cases reality gets close to the simulation results. If this is achieved, results of simulations can be taken as reliable references for dimensioning.

Slight modifications to the circle-packing algorithm have been included, and the air gaps between cables have been considered independent regions with the heat conductivity and capacity of still air. However, the wire cores are modeled as in [12], calculating the filling factor and carrying out the harmonic average of the heat conductivities of copper and still air.

The used value of resistivity of copper has been taken from automotive wire standard VW60306, where the maximum acceptable unit-length resistance is established for the cable suppliers. This is a worst-case value. Likewise, dimensions of the wires are delimited with minimum and maximum diameters, as well as minimum and maximum insulation thickness. The worst combination has been chosen, so that the resulting simulation provides the fastest and hottest results.

The validated cases include different tape types. Fleeces are assumed to be composed by still air and a polymeric material, such as PET. The exact proportion of air has been fitted after getting the measured results.

6.3.2. Mesh resolution and time step

In order to evaluate the need for a fine mesh, several tests have been carried out. Since the approach of this research is not to obtain high accuracy but rather good estimations of the heating time of a cable in different situations, it is thus acceptable to have a low-resolution mesh, so that the error is approximately a tenth of one Kelvin.

Fig. 62 shows a comparison of a fine mesh the finally selected resolution. Below the mesh representations, the obtained transient temperatures are plotted, with no significant differences.

Fig. 63 and Fig. 64 show the effects of varying the time step of the simulation. These effects are significant, but just in the first moments, near $t = 0$. Then, as the curve stabilizes, a long time step does not cause a significant error. It would be a good approach to use an adaptive time step.

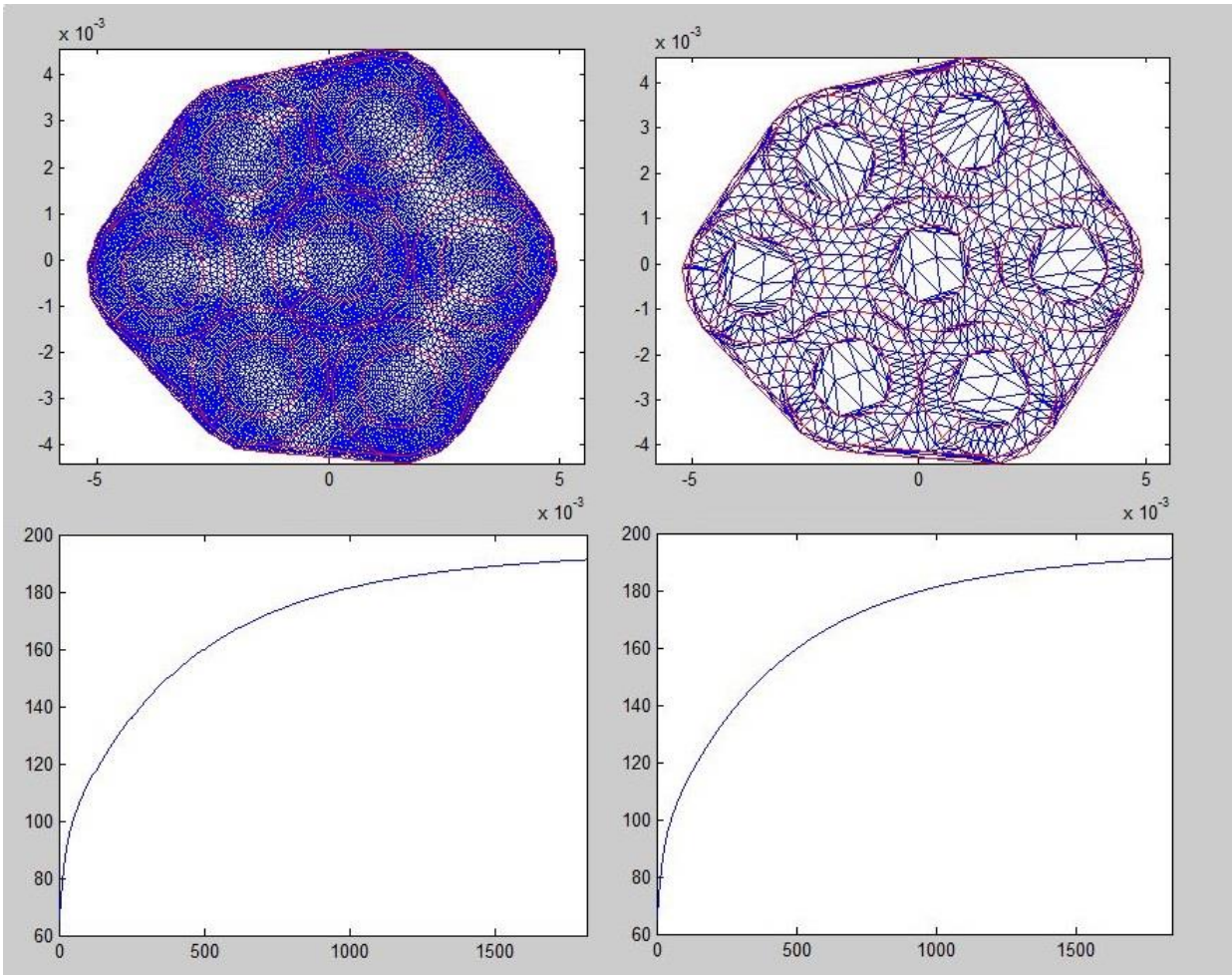

Fig. 62: High resolution versus the finally chosen resolution for the FEM mesh

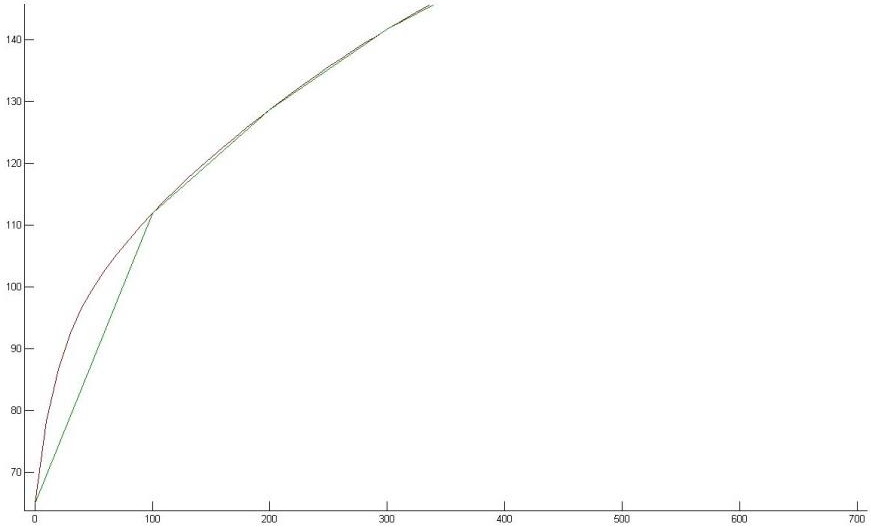

Fig. 63: Effects of variations of the time step in the transient, near $t = 0$

As time passes, the obtained curve seems satisfactory.

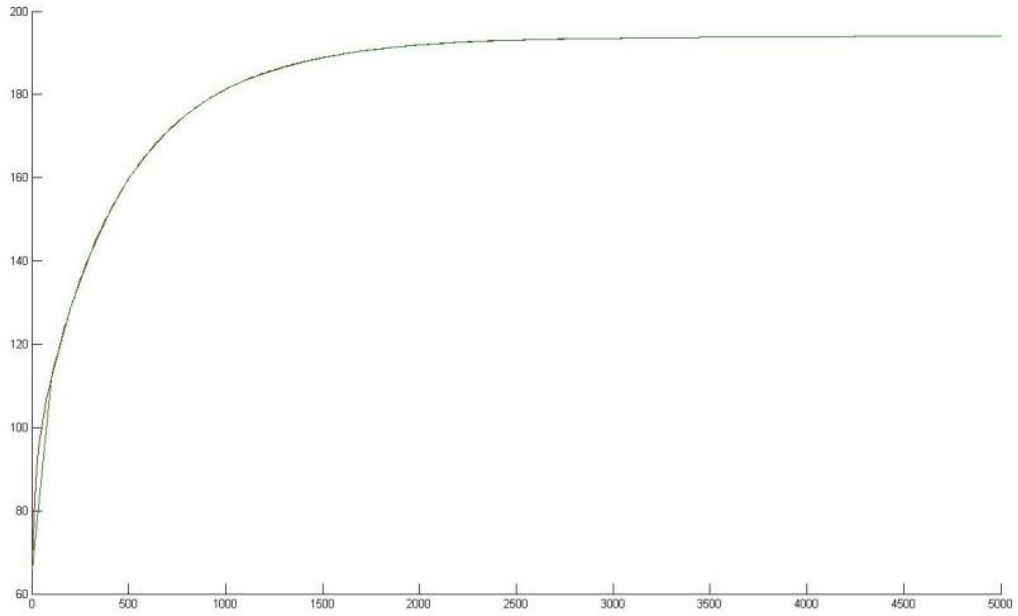

Fig. 64: Effects of variations of the time step

6.3.3. Validation

In order to validate the simulator, different experiments have been carried out. Fig. 65 shows, in red, the measured results of temperature. In blue, the simulated temperature.

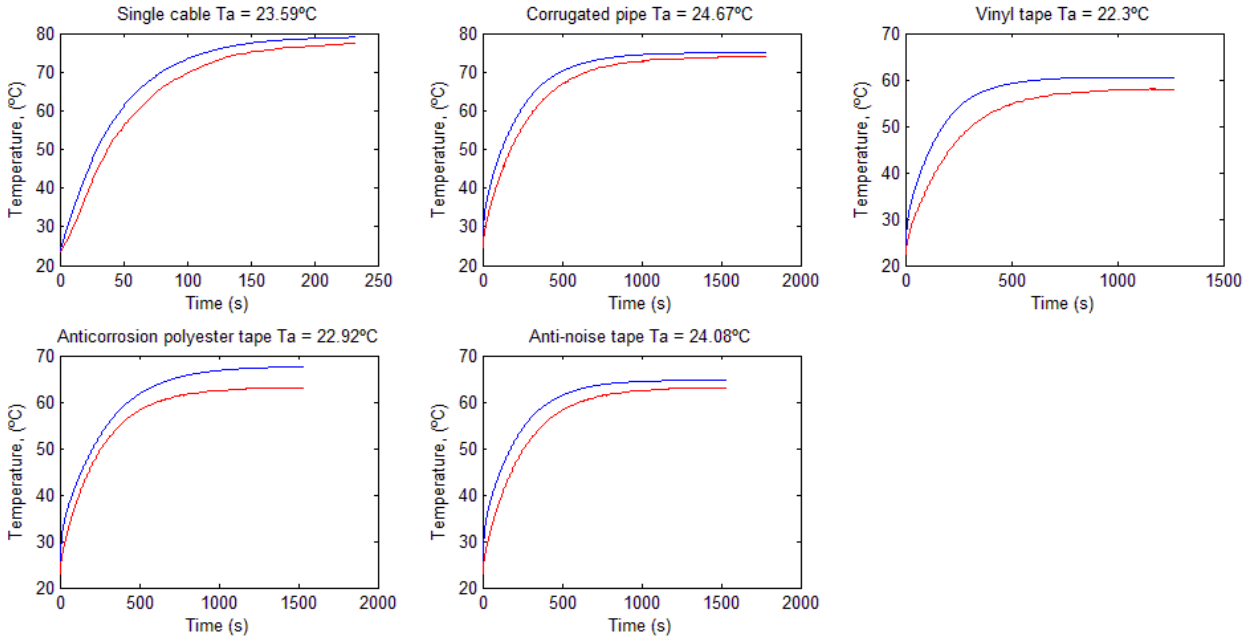

Fig. 65: Measured results and simulations of multiple cases of wire bundles

All of the experiments consisted of a bundle made of seven cables forming a hexagonal cross-section. The cable in the center was conducting. The temperature of the cable and the ambient temperature are the only parameters that have been measured.

The rest of parameters have been taken from catalogues, except from those related to unknown effects such as the exact geometry of the bundle or the exact number of layers of tape. It is not useful to measure them because this research aims to predict the worst case.

The fact that the blue curves are always over the red curves is a good sign, because the selection of worst-case parameters whenever the parameter is unknown has lead the result to be, indeed, worse than the actual experiment, which agrees with the initial aim of the simulator. In these particular experiments, cables were 1-metre long, which places the length-to-radius ratio over 1,400. Thus, it is a good approximation to ignore the axial heat.

It is remarkable that the fastest and warmest curve corresponds to the single wire. All of the types of bundle appear to have a good correlation to the simulated cases.

In a second experiment, an actual harness of a car has been taken. The actual geometry of the bundle cannot be described, since it was composed by 25 cables. Two temperatures have been measured: one in a single cable stretch, and the second one in a bundle with a discontinuous tape. The important –and known– aspect of the geometry was that the cable under study was not in the center of the bundle, but directly in contact with external air on the exterior of the bundle. Again, the axial heat between both stretches has been neglected. Results show that this is a good approximation.

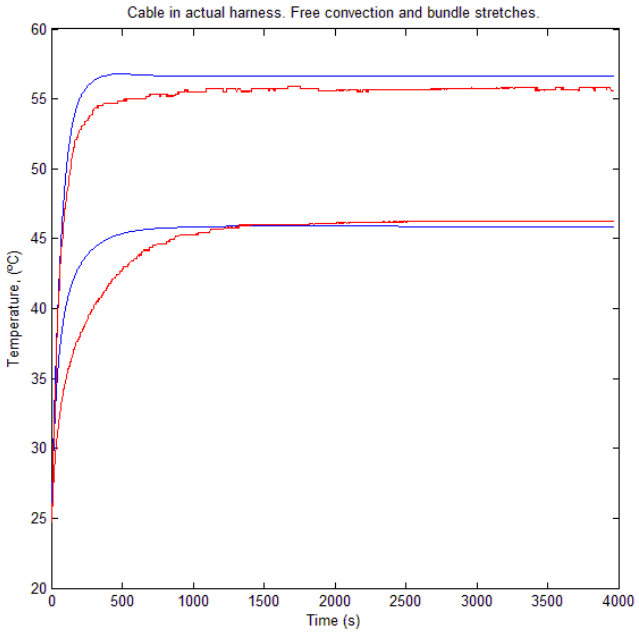

Fig. 66: Experimental and simulated heating curves for bundle and free convection branch segments of one wire

Fig. 66 shows the results of the experiment (red), as well as the simulation results (blue). A good accordance can be observed.

However, the lower curve corresponding to the wire inside the bundle is not above the red line all the time. This is failing to fulfill the requirement of worst-case for the simulator. The explanation for this is the axial heat. The segment wherein the cable was in contact with other cables was considerably shorter than the other segment where the cable was alone. The hotter part of the cable unavoidably transmits heat to the other part, which was not long enough to avoid experiencing a slight temperature rise. Anyway, the same phenomenon produces a positive effect on the overall temperature prediction, because the actual temperature of the single wire exposed to air is lower than the estimated.

A third experiment was carried out. It consisted of the same seven cables protected by anti-abrasive tape. This time two of them were carrying current and their temperature was measured in two points. These current-carrying cables were the exterior ones, i.e., none of them were the one in the middle of the bundle. The points wherein the temperature was measured were the following:

1. The contact point between the two current-carrying cables, in the midpoint of the bundle extent

2. The midpoint of the exposed stretch of one of these current-carrying cables, between the end of the bundle and the connector

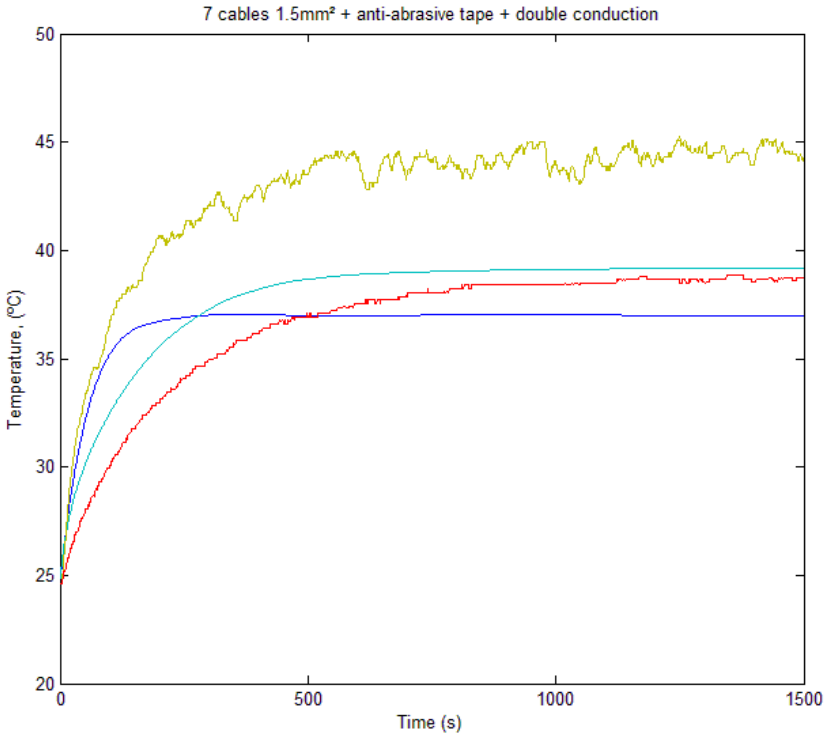

Fig. 67: Experimental and simulated heating curves for bundle and free convection branch segments of two wires (12A)

Cyan and red curves correspond to the temperature in the bundle, whereas the blue and yellow curves correspond to the temperature in the exposed stretch. The cyan and red curves match correctly, but the blue-yellow pair does not.

A reason for this behavior can be a wrong assumption for the ambient temperature. It has been assumed constant and equal along the cable, but the truth is that a hot cable was close enough to the other cable in the exposed stretch to cause an increase of the temperature in the surrounding air.

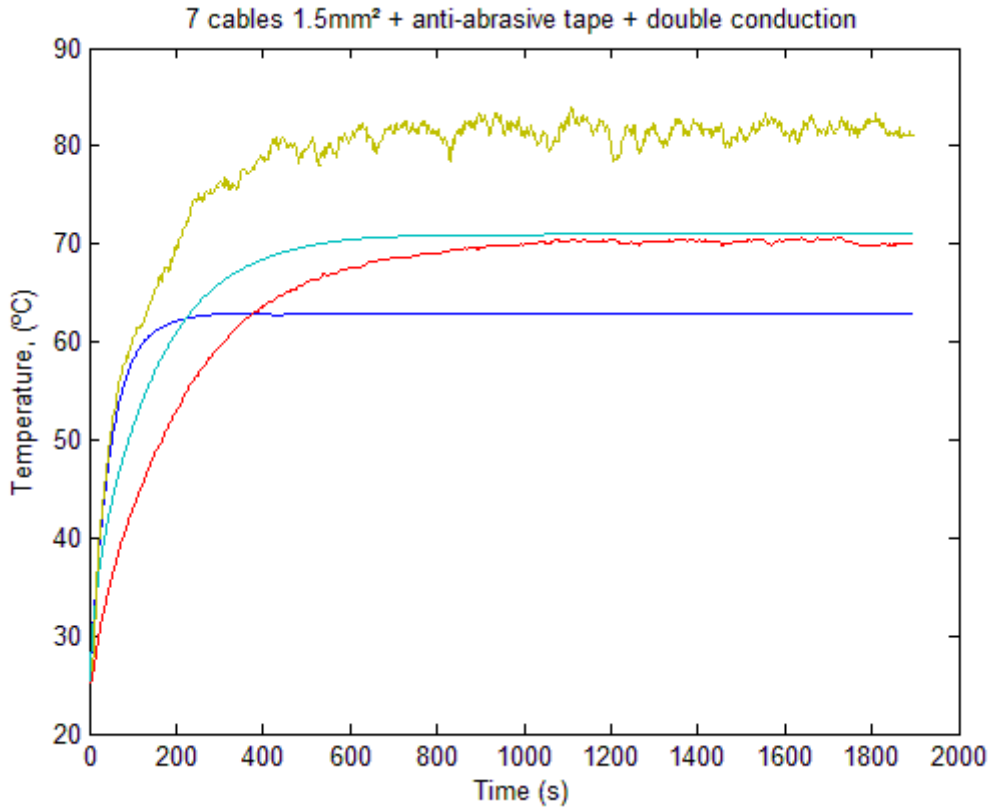

Fig. 68: Experimental and simulated heating curves for bundle and free convection branch segments of two wires (24A)

Fig. 68 shows the same experiment as Fig. 67, but using 24A instead of 12A. No significant changes in the behaviors of the curves can be noticed.

6.4. Comparison of the FEM simulator with COMSOL® Multiphysics

In order to assess the correct results of the finite elements simulations carried out with Matlab®, COMSOL Multiphysics (shown in Fig. 69) has been used. In this section, it is detailed how a simulation of a 0.35mm² wire has been carried out and compared.

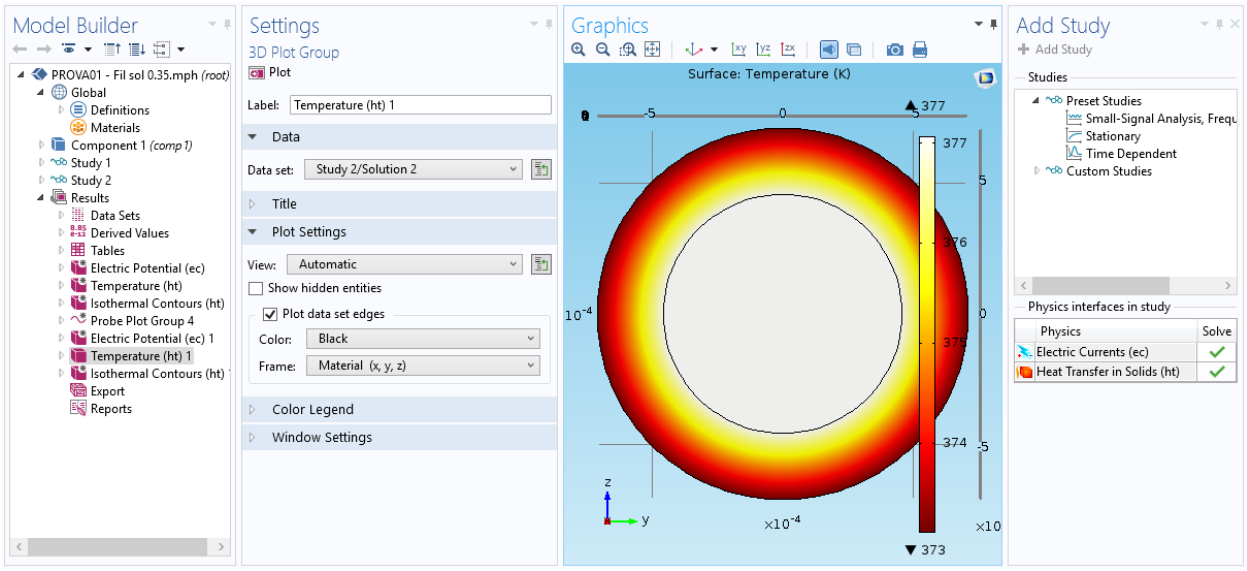

Fig. 69. Overview of the COMSOL project for comparing FEM results

6.4.1. COMSOL Multiphysics

COMSOL Multiphysics (formerly known as FEMLAB) is a software package of analysis and resolution via finite elements for several physical or engineering applications. It is especially used for multiphysical or coupled phenomena, and offers a wide and well managed interface into MATLAB and its toolboxes, providing variety of possibilities for programming, preprocessing and post-processing. COMSOL Multiphyics also allows for introducing coupled systems under partial differential equations, either directly or in weak form.

The AC/DC module

This module simulates components and electrical devices depending on electrostatic, magnetostatic and quasistatic electromagnetic applications, particularly coupled to other physics. It consists of specific interfaces for applications of rotatory machines and importation of SPICE circuit lists.

The heat transfer module

The heat transfer module includes advanced application modes for analysis of heat transfer by conduction, convection and radiation. It is suitable for industrial applications such as electronic cooling and process engineering.

The material library

The material library of COMSOL Multiphyics is an internal database of material properties with more than 2,500 materials and 20,000 properties. This database contains temperature dependencies of electrical, mechanical and structural properties of solid materials. The material library also accepts files generated by the material properties database MatWeb, which is a database with search capabilities with more than 59,000 material datasheets, including information of properties about thermoplastic and thermostable polymers, metals and other engineering materials.

6.4.2. Comparing the simulation of a 0.35mm² wire

In order to carry out the transient-state coupled electrical-thermal simulation of a 0.35mm² copper-PVC class B wire some definitions must be made.

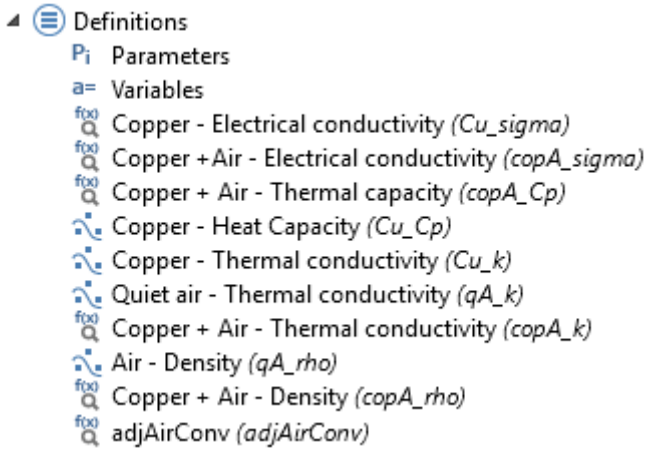

Fig. 70. List of global definitions showing parameters, variables, analytic formulas and look-up tables

Fig. 70 shows the structure of global definitions amongst which there are the global parameters and variables that are necessary for this problem. Parameters in Fig. 71 are necessary to define the size of the wire with its external radius *ex_rad*, internal diameter *int_diam*, and copper cross-section *xs*. Here it is also stored the ambient temperature *Tamb*, the Earth gravity *g* used for the convection coefficient calculation, and the current applied to the wire, in this particular simulation 9.5A.

Name	Expression	Value
ex_rad	0.7e-3 [m]	7.0000E-4 m
Tamb	273.15+55[K]	328.15 K
g	9.8062 [N/kg]	9.8062 m/s²
int_diam	0.9 [mm]	9.0000E-4 m
xs	0.35 [mm^2]	3.5000E-7 m²
current	9.5 [A]	9.5 A

Fig. 71. Definition of the global parameters

The wire is composed by three materials, which are polyvinylchloride, copper and air. However, since the copper core is made of very thin strands, the resulting mesh would be excessively fine, lengthening the calculation time drastically. For that reason, the core is simplified to an equivalent material, a mix of air and copper. The parameter β is defined as shown in Fig. 72, being the relation between the internal area of the core and the real copper cross-section. Fig. 72 shows the defined global variables.

Name	Expression	Unit
qA_Cp	1006 [J/(kg*K)]	J/(kg·K)
Cu_rho	8960 [kg/(m^3)]	kg/m³
ex_diam	2*ex_rad	m
beta	xs/(pi*(int_diam/2)^2)...	

Fig. 72. Definition of the global variables

In order to define the mixed material air + copper, the thermal and the electrical parameters have been defined separately in the structure of global definitions, as shown in Fig. 70.

The analytical formulas listed in Fig. 70 give values of variables related to the air and copper material, shown in Fig. 73, where the dependency with temperature and β can be seen, as well as their units. These variables are used along the definition of the simulation.

Name	Expression	Unit
copA_sigma_var	copA_sigma(T,beta)	S/m
copA_Cp_var	copA_Cp(T,beta)	J/(kg·K)
copA_k_var	copA_k(T,beta)	W/(m·K)
copA_rho_var	copA_rho(T,beta)	kg/m³
Cu_rho	8960 [kg/(m^3)]	kg/m³
h_var	adjAirConv(T)	W/(m²·K)
f	(current/xs)^2/Cu_sigma(T)	W/m³

Fig. 73. Definition of variables for copper + air

The next step is to define the geometry of the wire. With the aim of using these definitions in the future in order to simulate heat transfer along the axis of wires, the definition has been made in three dimensions, but blocking heat transfer in the axis direction. In this way, the geometry description seen in Fig. 74 and Fig. 75 consists of the set made of a pipe and a cylinder of PVC and air-copper respectively.

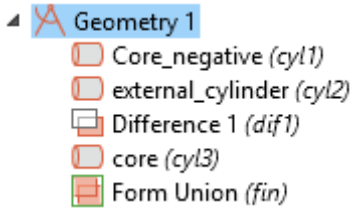

Fig. 74. Structure of the geometry description

The geometry description is made by means of a negative cylindrical core with an internal diameter *int_diam* that is subtracted to a positive and bigger cylinder with an external diameter *ext_diam*. This subtraction configures the external PVC pipe. Finally, the core is defined by a cylinder that is exactly equal to the first negative cylinder used for the core. The resulting geometry can be seen in Fig. 75.

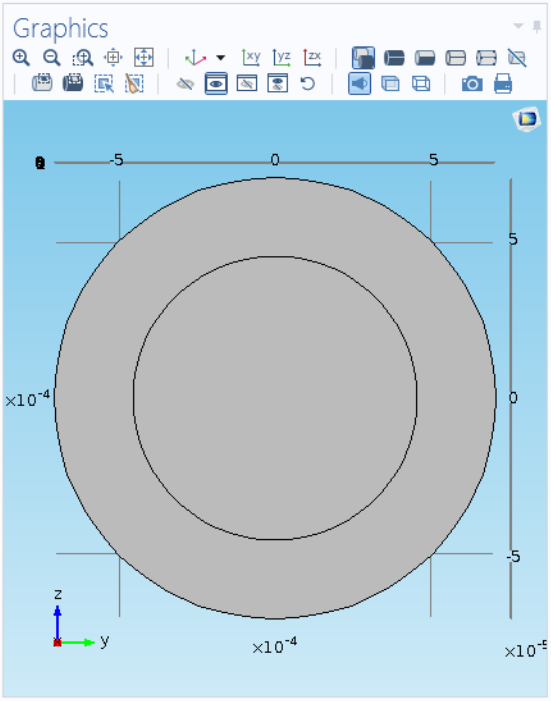

Fig. 75. Caption of the geometry description in Fig. 74

Now that the geometry with its region is defined, the materials must be assigned. These two materials are PVC and mixed air and copper. The definition of polyvinylchloride can be seen in Fig. 76, as well as the definition of the mixed copper and air can be seen in Fig. 77. This latter one is particular because its parameters are represented by the variables shown in Fig. 73, which depend on β as well as on the temperature.

Property	Name	Value	Unit
Density	rho	1100[kg/m^3]	kg/m³
Thermal conductivity	k	0.14[W/(m*K)]	W/(m·K)
Heat capacity at constant pressure	Cp	900	J/(kg·K)
Coefficient of thermal expansion	alpha	100e-6[1/K]	1/K
Relative permittivity	epsilonr	2.9	1
Electrical conductivity	sigma	eps	S/m
Young's modulus	E	2.9e9[Pa]	Pa
Poisson's ratio	nu	0.5	1

Fig. 76. Definition of the polyvinylchloride material

In order to be able to simulate, it is necessary to define the heat transfer in solids, as in Fig. 78. It configures the equations of heat transfer and takes parameters from the different defined materials. It is

necessary to set a value of initial temperature, which is the ambient temperature *Tamb*. It is also here where the thermal insulation is defined, which correspond to the front and rear surfaces of the wire, so that no heat is transferred in axial direction. The heat flux defines convection, and the convection coefficient has been taken from its definition in [1]. The radiation effect is described in *diffuse surface*, which takes a surface emissivity for PVC of 0.93, as in [12]. The Joule effect is incorporated converting the inner region in Fig. 75 into a heat source of constant specific power of *f*, calculated through *β*, the electrical conductivity of copper and the cross-section of the core.

Property	Name	Value	Unit
Electrical conductivity	sigma	copA_sigma_var	S/m
Relative permittivity	epsilonr	1	1
Thermal conductivity	k	copA_k_var	W/(m·K)
Density	rho	copA_rho_var	kg/m^3
Heat capacity at constant pressure	Cp	copA_Cp_var	J/(kg·K)

Fig. 77. Definition of the mixed air and copper material, depending on the *β* parameter

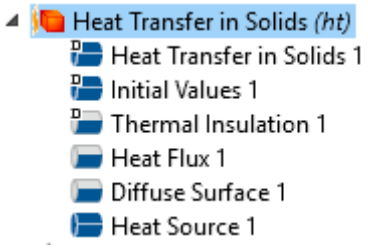

Fig. 78. Structure of the heat transfer definition of the 0.35mm² wire

Since the domains are in three dimensions, the corresponding mesh must be in three dimensions as well. Therefore, the mesh is tetrahedral, as shown in Fig. 79.

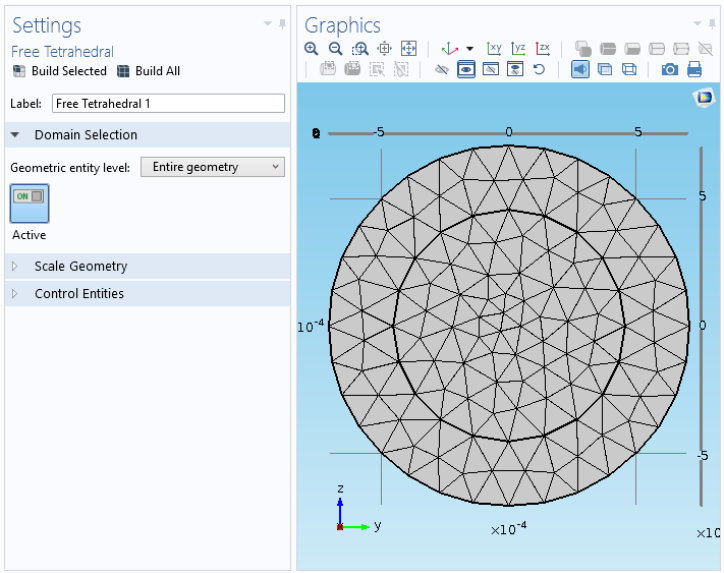

Fig. 79. Caption of the mesh definition of the wire

In order to get results of simulation revealing the maximum temperature of the PVC, it is necessary to place a temperature probe at the surface separating the core from the insulator, as can be seen in Fig. 80 (red dot).

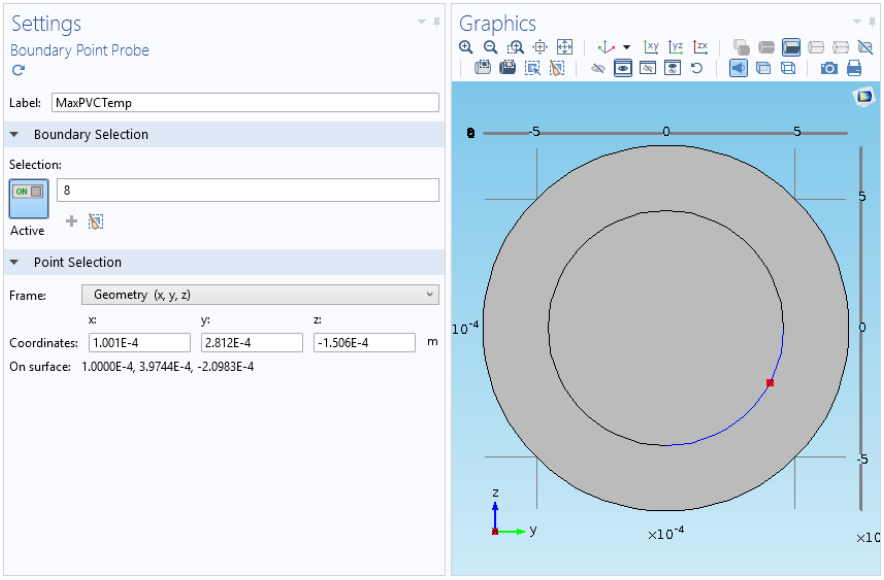

Fig. 80. Position of the temperature probe

Once the simulation has been configured as explained in the previous paragraphs, a transient temperature study can be calculated, revealing results in Fig. 81.

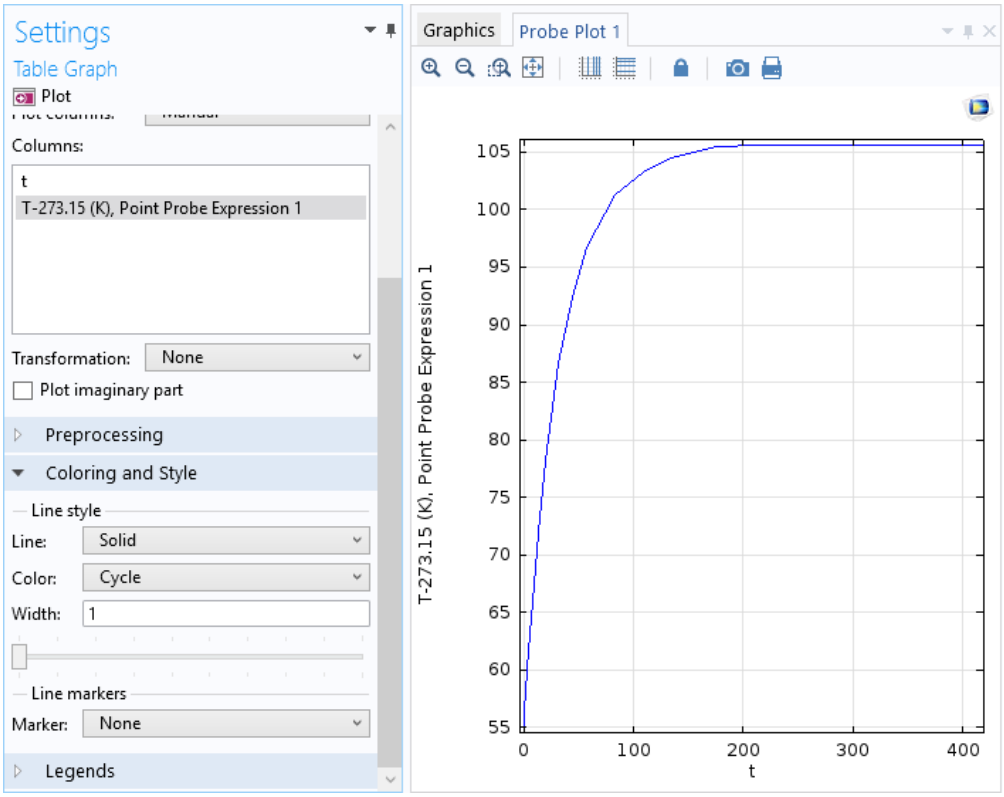

Fig. 81. Results of the transient simulation showing maximum temperature of the polyvinylchloride insulator of the wire

Passing 9.5A through this 0.35mm² produces a temperature slightly above 105ºC, according to results provides by the defined simulation in COMSOL Multiphysics. These 9.5A are precisely the maximum acceptable value of current indicated by the VW75212 regulation for this wire, so that the wire withstands in continuous operation. Therefore, the result is very satisfactory. Additionally, it gives equivalent results to the simulations in section 6.3, as can be seen in Fig. 82.

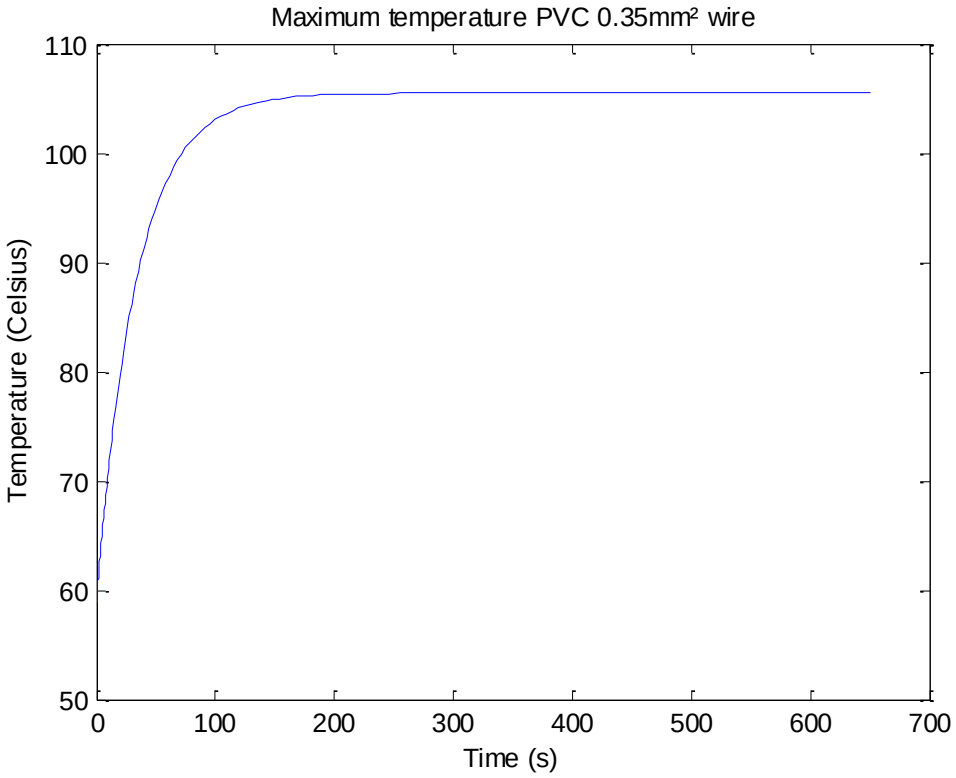

Fig. 82. Results of simulation of a 0.35mm² wire made with the FEM simulator described in section 6.3

6.5. Optimization process proposal

In this chapter, a novel optimization method for automotive wiring harnesses is introduced. It provides optimum sizes for all of the wires, assuring safety by correctly matching all of them with their fuses.

An overview of the method can be seen in Fig. 83. All of the unexplained details of the process in this diagram will be expounded in the next sections.

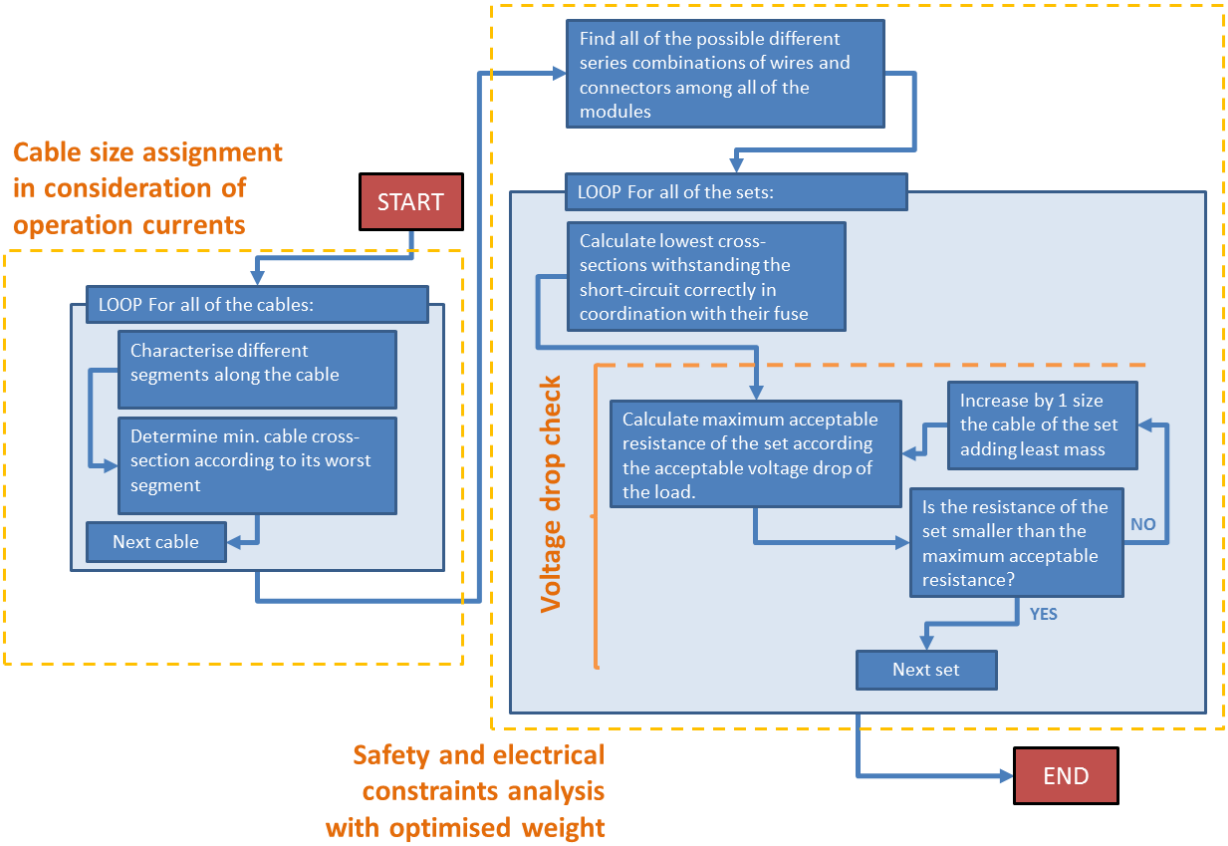

Fig. 83: Diagram of the proposed optimization method

6.5.1. Characterization of the branch segments of a wire

It is necessary to identify the segments of a cable. A segment is the stretch of the harness between two nodes, which are the points of bifurcation of the bundle branches. Each of the segments is defined by its composition, i.e. which cables are together in this segment, as well as its packing solution (tape, corrugated pipe, etc.) and the temperature of the ambient.

The different segments are defined in the context of the 3D routing, but their composition is not defined explicitly. The composition of each of the segments is defined when the information from the wiring schematics (KBL format) is joined with the 3D information (XML format) with a special application. At this stage, a one-by-one correlation of all of the components is checked, but the wire composition of each of the segments is not explicitly defined. Instead, the tool can automatically decide which segments of the

harness are the most logical for each of the wires, because the wiring schematics contain information of connectors and components so that every pin is associated to one cable.

Thus, this necessary information is stored in the resulting KBL files after the coupling process of the wiring schematics and the 3D files.

Once the segments are identified, the corresponding dimensioning must be done according to the thermal characteristics of the bundle in that segment.

6.5.2. Possible different series combinations of wires

In a wire list, each of the rows is a wire with an associated number. Its origin and destination are written as well. The origin and the destination can be connectors, components, or splices. These origins and destinations must be tracked, so that the applicable fuse and component of the observed wire can be identified.

For those cables supplying more than one component, each of the components defines a particular electric path. Additionally, modular combinations could produce extra combinations. Each of these series combinations of wires connected to one observed wire must be identified and prepared as a wire set.

6.5.3. Lowest short-circuit current of a series-connected wire set

The lowest short-circuit current must be calculated, because the lowest faulty current is the one with higher potential of overheating the cable, due to the longer tripping time of the fuse compared to higher currents. This has been previously explained.

The short-circuit current depends on the resistance of the short-circuit path, which is defined by the resistance of the wires and junctions along its extent. Regardless of how the short circuit is produced, applicable short circuits are direct connections to earth. In this case, with the highest resistance, in order to find the minimum short-circuit current.

The minimum short-circuit current will appear when a connection occurs between the furthest point of the series-connected set and the thinnest earth cable. It is difficult to know how far these points are from each other, it is enough to consider always the longest and thinnest earth cable of the car. This way, the short-circuit resistance will be always the worst. The resistance of the earth, i.e. the bodywork, can be considered of some orders of magnitude below the values of the wires. In addition, it is sure that the short-circuit current will always go through the battery cables.

On the other hand, the contact resistance of junctions in connectors can be high enough to be relevant in the resulting short-circuit current. A maximum value depending on the contact area (e.g. based on the cable cross-section) must be used as a worst case of contact resistance.

Since the suitability of the fuse with respect to the observed cable is checked iteratively, this evaluation will be performed more than once for those cables in contact with a splice. The result of the cable cross-section will be the larger among the required for all of the possible short-circuit paths.

If any of the cables of the set of series-connected cables is found to gain temperature above the thermal overload value for the minimum short-circuit current, then the problem must be solved. Here, two strategies are proposed, which must be conducted and compared in any case. The need for using two strategies resides in the fact that the suitability of a wire exposed to short circuit considering its fuse depends much on the thermal behavior of the cable, which is defined by external parameters that are not related to the resistance of the short-circuit path.

6.6. Optimization approaches for wire bundles

In the previous section it has been exposed that wire segments must be identified and studied so that correct dimensions are assigned considering the thermal load of each branch segment. This will be extended and described in this section.

Since wiring harnesses are generally assembled manually, it is impossible to assume any determined internal distribution of wires in bundles. The position of the wires is generally not controlled. However, it is possible to observe the worst case. Given a maximum value of current density, corresponding to a wire inside the bundle, the worst case occurs when all of them have the same current density. For this purpose, all simulated bundles and the derived formulae and optimization algorithms will assume constant current density in bundles. If this is accomplished, given a set of wires, their position inside the bundles can only produce small variations on the maximum temperature.

This assumption demands that all bundles have homogeneity in their heat generation, viewed as the f parameter (W/m³) in the heat dissipation equation, which must be roughly uniform all over the cross-section of any random wire bundle. The power per unit volume f equals to zero in all regions of a wire bundle except in conductor regions, wherein the Joule effect heat depends on the density J and resistivity, ρ, (84**)**:

$$f = J^2 \rho(T) \tag{84}$$

Equation (84) presents the resistivity of copper ρ as a function of the temperature, T. Its expression depends on the material, and this document explores exclusively the case of bundles with a unique and common composition of materials (copper and polyvinylchloride).

Power wire bundles will frequently come along with signal wires carrying negligible currents. This prevents to maintain this desired unique Joule heat per unit volume, f, for all of the wires. These signal wires will have nearly zero heat dissipation in their cores, since the wire manufacturers cannot provide wires with unlimitedly thin diameters. In many cases, the current is so low that there is no available gauge in the market thin enough to produce a relevant heat power.

Consequently, it is possible to ensure that these wires are always *cold*, i.e. providing nearly $f = 0$ heat to the system. If a bundle with signal wires is compared to the same bundle with these wires removed, the average current density J is reduced, due to their lack of any contribution of heat to the system. Additionally, their presence makes the diameter of the bundle increase when compared to the same bundle without them, which means slightly allowing more heat dissipation by means of convection and radiation. These two aspects suggest that these cold wires can only benefit bundles by lowering their maximum expected temperature for given currents. Since wire dimensioning must be done according to a

reasonable worst case, this chapter deals with bundles containing merely power wires with approximately uniform current density, *J*.

6.6.1. Critical dimensions of a homogeneous conductive cylinder with uniform current density

If all of the wires in the bundle are made of the same materials and they have the same current density, the temperature of the center will increase with the radius of the bundle. The particular case of a cylindrical conductor exposed to air in Fig. 84 is compared to wire bundles in order to validate the obtained curves of the response surfaces. The resulting equations (85) and (86) are plotted in Fig. 85 and Fig. 87.

$$T_{centre} = f\left(\frac{A}{4\pi\lambda} + \frac{\sqrt{A}}{2\tilde{\alpha}\sqrt{\pi}}\right) + T_{amb} \tag{85}$$

$$A_{max} = 4\pi\lambda^2\left(-\frac{\lambda}{2\tilde{\alpha}} + \sqrt{\frac{1}{4\tilde{\alpha}} + \frac{T_0 - T_{amb}}{\lambda J^2 \rho}}\right)^2 \tag{86}$$

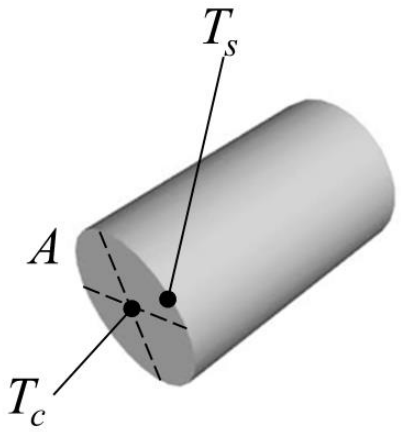

Fig. 84. Ideal cylindrical conductor exposed to air, with uniform current density *J*

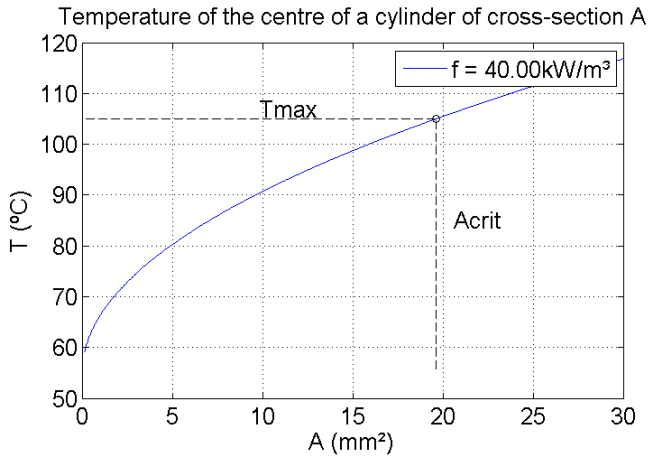

Fig. 85. Center temperature of a conductive cylinder with uniform current density and cross-section *A*

In equations (85) and (86), λ is the thermal conductivity of the cylinder material, and $\tilde{\alpha}$ is the averaged convection and radiation term of heat transfer.

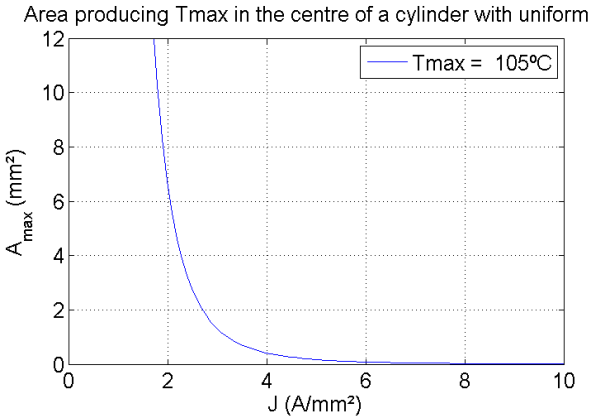

Fig. 86. Maximum area of a cylindrical conductor set to current density J

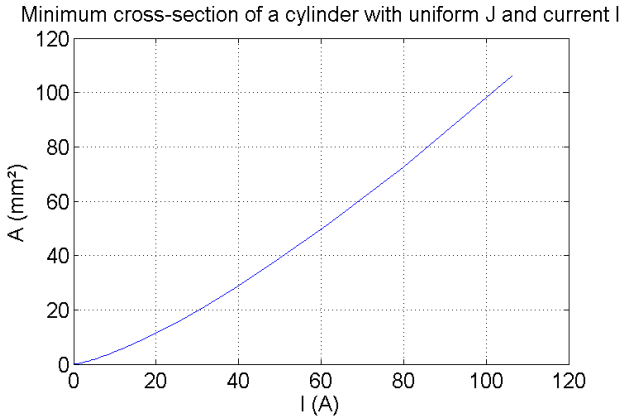

Fig. 87. Minimum cross-sectional area of a cylindrical conductor subjected to a current I and uniform current density. Smaller areas would produce temperatures above T_{max}

Conversely, it is useful to consider the minimum area A_{min} as a function of the total current I rather than the current density. This resulting curve is shown in Fig. 87.

It is also convenient to consider the maximum current I_{max} as a function of the total cross-sectional area of the cylinder. This is shown in Fig. 88. These latter relations are interesting to ascertain the maximum area of an arbitrary bundle, given the sum of its currents, which will be used later in this document.

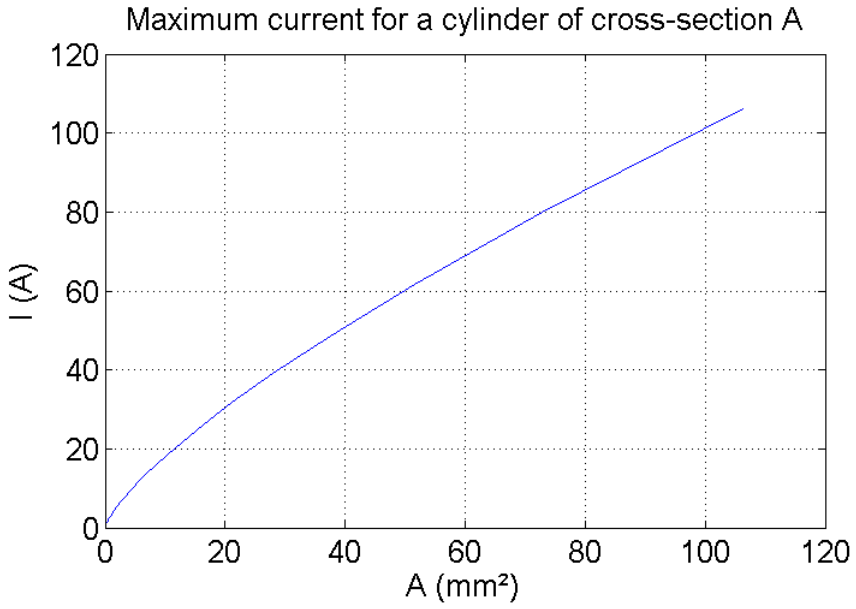

Fig. 88. Maximum current for a cylindrical conductor with cross-sectional area A. Greater currents would produce temperatures above the maximum acceptable value

6.6.2. Response surfaces

It is desired to apply the response surface methodology (RSM) in order to be able to optimize wire bundles without using on-line simulations.

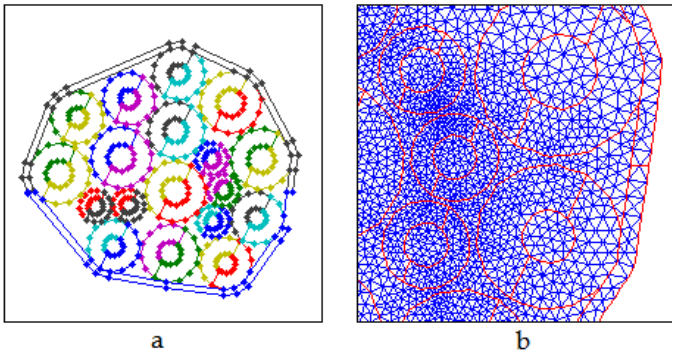

Fig. 89. a. Bundle geometry decomposition b. Mesh detail

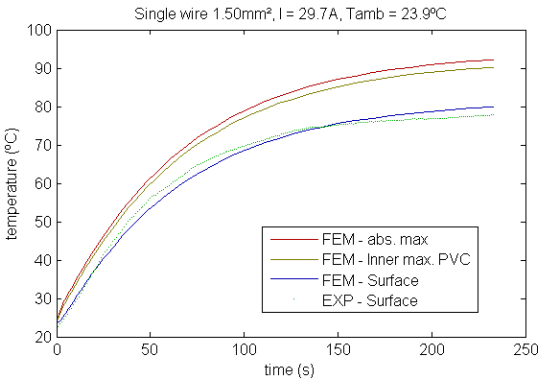

Fig. 90. Experimental results vs. FEM simulation of a single wire

It is necessary to obtain similar curves to those exposed in the previous section, this time for actual wire bundles, which can be regarded as a heterogeneous mix of different materials. This chapter explores only the possibilities of different approaches with a limited set of materials composing the bundles, which are copper, still dry air, polyvinylchloride (PVC) and polyethylene terephthalate (PET) fleece. The behavior of this system is similar to the case of the prior plotted homogeneous cylinder, yet not as simple to express by means of its parameters, such as λ or ρ.

Obtaining the response surfaces of wire bundles requires a set of samples obtained either by simulation or experimentation. For this purpose, a special algorithm capable of generating bundle geometries with their PET fleece and simulating them using the finite element method has been created. Fig. 89 shows an example of generated geometry with its mesh ready to be simulated. Experimental validation shows good accuracy for both single wires and bundles. Fig. 90 and Fig. 91 show temperature transients of a single wire and a wire bundle, comparing simulation results with experimental results. In these figures, the experimental temperature corresponds to the external surface of wires, whereas the simulator can provide also the maximum temperature of the copper core of the wires and the minimum and maximum temperature of their insulation.

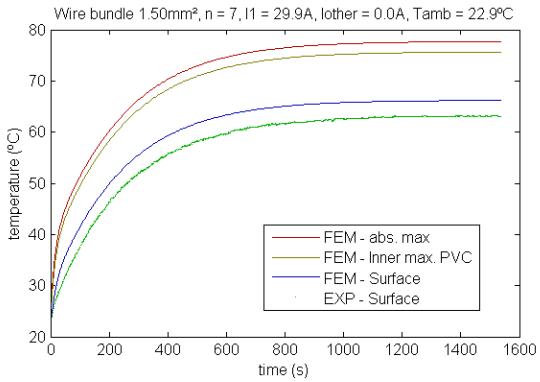

Fig. 91. Experimental results vs. FEM simulation of a wire bundle

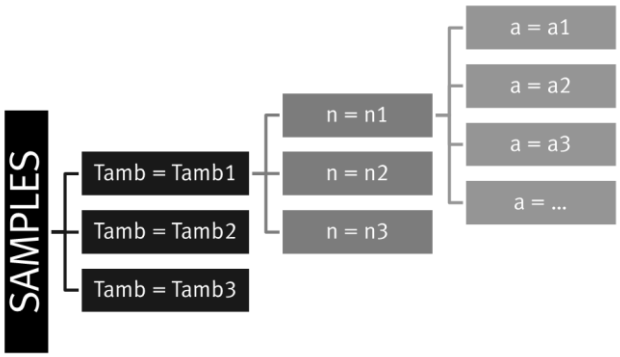

Fig. 92. Diagram of the factorial experiment, where *a* is the cross section of the conductors, n is the number of wires and T_{amb} is the ambient temperature.

All simulations foresee temperatures and behaviors slightly more pessimistic than those found in experiments. This is a desired effect, since the simulation results are at the worst case, which allows for using them as reference for wire-sizing.

This simulator has been included in an algorithm capable of generating multiple wire bundle samples following the factorial design in Fig. 92. A first evaluation of the results is used to compare the behavior of wire bundles with the curves of an ideal conductive cylinder. It has shown similitude between these curves and the obtained simulation curves for actual wire bundles with heterogeneous composition of materials. Despite the heterogeneity of the wire bundles, it is possible to obtain similar curves with non-linear response surfaces obtained by the least-squares method.

The least squares method is commonly used in many different engineering areas to produce response surfaces. In this chapter, polynomial fits have been carried out with the aim of obtaining the response surfaces describing both the critical area and the critical current of arbitrary wire bundles.

The set of samples consists of 171 different geometries of bundles with different ambient temperatures, to which the critical current is found and registered. Expressions for the logarithms of the critical area and the critical current (87) and (88) are found.

$$\log A_{crit} = f_1(n, I_{total}, T_{amb}) + \varepsilon \tag{87}$$

$$A_{crit} \sim e^{f_1(n, I_{total}, T_{amb})} \tag{88}$$

$$\log I_{crit} = f_2\left(n, A_{Cu}, A_{pvc}, T_{amb}\right) + \varepsilon \tag{89}$$

$$I_{crit} \sim e^{f_2(n, A_{Cu}, A_{pvc}, T_{amb})} \tag{90}$$

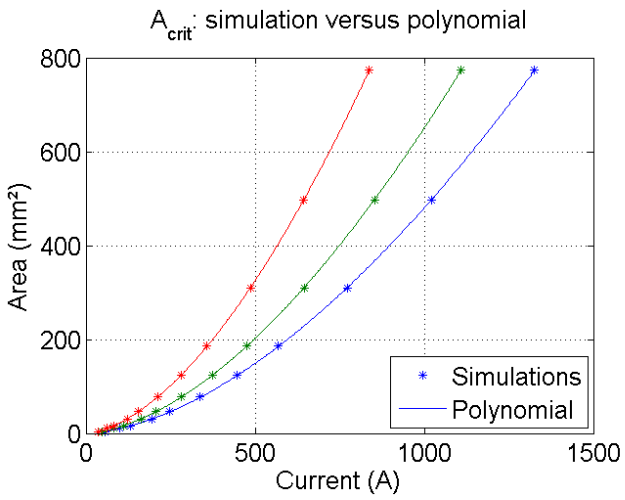

Fig. 93. Response surface: minimum area of the bundle versus its sum of currents and different ambient temperatures

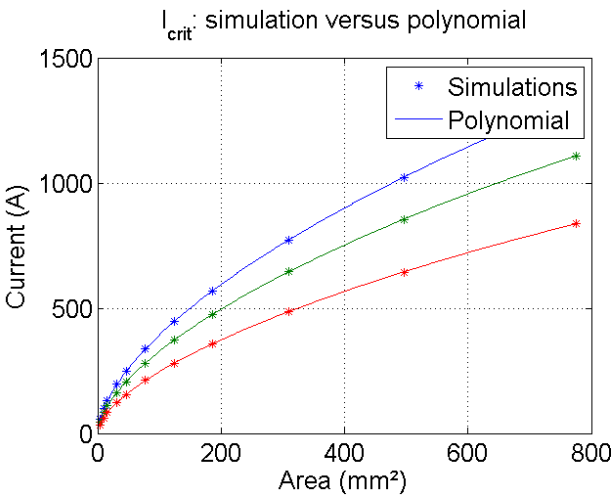

Fig. 94. Response surface: maximum current of the bundle versus its sum of cross-sections and different ambient temperatures

The critical area surface uses the number of wires n, the sum of their currents, I_{total}, and the ambient temperature T_{amb} as predictors, as in (87) and (88). On the other hand, the response surface of critical current I_{crit} uses the areas of copper and PVC, A_{Cu} and A_{pvc} as predictors (89) and (90). Fig. 93 and Fig. 94 can be observed to evaluate graphically the results of the polynomial fit.

6.6.3. Integer optimization algorithms for cross-section assignment of wires in bundles

As previously discussed, once the critical area is obtained, the cross-sections of the wires must be chosen so that the final area is minimized but still greater than its critical value. If it were possible to buy wires with unconstrained cross-sections –i.e. continuous and infinite availability of sizes–, then the problem would be easily solved. The cross-sections can be found by dividing each current by the obtained value of critical current density J_{crit}, obtained at the same time by dividing the total current of the bundle by the critical area $\left(J_{crit} = \frac{I}{A_{crit}}\right)$. However, cross-sections can only pertain to sets of discrete values, and it is not trivial to assign them in an optimum way.

For the purpose of cross-section assignment, three different optimization algorithms have been created and compared. The first one is an integer linear program. The other two algorithms are custom methods presented in this document. They use respectively the response surface of the critical area of the bundle and a combination of this one and the response surface of critical current. The main difference between these two latter approaches is the fact that the critical current must be recalculated in each iteration of the optimization loop, whereas the critical area is calculated only once before the optimization loop starts. These three algorithms are detailed in the following sections.

6.6.3.1. Integer linear programming

The decision of which standard cross-sections should be used for each of the wires in the bundle, given their currents, is a problem that can be formulated as a linear program. This is possible whenever variables of a problem represent integer quantities (e.g. amount of people) or integer variables representing states or decisions. In this case, the problem is described by integer variables representing the decision of which wire size is applied to each of the wires in the bundle.

Wires are indexed from $k = 1, \ldots, N$ being N the number of wires in the bundle. In order to solve the integer optimization problem in matrix form, it is necessary to express the available cross-sections for each of the wires by means of a set of N vectors called Q_k. Each of these vectors contain S values of cross-sectional areas a_{ki} ($i = 1, 2, \ldots, S$) for the wire k (91).

$$Q_k = [a_{k1}, a_{k2}, \ldots, a_{kS}] \tag{91}$$

Each of the wires must have only one cross-section. For that reason, there are exactly S Boolean variables for each of the wires, i.e. there are totally $S \cdot N$ Boolean variables (92). Since it is imposed that all of the wires must have the same current density, S must be equal to 2. With S=2, each wire have two possible cross-sections, being the first the greatest cross-section below the critical value of J, and being the second the smallest value above the critical J.

The Boolean b_{ki} is true if the wire k receives its cross-section i, and false otherwise. They are actually integer variables, and it is necessary to convert them into Booleans by forcing them to be at least 0 and not higher than 1 (93).

$$x = [b_{11}, \ldots, b_{1S}, \ldots, b_{2S}, \ldots, b_{N1}, \ldots, b_{NS}]^T \tag{92}$$

$$\begin{aligned} x_{min} &= [0 \ldots 0]^T \\ x_{max} &= [1 \ldots 1]^T \end{aligned} \tag{93}$$

The constraint that one wire must have only one cross-section is programmed by imposing that the sum of all of the b_{ki} for the wire k equals 1:

$$\sum_{t=1}^{S} b_{kt} = 1, \qquad k = 1, \ldots, N \tag{94}$$

This latter constraint is expressed in matrix form as follows:

$$A_{eq} \cdot x = b_{eq} \tag{95}$$

$$A_{eq} = \begin{bmatrix} 1 & 1 & \cdots & 1 & & \cdots & & 0 \\ \vdots & & & 1 & 1 & \cdots & 1 & \vdots \\ 0 & & & \cdots & & & 1 & 1 \cdots 1 \end{bmatrix} \tag{96}$$

$$b_{eq} = [1 \dots 1]^T \tag{97}$$

Notwithstanding that these logical definitions are more complex, the main constraint of the problem consists of the sum of all of the cross-sectional areas of the bundle not exceeding the critical area (A_{crit}):

$$\sum_{k=1}^{N} \sum_{i=1}^{S} b_{kt} \cdot a_t \geq A_{crit} \tag{98}$$

This sum of areas must be expressed in matrix form as follows, using Q_k:

$$A \cdot x \geq A_{crit} \tag{99}$$

$$A = [Q_1 \dots Q_N] \tag{100}$$

The objective function is the volume of copper, V (101), since a minimized volume of copper will bring also its minimized mass, which is the real objective. This is obtained through the product of the length of each of the wires, l_k, and their cross-section, a_k, as well as their commercial mix, w_k. The commercial mix is such that $w_k \in (0,1]$ and it permits a fleet-oriented optimization, which minimizes the volume of copper used by the entire automotive brand, and not only the volume of copper used in one car. As a result, wires that are installed in many cars tend to be thinner, so that the mass of copper used in the fleet of sold cars is minimized. Conversely, *rare* wires tend to be thicker. If the optimization is only applied to one car and not to an entire fleet, these w_k's must be equal and non-zero (in that case, their recommended value would be 1).

$$V = [Q_1 \cdot l_1 \cdot w_1 \ \cdots \ Q_N l_N w_N] \cdot x \tag{101}$$

6.6.3.2. Custom optimization method based on the critical area

As opposed to the optimization method described in the previous section, a custom code has been developed in order to achieve one important goal in this optimization: speed. This custom method uses the value of critical area of the bundle in order to achieve the same result as the described linear optimization, but using in this case a specific optimization algorithm for this stated problem.

The value of critical area A_{crit} is obtained from the sum of the currents of the wires, and unlike in the integer linear programming, here each of the particular values of current of the wires is necessary to calculate the preliminary cross-section a_k^{pre}, by dividing these currents by the critical current density J_{crit}:

$$J_{crit} = \frac{\sum_{k=1}^{N} I_k}{A_{crit}} \tag{102}$$

$$a_k^{pre} = \frac{I_k}{J_{crit}} \tag{103}$$

Using the obtained value of J_{crit} each wire is given a preliminary hypothetical cross-section a_k^{pre}, whose value is not necessarily available in the industry. Actually, from a mathematical point of view the preliminary cross-section can be a standard one, but this is just unlikely. For this reason, exactly as in the linear method, the gauge options of each wire are a set of industrial values of cross-section, Q_k. The algorithm could take any set of values for each of the Q_k vectors, but all optimization results shown in this chapter have been carried out with $S = 2$. The initialization process of the algorithm selects the closest two standard cross-sections to a_k^{pre}: one smaller,a_k^-, and one greater, a_k^+.

The algorithm starts assigning the lightest areas of Q_k to all of the wires and upgrades repeatedly the cross-section of the "lightest" wire (if possible), until the sum of all of the cross-sections surpasses the critical area A_{crit}. The concept of lightest wire is once more related to the volume and the mix w_k of the wires and not just to their cross-sectional area. Whenever a wire is the lightest but has the thickest available cross-section, the modified wire is the second lightest, and so on and so forth.

This Alg. 1 is exposed below and uses A_{crit}, a^{pre}, w, 1, a^{st} and S as inputs. A^{crit} is a single float value representing the critical sum of areas of the bundle. a^{pre} is a vector of N elements containing the preliminary cross-sectional areas of the N wires. w and l are respectively the mixes and the lengths of all of the wires. a^{st} is the complete list of standard available cross-sections that these wires can take, and S is the number of considered cross-sections for each wire. As previously discussed, when $S = 2$, the algorithm considers only one smaller and one greater areas for each of the a_k^{pre}, i.e. a_k^- and a_k^+.

The output of the algorithm is *a_opt*, a vector of N standard areas accomplishing $\sum_{k=1}^{N} a\_opt(k) \geq A_{crit}$ with minimum volume of copper. The volume of copper is calculated intrinsically in the *get_min_index* function, as the sum of the element-wise product of the w, 1 and a vectors. This function returns the index of the wire with least volume, among those that are still able to take greater cross-sections. The increase of cross-section for each of the wires is limited by S, and that is why this argument is also passed to this *get_min_index* function. Alg. 1 includes also the *initialize_Q* function, which mounts the Q matrix as follows:

$$Q = \begin{bmatrix} a_{k1} & a_{k2} & \dots & a_{kS} \\ \vdots & \vdots & \ddots & \vdots \\ a_{N1} & a_{N2} & \dots & a_{NS} \end{bmatrix} \tag{104}$$

The values of cross-sections belong to Q and they are selected by means of the *selection* vector, which contains only integers from 1 to S: *selection* = [s_1 … s_N]. The s_k component of *selection* selects the column of Q in its k-row: $a_k = Q(k, selection(k))$. This access to the Q matrix is performed in the function *select_areas*.

Input: A_{crit}, a^{pre}, w, l, a^{st}, S
Output: *a_opt*
Q = initialize_Q(*a_pre*, *a_st*, *S*)
selection = array_of_ones(length(*a_pre*))
a_opt = select_areas(*Q*, *selection*)
while $\sum_{k=1}^{N} a\_opt < A_{crit}$ **do**
    assert(**not** all(selection == *S*), "All wires reached their upper limit of cross-sections")
    min_index = get_min_index(*w*, *l*, *a_opt*, *selection*, *S*)
    selection(*min_index*) = *selection*(*min_index*) + 1
    a_opt = select_areas(*Q*, *selection*)
end

Alg. 1. Custom optimization algorithm with critical area criterion

6.6.3.3. Custom optimization method based on the critical current

The presented custom optimization algorithm shows accordance with the objectives of reduced computation time and maximum temperature of the bundles. This approach uses the obtained response surface of critical area of the bundles, as in the linear method. Yet, this document presents a formula for the critical current of bundles as well, which has impelled the authors to create a specific algorithm using this model.

As in the custom method based on the critical area, the main input of the algorithm is the expected current of each of the wires. The first step is to calculate the optimum areas as explained in section V-B. Afterwards, the algorithm starts providing normalized cross-sections to each of the wires, but in this occasion the suitability of the result is checked using the critical current model in each iteration. Since the input currents of the wires does not change during the execution of the algorithm, the custom method based on the critical area calculates the critical area only once at the beginning of the algorithm. As opposed to this, the custom method based on critical current must calculate the critical current in each new iteration, since the total area of the bundle is changing.

Since two different models are used in the same algorithm, the result of the algorithm accomplishes both restrictions of critical current and critical area in a reciprocal way. In other terms, the critical area is respected and the critical current calculated from the final value of area is respected as well.

Due to all of these reasons, this new approach, Alg. 2, can be considered an expansion of the prior custom method based merely on the critical area of the bundle (Alg. 1).

Input: A_{crit}, a^{pre}, T_{amb}, w, l, a^{st}, S_-, S_+
Output: *a_opt*
Q = initialize_Q(*a_pre*, *a_st*, S_-, S_+)
selection = array_of_ones(length(*a_pre*))
a_opt = select_areas(*Q*, *selection*)
a_pvc = getPVCAreas(*a_opt*)
while $\sum_{k=1}^{N} I_k > I_{crit}$ **or** $\sum_{k=1}^{N} a\_opt < A_{crit}$ **do**
    assert(**not** all(selection == S_- + S_+), "All wires reached their upper limit of cross-sections")
    min_index = get_min_index(*w*, *l*, *a_opt*, *selection*, S_-, S_+)
    selection(*min_index*) = *selection*(*min_index*) + 1
    a_opt = select_areas(*Q*, *selection*)
    a_pvc = getPVCAreas(*a_opt*)
    I_{crit} = getIcrit(*a_opt*, *a_pvc*, T_{amb})
end

Alg. 2. Custom optimization algorithm with critical current criterion

6.6.3.4. Comparison of the three methods

In order to compare the optimization methods, 200 random wire bundle cases have been passed to these assignment algorithms. Fig. 95 shows the comparison between their computation times, where the *x*-axis enumerates the 200 different bundle cases and the *y*-axis indicates the elapsed time after the execution of the three different algorithms for each of the cases. These times were obtained running the algorithms via Matlab® through an Intel® CORE™ i5 processor, without disabling hyper threading.

Fig. 96 compares the obtained areas of the bundles. Specifically, it shows the relative difference between the two custom methods and the integer linear programming approach, in such a way that the zero-level at the *y*-axis represents the reference value of total area of the bundle obtained by means of the linear method, and non-zero values correspond to the relative difference obtained with respect to this value. It is remarkable how the total areas are nearly identical between the custom method with critical area and the linear method, whereas the critical current method provides bigger bundles. The extreme value probability density distribution of the obtained maximum temperature of the 200 cases with the three different methods has been fitted, and can be seen in Fig. 97.

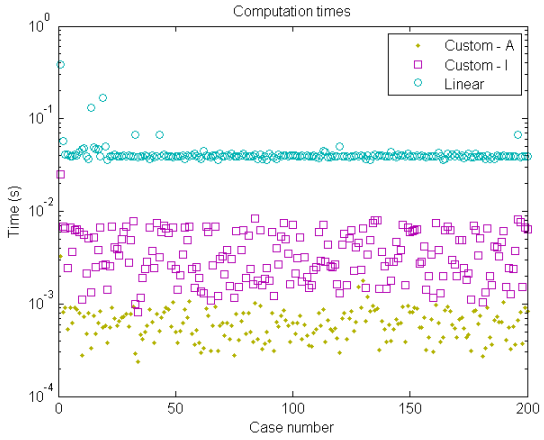

Fig. 95. Comparison of the computation times of 200 optimization cases using the three different methods

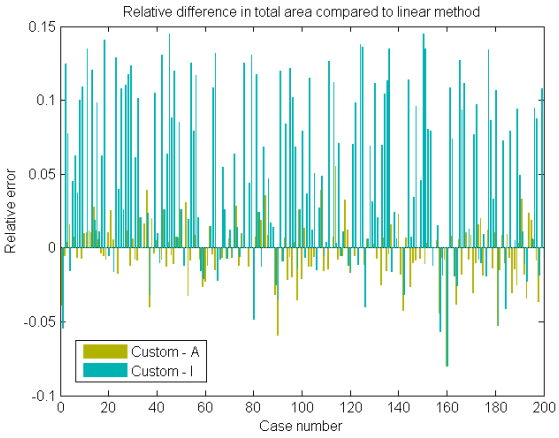

Fig. 96. Relative difference in total area of copper in the bundle compared to the linear method, calculated for 200 cases

Additionally, the reduced computation time makes the custom methods especially suitable for the purpose of the global optimization of the wiring harnesses of a complete vehicle.

Among all of these 600 results, eighteen particular cases have been selected. The first nine correspond to those with lower temperatures (Table 7). Conversely, the other nine cases (Table 8) correspond to those cases with higher temperatures.

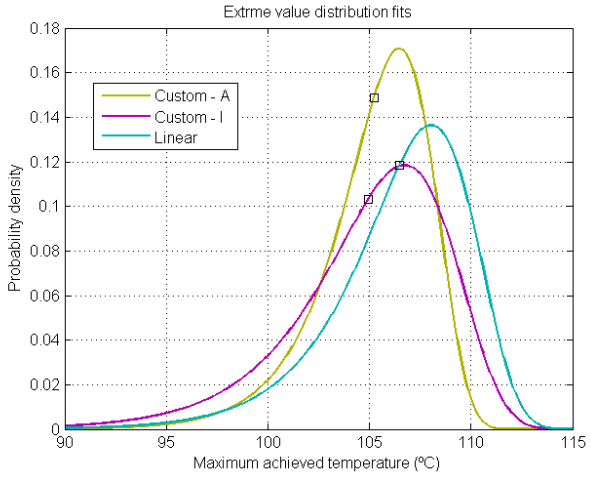

Fig. 97. Probability density function fit of the maximum temperature and their mean values

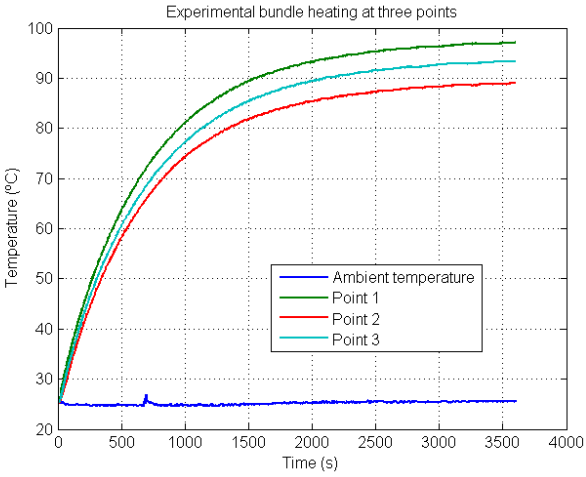

Fig. 98. Temperature evolution measured in three different points of a bundle dimensioned via the custom method with area criterion

Case	T_{amb} (ºC)	N	$\sum I$ (A)	Method	A_{crit} (mm²)	A_{total} (mm²)	T_{max} (ºC)
124	55.7	25	348.8	I	79.52	91.00	99.5
25	65.4	23	287.4	I	69.13	77.00	100.0
36	58.9	13	188.9	A	32.00	33.50	100.2
45	76.7	25	366.3	I	140.43	162.00	100.3
1	64.2	10	108.6	I	14.49	14.75	100.3
165	58.1	27	356.7	I	86.32	97.50	100.5
81	59.2	24	310.6	I	69.45	78.50	100.5
56	71.3	28	354.6	I	114.94	129.00	100.5
103	55.2	24	353.8	I	80.79	92.00	100.7

Table 7. Optimization results (FEM) – Coldest

Note that these Table 7 and Table 8 describe the bundle case with its number of case between 1 and 200, the ambient temperature, the number of wires, their sum of currents and the method used for dimensioning. The columns on the right show their calculated critical area and the results of optimization of each case, which are described by means of the obtained copper area of the bundle and the maximum temperature of the bundle after optimization. This maximum temperature has been calculated as the maximum temperature of polymer in the bundle, by means of the FEM simulator.

Case	T_{amb} (ºC)	N	$\sum I$ (A)	Method	A_{crit} (mm²)	A_{total} (mm²)	T_{max} (ºC)
144	65.9	23	348.9	Linear	96.43	96.50	116.0
74	64.3	17	214.8	I	42.70	43.00	114.1
174	59.8	12	158.7	Linear	24.44	24.75	113.0
106	64.1	14	178.8	I	32.10	33.00	113.2
187	56.3	20	228.7	I	40.14	41.50	113.0
138	58.6	19	228.6	I	41.89	43.00	113.0
27	61.0	23	287.4	Linear	63.06	63.50	112.8
81	59.3	24	310.7	Linear	69.45	70.25	112.2
146	61.1	20	249.6	Linear	50.47	51.25	111.7

Table 8. Optimization results (FEM) – Warmest

6.6.4.Experimental validation

In order to validate the optimization approaches, an arbitrary bundle has been optimized via the custom method with area criterion. It is a bundle made of twenty wires with currents ranging from 1.9A to 44.8A. Details of the bundle can be seen in Table 9.

The values of currents and ambient temperature of the laboratory have been passed to the algorithm and the cross-sectional areas have been obtained as outputs. FEM element simulations have been used to

predict the temperature of the bundle, revealing that in the worst layout the temperature could reach 113.9ºC and only 83.4ºC in the best case. These cases correspond to a controlled distribution of the wires: in the first one the wires with highest current density are placed in the center of the bundle, while in the second one these hotter wires are placed outwards.

The bundle has been built in laboratory and subjected to the aforementioned input currents. The temperature has been measured in three different points of the bundle nearly in its center. The achieved maximum stable temperature was 97.13ºC, which validates both the simulations and the optimization approach, and meets the hypotheses. Temperature measures can be seen in Fig. 98.

Wire number	Current (A)	Cross-section (mm^2)	Wire number	Current (A)	Cross-section (mm^2)
1	1.94	0.50	11	20.13	4.00
2	2.75	0.75	12	22.59	6.00
3	3.56	0.75	13	25.11	6.00
4	4.38	1.00	14	27.70	6.00
5	6.49	1.50	15	30.36	6.00
6	8.64	2.50	16	33.09	6.00
7	10.83	2.50	17	35.90	6.00
8	13.08	4.00	18	38.79	6.00
9	15.37	4.00	19	41.76	6.00
10	17.72	4.00	20	44.82	6.00

Table 9. Experimental bundle setup

6.6.5. Conclusions

Expressions providing the response surface of minimum sum of cross-sections of a wire bundle with given currents were obtained. Results show great accordance between the models and the finite-element simulations.

The integer linear programming method is used to find the optimum dimensions of wires in bundles, taking their surface of critical area as constraint. Additionally, in order to improve the computation time, custom algorithms have been created. The first of them uses merely the value of critical area of the bundle obtained by the response surface of critical area. The second one uses not only the critical area but also the critical current, which needs to be recalculated inside the loop of optimization. The custom methods obtain not only sufficiently good results, but also a remarkably improved computation time, which is one main goal in this research.

The custom methods achieve the objective of maximum temperature in average terms, being the custom method with area criterion the fastest and the one providing less variance of achieved maximum temperatures. This facts place the custom method with area criterion as the most suitable for wiring harnesses optimization.

The fact that the simulated results of the custom methods reveal temperatures above 105ºC makes it especially advisable to validate these results experimentally. Yet, the worst-case assumptions, such as the infinitely-long cylinders and the exclusion of signal wires in the bundles, suggest that experiments will reach lower temperatures than the finite element simulations. Once this is assessed, it would corroborate the quality of the optimized bundles. Note that the mean value of maximum temperature inside the bundle is below 105ºC with the custom methods. The statistical nature of these methods make it unavoidable to bring certain variance in the results, which forces to accept that pointing to 105ºC in the response surface will produce temperatures above this value. If this became undesired, the current of each of the wires should be rerated, so that the obtained cross-sections are bigger, thus reducing the statistical queue of values above 105ºC to a desired value, e.g. 5%.

The experimental validation of the custom method with area criterion has confirmed the expected hypothesis of more favorable temperature. The maximum achieved temperature of the experimental bundle, dimensioned through the custom optimization approach of critical area, reaches a high temperature but still under its objective temperature of 105ºC. This can be considered a positive result, validating the suitability of this method for wire bundle dimensioning.

6.7. Simulation and optimization of series connected wires subject to short circuit

The optimization process proposal in section 6.5 reveals the need for a short-circuit study of the series-connected wires in the network. This section introduces and describes a developed simulation and optimization method for this block of the optimization proposal.

The selection of the correct cross-section of a wire does not only depend on its steady-state behavior. Instead, it is necessary to dimension wires also ensuring that its temperature does not achieve dangerous values even in the case of a fault. For that purpose, the automotive industry has traditionally used melting fuses in order to protect wires from overheating. Automotive wire dimensioning standards such as ISO8820-4 demand using the characteristic tripping times of melting fuses in order to predict the maximum temperature of wires in the event of short circuits. On the other hand, it is also demanded that short circuit currents reach a minimum value, normally specified as a multiple of the rated current of the corresponding fuse.

Short circuits have different causes, locations and characteristics. They can be mechanical, i.e. short circuits produced by accidental contact between two conductors on account of foreign bodies, such as a tool or an animal. Other origin is the electrical one, corresponding to two conductors entering in contact because of the degradation of their insulation. And, last but not least, short circuits can be produced by a human error, due to a misuse of the network.

As regards the location of the short circuits, they can occur either inside or outside electrical equipment.

Finally, short circuits can also be classified considering their duration. Some short circuits disappear by themselves, resulting intrinsically temporary. Some other are considered fugitive, since the fault disappears due to the action of some kind of protection device, and does not reappear when the network is reenergized. One last type of short circuit is the permanent one. Permanent short circuits remain after re-energization and need intervention of operators to repair the network.

This chapter is focused on the optimization of series-connected conductors sharing one conventional automotive melting fuse. Like other circuit protection systems, there is a strong dependence on the characteristics of the fault and the tripping time of fuses. Mainly, the tripping time of a fuse depends of its temperature at the beginning of the fault and the current derived from it. In order to assess the suitability of a fuse, one can either use its characteristic curve or its nominal melting energy, depending on whether the fuse is going to be subjected to continuous currents or current pulses. The threshold between them is a matter of knowledge and control over the behavior of the fuse. Brief and intense pulses tend to cause adiabatic heating, and that is the reason why it is useful to simply calculate whether the pulse involves sufficient energy to melt the fuse or not.

The correct selection of an automotive fuse must ensure a certain desired life expectancy. This endurance can be essentially compromised by the current consumption nature of its electric loads, the ambient temperature and the temperature of the conductors in contact with the fuse.

So far, the natural way to proceed has been selecting the fuse first according to the electric loads. The wire cross-section is chosen afterwards depending on the breaking capabilities of the fuse. Eventually, the wire cross-section will be restricted by the limits of acceptable temperature of its insulation, voltage drop or desired short circuit current.

As usually, it is necessary to take the worst case as a reference to dimension the system. The dynamics of melting fuses and wires are different enough to roughly accept that their characteristic pre-arcing time and heating curves are divergent as the conducted current increases. In other terms, greater short circuit currents will melt the fuse faster, producing a smaller rise in temperature in the wire. As a result, the worst-case short circuit is the short circuit producing the smallest current.

This concept of worst-case short circuit with lowest current involves uncertainty. Some types of short circuits have the same cause as faults that cannot be considered short circuits due to the presence of a considerably resistive –and faulty– union between nodes of the circuit. This false short circuit would involve the lowest faulty currents, with the additional problem of the absolute uncertainty in the value of contact resistance. For this reason is crucial to be aware that the minimization of the short circuit current can be insufficient in front of possible mechanical short circuits with contact resistance. In some unfortunate occasions, an undesired resistive contact could cause a current low enough to heat the wire up rapidly without melting the fuse. This is a tremendously undesired effect, since it can produce a rapid corrosion of the wire insulation.

Therefore, one must be sure that there is no significant gap between the known and possible overload current and the minimized short circuit current. And, whenever there is any, a correct prevention measure must be carried out. This is going to be discussed in the next sections.

6.7.1. Scope

The objective of this study is to be able to decide the cross-sections of wires subjected to short circuits. In particular, the study is about series-connected wires connecting the positive and the negative terminals of a low-voltage DC source, and protected by one commercial automotive fuse. The series connection of wires is produced by the fact that power wires are connected between them by splices (Fig. 99) and short circuits can occur through one of the ramifications of these splices (Fig. 100).

The selection of cross-sections must respond to a desire of weight reduction. For this purpose, the optimum weight of the series-connected wire is desired. If the wires have different lengths, then the short circuit current is affected by their cross-sections with different sensibilities. Additionally, wires in

modular wiring systems are associated to a commercial mix, which can be very different for some combinations of wires. Therefore, wires with low mixes can be thicker than wires with high mixes, if it is necessary to produce higher short circuit currents to protect these series-connected wires correctly.

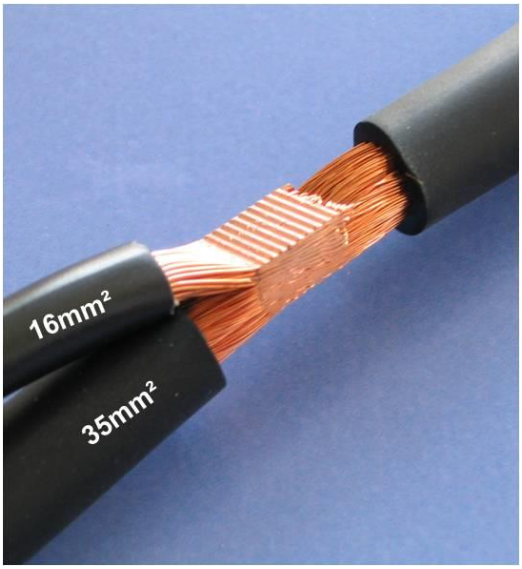

Fig. 99. Detail of an ultrasonic splice between two wires

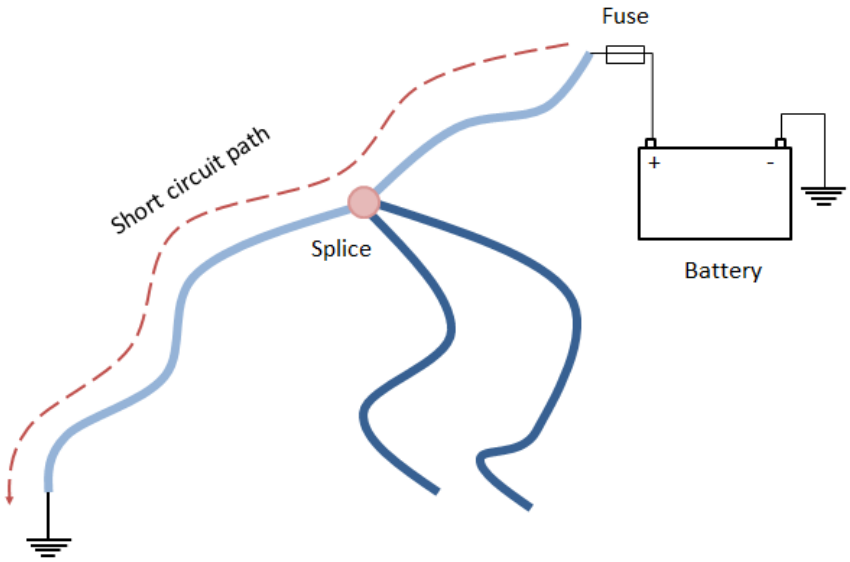

Fig. 100. Short circuit under study composed by series-connected wires

The final objective is thus being able to correctly predict the maximum achievable temperatures of series-connected wires after the corresponding short circuit. The simulation algorithm should be fast enough to properly provide information of the short circuit and use it as constraints inside a nonlinear optimization algorithm.

6.7.2. Simulation of short circuit across series-connected wires protected by one fuse

According to the objective of this chapter, it is necessary to have a simulator under the shape of a function capable of returning the maximum temperature of the wire and the short circuit current.

More specifically, this function must return the maximum temperature and its insulation separately, as well as the minimum and maximum values of the short circuit current. These set of four outputs will be used as constraints of the optimization problem, in such a way that the short circuit current reaches a minimum desired value, and the temperatures do not reach maximum acceptable values.

In order to have such simulator, it is necessary to have accurate and fast dynamic models of wires and fuses. The main resistance of short circuits studied here are due to the resistivity of copper, which varies with temperature as the short circuit lasts. This produces a variation on the short circuit current, which forces to use dynamic models.

Fuse model

Predicting the tripping time of a fuse can be performed in different ways. Normally, fuse manufacturers provide methods to estimate the tripping time for any given value of continuous current. One way to proceed is using the average tripping time curves provided by the fuse manufacturer. These curves give the average tripping time of the fuses and can be re-rated using the value of ambient temperature of the fuse. However, they assume that the current applied to the fuse is constant.

The fact that the short-circuit current is not constant makes these curves useful basically for high short-circuit currents, where the tripping time is fast enough to avoid any significant variation of current before the fuse trips. But calculating these constant-high-current short circuits is also done with the I^2t parameter (A^2s), which measures the necessary energy that the fuse must absorb to melt.

The higher the current is the more exact is the tripping time as calculated with the I^2t parameter, because the heating tends to be adiabatic. On the contrary, for low currents, the fuse can achieve a steady temperature at which the heat dissipation to its environment is equal to the power produced by the Joule effect. Theoretically, the current producing a steady temperature exactly equal to the melting temperature of the fuse equals its rated current, I_R.

Equivalent thermal circuit

Whereas the characteristic curves cannot be used with varying currents, a fuse model based on its absorbed energy (Fig. 101) can describe correctly the state of the fuse [17]-[18].

This equivalent electric circuit for the thermal model of the fuse uses the corresponding heat power per ohm ($i^2(t)$) as the current of a current source, I. As time passes, this power is stored in the capacitor. If R was infinite, any current would make the fuse blow after a finite time, but finite values of R produce a

certain value of current under which it is impossible to make the fuse blow. If the capacity C_{fuse} is set to I^2t, then the voltage at the capacitor v when an energy equal to I^2t has been absorbed is equal to 1. When the v voltage equals 1, the irreversible S switch opens and cannot close the circuit again.

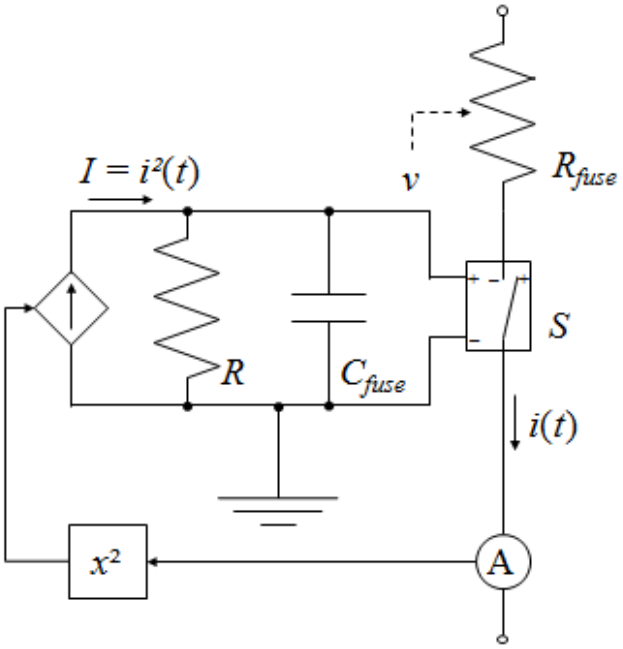

Fig. 101. Electric equivalent circuit for thermal fuse model

The fuse can open the electrical circuit from which $i(t)$ is taken. The fuse itself has a resistance that varies with temperature, R_{fuse}. This is modeled by assigning a certain maximum resistance of the fuse at the moment of melting, i.e. $v = 1$:

$$R_{fuse} = R_{cold} + v \cdot (R_{max} - R_{cold}) \tag{105}$$

For a constant current, the voltage at the capacitor follows an exponential law:

$$v = v_0 + IR\left(1 - \mathrm{e}^{-\frac{t}{RC}}\right) \tag{106}$$

From which one can derive that the minimum current capable of melting the fuse (assuming $v_0 = 0$) is:

$$I = \frac{v_{max}}{R} = \frac{1\mathrm{V}}{R} \tag{107}$$

This model can be coupled in a simulation system so that the charge of the capacitor varies with respect with current, predicting the tripping time for arbitrary variations of current.

***Least squares optimization for determination of* R**

The exact value of *R* should correspond to equation (107) and the rated current of a certain fuse. Still, a more satisfactory curve can be obtained using least square curve fit for a set of constant currents and melting times, given by manufacturer's datasheets. The initial value of *R* for a least squares minimization can be obtained as in (108):

$$R = \frac{1\text{V}}{I_R} \tag{108}$$

Figure 2 shows the experimental characteristic curve of a commercial fuse and the resulting curve obtained from the model, adjusting the value of *R* by the least squares method.

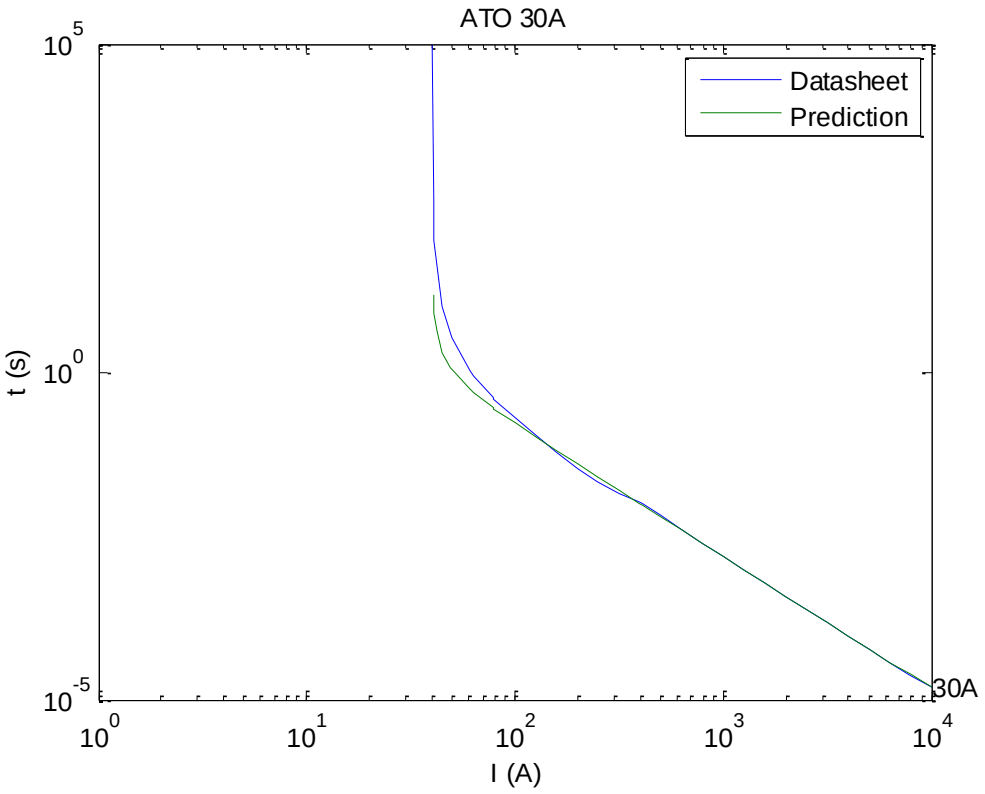

Fig. 102. Results of curve fitting to determine *R* for a commercial fuse

6.7.3. Wire model

The wire model in these calculations will assume that wires are surrounded by quiet air, being only able to dissipate heat through free convection and radiation. This is decided because the temperature increase of wires after a short circuit depends on both the heating time constant of the fuse and the wires. In particular, the faster the wire heats, the higher temperature it reaches. That is why the single wire behavior brings a reasonable worst case as regards heating time, because wires in contact with nothing else than air heat up faster than those in contact with other wires or other bodies. This produces the fastest

heating. Whenever a wire is in contact with other wires it will heat up more slowly, which reduces overheating during brief faults. In other terms, in the event of a short circuit the major risk occurs in exposed parts of the wire, and not at those stretches wherein the wire is in contact with other typical surfaces.

Finite volume method for series-connected wires

The finite volume method [9] is a well-known approach for heat transfer simulation. In this particular case, wires are sliced using a particular distance, Δx, and each of the resulting slices is divided at the same time in two different volumes, which are its core and its insulation, as shown in Fig. 103.

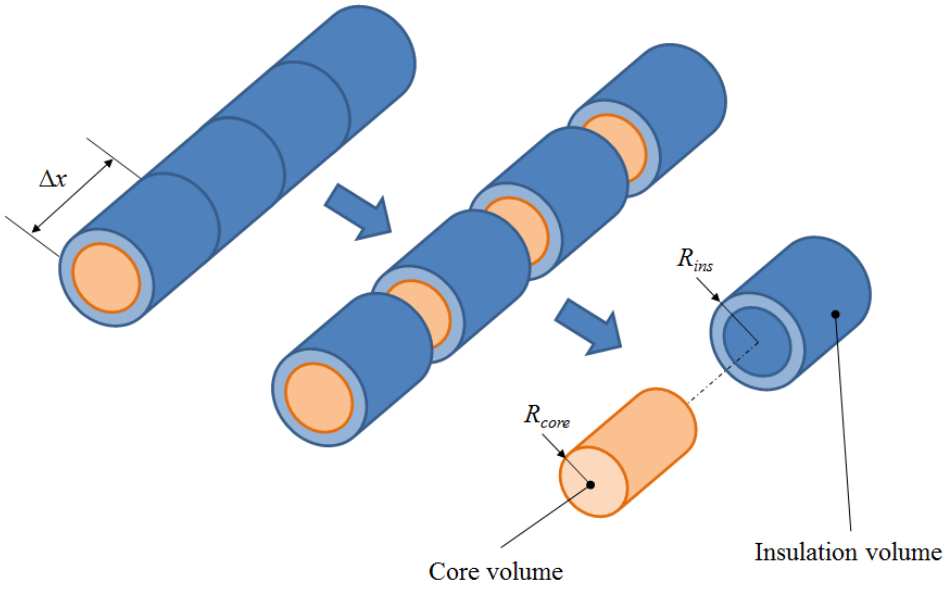

Fig. 103. Scheme of the finite volumes used for the wire heating model

Heat can flow from core elements to any other elements, and insulation elements can transmit heat to other insulation elements of the same wire, but not to insulation elements of different wires connected in series, because as seen in Fig. 99, isolation elements in splices are not in contact between them. This can be seen in Fig. 104. With this rule and the resulting equivalent electric circuit seen in Fig. 104, the connectivity matrix can be elaborated. The thermal conductance between elements depends on whether they are connected axially or radially, and depends also on its material and temperature.

Fig. 104 shows the equivalent thermal circuit of the problem. The Joule heat is expressed as current sources of the core volumes, so that the total heat is propagated as current across resistors. These resistances depend on the temperature of the volumes, so that they must be recalculated in each iteration. Since the ambient temperature is constant, it is expressed in Fig. 104 as a voltage source. The core and surface temperatures are the unknowns for each iteration.

The temperature of each of the volumes is in reality non-uniform in radial direction. Core volumes are composed of highly packed metal strands. Here, their behavior is described by averaging their thermal parameters according to the packing factor. Still, the triangular packing of the strands corresponds to a 93% of metal in the cores, which is equivalent to a high thermal conductivity. On account of this, elements are essentially metallic, which makes it a good estimation to consider a uniform temperature in their inside. On the contrary, there is a pronounced temperature drop between the core and the exterior surface of the wire (Fig. 105).

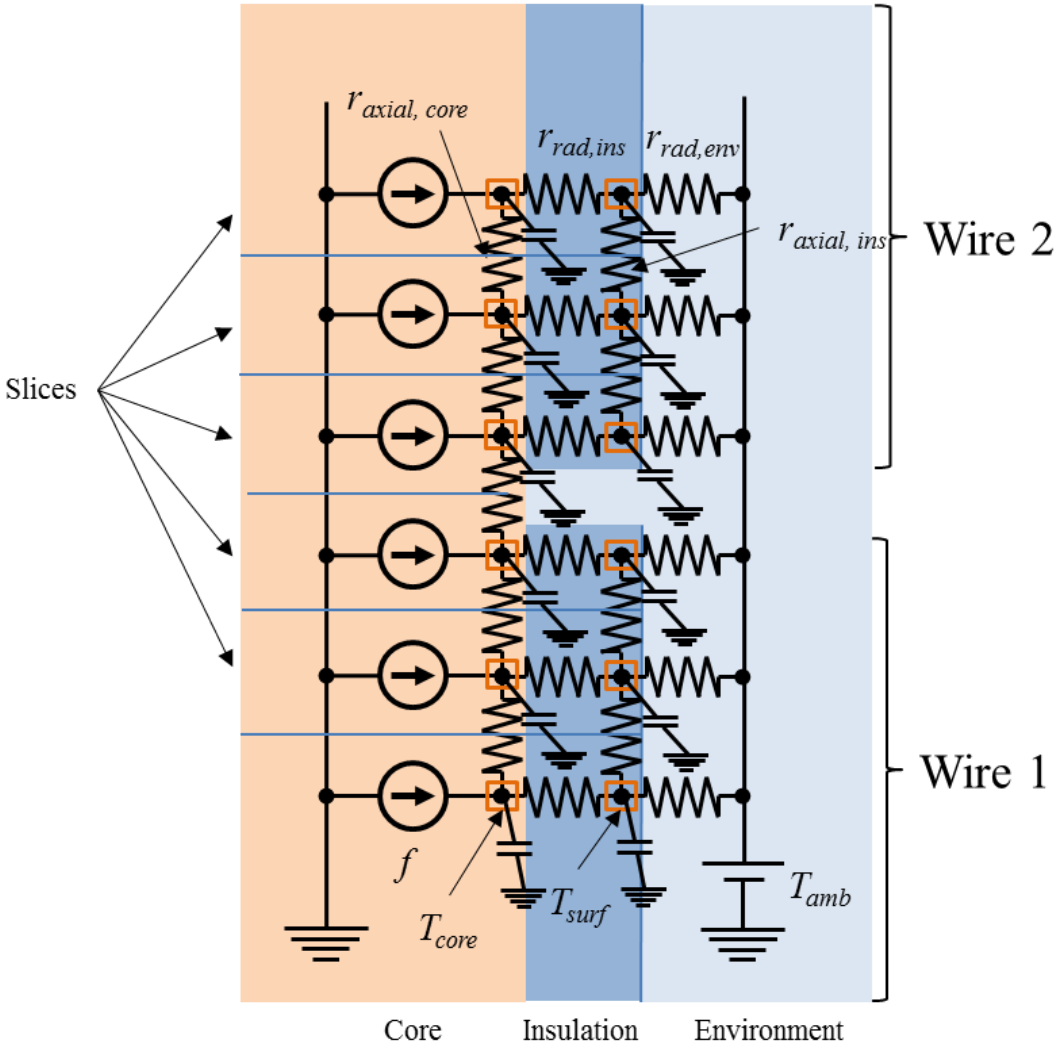

Fig. 104. Equivalent thermal circuit of the finite volume scheme

Despite both the temperature distributions in the core and in the insulation respond to non-linear expressions, they can be well approximated by linear equivalents. First, thanks to the aforementioned high thermal conductivity of the core, and secondly because normally the thickness of the insulation is small enough to produce nearly linear temperature drops (Fig. 105).

Solving the finite volume problem requires calculating the thermal conductance between different volumes and also with the environment, as well as their capacitance. The generated Joule power of core volumes is also needed. All of these parameters depend on temperature, but the fact that insulation volumes have a non-uniform temperature distribution forces to use a theoretical mean temperature of the insulation volume to calculate the thermal parameters of its material.

The temperature of the core volumes corresponds to the temperature exactly at the separation between core and insulation volumes. Likewise, the temperature of the insulation volumes corresponds to the temperature of the exterior surface of the wires. Therefore, obtained results provide the minimum and maximum temperatures of the insulation elements: T_{core}, T_{surf}. The uniform temperature of the core and the maximum temperature of the insulation are assumed to be equal, despite, in reality, the latter could be slightly lower due to certain contact resistances.

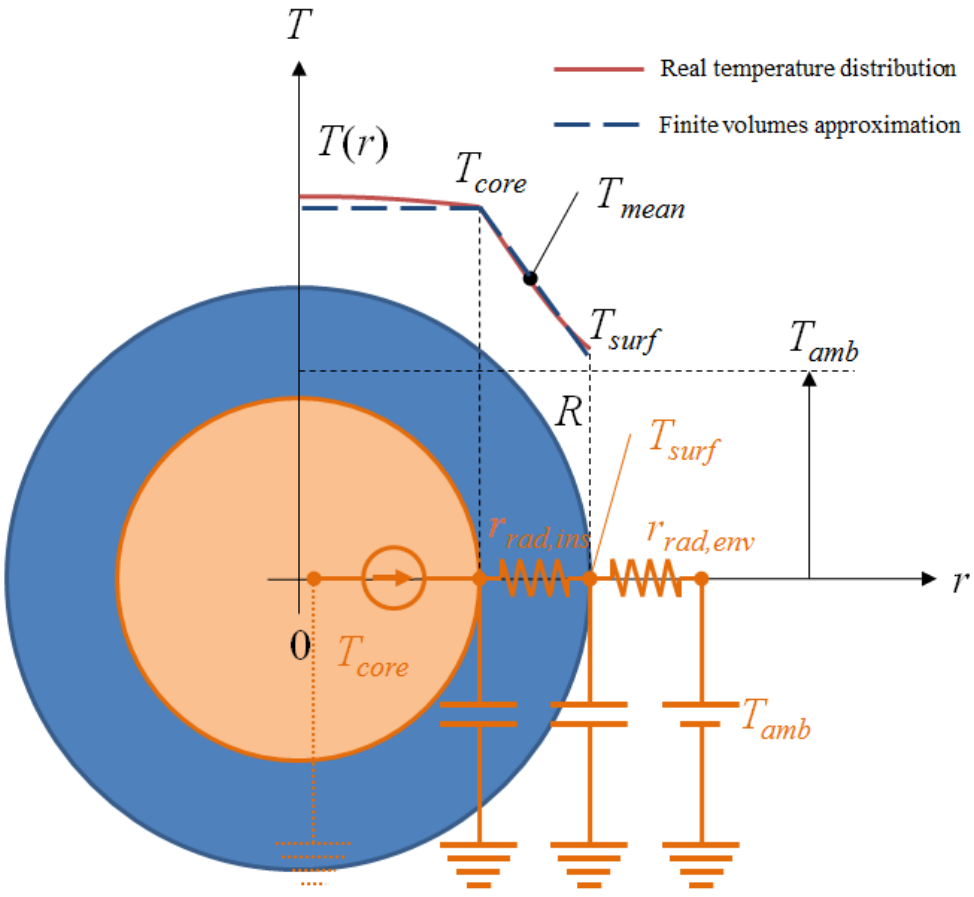

Fig. 105. Radial temperature distribution of wires

The finite volume method defines a system of linear equations. Once this problem is solved, the vector of temperatures of each of the elements, T, is obtained. T contains both T_{core} and T_{surf} of each of the slices of the wires, so the number of elements of this vector is twice the number of slices, $n_{volumes} = 2n_{slices}$.

The system of equations can be expressed in matrix form according to the implicit method:

$$C_k \frac{T_{k+1} - T_k}{\Delta t} = F_k + \left(G_k + G_{b,k}\right) T_{k+1} + b_k T_{amb} \tag{109}$$

$$b = \begin{bmatrix} b_1 \\ \vdots \\ b_n \end{bmatrix} \tag{110}$$

$$G_b = \begin{bmatrix} -b_1 & & 0 \\ & \ddots & \\ 0 & & -b_n \end{bmatrix} \tag{111}$$

Where G is the conductance matrix between elements, G_b is the conductance matrix between elements and the environment, T_k is a vector containing the temperatures at the current k-iteration, T_{amb} is the ambient temperature, and T_{k+1} is the vector of new temperatures after the time step, Δt. F is a vector containing the total heat power generated in each finite volume, and C is the heat capacity of each of the finite volumes. Since all matrices depend on temperature, they are calculated using T_k. b is the array of conductivities between each of the volumes and the environment, and its components are present in the diagonal of G_b. These conductivities are calculated considering convection and radiation. Compared to Fig. 104, they are the inverse of the $r_{rad,env}$ resistances.

The resulting T_{k+1} can be calculated then by just isolating this term:

$$T_{k+1} = \left(\frac{C_k}{\Delta t} - G_k - G_{k,b}\right)^{-1} \left(\frac{C_k}{\Delta t} T_k + F_k + b_k T_{amb}\right) \tag{112}$$

The implicit method provides good results with the heat equation, which is a parabolic partial differential equation, allowing larger time steps without compromising stability of the solutions. Still, precision can be improved if T_{k+1} are used to recalculate all of the matrices of the system before taking T_{k+1} for the next iteration.

The conductance values of G and G_b are calculated from certain radii, so that the observed temperatures correspond to points on the radius of the core and the external surface of the wire.

The F matrix is calculated from the total current crossing the finite volumes and the resistance of each of them. This current can be given for each simulation step, as coming from a current source, or it can be calculated externally after each simulation step. In the case of the short circuit, the calculation of the current requires the overall resistance of the series-connected wires, as the sum of all of the resistances of the core volumes that have been used for the calculation F.

6.7.4. Short circuit simulation

The short-circuit current throughout a set of series connected wires depends on several parameters of the entire short-circuit path. Particularly, parameters taken into account here are the resistance of the wires, the resistance of the fuse and one constant value of additional resistance present in the path (113).

$$I = \frac{V}{R_0 + R_{f,cold} + R_{wires}} \tag{113}$$

$$R_{wires} = \int_0^{\sum L_w} \frac{\partial R(x,T)}{\partial x} dx \tag{114}$$

Where V is the voltage of the battery, R_0 is the imposed minimum resistance of the path, $\frac{\partial R_i(x,T)}{\partial x}$ is the unit length resistance of the wire i as a function of its temperature, T, and a given point x of the wire. R_{wires} represent the total resistance of the series-connected wires, calculated as the integral of the unit-length resistance along the wires. The limit of the integral, $\sum L_w$, is the sum of the lengths of the wires, $w = 1 \ldots N$. The discretization of this expression leads to the direct sum of the resistance of each of the core volumes in the finite volume method:

$$R_{wires} = \sum_{i=1}^{n} \rho_i(T) \cdot \frac{L_i}{a_i} \tag{115}$$

The resistance of each of the wires depends on the resistivity of their conductor material, which varies with temperature, $\rho_i(T)$. Then, the total resistance of the wire depends on the temperature distribution of the wire along its extension. L_i and a_i are respectively the length of the i-th volume and its conducting area.

In the first moment of the short circuit, the temperature of the wires is equal to the ambient temperature. This temperature will increase as the short circuit goes on, and therefore the resistance of the wires is going to be the minimum one along the entire short-circuit event. Thus, the maximum value of short-circuit current will be its starting value, and it will decrease rapidly as wires heat up, due to the increase in their resistance.

If the short circuit persists, both the temperature of the wires and the current will reach a stable value, after a certain time. This will normally correspond to very high temperatures of the wires. This would occur if no circuit breaker was included in the set, but it the fuse is correctly chosen, it will blow before

the temperature is too high. Still, the simulation of the short circuit must be able to give a correct result regardless of whether the fuse blows or not.

The short-circuit current will reach a minimum value right before becoming zero when the fuse blows and opens the circuit.

The variation of the short-circuit current depends also on the inductance of the short-circuit path. Still, it is expected to be low enough to be negligible, because the time constants of wires are much greater than the possible delay produced by the inductance of the short-circuit path.

Description of the algorithm

The short-circuit simulation algorithm (Alg. 3) calculates iteratively the short-circuit current. As a first step, the short-circuit current is calculated as in equation (113). Then, the *solve_FM* function simulates the evolution of the short circuit. This function couples the fuse and the wire models, so that each time step varies the stored energy of the fuse according to the fuse model in Fig. 101.

This way, the function is first called in "fuseTrip" mode. Under this mode, the short circuit simulation persists with a small time step, *dt1*, until either the fuse blows or the maximum number of iterations is reached. If the short circuit is such that the fuse can blow before the maximum iterations are reached, then the value of fuse tripping time is returned in *ftt*, in seconds.

On account of heat diffusion, the external temperature of the wire reaches its maximum value later than the maximum temperature in its core. For that reason the short circuit calculation includes a second part, where the evolution of temperature after the fuse blows is calculated. This time it is calculated with larger time step, *dt2*, because now that the fuse has already blown, less precision is needed.

```
Input fuse_data, fuse_type, fuse_rated_current, fuse_Tamb, areas, lengths,
wires_Tamb, voltage, R0

Output time,Tmax_core,Tmax_ins,I,Imin,Imax,ftt

N = length(areas)
dt1 = 0.001          %seconds
dt2 = 0.1            %seconds
dt3 = 0.005          %seconds
dx = 0.01            %meters

maxtime = 10         %seconds
max_iterations_1 = ceil(maxtime/dt1)
max_iterations_2 = max(max_iterations1,60)
iterations_2 = 2
iterations_3 = 3
queue_time = 10      %seconds

FVMS = get_FV_information(lengths, dx, areas, wires_Tamb)
fuse = filterFuseData(fuse_data,fuse_type,fuse_rated_current)

I_ini = FV_get_current(FVMS,wires_Tamb,voltage,R0+fuse.RF)
SE_INI = 0

[time1,I1,T1,ftt,SE_FIN] =
solve_FV(FVMS,wires_Tamb,I_ini,SE_INI,dt1,max_iterations1,voltage,
fuse,R0,'fuseTrip')

Imin = min(I1(I1>0))
Imax = max(I1)

[time2,I2,T2,ftt,SE_FIN] =
solve_FV(FVMS,T1(end),I1(end),SE_FIN,dt2,max_iterations2,voltage,
fuse,R0,'fuseTrip')

I = concatenate(I1,I2(2:end))
T = concatenate(T1,T2(2:end))
time = concatenate(time1,time1(end)+time2(2:end))

[Tmax_core,Tmax_ins] = split_temperatures(FVMS,T,N,time)
```

Alg. 3. Short circuit simulation

The *solve_FV* function uses initial values of current and stored energy of the fuse. At the beginning of the short circuit calculation, the value of current occurs when all of the temperatures of the finite volumes are equal to the ambient temperature. Then, having the values of temperatures ($T_0 = T_{amb}$) and current, the set of matrices for the first iteration can be generated. From this set of matrices, the temperature of the next iteration is achieved ($T(1{:}N,1) = T_1$). Additionally, the resistance of the wires at this new temperature is also obtained (R_w). At the same time, the value of current of this iteration is passed to the fuse model, so that the fuse stores energy, and the new energy of the fuse (V_1) and its resistance after this iteration (R_f) are obtained. In the first moment, the energy, *SE_INI*, of the fuse is $V_0 = 0$. In the new iteration, the current is calculated using R_w and R_f. With this new current, a new temperature of the wires is calculated from a new T_0 taking the value of T_1, and likewise does the fuse with V_0 and V_1. And so on and so forth.

Experimental validation

A set of different combinations of series-connected wires with different cross-sections and lengths has been subjected to short circuits. The sets have been protected with different fuses to produce different combinations. Results of the short circuit and its simulation can be seen in Fig. 106, with just one wire. The same experiment can be seen in Fig. 107 with 3 wires.

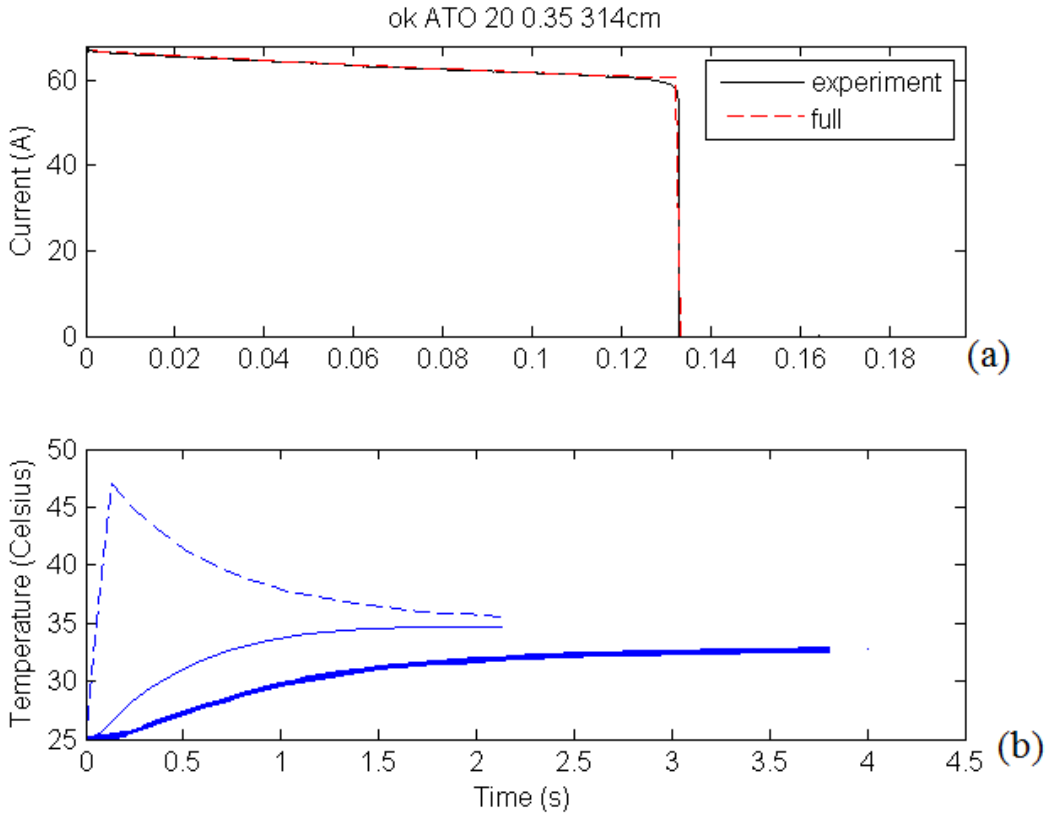

Fig. 106. Experimental validation of a short circuit (one wire)
a. Experimental versus simulated short-circuit current
b. Experimental (thick solid line) versus simulated (thin and dashed lines) temperatures of the wire

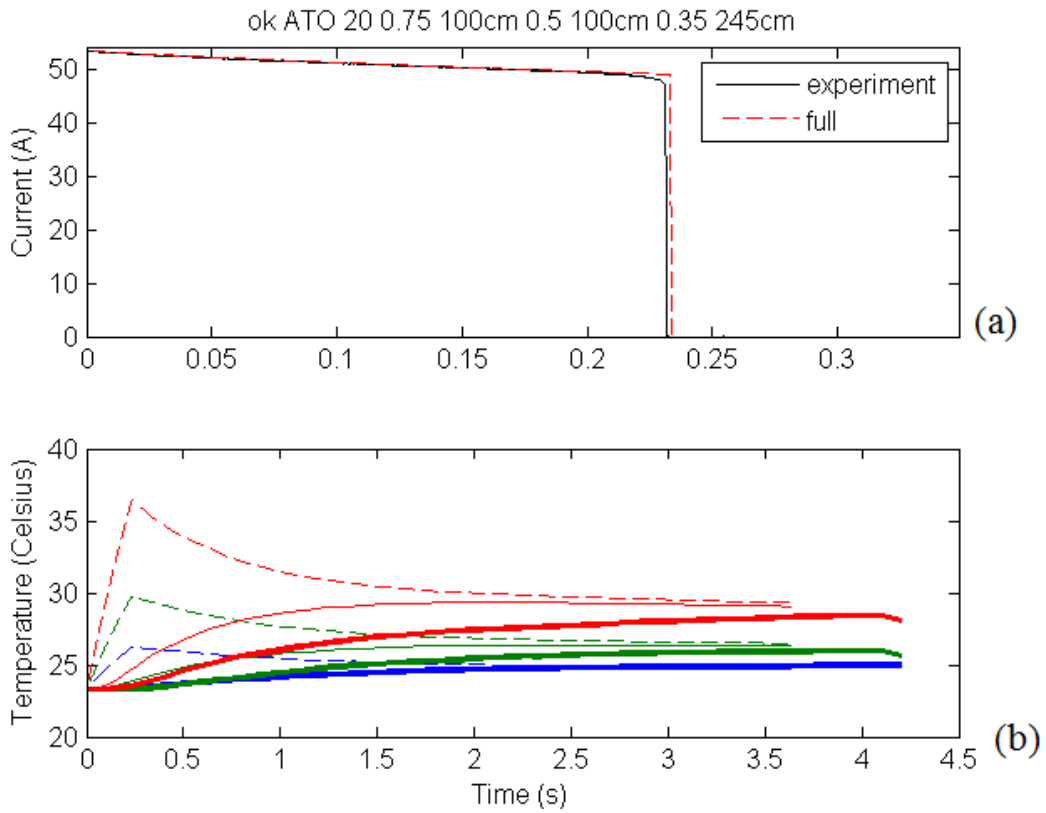

Fig. 107. Experimental validation of a short circuit (three wires)
a. Experimental versus simulated short-circuit current
b. Experimental (thick solid line) versus simulated (thin and dashed lines) temperatures of the wires

In both figures Fig. 106 and Fig. 107, two graphs are shown. The upper graph shows the measured current during the short circuit compared to the simulated current. In the lower graphs, the simulated temperature of the wires versus the obtained temperatures are shown. The dashed lines represent the simulated temperature in the internal surface of the insulation of the wires. The solid, thin lines represent the simulated temperature of the external surface. The measured temperature is depicted by thicker lines. In Fig. 107, each of the wires is associated to a color: red, green and blue.

Results show accordance between the simulated current and the real measured current, as well as the tripping time of the fuse. The temperature of the wires shows also good accordance, despite the dimensions of the thermocouples made the temperature transient slower than the simulated external temperature.

6.7.5. Cross-section optimization of series-connected wires subjected to short circuit and protected by one fuse

When two or more wires are connected in series and subjected to short circuit, the resulting short circuit current depends on their resistance. This resistance depends at the same time on the resistivity of their core material, their temperature, their cross-section, and their length. As the wires gain temperature, this

short circuit current will decrease more or less depending on the relation between the resistivity of the materials and their temperature.

For instance, if two wires are connected in series and subjected to a short circuit, the resulting maximum and minimum short circuit currents vary as shown in Fig. 108. In this figure, the two cross-sections are considered variables, and the z-coordinate shows the value of current for this combination of cross-sections.

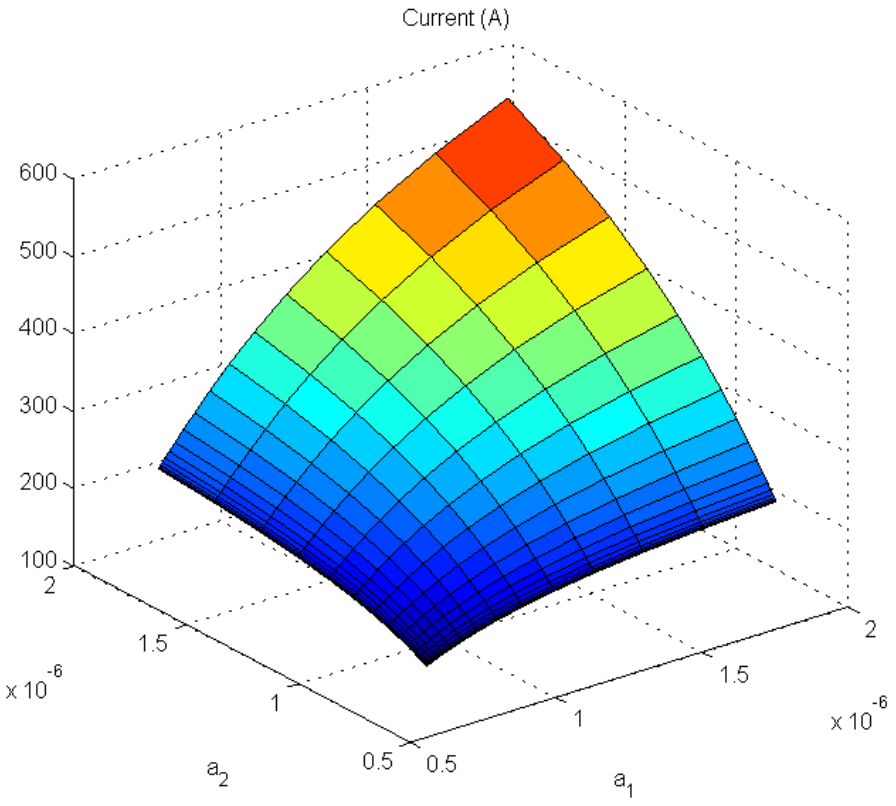

Fig. 108. Short circuit current for different cross-sections of two series-connected wires of equal lengths

This way, and given other constants like the type of fuse and the ambient temperatures, the short circuit current can be seen as a function of *N* variables, being *N* the number of series-connected wires. The values of each of the variables a_i $i = 1 \ldots N$ is the cross-section of each of them (116). Likewise, the tripping time of the fuse will also vary with these variables (117). This can be also done with the maximum temperature of the wires, which is exemplified in Fig. 109.

$$I_{sc} \equiv I_{sc}(a_1, a_2, \ldots, a_N) \tag{116}$$

$$t_{pa} \equiv t_{pa}(a_1, a_2, \ldots, a_N) \tag{117}$$

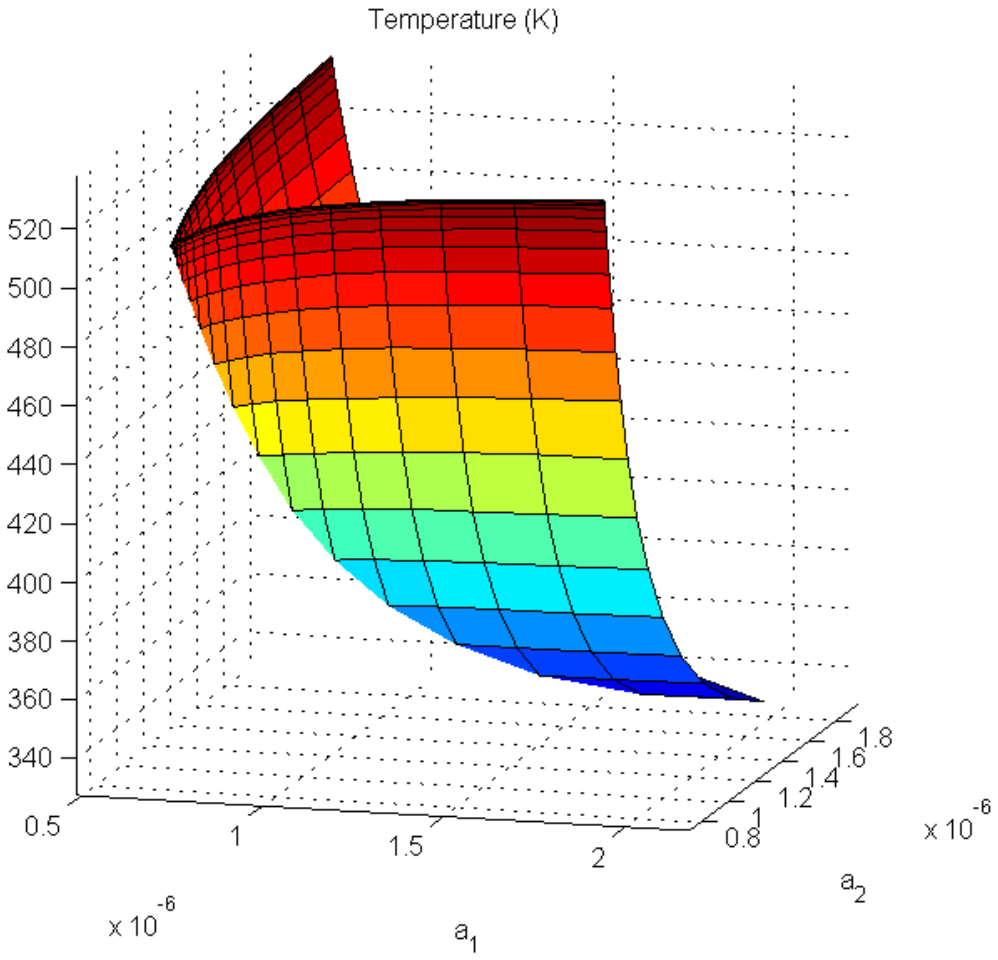

Fig. 109. Maximum reached temperature along two wires of equal lengths after the short circuit, for different cross-sections a_1 and a_2

This information of the short circuit can be associated to limits defining constraints of minimum short circuit current, maximum tripping time, and maximum temperature of the insulation of wires.

The cost function

The cost function is the volume of copper. The volume of copper determines the mass of copper, and it is calculated as the product of the cross section and the length of each of the wires. As in previous sections there is also a weight coefficient corresponding to the installation ratio or *mix* of the wires. This is made because the selection of cross-sections for a particular wire is shared by any manufactured vehicle of the same type. The cross-section of the wire cannot be adapted to every customer, but merely whether the wire is present or not. Therefore, instead of optimizing particular instances of cars, it is necessary to optimize the entire fleet of sold cars of the same type, by assigning a ratio to the cost of each of the wires of the vehicle. This *mix* influences the optimization in such a way that rare wires tend to be thicker and frequent wires tend to be thinner, in order to have a light fleet of cars. Following these rules, the cost function is defined as in equation (118). For $N = 2$, the cost function looks like a plane, as in Fig. 110.

$$V = \sum_{i=1}^{N} a_i \cdot L_i \cdot w_i \tag{118}$$

$$\nabla V = [L_1 w_1, \dots, L_N w_N] \tag{119}$$

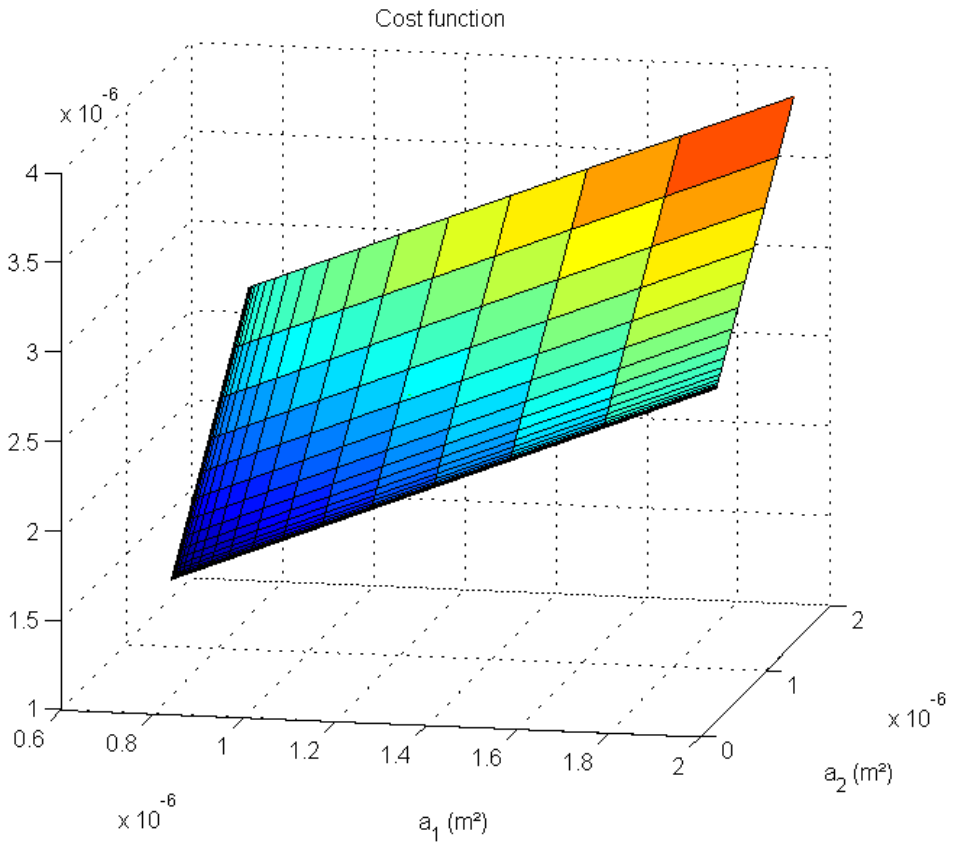

Fig. 110. Cost function seen as plane of two variables, representing different cross-sections of two series-connected wires with equal lengths and mixes

For larger *N*, the cost function becomes an *N*–1-dimensional hyperplane in an *N*-dimensional space, and cannot be hence depicted in the same way. The gradient of the function is always a constant vector, composed by the product of the lengths and the mixes of the wires (119).

Constraints

The values of minimum and maximum short circuit current, maximum temperature of each of the wires and tripping time of the fuse are obtained by means of the simulation of short circuits. These values must be compared to certain boundaries to define constraints. In particular, the short circuit current must accomplish a minimum value, which is proportional to the rated current of the fuse. This constraint is imposed to ensure that the fuse always blows in case of short circuit (120). A safety coefficient C_{SC} multiplies the rated current of the fuse, I_R.

$$I_{sc}(a_1, a_2, \dots, a_N) \geq C_{sc} \cdot I_R \tag{120}$$

The achieved temperatures of each of the wires cannot exceed the particular maximum acceptable temperature in short term of that insulation material (121).

$$\begin{matrix} \Theta_1(a_1, a_2, \dots, a_N) \leq T_1^{max} \\ \vdots \\ \Theta_N(a_1, a_2, \dots, a_N) \leq T_N^{max} \end{matrix} \tag{121}$$

Figure Fig. 111 shows the characteristic hyperbolic-like shape of the boundaries defined by these different constraints, for $N = 2$.

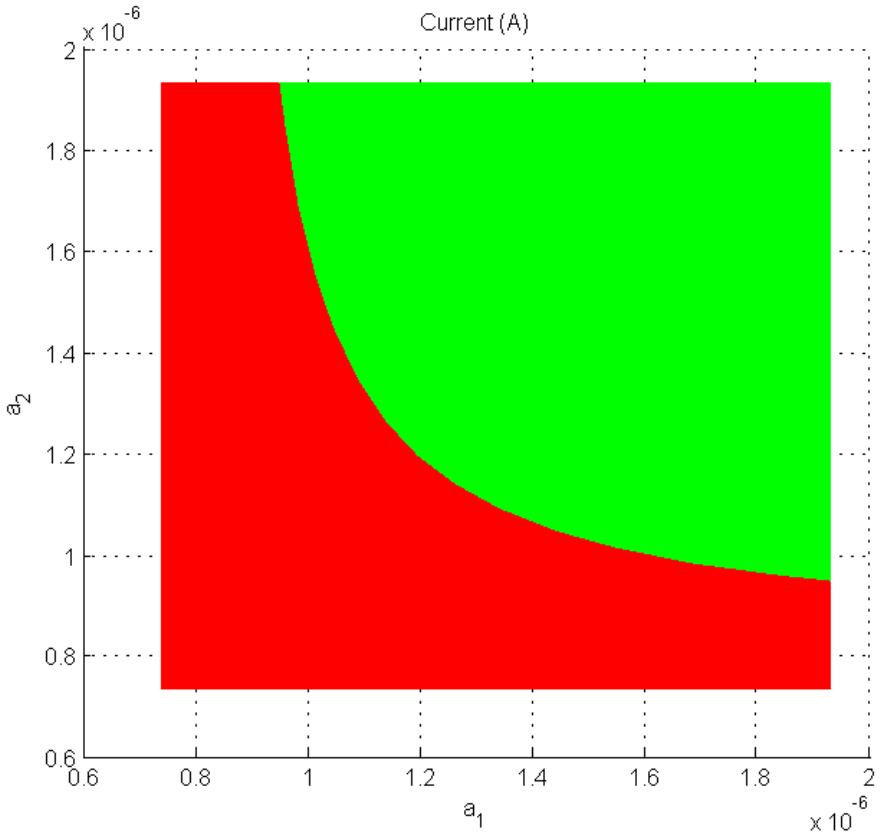

Fig. 111. Feasible (green) and unfeasible (red) combinations of cross-sections a1 and a2 according to the minimum short circuit current constraint

Likewise, Fig. 112 shows the same boundaries, this time for three variables.

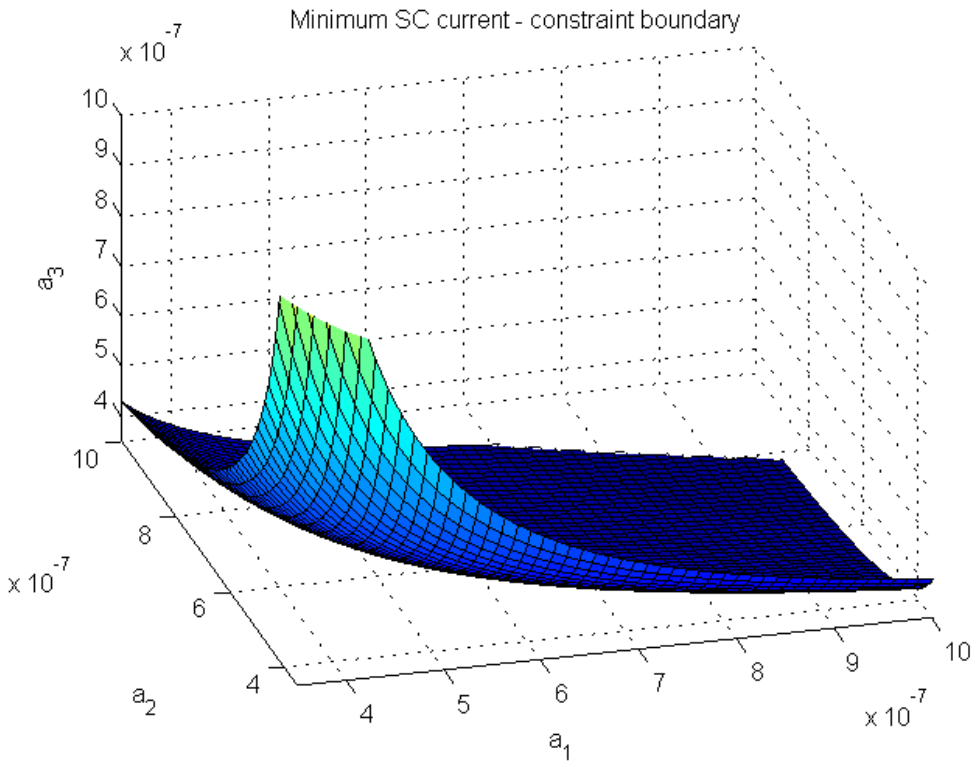

Fig. 112. Constraint boundary of the minimum short circuit current for three variable cross-sections. Values of [a_1, a_2, a_3] below the surface are unfeasible solutions and vice versa

Resolution

The problem is solved with the *fmincon* function in Matlab®, which finds the minimum of constrained nonlinear multivariable functions. It needs a set of matrices and vectors containing the information of the optimization problem. This function can operate using different algorithms [19]-[23], starting always at a given initial point x_0 and attempting to find a minimizer x of the cost function subject to linear and nonlinear constraints.

The cost function must give its value and optionally its gradient. If the gradient was not given, then the algorithm would calculate it through finite differences, which would slow down the optimization due to the corresponding and severe increase of function calls.

The constraints must be expressed so that feasible values of the variables result in negative values of the constraint functions. Marginal and unfeasible values of the cross-sections must provide respectively zero and positive values of the constraining functions. Taking all of the aforementioned constraints, this vector of non-linear constraints looks as in equation (122). Then, feasible solutions are such like all components of c are negative or zero.

$$c = \begin{bmatrix} C_s I_R - I_{sc}(a_1, a_2, \dots, a_N) \\ \Theta_1(a_1, a_2, \dots, a_N) - T_1^{max} \\ \vdots \\ \Theta_N(a_1, a_2, \dots, a_N) - T_N^{max} \end{bmatrix} \tag{122}$$

This algorithm does not work with integer variables, and thus the resolution of the problem provides the optimum values of areas. For each obtained area, it must be selected between the closest standard values. These standard values are normally two values: one greater and one lower. When the obtained value of area for a wire is lower than the minimum available cross-section or greater than the maximum one, then there is only one option available. In this study, the way to choose the final cross-section is carrying out an ordered and exhaustive evaluation of the *V* function for different possibilities. The evaluations start with the lightest. The first time one combination of standard cross-sections results in a feasible result, it is considered optimum and the search ends. This is depicted in two dimensions in Fig. 113, where there is only one feasible solution with standard wire cross-sections, indicated as a check symbol. The remaining three solutions are unfeasible in accordance with this constraint of minimum short circuit current, and they are indicated as crosses. The floating optimum is indicated as a blue point, and the gradient of the cost function is represented as an arrow.

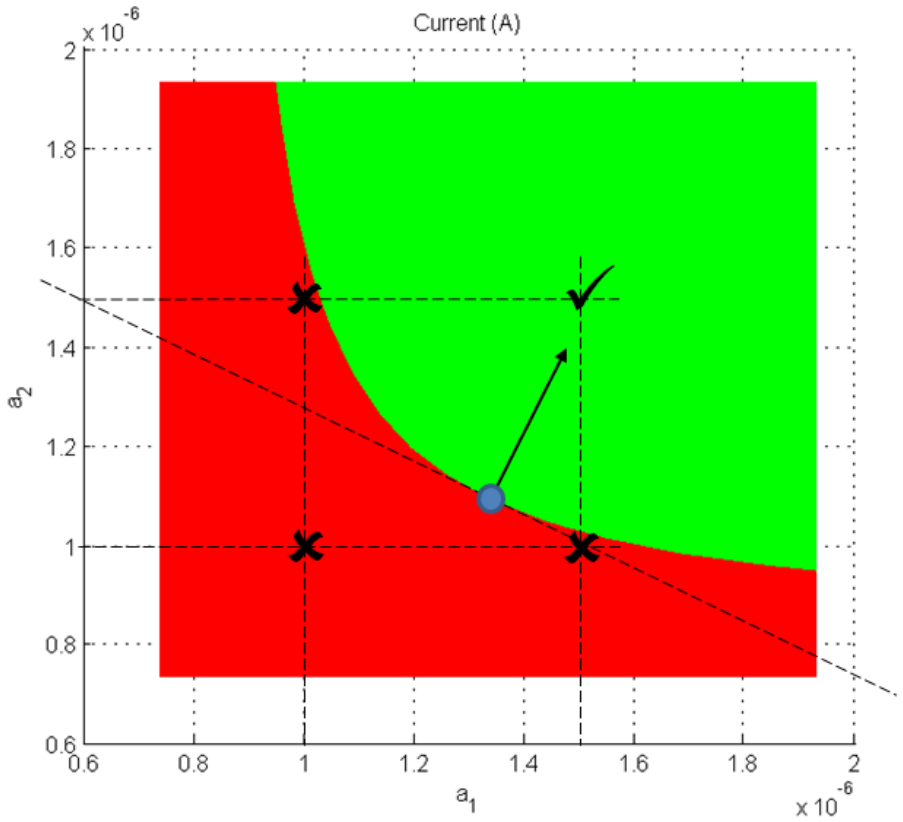

Fig. 113. Evaluation of four different standard values of cross sections around the found floating optimum (blue point): only one combination of standard cross section is feasible (check) and the other three are unfeasible (cross)

Initial values of cross-sections

Due to the characteristic shape of the constraints, the optimum is usually close to the edge defined by equal values of cross-section for all of the wires, as seen in Fig. 113, where the optimum corresponds to 1.5mm² for both wires. This fact can only change for extreme differences of mix, so that the gradient of the cost function is almost parallel to the axis of one of the variables. Fig. 114 shows a similar case, this time with dissimilar mixes of the wires, so that the gradient is nearly vertical. This time, the optimum cross-sections are not the same: a_1 = 2.5mm² and a_2 = 1mm². Despite variations in the cross-section of any wire produces notable changes in the short circuit current and in the temperatures, the same variations can produce insignificant changes in the cost function, if some of the mixes are very low compared to the rest of mixes of the wires. In Fig. 114, it is visible how the cost function is substantially less sensible to a_1 than to a_2.

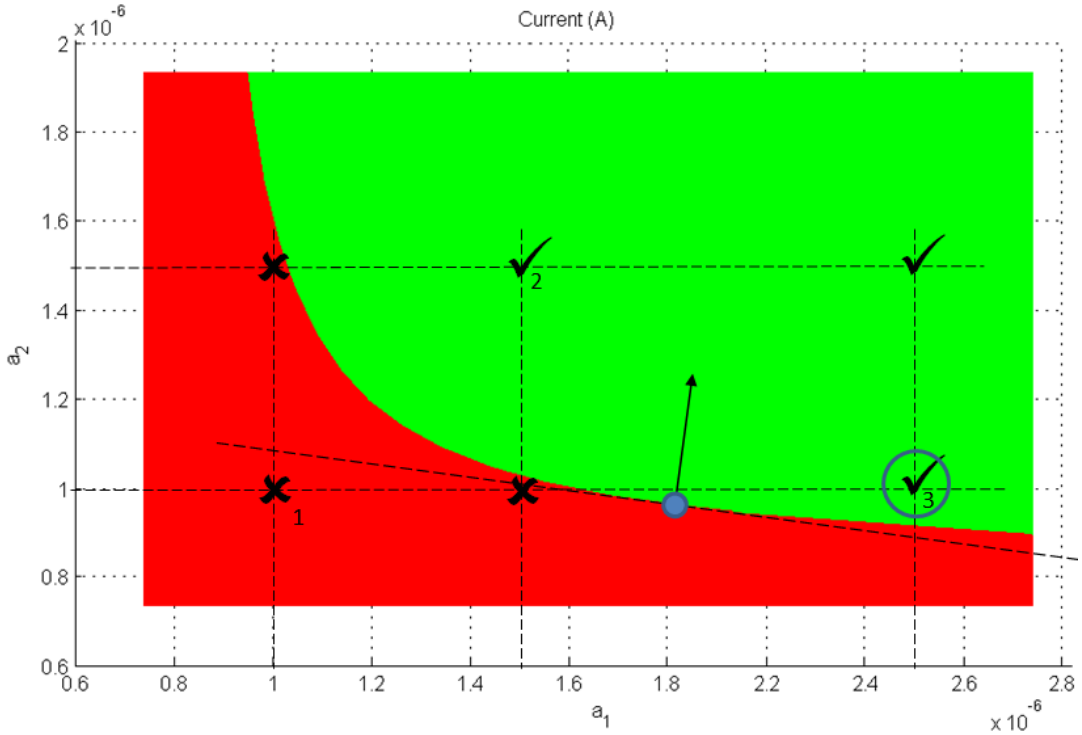

Fig. 114. Evaluation of four different standard values of cross sections around the found floating optimum (blue point), for dissimilar mixes: the standard optimum is encircled

In spite of these dissimilar mixes displacing the optimum, it is chosen in this study to give initial values of cross-sections assuming that they will be identical for all of the wires. Therefore, the first feasible solution passed to the optimization algorithm must be such that all of the wires have the same cross section. This is done iteratively starting from a first guess until the lightest feasible and standard solution is found. Afterwards, the optimization algorithm must either confirm or reject this first guess. These steps are marked in Fig. 114 as 1, 2 and 3. Steps 1 and 2 are the successive tries for feasible symmetric solutions. After solution 2 is found to be feasible, the optimization algorithm finds solution 3 as the optimum.

Analysis of results

The simplest case of problem is the one having just one wire. This configures the problem in such a way that there is only one variable, i.e. one cross-section to determine. As previously explained, the optimum is a free value of area, but the final optimum cross-section is the lightest value comprised by the set of available standard cross-sections, as seen in Fig. 115. For just one wire, the problem is simple: the lower cross-section, the better result. In fact, the linearity of the cost function implies that the free optimum will always lie right on one of the boundaries. This can be seen also in Fig. 115, were the minimum current is the active constraint. Finally, the chosen value of cross-section is the immediately greater standard value, because the immediately lower one does not match the constraints.

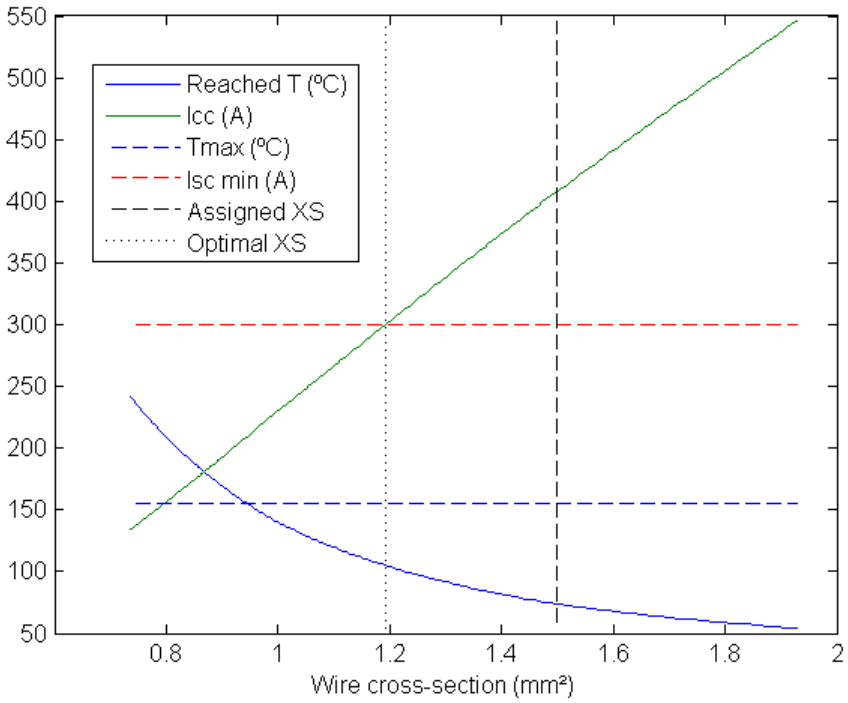

Fig. 115. Results of optimization for one wire. The active constraint is the short circuit current

The same problem can be solved, in this case imposing less minimum short circuit current, as seen in Fig. 116. Now the active constraint is the temperature, which is equal to the maximum acceptable value for the free optimum. Once again the final optimum is the immediately greater value.

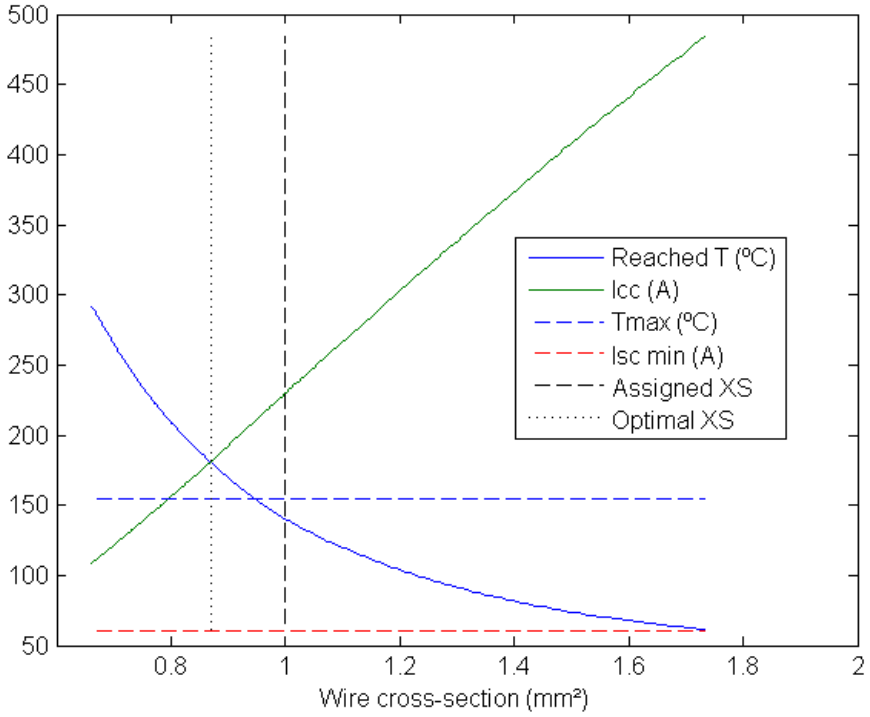

Fig. 116. Results of optimization for one wire. The active constraint is the wire temperature.

In order to see the results of optimization for two wires, it is necessary to use a 3D plot, as seen in Fig. 117. The cost function here is seen as a plane, which has a constant gradient vector pointing to the direction of maximum slope. The short circuit current and temperature form surfaces intersecting their limit values with hyperbolic-looking boundaries, separating the feasible solutions in the most positive regions. Once again, the free optimum lies right on one of the boundaries, and in this case it is possible to observe how the gradient is perpendicular to the boundaries. This can be better seen in Fig. 118.

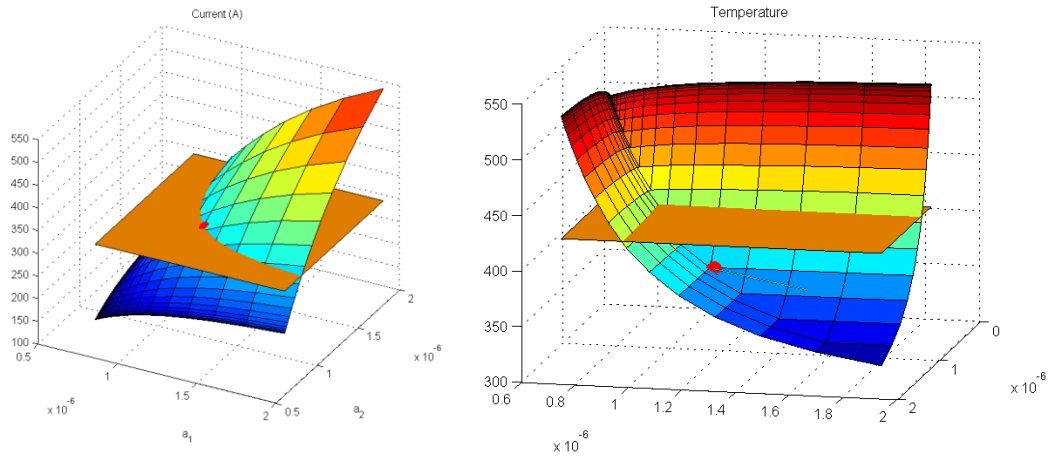

Fig. 117. Results of optimization for two wires. The active constraint is the short circuit current

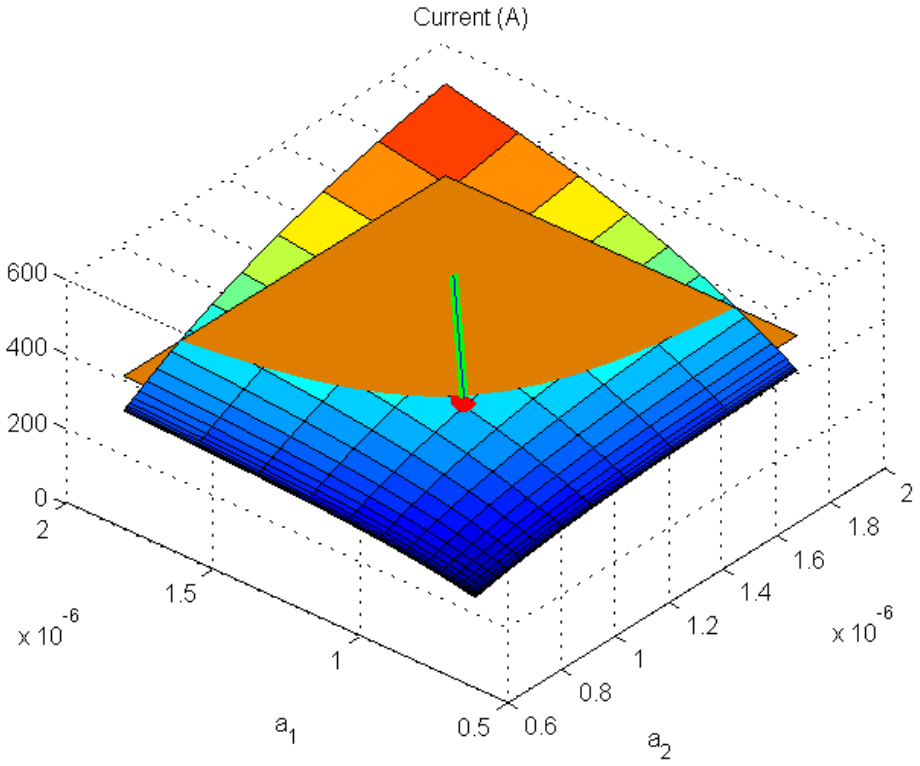

Fig. 118. Results of optimization for two wires. Better angle to see the gradient vector and its perpendicularity to the boundary

For three wires, the cost function is a hyperplane and cannot be plotted as a function of three variables. Each point of the space has a different value of volume, of short circuit current and temperature. None of those can be depicted. However, the loci defined by equaling the current and temperature to their critical value define 3D surfaces that can be seen in Fig. 119. In this figure, the gradient of the cost function can also be seen, as well as the optimum. Once again, it is also possible to see how the gradient is perpendicular to the boundaries.

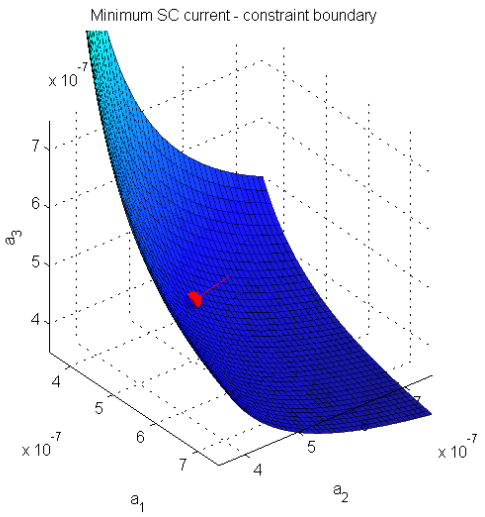

Fig. 119. Results of optimization for three wires, showing the short circuit boundary, the optimum and the gradient vector

Optimality tests

As seen in the prior sections, the optimum is always in contact with the boundaries, in a point where the gradient is perpendicular to them. If the obtained point is the absolute optimum, then a linear region of the space is tangent to the boundary will not cross any other point of the boundaries as seen in Fig. 120. Using this principle, an algorithm capable of answering to whether the free optimum is the absolute optimum has been created. Alg. 4 defines a set of points surrounding the free optimum and propagates them throughout a growing radius until all of the propagated points are out of the bounds of cross-section. This test is unnecessary for problems with just one wire.

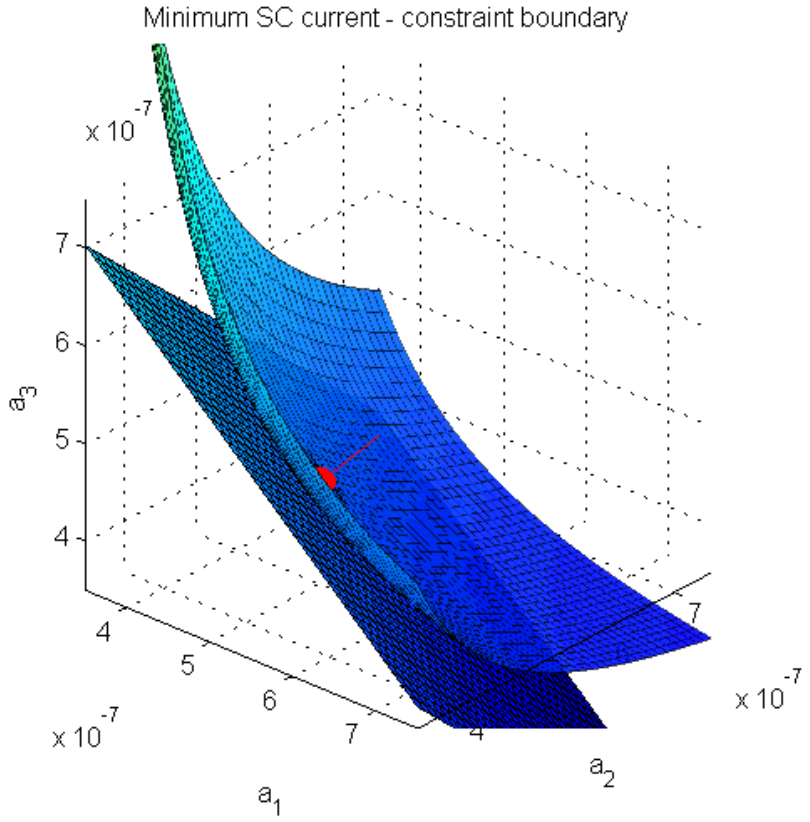

Fig. 120. Results of optimization for three wires. The tangency of the plane defined by the gradient vector (red) with respect to the short circuit current boundary indicates that the optimum is correct

```
Input cost_fun, x, dr, offset, lb, ub, constraint_fun, TolCon

Output answer

R = dr
ex = (R+dr)/dr
answer = true

C_1 = checkBounds(lb,ub,x)
if not C_1
       print("The evaluated point is either invalid or out of the specified
       bounds")
       answer = false
       return
end

[points,x] = getPointsOnce(cost_fun,x,R,offset)
C1 = checkBounds(lb,ub,points)   %C1 is true for points inside the hypercube
                                 %defined by lb and ub and false for
                                 %outliers
if not any(C1)
       print("The evaluated point is too close to a vertex of the bounding
       hypercube")
       answer = false
       return
end

while any(C1)
       C0 = checkConstraints(lb,ub,constraint_fun,points,TolCon)
       if any(C0)
              answer = false
              break
       end

       [points,R] = expandPoints(x,points,R,ex)
       C1 = checkBounds(lb,ub,points)
end

if answer
       print("Optimality test successful")
else
       print("Optimality test unsuccessful")
end
```

Alg. 4. Optimality test algorithm

The *checkBounds* function returns true if the point *x* is inside the region defined by the *lb* and *ub* vectors, which stand for lower bounds and upper bounds. These vectors contain the minimum and maximum available cross-sections for each of the wires, and therefore they have the same dimensions as *x*, which is the solution vector with the cross-sections of the *N* wires at their candidate for optimum point. This region is a segment for one wire, a rectangle for two wires, a right cuboid (a box) for three wires, and *n*-polytope figures for higher number of wires, *N*.

getPointsOnce generates checkpoints around *x* with certain offset. These points form a figure with *n*–1 dimensions correctly allocated in the *n*-dimensions space. For two wires, the *getPointsOnce* function will return two aligned points lying on a line that is perpendicular to the gradient of the cost function, as seen in Fig. 121. For three wires, the function will return eight points in a plane that is perpendicular to the gradient, forming a square, which is shown in Fig. 122.

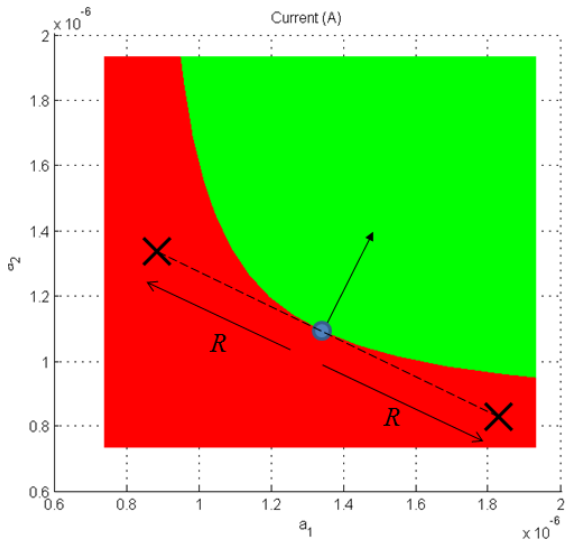

Fig. 121. Test points of the tangent plane of a 2-wire problem. These two points propagate outwards checking for compatible solutions in the optimality test algorithm

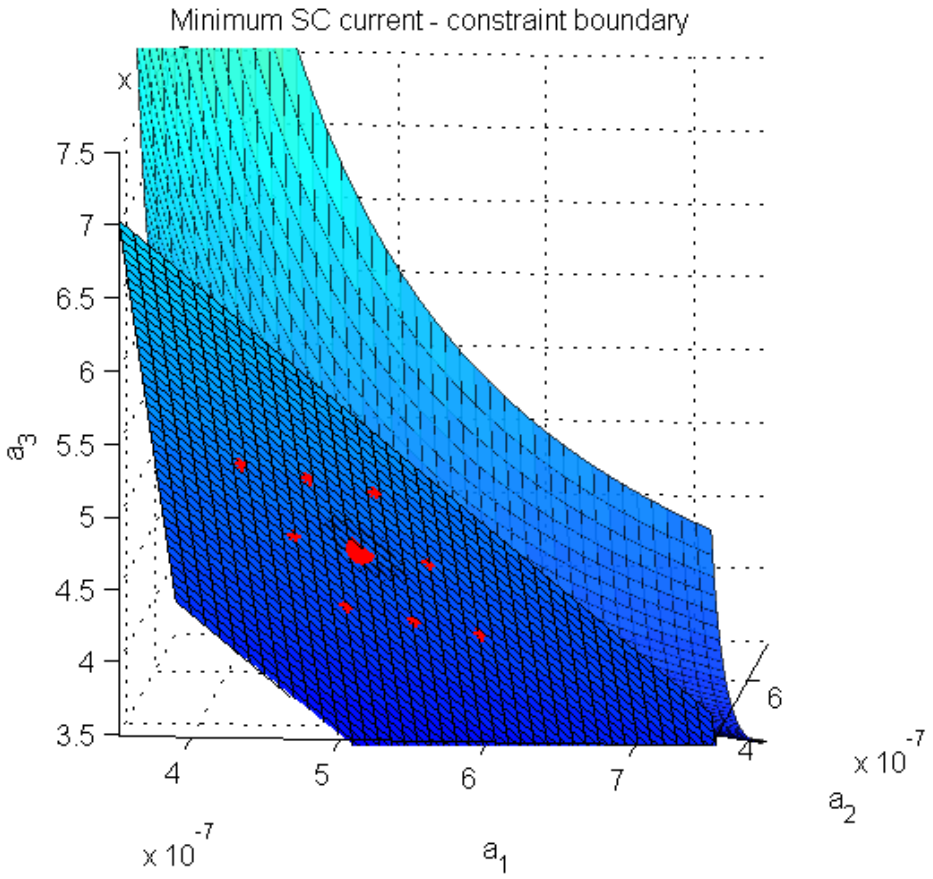

Fig. 122. Test points of the tangent plane of a 3-wire problem. These eight points propagate outwards checking for compatible solutions in the optimality test algorithm

For four wires, the function will return 26 4-dimension points forming a cube inside the space that is perpendicular to the 4-dimesioned gradient vector. Projected according to the direction of this gradient vector, this can be depicted as in cube. The subspace of n–1 dimensions is always displaced according to the offset parameter moving to the opposite direction of the gradient, giving certain margin to avoid mistakes in the test. Normally the offset is set to zero.

Once these points are obtained and evaluated the *expandPoints* function expands them in their subspace following the *ex* parameter, which is a ratio of expansion. After each expansion the test is successful if no point lies on the compatible side of the solutions, i.e. all of the points give negative results to the constraint evaluation.

6.7.6. Conclusions

With the aim of carrying out predictions of the temperature of wires after suffering a short circuit in automotive wiring harnesses, a system of simulation of series connected wires have been created. This system incorporates the behavior of the conventional automotive melting fuses in order to predict the duration of the short circuit. Additionally and using this simulation system, the sets of series-connected wires can be optimized using a particular optimization approach developed and described in this study. Finally, in order to ensure that the optimization algorithm is providing correct results, a test algorithm has been created and described.

The simulation of the short circuit shows good results for the prediction of the tripping time of the fuse, as well as the wire heating. The main challenge of his approach is to correctly determine the parameters of the fuse, which have been obtained by means of the least square method and the empirical curves of the fuse, given by its manufacturer. The wire heating model for single wires surrounded by still air provides good results of simulation.

The optimization approach used for these series-connected wires finds the optimum with the correct dimensions to withstand the short circuits, given the acceptable values of short circuit current and wire temperature. The optimum is normally associated to a unique value of cross-section of all of the wires, and this rule is in general only broken when the mixes of the wires are very different. In these cases, results reveal that the optimization approach could be applied assuming just one wire with the sum of the lengths of the considered wires, which would speed up the process. It is precisely in these cases of dissimilar mixes when this optimization approach can give solutions to the cross-section selection of wires in modular automotive wiring harnesses.

6.8. Entire network optimization

In this chapter, a novel optimization method for automotive wiring harnesses is introduced. It provides optimum sizes for all of the wires, assuring safety by correctly matching all of them with their fuses. This chapter is the result of concretizing the optimization process proposal in section 6.5, integrating the developments in sections 6.6 and 6.7.

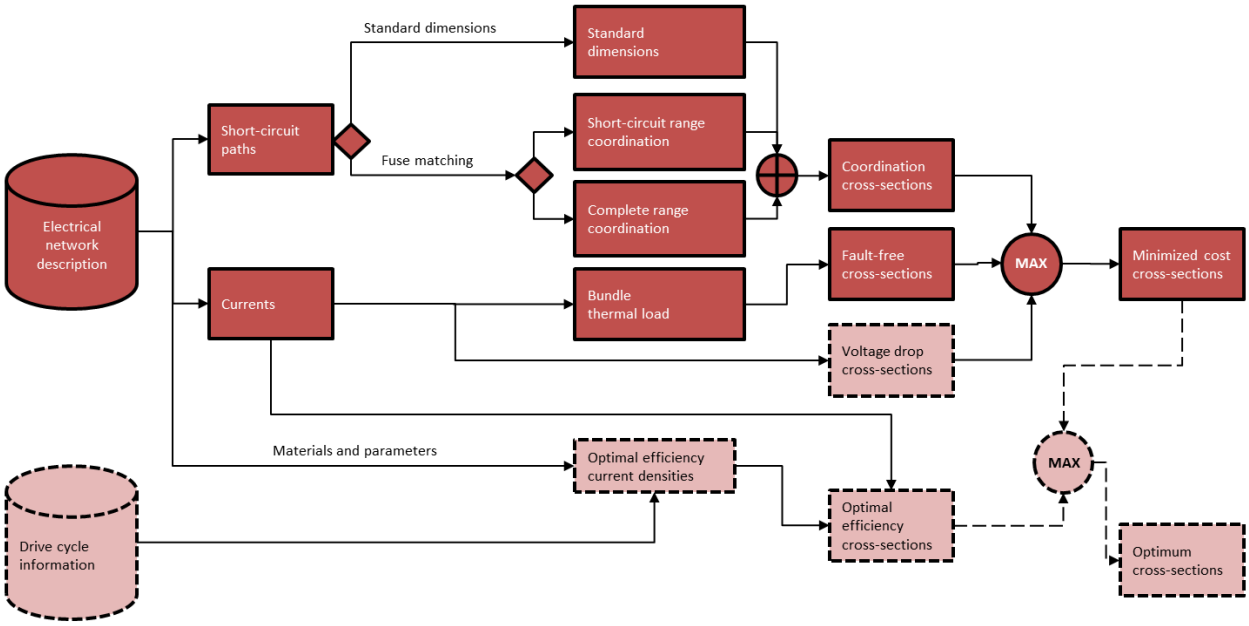

Fig. 123. Entire network optimization flux diagram

Fig. 123 shows a complete flux diagram describing the optimization proposed by this study. It reduces the process to two different concepts of optimization: the minimization of costs and the efficiency optimization in [15]. The minimization of cost stands for the minimization of copper weight, i.e. the cross-sections of wires, but as explained in [15], the minimization of costs is not necessarily the most efficient solution for the network, since thinner cross-sections imply higher energy losses. Finding the most efficient cross-sections is not under the scope of this study, and that is the reason why these blocks appear with dashed contours in Fig. 123. Neither is the calculation of voltage drops, which would be used to assess that the assigned cross-sections do not produce excessively high voltage drops.

The minimization of cross-sections consists of assigning the minimum cross-sections considering the thermal load of bundles, following the approaches in section 6.6, as well as studying the short-circuit breaking capability of each of the fuses of the network, using the approach in section 6.7. These two assignments of cross-sections are stored for every wire and the larger are selected at the end of the process. This way all of the wires will withstand short circuits as well as hot spots inside the bundles. It must be remarked that setting cross-sections influence results of optimizations for both criteria. This means that if a wire needs a certain cross-section *a* as a conclusion of the bundle thermal load optimization, and the same wire needs a cross-section *b* as a conclusion of the series-connected wires

optimization, such that $a < b$, the b cross-section will be assigned. However now that the wire has a set cross-section b, the same optimization in the bundle might produce different results for some of its neighbor wires. In particular, some of the neighbor wires could become thinner. Therefore, the optimization can be repeated setting constant values the new cross-sections, starting from the lightest wires. The iteration would finish when no cross-section changes.

The optimization oriented to short-circuit needs the detection of the short-circuit paths. The set of short-circuit paths is composed by the paths through which currents would flow when shorting all of the pins. Then, there is at least one short-circuit path for each pin.

In the flux diagram in Fig. 123, there is a complete branch for the *short-circuit paths*. These are the different possible calculations that can be made with the short-circuit paths. These options are the assignment of the standard cross-sections for each path and two different types of fuse-wire coordination. The first fuse-wire coordination, the *short-circuit range* coordination, finds the minimum cross-sections of the wires composing these paths that are still well protected by the fuses after ground short-circuits. The minimum impedance of the path can be set, so that simulated short-circuits are not free of extra impedances. This lowers the short-circuit current to be on the safe side. The second option is the *full range* coordination, which ensures that no current applied to the path can make the wire reach undesired temperatures. In both cases, the maximum acceptable temperature can be selected.

The other branch starts with the currents of the network. Once the current of each of the wires is known, it can be applied to calculate the optimum cross-sections of the bundles or the voltage drops. They can also be used to assess the correct selection of fuses.

The optimization applied to the network should include the possibility of using the minimum cross-sections of wires ensuring the correct temperatures for both the steady state and the transient state in the event of short circuit. The concept of an optimization tool would look like in Fig. 124.

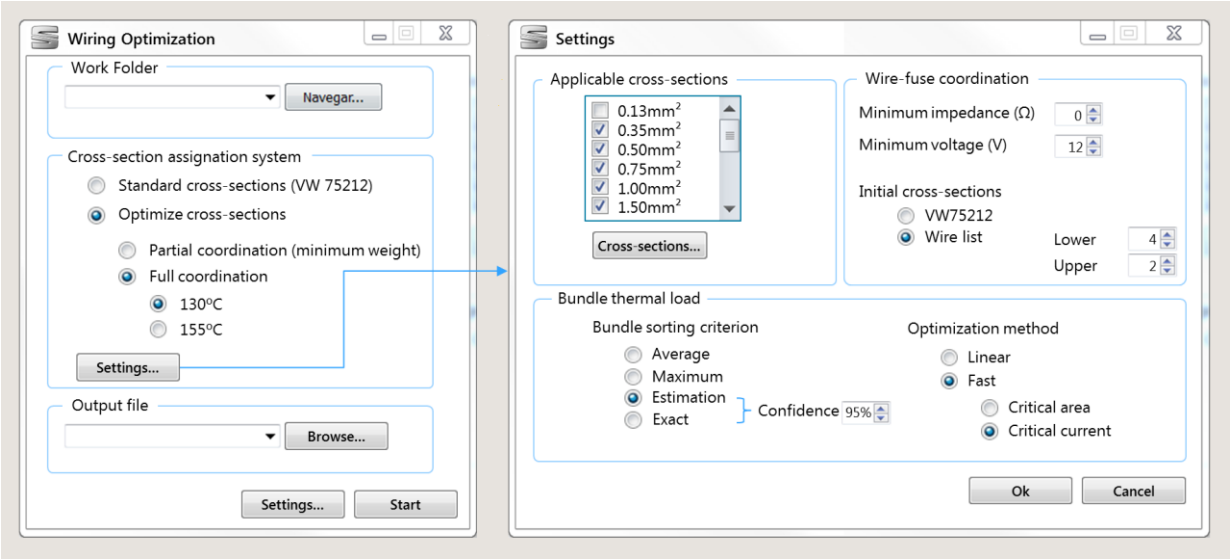

Fig. 124. Concept of optimization tool for wiring harnesses

The main option would allow choosing if a optimization is desired or just the standard cross-sections are desired. The optimization should be configurable so that:

- Some cross-sections can be used and some other are not allowed (applicable cross-sections).
- There are options of fuse-wire coordination: A) The weight of the wires is reduced by applying ISO 8820, in such a way that wires are protected against ground short circuits. B) The coordination is total, i.e. no current should be able to make wires exceed the given temperature (130ºC or 155ºC for class B wires)
- The fuse-wire coordination is defined by a minimum impedance of short-circuit and the voltage producing the weakest short-circuit (minimum impedance and minimum voltage)
- The cross-sections at the beginning can either be the cross-sections in the wire lists or re-assigned in the first step as VW75212 (standard cross-sections).
- The optimization of bundles allows choosing the sorting method of the modular combinations. “Average” would use the root mean square currents of the wires in the bundles; “Maximum” would use the maximum given value of currents in the wires; “Estimation” or “Exact” would calculate maximum current of the bundle with a selectable confidence, “Maximum” corresponds to 100%. “Estimation” would approximate the confident value of current by means of the normal distribution, whereas “Exact” would add distributions of currents to get an accurate value. This way, the bundles can be dimensioned according to the maximum expectable current but in a realistic way, so that they are not oversized.
- The bundle optimization method can be selected between the approaches described in section 6.6.

6.8.1. The harness description list

It is crucial to know the history of wiring harness development to understand why, in general terms, the main concern of this engineering has been always make the assembly of harnesses feasible and fast to modify. All of the information used by software tools and engineers is basically responding to one objective, which is being able to assembly the harnesses.

The data containers used for the harness development software tools lack the necessary information for simulation that has been discussed and explained in the previous chapters. This is because, so far, the main issues and problems within the wiring harness development and manufacturing have been traditionally related to geometries and mechanical aspects of the harnesses rather than to the electrical aspects of the network such as the optimal selection of fuses and wires. On the other hand, electrical or thermal problems can be solved without new investments whenever these problems affect only to the cross sections of wires or the fuse rated current or type.

The available information is the needed to exchange harness design data within car manufacturers and their suppliers:

1. Harness, variants and modules
2. Components like connectors of wires
3. Part lists
4. Connectivity lists
5. Topology

Innovations in automotive industry define themselves by electric and electronic components. As the electrical wiring system builds the essential infrastructure for automobile electronics, the wire harness becomes increasingly complex. This need for increased complexity comes along with the minimizing of design time and shortening of lead times.

Therefore, the collaboration of car manufacturers and harness suppliers is a challenge. He traditional way that a supplier receives harness design data from the car manufacturer has to change. Instead of various drawings and lists in proprietary formats, they need a specification, which describes the wire harness in its entirely so that the manufacturer can plan the manufacturing and assembly of the harness, based on the received data. Such a specification should be based on standards to fulfill the requirements for open development partnerships.

The exchange data containers have been developed under recommendations of the VDA Working Group “Car Electric”, whose objectives are the harmonization of requirements and the development of recommendations for the exchange of product data in the area of car electrical systems. This specification is also known as “KBL”, which stands for “Kabelbaumliste”, German for “Harness description list”. The

recommendation defines how harness design data coming from various sources like 3D CAD systems or CAE system can be represented in an aggregated view. It also describes how the international standard ISO 10303-212 “Electrical Design and Installation” [ISO 10303] should be used for this purpose.

The achievements of these recommendations are the basis for reference standards for data quality, standardized viewing solutions, independency of harness data from proprietary software tools, simple comparability of development status and variants or standardized data exchange processes.

The typical harness development process starts with the system design where the functionality of the new developed system will be described. The top level view gives the overview of all items needed. With wiring diagrams, engineers start to define the parts needed to fulfill the expected functions. Components are selected according to the required specification and are documented in part lists. Connections are defined to combine the components logically. The first harness concept takes place, the position of the components and paths for wires are planned and described in wire lists and harness layouts. The net list (connection list) can be used to start the harness routing.

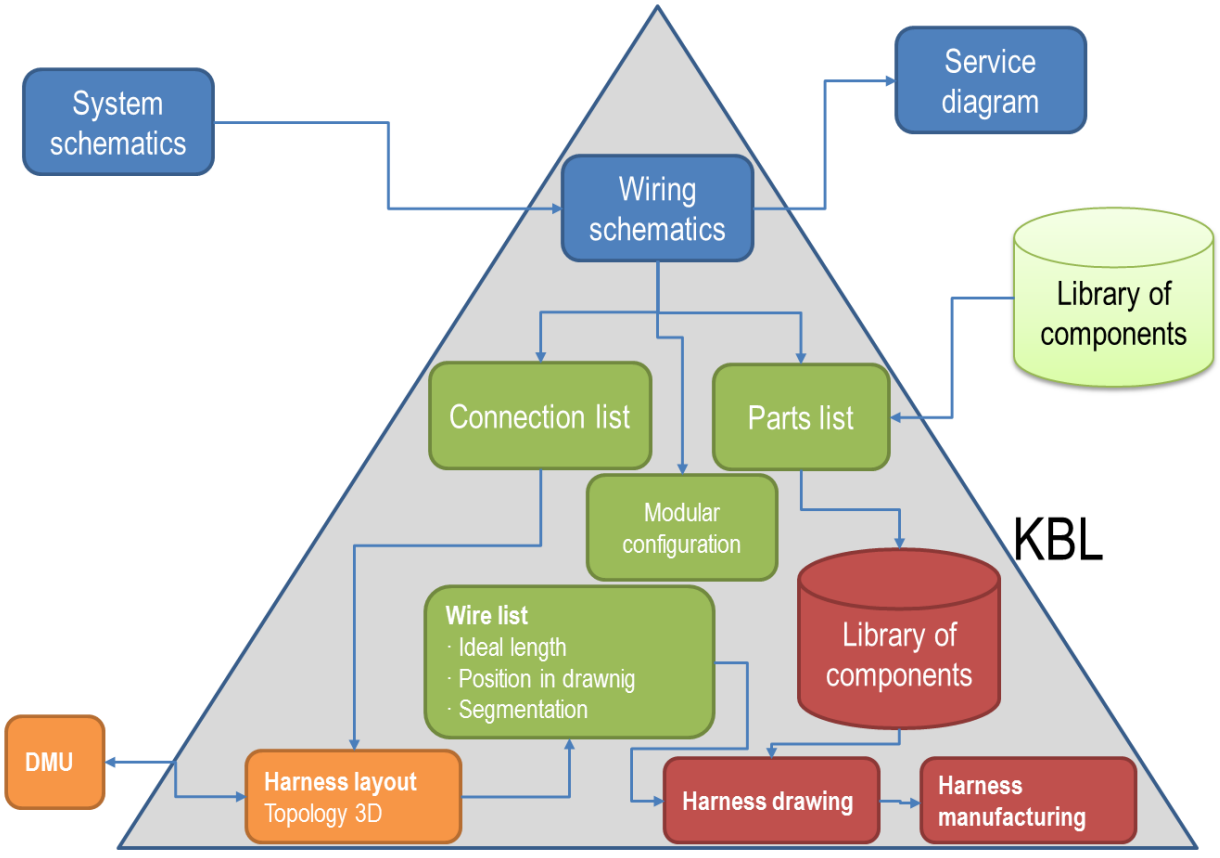

Fig. 125. Scope of the KBL data container within the harness design process

Unfortunately, the library of components inside the KBL files do not contain any information related to the electrical behavior of the parts. These parts are just described by their part number, number of pins

and other relevant information for the wiring harness assembly. For example, a motor may be referenced, but not its power nor an equivalent electrical circuit will be described in the KBL file.

6.8.2. Necessary data for simulation

The on-board network of a vehicle is large enough to result complex compared to the typical simulated circuits in research, but compared to power distribution networks it is small enough to encourage designers to get as many details as possible.

If the network is simulated with its total definition, it is necessary to include a simulation model of all of the electrical loads, as well as models for the switches, control units, fuses or other protection devices, relays and so on and so forth. Only in this manner, it will be possible to know the exact current circulating through every wire. Of course, it is not only necessary to know currents, but also to know how much current can withstand all parts involved (connectors, relays, etc.).

The maximum reachable temperature of each wire results from all of the aspects described in previous sections. The complete simulation of the network would use the temperature of the wires to provide better information of the voltage drops. Therefore, a temperature map of the car associated to each position of the car would be useful.

The state of the art of thermal and electrical simulation would allow for an ultimate concept of simulation capable of simulating the behavior of the car and the associated temperature increase. This way, the temperature in the 3D geometries could be calculated as the simulation time goes on, relating with highest precision the electrical and the thermal state of the vehicle. However, this type of simulations is still far to be achieved from the point of view of practical industrial use.

6.8.2.The data container prototype

Some of the used data for the assembly of wiring harnesses can be used for the simulation of the electrical network of the vehicle. Basically, this information is the connectivity list containing to which user location connects each end of the wires, which modules include each part and wires, and through which harness segments extend these wires. However, the connection between different harnesses is not contained in the KBL files, as well as other information that would be necessary in order to carry out the simulations and optimizations proposed in this study.

The data container prototype proposed here consists of a set of tables with the necessary information to simulate and optimize. This file is called “QT”, which stands for Catalan *“quadern tècnic”*, i.e. “technical booklet”. This name has been chosen because this so-called technical booklet is a technical set of worksheets containing information of the on-board wiring system. First of all, it resumes the different wiring harnesses and how they connect between them through couplings. It also details how the fuse boxes are structured, among other relevant information.

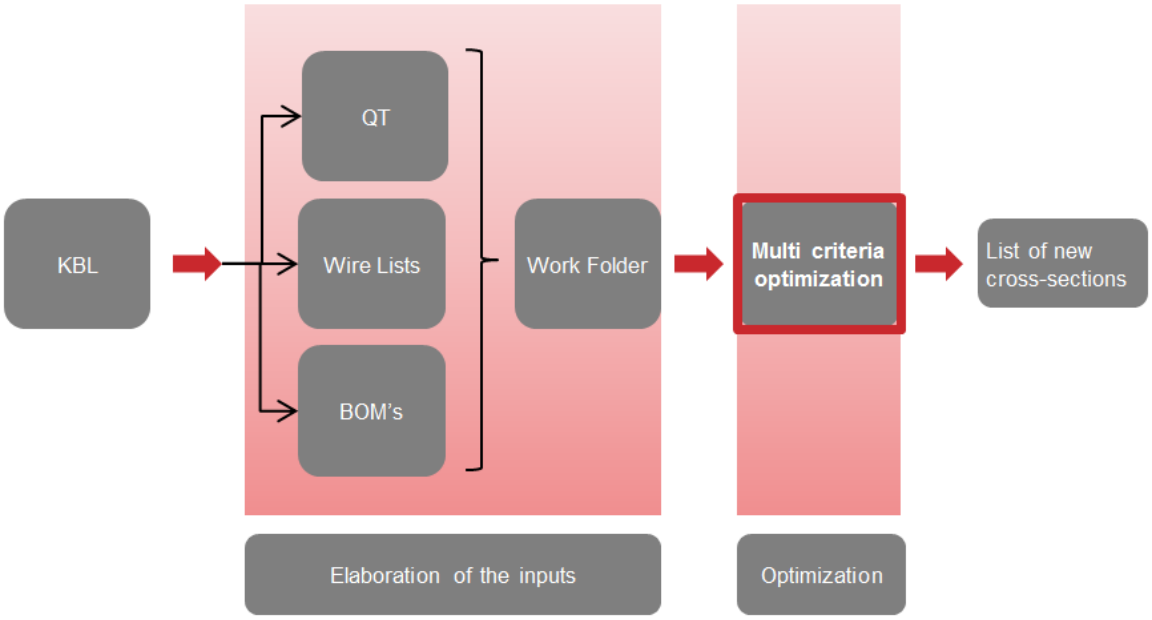

Fig. 126. Prototype process of optimization using the *QT* file

One important aspect of the traditional technical booklets is that they are only made manually by humans, and they are only read by humans. The information contained can usually present inconsistencies due to transcription errors, mistakes, inattentions, or just because not the entire booklet has been updated at the same time.

Still, these technical booklets inspired the *QT*, because an important part of the contained information is necessary to simulate and to optimize the network. What the *QT* brings is a new format that a computer can read, so all the information can be taken directly for simulation. In this state of research, the *QT* has been design so that in works in parallel with two other documents, which are the *wire list* and the *bill of materials*. These three documents can provide enough information to simulate the network with constant power consumptions and to optimize wire cross-sections as described in this dissertation.

In origin, the *QT* is a Microsoft Excel® file with 13 worksheets:

1. List of harnesses

   The list of harnesses contains information of all of the harnesses composing the on-board network of the vehicle. All of them have one identifier that must be a unique name for this harness, and which is used constantly during the analysis of the network. Normally, this name is the original table number of the harness or its part number. Each of them is also related to the corresponding wire list and bill of materials.

harness	bom_filename	wirelist_filename
Harness_1	bom_harness_1.csv	wire_harness_1.csv
Harness_2	bom_harness_2.csv	wire_harness_3.csv
…	…	…
Harness_N	bom_harness_N.csv	wire_harness_N.csv

Table 10. Example of the list of harnesses in the *QT* file

2. Supplementary families

As previously explained, wiring modules are indivisible sets of parts related to a set of functions that are either completely assembled or completely ignored at the manufacturing stage of the harnesses. The necessity of assembly depends on the required functions of the car that the customer has demanded. Modules are grouped by families and in general modules of the same family cannot be installed at the same time. However, there are some families called *supplementary* families, which group their modules but permit their coexistence in the vehicle. In other terms, more than one module pertaining to supplementary families can be installed at the same time. These supplementary families are an exception to this rule, and therefore, it is necessary to list them in the *QT*. This worksheet is just a list of the names of these families, just as they appear in the KBL files and consequently in the bills of materials and wire lists.

3. Battery

All contacts are listed in the wire lists and the available information of the harnesses, but the exact name of the terminals of the battery is not specified. It is necessary to specify which are the positive and negative terminals of the batteries and their harnesses so that the simulation interprets correctly which is the block of representing a battery in the system diagrams and considers it correctly in the simulation. In improved simulations, the alternator should be consider as well if one wants to study the behavior of the network when the battery is exchanging energy in two directions.

harness	location	Slot	pin	potential
drawing_bat_positive	A.3	A	1	positive
drawing_bat_negative	A.3	B	1	negative

Table 11. Example of the battery information in the *QT* file

Moreover, this information is expected to be extended for cars with more than one level of voltage. These tables should be extended with one or more additional columns expressing the voltage of the batteries or other necessary information like their maximum current, power and capacity.

4. Locations master

This table resumes all the information of the so-called *user locations* (*Verwendungsstelle* or "use location" in German). They are associated to functions in a conceptual way, and they are not strictly associated to a particular part. Particular part numbers for electrical loads and their corresponding 3D models are associated to user locations, whose names are standard and shared between cars, despite the particular parts used for these locations change from project to project or even throughout the same project, as they are updated or replaced.

This way, connections in system schematics are expressed to user locations and not to parts. The particular parts in the same user location will share the number of pins and their function, so that the connections to the same user location do not depend on the final component used for this electrical function.

The master table of user locations contains their name, their description, harnesses where they appear, their type and additional information for their particular type when necessary. During the status of this dissertation, the additional information is just related to fuse boxes, though this information might be extended when necessary in the future.

The current types of elements of simulation are the splices, fuse boxes, ground bolts, couplings, batteries and other components. With this classification is possible to carry out the first analysis of the network. They identify all the different types of places where a wire can end.

location	harness	description	type	fusebox_ name	fusebox_ temperature
vws1	drawing01	User location 1	FuseBox	LVI	80
spl1	drawing01	Splice 1	Splice		
vws2	drawing01	User location 2	Component		
vws3	drawing01	User location 3	Coupling		

Table 12. Example of the location master table in the *QT* file

5. Wires-Segments

The wires-segment table identifies which segments of the wiring harness includes each wire. By definition, the extremities of wires must coincide with the extremities of the segments, called *junctions* in the *QT*. Therefore, it is necessary to indicate in which segment/s a wire is present.

harness	wire_number	segment_id
drawing01	1	s1
drawing01	16	s1
drawing02	2	s111
drawing02	3	s112
drawing02	3	s1121

Table 13. Example of the wires-segment table in the *QT* file

6. Segments-Junctions

In a similar way, the *segments-junctions* table gathers the relations between segments and junctions. Since one segment is defined by exactly two junctions, this could be also called the master table for segments. Each segment has also its value of ambient temperature.

harness	segment_id	junction_id_1	junction_id_2	Tamb
drawing01	s1	j1	j2	55
drawing01	s11	j2	j3	55
drawing01	s12	j2	j5	55
drawing01	s111	j3	jc01	55
drawing01	s112	j3	j4	55
drawing01	s1121	j4	jc02	55
drawing01	s1122	j4	jc05	55

Table 14. Example of the segments-junctions table in the *QT* file

7. Junctions

The *junctions* table contains the master information about junctions, composed by an identification of the node, the harness to which it belongs and its coordinates in the drawing. This latter parameter has not been used in this research but it will be useful for future graphical representations of the simulation and optimization results.

harness	junction_id	x	y
drawing01	j1	137	123
drawing01	j2	384	761
drawing01	j3	123	132
drawing01	j4	872	129
drawing01	j5	423	674

Table 15. Example of the *junctions* table in the *QT* file

8. Modules

The *modules* table contains all of the necessary information of the modules, consisting on their name, their family, their installation condition formula and their installation ratio or *mix*.

module_name	pr_formula	family	mix
module01	06+07+08	family01	31%
module02	06+07+08+01+05	family01	39%
module03	06+07+08+01+05+03+04	family01	30%

Table 16. Example of the *modules* table in the *QT* file

9. Device pin-out

This table tries so solve the black box problem within the wiring development. Components as switches or relays lack any digitalized description of their internal connection and states. Therefore, it is necessary to know through which pins flows the electrical current. For instance, this table relates the coil pins of a relay between them, and the power pins between them accordingly, so that the simulator knows how to transport continuously the current from node to node. This table incorporates all types of electrical loads, switches and control units, but it lacks information about their states. For a complete simulation, it should be done in a smart way. The utility of this table is to correctly know how currents distribute inside the network as well as detecting the short circuit paths.

partnumber	pin_in	slot_in	pin_out	slot_out
pn021	1	A	2	A
pn021	1	A	3	A
pn021	1	A	4	A
pn041	1	A	2	A
pn041	1	A	3	A
pn051	1	A	2	A

Table 17. Example of the *device pin-out* table in the *QT* file

10. Pin master

The pin master table contains the information about all of the pins included in the different components of the electrical system of the vehicle. So far, the only information of current consumption of loads that is stored in data bases comes under the form of six different values of current and two characteristic times. Depending on the time of pin (ECU Drain, ECU Source, Sink, Signal, Switch contact, Coil, or not connected), these values from 1 to 6 have different meanings, as well as the two values of time.

The database provides also information about the pins, being these ones ohmic, motor, capacitor, glow or coil.

partnumber	slot	pin	pin_type	pin_characteristic	i1	i2	i3	i4	i5	i6	t1	t2
pn021		1	Senke (SG Last)	Ohmic	30,01	30,01	30,01					
pn021		2	Signal (CAN, Messein/-ausgang)	Ohmic	0,02	0,01	0,01					
pn021		3	Quelle (SG Ausgang)	Ohmic	30,01	30,01	30,01					
pn021		4	Senke (Komponente)	Ohmic	0,51	1,01	1,11					

Table 18. Example of the pin master table in the *QT* file

11. Couplings

The couplings are the unions between different harnesses. They are identified in the system schematics are user locations by themselves, but no information of the harnesses at the other side is stored. Therefore, it is necessary to relate these user locations between them in order to state connections.

location_1	location_2
vws_02.1	vws_06.1

Table 19. Example of the couplings table in the *QT* file

12. Fuse boxes pin-out

Fuses have the particularity that, unless they are floating fuses, they are not in contact directly with wires. Instead, is the fuse box as user location the block that is in contact with the wires, appearing in the wire list. The pin and slot of the fuse box is contained in wire lists, but the information about the fuses is contained in the KBL file.

Additionally, the fuse box has an internal connectivity, in such a way that some pins are connected between them and some others are not. Relays are also connected to the fuse boxes and it is necessary to relate pins of the fuse box to pins of the parts connected to it, which can be relays or fuses.

location	slot_1	pin_1	part_slot_1	part_pin_1	connection_id	connection_type	slot_2	pin_2	part_slot_2	part_pin_2
vws_fuse01.1	A	1			F1	fuse	F	1A		
vws_fuse01.1	A	1			F2	fuse	F	2A		
vws_fuse01.1	A	1			kl30..C1	plate	C	1		
vws_fuse01.1	F	4			F4	fuse	F	4A		
vws_fuse01.1	A	1			F5	fuse	F	5A		
vws_fuse01.1	F	3			F3	fuse	F	3A		
vws_fuse01.1	F	50		1	R1_coil	relay_coil	F	51		2
vws_fuse01.1	F	52		3	R1_switch	relay_switch	F	53		4

Table 20. Example of the fuse box pin-out table in the *QT* file

13. Fuse boxes modularity

Each fuse should be dependent to a set of PR's and modules. This table states relations between each of the fuses and the active modules.

location	connection_id	module	partnumber
vws_fuse01.1	F1	module01	fuseref01
vws_fuse01.1	F1	module02	fuseref02
vws_fuse01.1	F1	module03	fuseref03
vws_fuse01.1	F2	module02	fuseref04
vws_fuse01.1	F2	module03	fuseref04

Table 21. Example of a fuse box modularity table in the *QT* file

6.8.3. Optimization

Since the available information about power consumption of the different loads is their current consumption as expressed in the *pins master* table and it lacks a correct orientation of these currents, it is necessary to detect the current flow in the network.

This detection of the current flow is carried out using the wire lists, the type of components, the type of pins and the device pin-out explained in the previous section. An algorithm capable of finding the current paths have been developed. It search possible ways for the current to flow from the positive battery terminal crossing all components until it reaches the negative battery terminal. This way all current consumptions detailed in *pin master* can be translated and added through the entire network until the current of each wire is known.

Additionally, this search allows for knowing the short-circuit paths, which relates the set of wires being protected by particular fuses. This way the cross-section assignment can be done to every wire in a correct way. The modules of the wires are also taken into account so that no impossible paths are considered.

Once the short-circuit paths are detected, the normative cross-section assignment can be performed just using a look-up table. This look-up table is an adaptation coming from the regulation, as explained in previous chapters. It is especially made in order to be able to compare the results of optimization. The standard cross-section is the reference.

In order to apply the optimization explained in section 6.6, it is necessary to identify all the wires in the different segments. After the current distribution is known, all wires have their currents depending on the modular configuration. Before the optimization starts, in every segment it is necessary to consider all of the different combinations of bundles and to sort them from higher to lower sum of currents. Different optimizations are carried out following this order until all of the wires have been dimensioned. If one combination of modules does not introduce a new wire dimension, the calculation is skipped. This way, the search ends once all of the wires in a segment are dimensioned. This is made for all of the segments

and wires in the on-board network. After this process, the wires take the bigger cross-section between all of the different cross-sections they could take, so that the wire is ready for all of the considered situations.

The last stage of optimization is reached by applying the optimization approach described in section 6.7. Wires in the network are grouped and sorted by short-circuit paths. Each of these short-circuit paths is taken by the optimization algorithm in section 6.7 and optimized. These groups can be formed by two or more wires.

7. Conclusions

With the aim of optimizing the cross-sections of the modular wiring harnesses in the on-board network of cars, a general FEM simulator for single wires and wire bundles has been developed. It can realize steady and transient state simulations. The materials and geometry of the bundle and the packing solution, such as tape, can be configured. This particular simulator does not include the axial heat transfer. The correct definition of materials have led to good accordance with experimental results.

The good results of the FEM simulator have been used to create adjusted response surfaces so that the response surface optimization method can be applied to bundles. These surfaces respond to bundles with uniform current densities, and that is why signal wires must be excluded from the study. In order to introduce them in the study, the response surfaces would need extra independent variables to describe the amount of *cold* wires in the bundle. Their worst-case distribution should be such that the current density is focused in the center of the bundles. Still, the exclusion of the *cold* wires is considered worse than reality, which keeps the dimensioning on the safe side. The obtained response surfaces provide very similar results compared to the direct FEM simulations, in a really fast calculation time due to its polynomial form, which allows analyzing a large amount of modular combinations of bundles in a reduced time.

In fact, the response surfaces are related to the critical dimensions of the bundles in order to focus on the necessity of the optimization algorithms. These bundle optimizers do not need temperature predictions directly, and that is why a temperature-predicting response surface has not been developed. In spite of this, it would have been useful for the wiring development team in order to quickly assess the temperature of wire bundles, instead of affording directly the optimization.

In order to also give dimensions considering the protection devices –in this case melting fuses–, a single wire simulation approach with capability of axial heat transfer has been developed. The aim is to simulate short-circuits across wires of different cross-sections have been created using the finite volume method. The behavior of fuses has been replicated using an energy absorption model. The simulations are satisfactorily similar to experimental data. In comparison to the response surface method used for bundles, the finite volume method is not as fast. However is still fast enough to allow using these simulations on-line in optimization. In order to improve this, the same response surface method could be afforded with the short-circuit simulation in the future.

The sets of series-connected wires can be optimized using a particular optimization approach developed and described in this thesis. Finally, in order to ensure that the optimization algorithm is providing correct results, a test algorithm has been created and described.

The simulation of the short circuit shows good results for the prediction of the tripping time of the fuse, as well as the wire heating. The main challenge of his approach is to correctly determine the parameters of the fuse, which have been obtained by means of the least square method and the empirical curves of the

fuse, given by its manufacturer. The wire heating model for single wires surrounded by still air provides good results of simulation.

The optimization approach used for these series-connected wires finds the optimum with the correct dimensions to withstand the short circuits, given the acceptable values of short circuit current and wire temperature. The optimum is normally associated to a unique value of cross-section of all of the wires, and this rule is in general only broken when the mixes of the wires are very different. In these cases, results reveal that the optimization approach could be applied assuming just one wire with the sum of the lengths of the considered wires, which would speed up the process. It is precisely in these cases of dissimilar mixes when this optimization approach can give solutions to the cross-section selection of wires in modular automotive wiring harnesses.

Combining the optimization approaches for bundles and wires set to short-circuits, the analysis of the on-board network has been carried out. The basis of the entire network optimization have been described, and it sets the premises for a complete analysis of safety and optimization of the vehicle network, which sets the development one step closer to the complete zero-prototypes strategy.

Nevertheless it is still necessary to extract completely all the information of wiring contained in the format files used in the industry, to have a complete simulation of the network so that currents are correctly known. This means correctly interpreting all data containers of the wire development process, so that the entire information is structured and used as constraints or additional info for simulation of optimization.

The proposed system demands manual adaptation of information that makes this approach still not fast enough to be used in the highly demanding wiring development in the car industry. Fortunately, this research opens a set of defined tasks than can lead to a complete use of the developed approaches by the engineering of on-board network.

Bibliography

[1] Ilgevičius, A. *Analytical and numerical analysis and simulation of heat transfer in electrical conductors and fuses*. Universität der Bundeswehr München, September, 2004

[2] Lin, C., Rao, L., D'Ambrosio, J., Sangiovanni-Vincentelli, A. *Electrical architecture optimization and selection – Cost minimization via wire routing and wire sizing*. SAE International Journal of Passenger Cars – Electronic and electrical systems. January 2014.

[3] Short, T. A. *Electric power distribution handbook.* CRC Press LLC, 2004

[4] Čiegis, R., Ilgevičius, A., Ließ, H., Meilūnas, M., Suboč, O. *Numerical simulation of the heat conduction in the electrical wires*. Mathematical Modelling and analysis Vol. 12 No. 4. pages 425-439. 2007

[5] Combettes, S., Sontheimer, T., Rougemaille, S., Glize, P. *Weight optimization of aircraft harnesses*. Advances on practical applications of agents and multi-agent systems. Advances in intelligent and soft computing. Volume 155, 2012, pages 229-232.

[6] Frei, S., Diebig, M. *Simulation-based optimization of multi voltage automotive power supply systems*. Vehicle power and propulsion conference (VPPC), IEEE. Pages 1-6. 15-18 Oct. 2013

[7] Diebig, M., Frei, S., *Modeling of the automotive power supply network with VHDL-AMS*. Vehicle power and propulsion conference (VPPC), IEEE. Pages 1-3. Sept. 2010

[8] *VDI-Heat atlas*. Second edition. Springer-Verlag Berlin Heidelberg 2010

[9] Blomberg, Th. *Heat conduction in two and three dimensions*. Computer modelling of building physics applications. Lund University, Sweden. May, 1996

[10] Čiegis, R., Meilūnas, M., Jankevičiūtė, G., Ilgevičius, A. *Determination of heat conductivity coefficient of a wire bundle by inverse problem solution method*. ISSN 1392 – 1215 Electronics and electrical engineering. No. 2(90). 2009

[11] Lewis, R. W., Nithiarasu, P., Seetharamu, K. N. *Fundamentals of the finite element method for heat an fluid flow*. John Wiley & Sons, ltd. 2004

[12] Loos, F., Dvorsky, K., Ließ, H. *Two approaches for heat transfer simulation of current carrying multicables*. Mathematics and computers in simulation. Vol. 101, pages 13-30. July, 2014

[13] Benthem, R.C. van, Grave, W. de, Doctor, F., Nuyten, K., Taylor, S., Jacques, P.A. *Thermal analysis of wiring for weight reduction and improved safety*. National Aerospace Laboratory NLR. NLR-TP. AIAA/ICES Conference, Portland, Oregan, USA 18-21 July 2011

[14] Harbrecht, H., Loos, F. *Optimization of current carrying multicables*. Computational optimization and applications. June, 2013

[15] Ließ, H. *Optimal dimensions for electrical conductors in mobile systems*. Electric drives production conference (EDPC), 1st international. IEEE. Pages 139-142, Sept. 2011

[16] Loos, F., Ließ, H., Dvorsky, K. *Simulation methods for heat transfer processes in mechanical and electrical connections*. Electric drives production conference (EDPC), 1st international. IEEE, Sept. 2011.

[17] T. Robbins, *Fuse model for over-current protection simulation of dc distribution systems*, in Proceedings of Intelec 93: 15th International Telecommunications Energy Conference, vol. 2, pp. 336–340 vol.2, Sep 1993.

[18] D. Li and L. Qi, *Energy based fuse modeling and simulation,* 2013 IEEE Electric Ship Technologies Symposium (ESTS), Arlington, VA, 2013, pp. 487-492.

[19] R. H. Byrd, J. C. Gilbert, and J. Nocedal, *A trust region method based on interior point techniques for nonlinear programming*, Mathematical Programming, vol. 89, no. 1, pp. 149–185, 2000.

[20] R. H. Byrd, M. E. Hribar, and J. Nocedal, *An interior point algorithm for large-scale nonlinear programming*, SIAM Journal on Optimization, vol. 9, no. 4, pp. 877–900, 1999.

[21] T. F. Coleman and Y. Li, *An interior trust region approach for nonlinear minimization subject to bounds*, SIAM Journal on Optimization, vol. 6, no. 2, pp. 418–445, 1996.

[22] T. F. Coleman and Y. Li, *On the convergence of reflective newton methods for large-scale nonlinear minimization subject to bounds*, 1992.

[23] R. E. Ricketts, *Practical optimization*, Philip e. gill, Walter Murray and Margret h. wright, academic press inc. (London) limited, 1981, International Journal for Numerical Methods in Engineering, vol. 18, no. 6, pp. 954–954, 1982.

Conference presentations

A. Rius-Rueda, A. Garcia-Espinosa, Manuel A. Díaz-Millán, *Optimization of modular wiring harnesses by means of regression models for temperature prediction of wire bundles*, Simulation and Testing for Vehicle Technology, 7th Conference. Berlin, May 13th, 2016.

A. Rius-Rueda, A. Garcia-Espinosa, Manuel A. Díaz-Millán, *Custom integer optimization method for wire bundle dimensioning*[1], The 42nd annual conference of IEEE Industrial Electronics Society, Florence, Italy, October 25th, 2016.

Publications

A. Rius-Rueda, A. Garcia-Espinosa, E. Griful-Ponsati, Manuel A. Díaz-Millán. *Three optimization approaches for automotive wire bundles based on the response surface methodology (RSM)*, IEEE Transactions on Vehicular Technology. (Submitted and pending of acceptation)

A. Rius-Rueda, A. Garcia-Espinosa, Manuel A. Díaz-Millán. *Short circuit simulation and optimization of automotive wires*, IEEE Transactions on Industrial Electronics. (Submitted and pending of acceptation)

[1] Awarded for the best presentation in the *Transportation Electrification and Vehicle Systems* session.